

Cyclotetrabenzoin: Esterification, Host for Thin Guests, Purification, and By-Product Analysis

by
Corie Michele McHale

A dissertation submitted to the Department of Chemistry,
College of Natural Science and Mathematics
in partial fulfillment of the requirements for the degree of

Doctor of Philosophy
in Chemistry

Chair of Committee: Ognjen Š. Miljanić

Committee Member: Scott Gilbertson

Committee Member: Judy Wu

Committee Member: Melissa Zastrow

Committee Member: Jeffrey Rimer

University of Houston
April 2020

Copyright 2020, Corie Michele McHale

DEDICATION

I would like to dedicate this dissertation to my loving husband, Adam. His continued support and willingness to move across the country to help me pursue my goals have been instrumental in my success. I would also like to thank my parents Holly and Randy, sister and her husband Camryn and John, and my in-laws Kristin, Alan, and Kara for their continued support.

ACKNOWLEDGMENTS

When I started my PhD, I was very fortunate to join the Miljanić group. I found a group that was very welcoming and an advisor that was very supportive. I would like to thank Dr. Ognjen Š. Miljanić for his mentorship and guidance throughout the last five years working in his lab. I would also like to thank my colleagues and friends in the Miljanić group, Dr. Mohamed Hashim, Maymounah Alrayyani, Andrew Eisterhold, Zhenglin Zhang, Thamon Puangsamlee, Sumitra Karki, and Alexandra Robles for the research advice and welcoming environment. I would also like to thank close friends Dr. Sasha Oleynikchenko, Amy Boylan, Sabrina Aderibigbe, Suji Lam, and Cotton Starr for their support in and out of the lab.

ABSTRACT

Porous molecular crystals are a unique developing class of porous materials composed of discrete molecules. Macrocycles, which inherently have a central cavity, are a class of molecules that could be utilized in the continued development of porous molecular crystals. Cyclobenzoin is a class of macrocycles that were first reported in 2015 by the Miljanić group. Of the two reported macrocycles, cyclotribenzoin and cyclotetrabenzoin, this dissertation will mostly focus on our efforts to deepen the understanding and development of cyclotetrabenzoin. While published reaction conditions only produce one macrocycle with a 20% yield, analysis of other reaction components was attempted to determine what other products were being synthesized. A major limiting factor to studying cyclobenzoin is their insolubility in most common organic solvents. Previous modifications to cyclotetrabenzoin resulted in a major shape change in the pore, not enabling exploration of the intrinsic pore. Simple esterification with anhydrides was found to greatly increase cyclobenzoin solubility while not changing the shape of the intrinsic pore. Crystallization resulted in crystals with solvent molecules that could be removed resulting in a permanently porous crystal. A crystal structure was found to have CS₂ molecules in the intrinsic pore, which was the first indication of a small molecule interacting with the pore. Continued exploration to crystalize thin guest molecules resulted in several host-guest complexes with terminal alkynes and nitriles as guests. Lastly, CO₂ was shown in the crystal structure by X-ray crystallography and breakthrough curve analysis resulted in the ability to separate a N₂/CO₂ gas mixture.

TABLE OF CONTENTS

DEDICATION.....	iii
ACKNOWLEDGMENTS	iv
ABSTRACT	v
LIST OF TABLES	viii
LIST OF FIGURES	x
LIST OF SCHEMES.....	xiii
LIST OF ABBREVIATIONS	xiv
I. POROUS MATERIALS AND MACROCYCLES.....	1
1.1 Introduction.....	1
1.2 Porous Materials.....	2
1.2.1 Zeolites.....	2
1.2.2 Metal-Organic Frameworks (MOFs)	4
1.2.3 Porous Molecular Crystals (PMCs)	8
1.3 Macrocycle Synthesis Development	16
1.3.1 Brief History.....	16
1.3.2 Dynamic Combinatorial Chemistry	20
1.4 Benzoin Condensation	25
1.4.1 Reaction Discovery and Development.....	25
1.4.2 Applications of Benzoin Condensation.....	28
1.4.3 Macrocycle Synthesis by Benzoin Condensation	31
1.5 Conclusions and Outlook	34
II. POROSITY AND GUEST INCLUSION IN CYCLOBENZOIN ESTERS	36
2.1 Introduction.....	36
2.2 Cyclotribenzoin Synthesis and Reduction	37
2.3 Cyclotetrabenzoin Synthesis, Oxidation, and Diamine Condensation.....	39
2.4 Synthesis of Cyclobenzoin Esters	42
2.5 Conclusion.....	55
2.6 Experimental Section	55
2.6.1 General Methods.....	55
2.6.2 Synthetic Procedures and Characterization.....	57

2.6.3 Crystal Growth Conditions and X-ray Crystallographic Analysis.....	60
2.6.4 Gas Sorption Experiments.....	67
III. CYCLOBENZOIN ESTERS AS HOSTS FOR THIN GUESTS.....	71
3.1 Crystal Types and Crystal Growth.....	71
3.2 Host-Guest Complexes with Thin Molecular Guests.....	73
3.3 Thin Guest Inclusion.....	76
3.3.1 Inclusion of Aliphatic Alkyne and Nitrile Guests.....	81
3.3.2 Aromatic Alkyne and Nitrile Guest Inclusion	85
3.3.3 Aliphatic vs. Aromatic Guest Selectivity.....	91
3.4 CO ₂ Capture	95
3.5 Conclusion.....	101
3.6 Experimental Section	102
3.6.1 General Methods	102
3.6.2 Crystal Growth Conditions and Crystallographic Tables	102
IV. CYCLOTETRABENZOIN PURIFICATION AND BY-PRODUCT ANALYSIS ..	112
4.1 Benzoin Condensation	112
4.2 Reaction Condition Modifications	113
4.3 Cyanide Impact on Reaction Yield	117
4.4 Purification Methods.....	120
4.4.1 Cyclotetrabenzoin Purification.....	121
4.4.2 Purification After Oxidation to Cyclotetrabenzil	130
4.4.3 Purification After Esterification of Reaction Components	134
4.5 Conclusion.....	140
4.6 Experimental Section	141
4.6.1 General Methods	141
4.6.2 NMR Spectra of Isolated Compounds from Various Purification Methods	142
BIBLIOGRAPHY	145

LIST OF TABLES

1.1	Metal coordination by various crown ethers	17
2.1	Alkylation reaction conditions	42
2.2	Alkylation reaction solvent conditions.....	43
2.3	Esterification reaction conditions.....	44
2.4	Crystal data and structure refinement for cyclotribenzoin acetic ester	61
2.5	Crystal data and structure refinement for cyclotetrabenzoin acetic ester with ethyl acetate and hexanes	62
2.6	Crystal data and structure refinement for cyclotetrabenzoin acetic ester and acetone	63
2.7	Crystal data and structure refinement for cyclotetrabenzoin	64
2.8	Crystal data and structure refinement for cyclotetabenzoin propionic ester with acetone.....	65
2.9	Crystal data and structure refinement for cyclotetrabenzoin isobutyric ester with carbon disulfide.....	66
3.1	Calculated stabilization energies of host-guest interactions	93
3.2	Crystal data and structure refinement for cyclotetrabenzoin acetic ester and acetonitrile	102
3.3	Crystal data and structure refinement for cyclotetrabenzoin acetic ester and 3-butyne-2-one.....	103
3.4	Crystal data and structure refinement for cyclotetrabenzoin acetic ester and propargylic alcohol.....	104
3.5	Crystal data and structure refinement for cyclotetrabenzoin acetic ester and 4-phenyl-1-butyne.....	105
3.6	Crystal data and structure refinement for cyclotetrabenzoin propionic ester with benzonitrile.....	106
3.7	Crystal data and structure refinement for cyclotetrabenzoin isobutyric ester with benzonitrile.....	107
3.8	Crystal data and structure refinement for cyclotetrabenzoin isobutyric ester with phenylacetylene.....	109
3.9	Crystal data and structure refinement for cyclotetrabenzoin acetic ester with low concentration of CO ₂	110
3.10	Crystal data and structure refinement for cyclotetrabenzoin acetic ester with high concentration of CO ₂	111
4.1	Comparison of crude to isolated yield	113
4.2	Comparison of crude to calculated NMR yield.....	114

4.3	Comparison of crude and calculated NMR yield at lower temperatures	115
4.4	Comparison of crude, calculated NMR, and isolated yields.....	116
4.5	Comparison of nitrogen atmospheres.....	116
4.6	Solubility testing of cyclotetrabenzoin.....	122
4.7	Extended purification yeild	127

LIST OF FIGURES

1.1	Common zeolite building block.....	2
1.2	Crystallographic structure of Ga and Ge zeolite.....	4
1.3	Common SBUs used in MOF development.....	5
1.4	Chemical structure of second zinc MOF.....	7
1.5	Formation of extrinsically porous materials	9
1.6	Formation of intrinsically porous materials	10
1.7	Chemical structures of hemicryptophanes	12
1.8	Fluorinated PMCs with hexagonal pores	15
1.9	General structures of NHC salts.....	27
1.10	NHC salt catalysts development	28
2.1	Crystal structure of cyclotribenzoin	38
2.2	Crystal structure of cyclotetrabenzoin	40
2.3	Short contacts established in crystal of cyclotribenzoin acetic ester	46
2.4	Crystal structures of cyclotetrabenzoin esters.....	47
2.5	Packing diagrams of cyclobenzoin and cyclobenzoin esters.....	48
2.6	Short contacts established in crystal structure of cyclotetrabenzoin acetic ester	49
2.7	Short contacts established between layers of the crystal structure of cyclotetrabenzoin acetic ester.....	49
2.8	Short contacts established in the crystal structure of cyclotetrabenzoin propionic ester	50
2.9	Short contacts established between layers of the crystal structure of cyclotetrabenzoin propionic ester.....	50
2.10	Short contacts established in the crystal structure of cyclotetrabenzoin isobutyric ester	51
2.11	Crystal structure of cyclotetrabenzoin isobutyric ester with CS ₂ molecules located in the central pore.....	52
2.12	Nitrogen adsorption and desorption isotherms	53
2.13	Carbon dioxide gas sorption isotherm.....	53
2.14	PXRD patterns of cyclotetrabenzoin.....	54
2.15	Rouquerol plot for N ₂ gas sorption	68
2.16	BET surface area plot.....	68
2.17	NLDFT pore size distribution	69

2.18	Nitrogen gas sorption for cyclotribenzoin acetic ester, cyclotetrabenzoin propionic and isobutyric esters.....	69
3.1	Structure of adamantane derivatives crystal with alkynes	75
3.2	Cyclotetrabenzoin ester structures and resulting crystal packing	76
3.3	Crystallographic packing of cyclotetrabenzoin acetic ester with acetonitrile.....	78
3.4	Short contacts established in crystal structure of cyclotetrabenzoin acetic ester.....	78
3.5	Short contacts established between layers of crystal structure of cyclotetrabenzoin acetic ester.....	79
3.6	Short contacts established between cyclotetrabenzoin acetic ester and acetonitrile.....	80
3.7	Thin guest molecules used for co-crystallization experiments	80
3.8	Crystal structures with aliphatic thin guests.....	81
3.9	Crystal packing of cyclotetrabenzoin acetic ester with 3-butyne-2-one and propargylic alcohol.....	82
3.10	Short contacts established between cyclotetrabenzoin acetic ester and 3-butyne-2-one	83
3.11	Short contacts established between cyclotetrabenzoin acetic ester and propargylic alcohol.....	83
3.12	Crystal packing of cyclotetrabenzoin acetic ester with 4-phenyl-1-butyne.....	84
3.13	Short contacts established between cyclotetrabenzoin acetic ester in 4-phenyl-1-butyne crystal structure	84
3.14	Short contacts established between layers in the crystal of cyclotetrabenzoin acetic ester with 4-phenyl-1-butyne	85
3.15	Crystal packing of cyclotetrabenzoin propionic ester with benzonitrile.....	86
3.16	Short contacts established in the crystal structure of cyclotetrabenzoin propionic ester	86
3.17	Short contacts established between cyclotetrabenzoin propionic ester and benzonitrile	87
3.18	Short contacts established by π - π stacking	88
3.19	Crystal packing of cyclotetrabenzoin isobutyric ester with benzonitrile	88
3.20	Short contacts established in the crystal structure of cyclotetrabenzoin isobutyric ester	89
3.21	Short contacts established between cyclotetrabenzoin isobutyric ester with benzonitrile	89
3.22	Crystal packing of cyclotetrabenzoin isobutyric ester with phenylacetylene	90

3.23	Short contacts established in the crystal structure of cyclotetrabenzoin isobutyric ester and phenylacetylene	90
3.24	Short contacts established between cyclotetrabenzoin isobutyric ester and phenylacetylene.....	91
3.25	Liquid guest molecules used to test crystallization selectivity	92
3.26	Calculated energies and guest molecules approach the central pore of cyclotetrabenzoin acetic ester	94
3.27	Calculated geometries for π - π stacking calculated energies	94
3.28	Schematic of how to make crystallographic capillary tube filled with crystal and CO ₂	96
3.29	Crystal packing of cyclotetrabenzoin acetic ester with low concentration of CO ₂	97
3.30	Short contacts established between cyclotetrabenzoin acetic ester and CO ₂	98
3.31	Crystal packing of cyclotetrabenzoin acetic ester and high concentration of CO ₂	98
3.32	Short contacts established between cyclotetrabenzoin acetic ester and CO ₂	99
3.33	Breakthrough curves of gas separation	100
4.1	Mechanism of benzoin condensation	115
4.2	Stacked NMR spectra of selectively dissolved reaction components	123
4.3	Stacked NMR spectra of induced precipitation components	124
4.4	Mass spectrum analysis of induced precipitation components	125
4.5	Stacked NMR spectra of collected fractions with sephadex media	129
4.6	GPC analysis of oxidized reaction components.....	132
4.7	NMR spectra of second isolated fraction of DMSO solvent precipitate.....	137
4.8	Isomer products isolated in second fraction of DMSO solvent precipitate	138
4.9	Isomer product isolated from third fraction of DMSO solvent precipitate	138
4.10	Stacked NMR spectra of isolated precipitates of different purification methods of cyclotetrabenzoin	142
4.11	Stacked NMR spectra of sublimation fractions	143
4.12	NMR analysis of third isolated fraction of DMSO solvent precipitate.....	144

LIST OF SCHEMES

1.1	Synthesis of an early MOF.....	6
1.2	Dianin's templated synthesis of Schiff bases.....	9
1.3	Synthetic route to imine cages	11
1.4	Synthetic route to extrinsically porous materials.....	13
1.5	Synthesis of a crown ether	16
1.6	General synthesis of cucurbiturils.....	18
1.7	General route to pillararenes	19
1.8	Synthesis of first class of macrocycles by DCC	22
1.9	Synthesis of templated imine macrocycles	23
1.10	Synthesis of templated imine macrocycles	24
1.11	Lapworth's proposed benzoin condensation mechanism.....	26
1.12	NHC salt catalyzed natural products.....	30
1.13	Cyclobenzoin synthesis using sodium cyanide.....	32
1.14	Cyclobenzoin synthesis using NHC salt	34
2.1	Synthesis of cyclotetrabenzoin and cyclotribenzoin.....	37
2.2	Reduction of cyclotribenzoin	38
2.3	Oxidation of cyclotetrabenzoin and amine condensation	41
2.4	Microwave assisted silylation of cyclotetrabenzoin	43
2.5	Esterification of cyclobenzoin macrocycles.....	45
4.1	Synthesis of cyclotetrabenzoin.....	113
4.2	Synthetic reaction of cyclotetrabenzoin in buffered solution	118
4.3	Synthesis of cyclotetrabenzil.....	130
4.4	Synthesis of cyclotetrabenzoin acetic ester.....	134

LIST OF ABBREVIATIONS

1D	one dimensional
2D	two dimensional
3D	three dimensional
Ac	acetyl
AIE	aggregation-induced emission
BAL	benzaldehyde lyase
BDC	1,4-benzenedicarboxylate
BET	Brunauer-Emmett-Teller
BPY	4,4'-bipyridine
<i>t</i> BuOH	tert-butyl alcohol
CB	cucurbituril
CH ₃	methyl
COF	covalent organic framework
CTF	covalent triazine-based framework
DBU	1,8-diazabicyclo[5.4.0]undec-7-ene
DCC	dynamic combinatorial chemistry
DFT	density functional theory

DIPEA	<i>N,N</i> -diisopropylethylamine
DMF	dimethylformamide
DMSO	dimethyl sulfoxide
d.r.	diastereomer ratio
GPC	gel permeation chromatography
HPLC	high pressure liquid chromatography
<i>i</i> -Pr	isopropyl
Me	methyl
MOF	metal-organic framework
NHC	<i>N</i> -heterocyclic carbene
NION	nanoporous ionic organic network
NMR	nuclear magnetic resonance
PMC	porous molecular crystal
POE	points of extension
POP	porous organic polymer
PUNC	phthalocyanine unsolvated nanoporous crystals
PXRD	powder X-ray diffraction
SBU	secondary building unit

TBDMS-Cl	<i>tert</i> -butyldimethysilyl chloride
TEA	triethylamine
TIPS	triisopropylsilyl ether
ThDP	thiamine diphosphate
THF	tetrahydrofuran
TLC	thin layer chromatography

Chapter 1 Porous Materials and Macrocycles

1.1 Introduction

Materials that possess voids or pores within their structure are referred to as porous materials.¹ These materials are categorized based on the diameter of these voids. Materials containing pores that are larger than 50 nm are macroporous, those with pores in the 2–50 nm range are mesoporous, and those with pores smaller than 2 nm are microporous.² Of these, microporous materials have been the most explored in applications including catalysis, separation, filtration, and ion-exchange processes.^{3–5}

The field of porous materials initially focused on inorganic compounds, specifically zeolites. Zeolites are microporous aluminosilicate materials, formed by corner-sharing aluminum and silicon oxygen tetrahedra, that can be either naturally occurring or synthetically made. These materials have commonly been used for adsorption/separation,^{6,7} ion-exchange,^{8,9} and catalysis.^{10,11} As the interest in the field grew, focus began to include organic molecules in hybrid materials named metal-organic frameworks (MOFs).^{12–14} This field can be largely credited to Yaghi,¹⁵ Williams,¹⁶ and Kitagawa¹⁷ for their work in developing and popularizing this new class of materials. Yaghi's group was able to create a new class of permanently porous molecules with a measured surface area of $2,900 \text{ m}^2 \text{ g}^{-1}$ which is similar to that of activated carbon, $3,000 \text{ m}^2 \text{ g}^{-1}$.¹⁸ With the increased surface area, MOFs are being used in a variety of applications in catalysis, separation, gas storage, and molecular recognition.^{19,20} Purely organic compounds have been combined in a variety of ways which has led to the broad class of porous molecular crystals (PMCs).^{21–23} These materials are made up of discrete molecules held together by hydrogen bonds or other noncovalent interactions. The initial materials studied were shown to normally have their pores filled with disordered solvent, however, solvent removal

would result in pore collapse. Work was continued to develop materials that would remain permanently porous upon solvent removal. PMCs can be divided into two categories, intrinsic and extrinsic, depending on the type of pores present.²⁴ Intrinsically porous materials have pores contained within the building blocks, extrinsically porous materials form pores between building blocks, and a combination of both pore types is also possible. This chapter will introduce the three aforementioned types of well-established porous materials leading into the exploration and expansion of PMCs.

1.2 Porous Materials

1.2.1 Zeolites

Zeolites were the first explored porous materials, with naturally occurring zeolites chabazite and analcime showing the ability to separate straight-chained hydrocarbons from branched ones in 1944.²⁵ The first zeolites discovered were naturally occurring aluminosilicate three-dimensional microporous frameworks.²⁶ Crystalline materials show the tetrahedra of

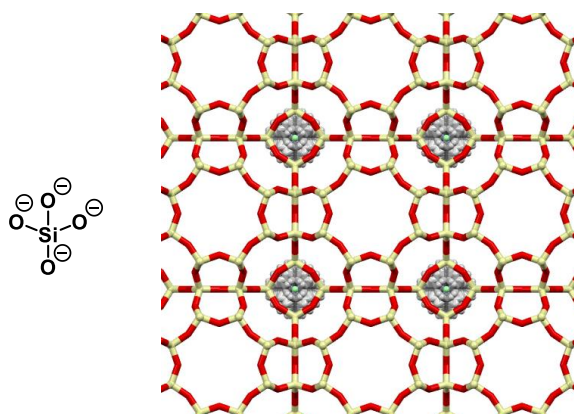


Figure 1.1 Common building block and resulting zeolite structure. Oxygens on silicon are shared with another silicon atom. Disordered molecules of tetramethylammonium fluoride can be observed. Element colors: Si—yellow, O—red, F—green, H—white.

$[\text{SiO}_4]^{4-}$ and $[\text{AlO}_4]^{5-}$ sharing corners to create channels and cages of molecular dimensions up to 10 Å (Figure 1.1). These large pores have led to the vast incorporation of zeolites into modern life in petroleum refining,²⁷ water treatment,^{28–30} gas adsorption,³¹ agriculture,³² production of animal feed additives,³³ and green chemistry.^{34,35} With increasing interest in this area, zeolite research has expanded to include synthetically made materials. While most zeolites are aluminosilicate materials, other common zeolite framework compositions include titanosilicates,³⁶ sodium tripolyphosphate, and trisodium phosphate.³⁷ Currently there are 234 different framework types recognized by the International Zeolite Association, with over 60 known to be naturally occurring.^{38,39}

The wide variety of applications of zeolites comes from the variety of porous structures present in each framework. Channels in these frameworks can be one-,⁴⁰ two-, or three-dimensional⁴¹ depending on the connectivity and the shape of building blocks.⁴² A large family of aluminophosphate-based materials were discovered in the 1980s, generating widespread interest in expanding zeolites to non-aluminosilicate-based materials.^{43–45} Stucky and coworkers have successfully synthesized a large family of germanate zeolite structures, that is materials made of germanates (GeO_4) and gallium (Ga).⁴⁶ These structures were of interest because of their metal–oxygen bond distances being longer than those of silicate materials and their ability of forming both even- and odd-membered rings, which created the opportunity to form new types of structures⁴⁷ and framework topologies. Utilizing these known parameters, eleven new materials were successfully synthesized. A germanium-based zeolite with both Ga and Ge (Figure 1.2) was the first germanium zeolite structure with five-membered rings, filled with piperazine solvent molecules, and the topology was not previously found in either natural or synthetic materials.⁴² The groundbreaking work developing porous zeolite materials has

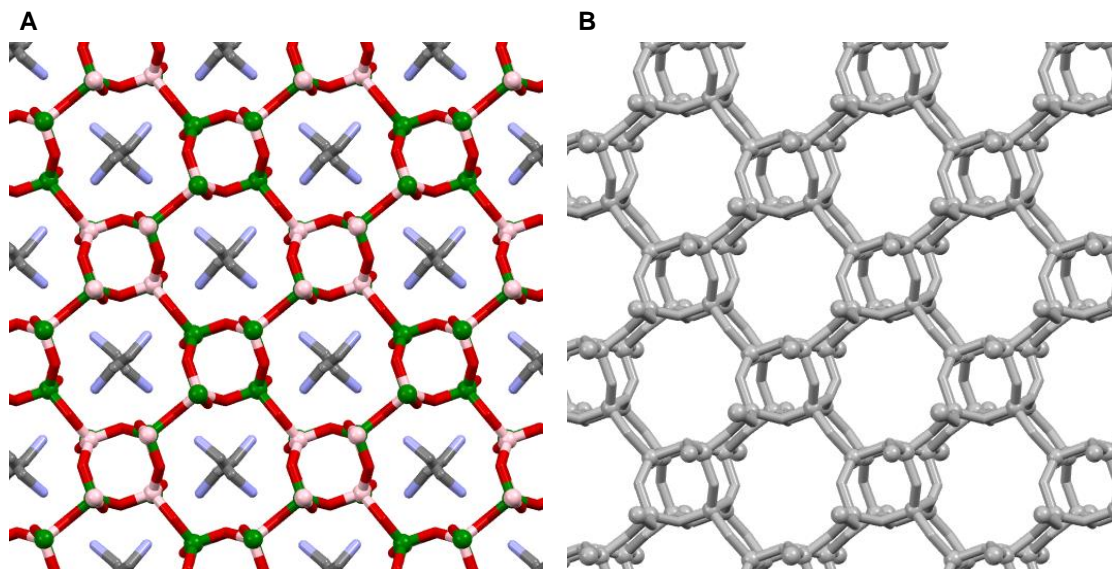


Figure 1.2 A) Crystallographic structure of Ga and Ge zeolite with disordered piperazine solvent molecules viewed along the crystallographic *a* axis. B) 1D channels formed with the two different sized macrocycles. Element colors: Ga—pink, Ge—green, O—red, N—blue, C—grey.

influenced all other types of porous materials that have since been invented. Despite the recent progress in zeolite science, continued growth in zeolite structures to incorporate new technologies or improve current applications remains very challenging.³⁷

1.2.2 Metal-Organic Frameworks (MOFs)

Combining inorganic and organic components resulted in the development of a new class of porous materials known as metal-organic frameworks (MOFs). MOFs consist of metal cluster nodes coordinated with an organic linker to form a framework. These frameworks can be either one-, two-, or three-dimensional which has led to the synthesis of a variety of structures. MOF frameworks are a class of coordination compounds, which is a class of compounds that has been understood since 1893 with Werner's explanation of coordination.⁴⁸ This coordination is utilized in the design of the secondary building units (SBUs) or metal

clusters used to form MOFs. Different SBUs can be classified by their points of extension (POE) which determines the number of connections able to be made to other clusters by organic linkers.⁴⁹ The minimum number of POE is three while the maximum reported is sixty-six⁵⁰. Commonly used SBUs include $\text{Cu}_2(-\text{COO})_4$, $\text{Zn}_4\text{O}(-\text{COO})_6$, and $\text{Fe}_3\text{O}(-\text{COO})_3$ which each create a POE of four, six, and six, respectively. While the last two create the same POE, their geometries are different which create different coordination geometries. SBU $\text{Cu}_2(-\text{COO})_4$ creates a square paddlewheel,^{51,52} $\text{Zn}_4\text{O}(-\text{COO})_6$ creates an octahedral,^{16,53} while $\text{Fe}_3\text{O}(-\text{COO})_3$ creates a trigonal prismatic cluster^{54,55} (Figure 1.3). Depending on which organic linkers are used, a variety of MOFs can be created from each SBU. While there are several carboxylate-decorated clusters reported,⁵⁶ only a few of them have been successfully utilized for MOFs.

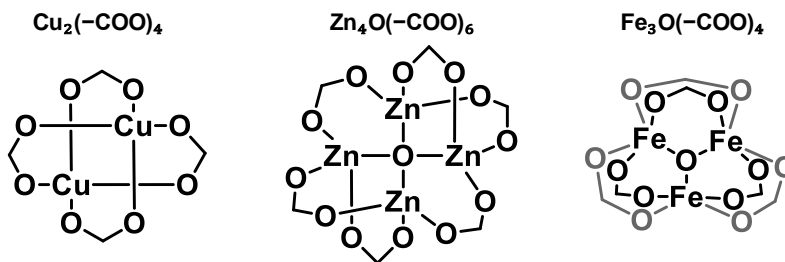
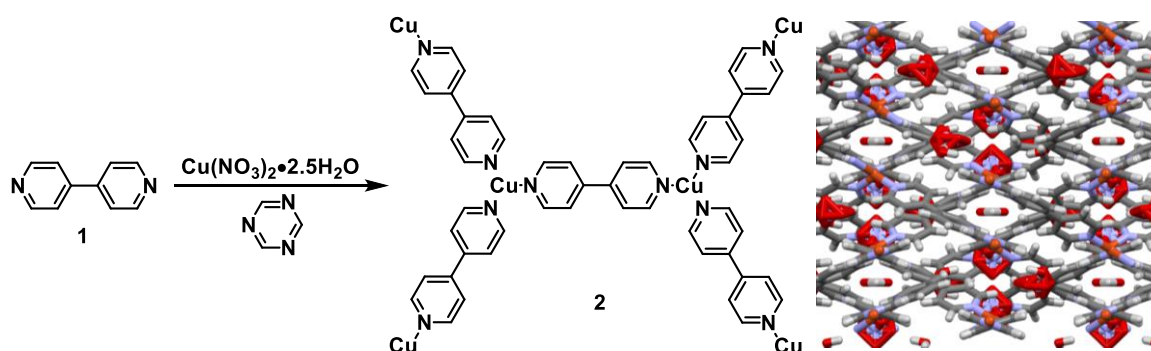


Figure 1.3 Common SBUs used in MOF development.

Combining SBUs with different metals and a mixture of organic linkers enables the synthesis of materials with greater complexity.⁵⁷

The building block approach has resulted in the initial development of metal-organic solids.⁵⁸ In 1995, this method proved successful in synthesizing an open framework with cavities or channels with simple ligands.⁵⁹ Utilizing Cu(I) dimers bridged by chloro ligands and linked to two 4,4'-bipyridine ligands forms a slightly distorted tetrahedron center. While this compound crystalizes with large pores, without the presence of large guest molecules to fill the pores sheets of the same structure are found to occupy the pores. The term MOF can be attributed to the work by Yaghi starting in 1995.¹⁵ His group showed that hydrothermal

synthesis is a viable method to develop zeolite-like materials. By combining $\text{Cu}(\text{NO}_3)_2 \cdot 2.5\text{H}_2\text{O}$, 4,4'-bipyridine (bpy) (**1**), 1,3,5-triazine, and water in a sealed stainless steel pressure vessel, placed in a programable furnace through a series of heating and cooling cycles they were able to produce crystals (Scheme 1.1). The crystals were found to be $\text{Cu}(4,4'\text{-bpy})_{1.5} \cdot \text{NO}_3(\text{H}_2\text{O})_{1.25}$ (**2**) that are stable in air and insoluble in water and common organic solvents. The unique trigonal planar geometry was the first example of an extended solid compound for a copper(I) center.



Scheme 1.1 Synthesis of an early MOF. Crystal structure viewed along the crystallographic *b* axis, showing water molecules located in the pore. Element colors: C—grey, O—red, N—blue, Cu—pink.

Structures that contain large voids are of interest for the ability to place guest molecules inside the voids or pores. A material's ability to fill these voids can be measured by gas sorption experiments. To measure this ability, a container of known volume is filled with a known amount of material, then sealed and evacuated. The container is slowly filled with a desired gas until a uniform pressure distribution is attained, allowing the ideal gas law to be used to calculate the pore volume. The calculated pore volume is the fraction of the total volume, or percent of the material that can interact with the gas molecules. This method assumes that the pores are empty so the gas molecules can interact with the material, which proved to be difficult with several MOF structures. Upon solvent removal, previously mentioned MOFs would lose stability and collapse. In 1998, Yaghi and coworkers were able to measure nitrogen adsorption

isotherms of $\text{Zn}(\text{BDC}) \cdot (\text{DMF})(\text{H}_2\text{O})\text{MOF}$ showing permanent porosity.⁶⁰ The MOF framework is composed of two zinc atoms bonded in a di-monodentate fashion with four 1,4-benzenedicarboxylate (BDC) units (**3**) (Figure 1.4A). Each zinc is also bonded to a terminal water molecule with disordered solvent molecules being dimethylformamide (DMF). The 2D

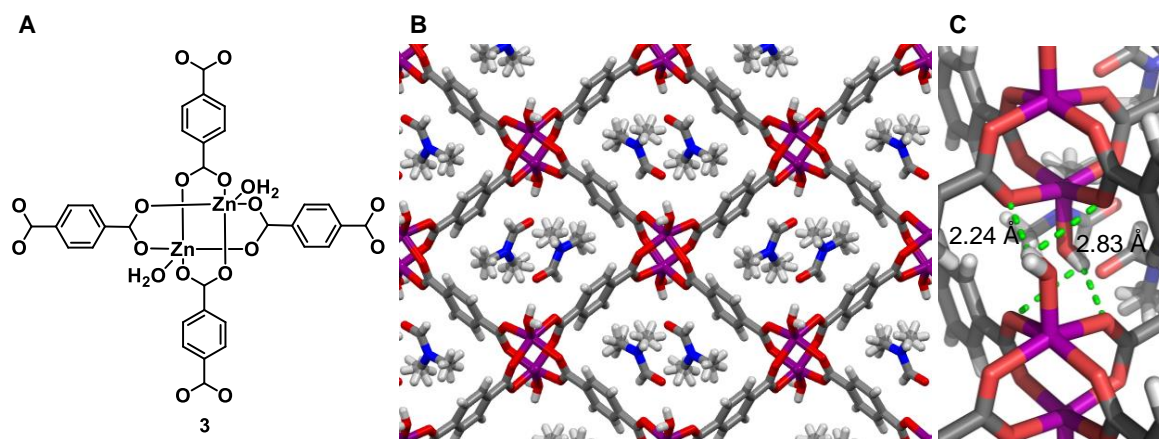


Figure 1.4 A) Chemical structure of the building block for $\text{Zn}(\text{BDC}) \cdot (\text{DMF})(\text{H}_2\text{O})$ MOF. B) Crystallographic structure of $\text{Zn}(\text{BDC}) \cdot (\text{DMF})(\text{H}_2\text{O})$ MOF with disordered solvent molecules in the pore, viewed along the crystallographic *a* axis. C) The hydrogen bonds formed to hold structure together. Element colors: C—grey, O—red, Zn—purple, N—blue, H—white.

layers are held together by two hydrogen bonds (2.23 and 2.83 Å Figure 1.4C), between water ligands and carboxylate oxygens of adjacent layers. Gas sorption was tested using N_2 and CO_2 , which showed an initial rapid uptake of both gasses. Both gas uptake graphs displayed a type I isotherm, typical of microporous materials, and had a Langmuir surface area between 270 and 310 $\text{m}^2 \text{g}^{-1}$ for N_2 and CO_2 , respectively.⁶⁰ The development of this MOF with permanent porosity acted as a springboard for the development of these materials. Synthetic pathways now include electrochemistry,^{61,62} microwave radiation,^{63,64} sonication,^{65,66} and mechanochemistry.^{67,68} With the growing variety of MOFs being produced, their applications have increased to include gas storage and separation,⁶⁹ sensing,⁷⁰ catalysis,⁷¹ drug delivery,⁷²

and energy storage.⁷³ The area of MOF chemistry continues to evolve and expand, with the potential to have practical applications.

1.2.3 Porous Molecular Crystals (PMCs)

Porous molecular crystals (PMCs)^{22,23,74–80} are a unique subset of porous materials as they are composed of discrete molecules and not polymeric in nature. Molecules tend to pack efficiently in the solid state due to entropic reasons and to maximize attractive intermolecular contact, making these types of materials rare. These discrete molecules are held together by non-covalent interactions, unlike the previously mentioned materials which have covalent bonds holding the materials together. Since PMCs are composed of discrete molecules, porosity can either be extrinsic or intrinsic, that is voids are formed between at least two molecules or within the molecule itself, respectively.²³ Intrinsically porous PMCs have most commonly been constructed from three-dimensional cages and macrocycles.^{18,21,81–88} Extrinsically porous PMCs are formed from small molecules that pack inefficiently leaving empty voids. Combinations of these two void types are possible as well.

Many PMCs show porosity in the solvated phase, where the voids are filled with disordered solvent or guest molecules. In most cases, once the solvent molecules are removed these voids collapse. This is most likely due to the removal of stabilizing interactions between the solvent and PMC, resulting in a less stable structure. Solvent removal produces three pathways for both intrinsic and extrinsic materials (Figure 1.5 and Figure 1.6);⁸⁹ resulting in an amorphous material (pathway A), denser packing (pathway B) or the desired result of a permanently porous crystal (pathway C). Structures with voids that result in a permanently

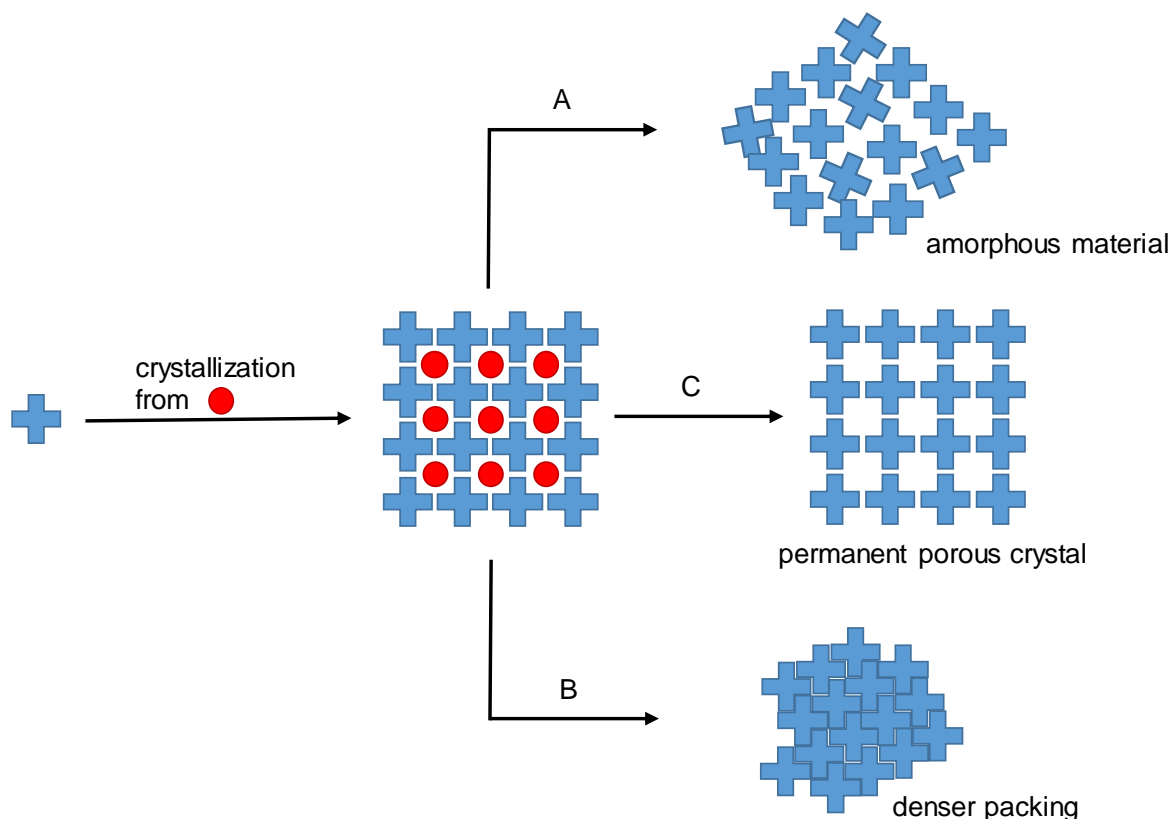
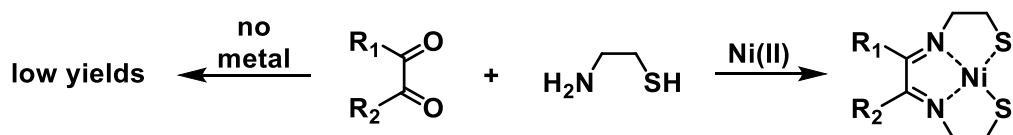


Figure 1.5 Generation of porous materials and the possible pathways upon guest removal for extrinsically porous materials.

porous crystal have been highly sought after, as they lend themselves to a variety of applications in energy^{90,91} and environment.^{92,93} One of the first examples was Dianin's compound reported in 1914 (Scheme 1.2).⁹⁴ Despite the appearance of porosity within the crystal structure, it is capable of sorbing a wide variety of gases.⁹⁵ This phenomenon can be explained through



Scheme 1.2 Dianin's synthesis of Schiff bases showing the effectiveness of templating a desired product from an equilibrium mixture.

dynamic van der Waals cooperativity, which allows for guest transport through the crystal.⁹⁶

Several years later, Atwood and coworkers demonstrated the same phenomenon in calixarenes

which contain voids that are not interconnected,⁹⁷ which led to the term “porosity without pores”.⁹⁸

Intrinsic and extrinsically porous materials are most commonly composed of caged compounds. With a rigid structure built into the starting materials, these materials tend to retain more porosity upon solvent removal. While some of the overall porosity may be lost to a more densely packed structure (Figure 1.6, pathway B), the central cavity can often still be accessed.

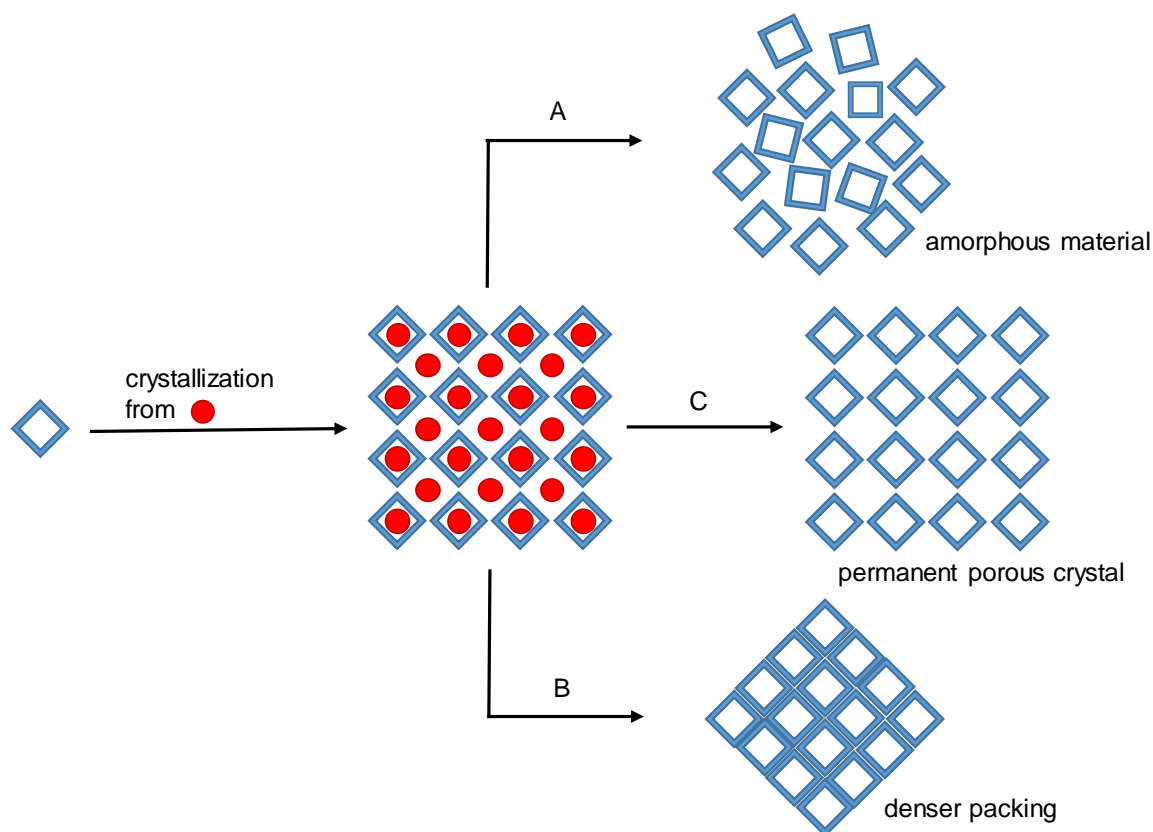
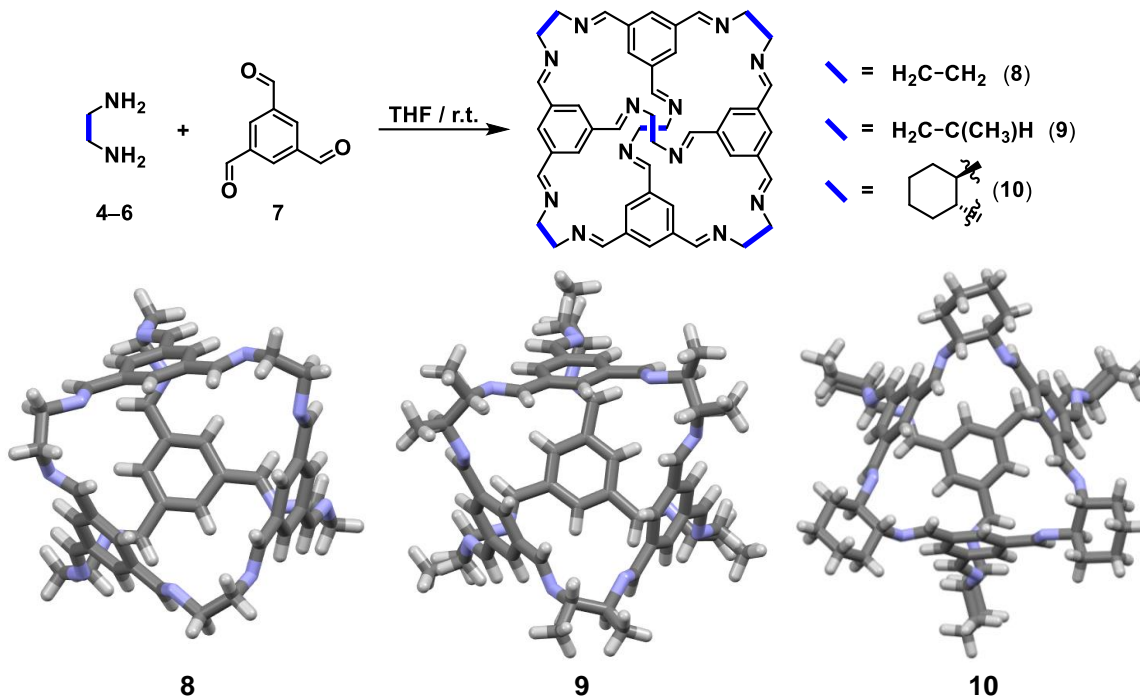


Figure 1.6 Generation of porous materials and the possible pathways upon guest removal for intrinsically porous materials.

A porous organic cage molecule was synthesized in 2009 by Cooper and coworkers.⁹⁹ They were able to synthesize three tetrahedral cages utilizing imine condensation of 1,3,5-triformylbenzene (**7**) with 1,2-ethylenediamine (**4**), 1,2-propylenediamine (**5**), and (*R,R*)-1,2-diaminocyclohexane (**6**) (Scheme 1.3). All three resulting cages—**8**, **9**, and **10**—have four



Scheme 1.3 Synthetic route to imine cages **8**, **9**, and **10**. Crystallographic images of synthesized cages. Element colors: C—grey, N—blue, H—white.

approximately triangular faces with diameters of 5.8, 6.1, and 5.8 Å respectively, measured from the center of the triangular face to the three arene hydrogens. The difference in the three cages is the steric group that is attached to the six vertices. These groups, as expected, drastically impact how the cages pack in the solid state. Cage **8** packs face-to-edge resulting in efficient packing, producing a material that only has the intrinsic pore. Cage **9** packs in a similar manner but has slightly more space which creates a channel between the cages along with the intrinsic pore. Cage **10** packs altogether differently in that the cages pack face-to-face, creating a continuous channel that goes through the interlocking faces. All three cages can absorb gases in the desolvated state, however cage **8** does not show N_2 uptake like cages **9** and **10**. Cage **8** does show CH_4 and CO_2 uptake indicating it is porous, while cages **9** and **10** show type I isotherms with N_2 , suggesting Brunauer-Emmett-Teller (BET) surface areas of $533 \text{ m}^2 \text{ g}^{-1}$ and $624 \text{ m}^2 \text{ g}^{-1}$, respectively.

Another application for which intrinsically porous molecular crystals have been utilized is facilitating reactions. One example has been accomplished by Martinez and coworkers to show that cages can be used in the oxidation of methane.¹⁰⁰ This issue has been sought after to improve the current industrial standards of needing high temperatures resulting in low selectivity.¹⁰¹ Selective oxidation of aliphatic C–H bonds has been achieved by supramolecular catalysts when hydrogen bonding,⁴⁸ ligand to metal coordination,¹⁰² hydrophobic effects,¹⁰³ or hydrophobic cavity for the catalytic center⁹⁰ have been utilized to facilitate substrate interactions. Of these, creating a hydrophobic cavity with Cu(II)-⁹¹ and V(V)- based

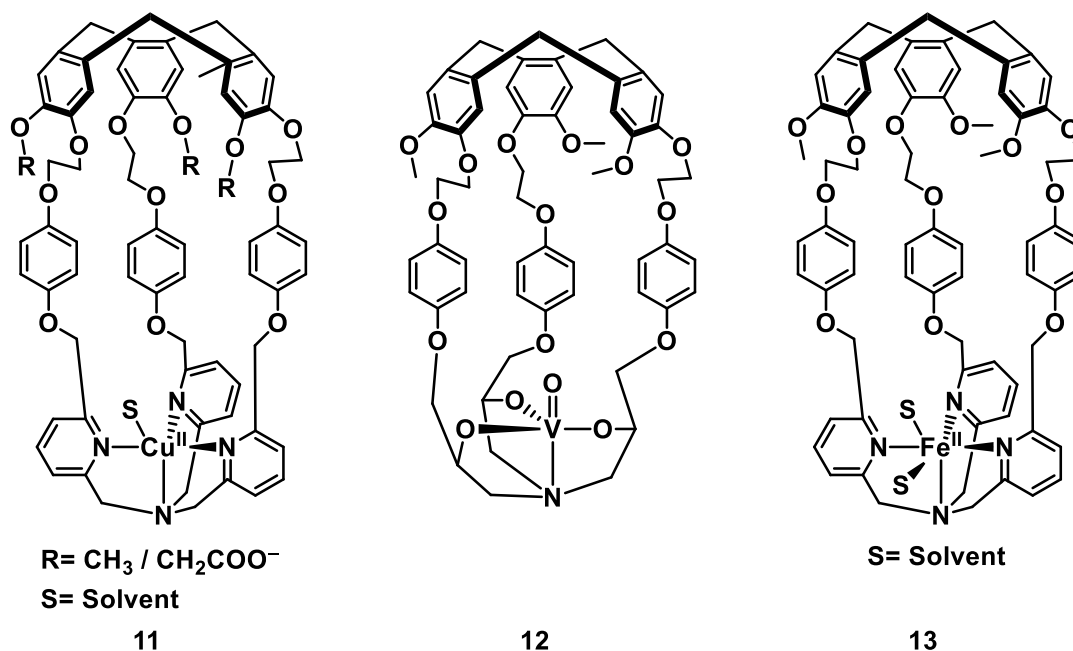
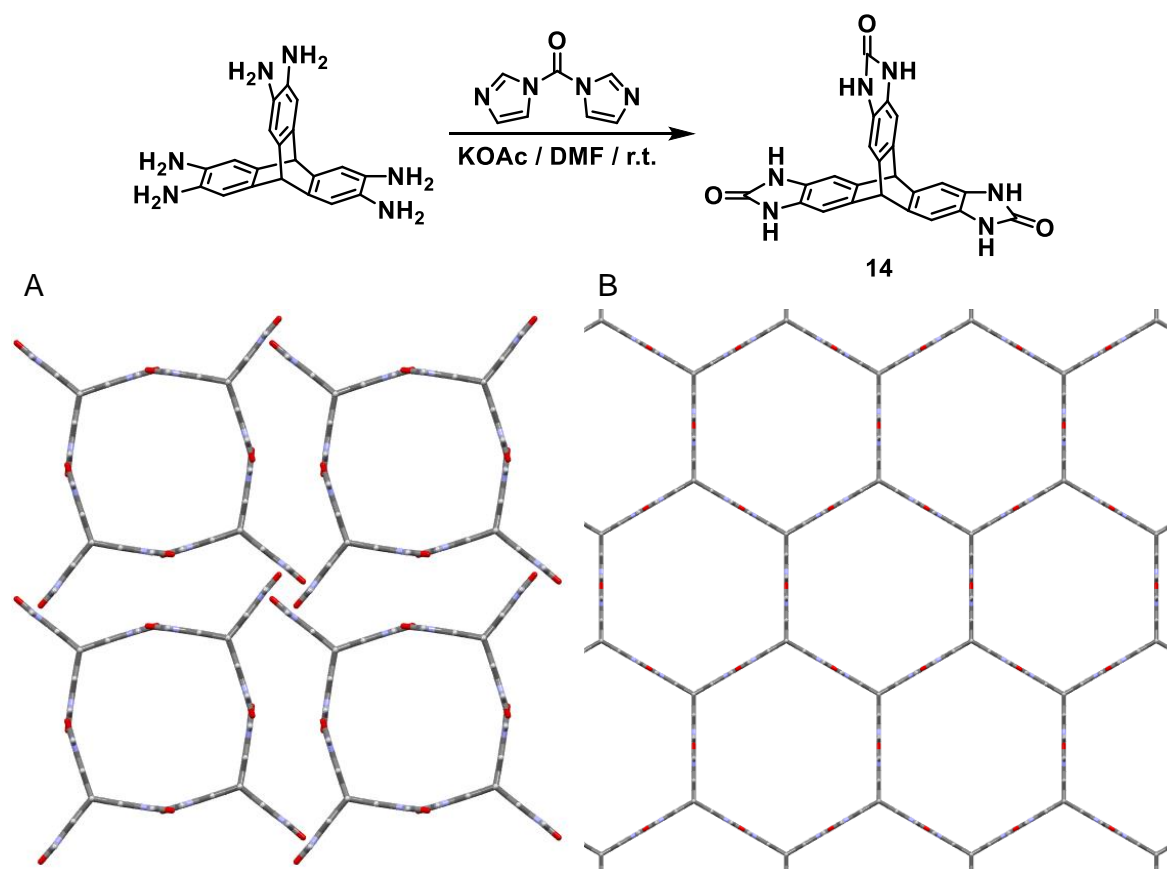


Figure 1.7 Chemical structures of hemicryptophanes.

hemicryptophanes⁹² have been the most successful (**11** and **12** in Figure 1.7). Expanding on this finding, Martinez and coworkers were able to show an Fe (**13**) center in a hemicryptophane hydrophobic cavity has the best selectivity for primary oxidation of methane to methanol.

Extrinsically porous materials were synthesized before^{95,104} intrinsically porous materials. Most early extrinsically porous materials show low BET surface areas, less than 500 m² g⁻¹,^{98,105} resulting from the increased density in packing upon solvent removal which results in a loss of accessible surface. In 2012, Mastalerz and coworkers synthesized triptycene trisbenzimidazolone (**14**)¹⁰⁶ with the goal to achieve an extrinsically porous material (Scheme 1.4). This molecule was a good candidate as benzimidazolones are known for forming ribbon like structures¹⁰⁷ and incorporating a triptycene subunit could facilitate a trigonal orientation of



Scheme 1.4 Synthetic route for **14**. Crystal structure showing large extrinsic pores that form in the solid state. Element colors: C—grey, O—red, N—blue.

the hydrogen bond donors to form an extended porous framework. Mastalerz first reported the crystal packing shown in Scheme 1.4A which resulted in a BET surface area of 2796 m² g⁻¹, however, by changing crystallization conditions Cooper, Day and coworkers reported a second

packing method shown in Scheme 1.4B which increased the BET surface area to $3425 \text{ m}^2 \text{ g}^{-1}$,¹⁰⁸ which is one of the highest reported surface areas for PMCs. The building blocks of **14** were able to arrange into large hexagonal pores enabling an increase in the measured porosity. Another family of extrinsically porous materials with a high BET surface area are phthalocyanine unsolvated nanoporous crystals (PUNC) synthesized by McKeown and coworkers.¹⁰⁹ The bulky groups surrounding the central metal prevents the molecules from packing tightly, creating two different foci within the crystal lattice. This inability to densely pack resulted in a BET surface area of $1002 \text{ m}^2 \text{ g}^{-1}$.¹⁰⁹

Fluorinated organic compounds have been successfully synthesized and used in the development of PMCs as well. In 2015, the Miljanić group was working to prepare a MOF based on fluorinated trispyrazole ligand, but upon X-ray analysis they found they had instead crystallized a PMC.^{110,111} The pyrazole precursor (**15**) creates a combination of $[\text{N}-\text{H}\cdots\text{N}]$ hydrogen bonds between terminal pyrazoles and aromatic $[\pi\cdots\pi]$ stacking interactions. The trigonal shape and the non-covalent interactions resulted in a robust framework that showed large hexagonal pores with a surface area of $1159 \text{ m}^2 \text{ g}^{-1}$ (Figure 1.8).¹¹² This material has been proven to be an effective adsorbent for hydrocarbons, chlorofluorocarbons, fluorocarbons, and fluorinated anesthetics.¹¹³ Derivatives of **15** were studied and found that geometry and fluorinated benzene rings played a significant role in establishing a porous framework. Replacing the central benzene ring with a triazine ring yielded a porous material with the same crystal packing (Figure 1.8). Both materials show similar properties, however, with the removal of the central hydrogens on **16** the rotation of the tetrafluorobenzenes around the C–C bond becomes easier which impacts emissive properties. When dissolved in DMF, **15** remains

emissive while **16** does not become emissive until water is added to the solution turning the emission back on by aggregation-induced emission (AIE).¹¹⁴

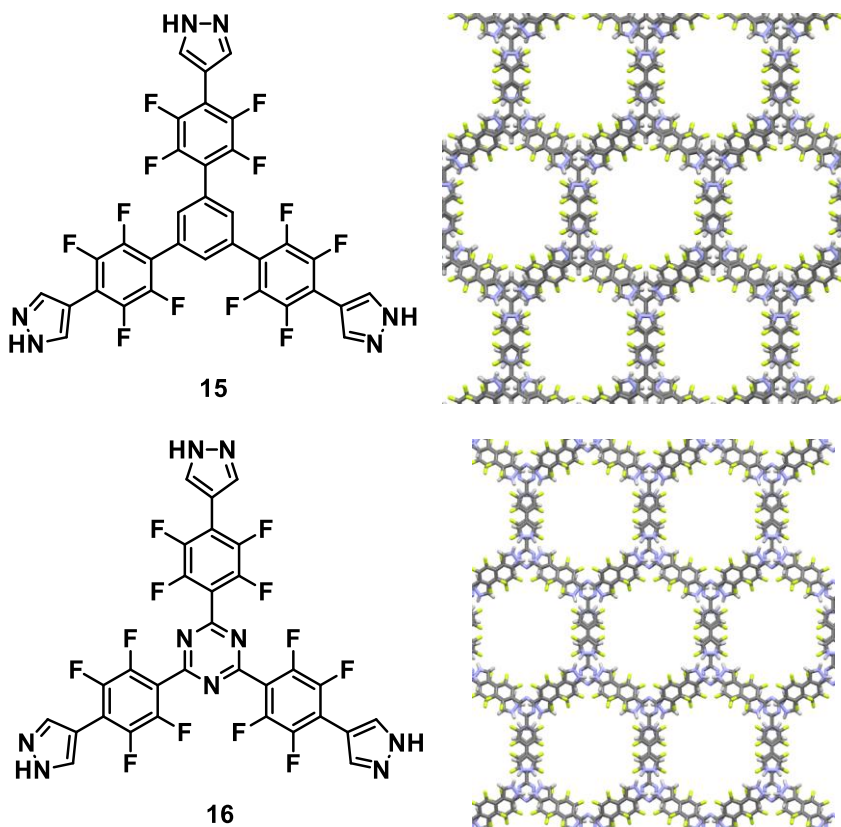


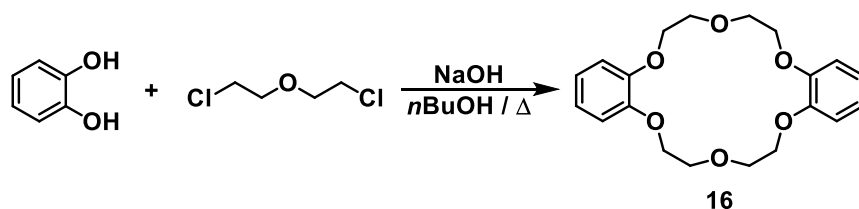
Figure 1.8 Fluorinated PMCs with hexagonal pores. Element colors: C—grey, N—blue, F—green, H—white.

Porous molecular crystals encompass a myriad of different compounds with different geometries making the applications of these materials just as varied. The limitations to these materials will remain to be the unpredictability of forming stable frameworks by noncovalent interactions. As calculations and additional understanding of molecular tendencies continue to be explored, the predictability of forming these frameworks could be more reliable. While most PMCs have been studied with cage molecules or small organic molecules, macrocycles have been less successful in forming PMCs. Macrocycles, like cages, already contain a central void which could enable them to be good building blocks for PMCs.

1.3 Macrocycle Synthesis Development

1.3.1 Brief History

Macrocycles are defined as molecules containing twelve or more atoms connected in a cyclic framework. This area of chemistry contains both naturally occurring compounds such as cyclodextrins^{115,116} and porphyrins,¹¹⁷ and synthetic compounds such as crown ethers,¹¹⁸ pillarenes,¹¹⁹ cyclophanes,¹²⁰ and cucurbiturils.¹²¹ These types of molecules are of interest since they contain voids in the middle of the molecule, which endows them with an ability to interact with other molecules. Cyclodextrins were first described by Villiers in 1891¹²² and called cellulosine. The three naturally occurring cyclodextrins were discovered by Schardinger in the 1930s¹²² which are isolated by enzymatic treatment of starch molecules found in corn.¹²³ These have also been found useful in drug delivery¹²⁴ and household cleaners.¹²⁵ The active ingredient in Febreze is β -cyclodextrin, which contains seven glucose molecules bonded through α -1,4 glycosidic bonds, and it works by interacting with small volatile odor molecules with the central void. When this happens, the small molecule is no longer volatile and cannot be detected by the human nose, therefore eliminating odors.¹²⁶ In the late 1960s, Charles Pedersen reported the synthesis of crown ethers (Scheme 1.5), with the first reported crown ether being

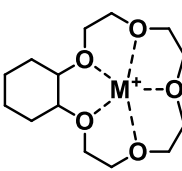


Scheme 1.5 Synthesis of a crown ether.

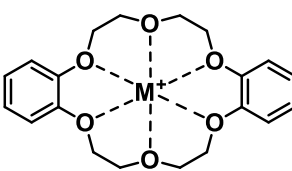
dibenzo[18]crown-6 (**16**), where 18 represented the total number of atoms in the ring and 6 represents the number of oxygens. During the synthetic process, it was found that crown ethers had the ability to complex with metal cations. This was tested by extraction with equal volume

of a 7×10^{-5} M aqueous solution of alkali metal salt (picrate) and 7×10^{-5} M solution of the desired crown ether in dichloromethane.¹²⁷ Different sized crown ethers and metal cations were tested, the percentage of picrate extracted from solution is reported in Table 1.1. These findings also indicated that size influences how effectively a crown ether can remove a specific cation. This discovery had a large impact on the emergence of host–guest chemistry with pioneering work done by Donald Cram¹²⁸ and the broader field of supramolecular chemistry and its development by Jean-Marie Lehn.¹²⁹

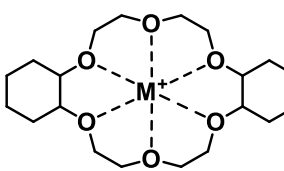
Table 1.1 Metal coordination of various crown ethers measured by the percentage of picrate extracted from solution



17



18

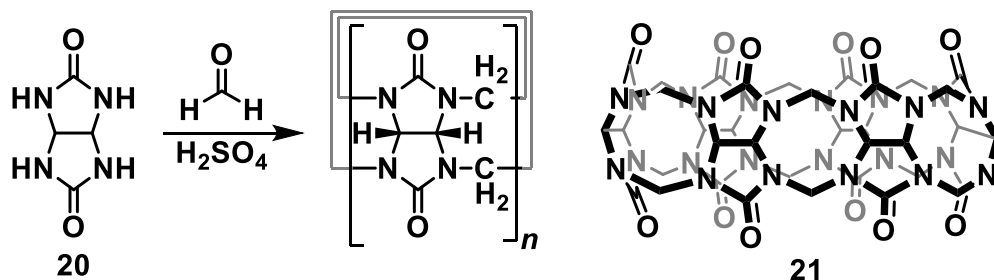


19

	Na ⁺ (%)	K ⁺ (%)	Cs ⁺ (%)
17	19.7	8.7	4.0
18	1.6	25.2	5.8
19	25.6	77.8	44.2

From the work done by Pedersen, Lehn was able to expand from the 2D encapsulation shown by crown ethers to 3D encapsulation with a new class of molecules called cryptands.^{129–133} While crown ethers encapsulate alkali and ammonium salts, the added degree of preorganization enables cryptands to have higher binding constants and encapsulate alkali and alkaline earth metal cations as well as lanthanides and ammonium ions.¹³⁴ The first, and most common, cryptand reported was called [2.2.2]cryptand, where the numbers inside the brackets indicated the number of ether oxygen atoms between the nitrogen atoms. The [2.2.2]cryptand exhibited a 10^4 times stronger binding of K⁺ in MeOH than the crown ether analog of 18-crown-6, due to the preorganization of binding sites.

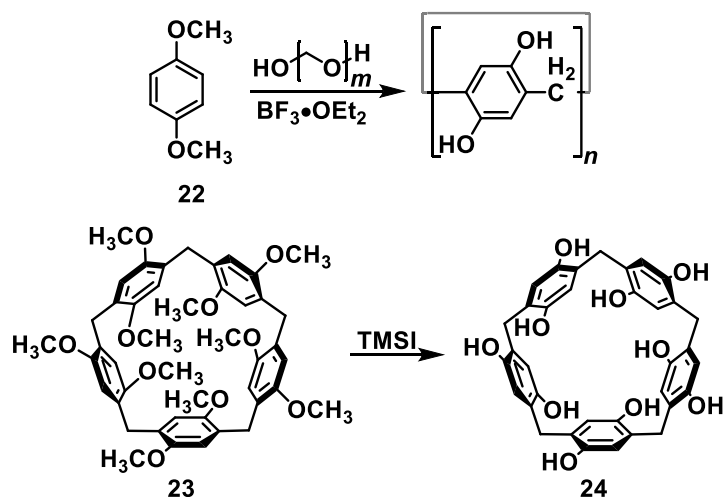
Originally discovered in 1905 by Behrend and coworkers,¹³⁵ cucurbiturils were formed by the condensation of glycoluril (**20**) and formaldehyde under acidic conditions (Scheme 1.6).



Scheme 1.6 General route for synthesis of cucurbiturils with the chemical structure of the first known macrocycle of this class **21**.

However, the molecular structure was not revealed until 1981 by Mock and coworkers¹³⁶ when they repeated the experiment. This macrocycle consists of six glycoluril units linked by twelve methylene bridges resulting in cucurbit[6]uril (CB[6]) (**21**). Upon this discovery, several groups explored the reaction to produce other derivatives of CB[6]. This has been successful in expanding the family of cucurbiturils to CB[5], CB[7], and CB[8] by Kim and coworkers,¹³⁷ CB[5] entrapped by CB[10] by Day and coworkers,^{138,139} and CB[14] by Tao and coworkers.¹⁴⁰ The expansion of this class has created a catalog of macrocycles with the ability to encapsulate different molecules. The hydrophilic carbonylated rims and typically hydrophobic cavity enable cucurbiturils to interact with organic species and inorganic ions through a combination of dipole-ion interaction, hydrogen bonding, and hydrophobic cavity interactions. With a large variety of possible macrocycles several applications have been found in water treatment, catalysis, drug delivery, stimuli-responsive systems, and artificial molecular machines.^{141–143}

A relatively new class of synthetic macrocycles, pillar[*n*]arenes have become a focus since they can provide different sizes of electron-rich cavities to interact with electron-deficient species. This class of macrocycles were initially introduced in 2008 by Ogoshi and coworkers¹⁴⁴ with the synthesis of pillar[5]arene (**24**) from the reaction of 1,4-dimethoxybenzene (**22**) with paraformaldehyde to form 1,4-dimethoxypillar[5]arene (**23**), followed by the reduction of the methoxy groups (Scheme 1.7). The terminal hydroxyl groups enable a variety of possible



Scheme 1.7 General route to pillararenes with the chemical structure of the first pillararene **24**.

functionalization to provide various derivatives and a wide range of applications in supramolecular chemistry,^{145–147} materials science,^{148,149} and biology.^{150–152} Common strategies for functionalization include deprotection,¹⁵³ cocyclisation,¹⁵⁴ peroxidation and reduction,¹⁵⁵ simultaneous deprotection and cyclisation,¹⁵⁶ deprotection-followed-by-activation,¹⁵⁷ and phenylene substitution.¹⁵⁸ The development in new classes of macrocycles has led to the expansion of different areas of chemistry, host-guest and supramolecular chemistry, which has increased the variety of applications found and continued to be explored.

1.3.2 Dynamic Combinatorial Chemistry

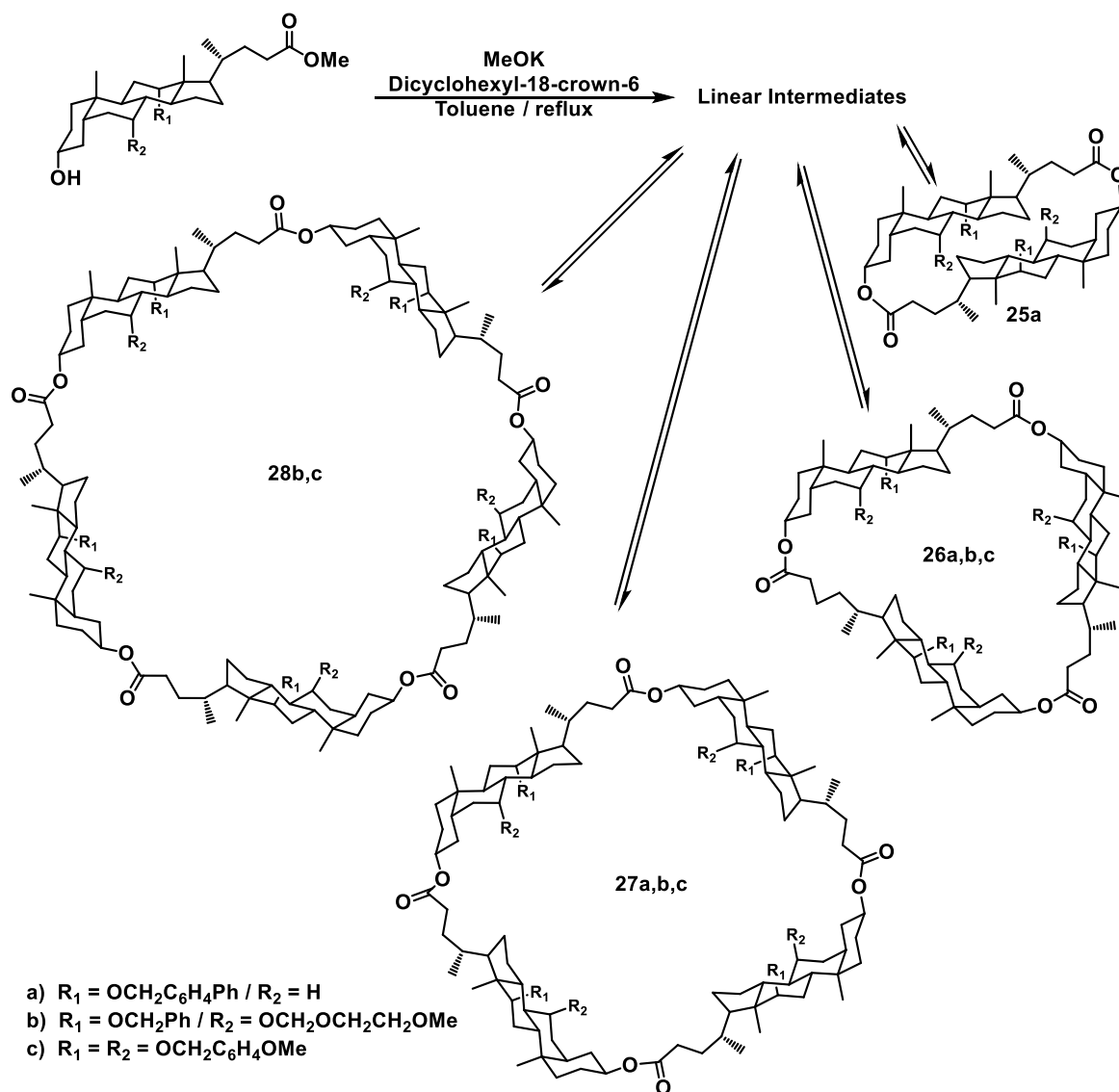
Dynamic combinatorial chemistry (DCC) utilizes a thermodynamic equilibrium, where all species can interconvert into each other, as a method to generate a library of products.^{159–163} The library of products establishes an equilibrium determined by the thermodynamic stability of individual products. The interconversion between products could be through coordinative, covalent bonds, or noncovalent interactions.¹⁶⁴ Under DCC conditions the most thermodynamically stable product, and relative stability of other reaction products, can be determined to better understand chemical reactions. A thermodynamically controlled reaction would also suggest that external stimuli such as, temperature, pressure, solvent, and light would influence the outcome of the equilibrium. Several templating reactions have been successful utilizing DCC properties to amplify the compound that is most stabilized through noncovalent interactions with either the template, itself, or other reaction compounds.¹⁶⁵

While templating synthesis had been seen before, the work by Busch in the 1960s led to a better understanding of templating in macrocycle synthesis.¹⁶⁶ The synthesis of Schiff bases from α -diketones and β -mercaptoethylamines typically yield thiazolines as the major product, however with the inclusion of Ni^{2+} yields of the desired base are found to be greater than 70%. This led to the expansion of templating reactions in transesterification,¹⁶⁷ transallylesterification,¹⁶⁸ transamination,¹⁶⁹ aldol exchange,¹⁷⁰ transthioesterification,¹⁷¹ Michael/retro-Michael reactions,¹⁷² acetal exchange,¹⁷³ thioacetal exchange,¹⁷⁴ pyrazolotriazon metathesis,¹⁷⁵ transimination,¹⁷⁶ hydrazone exchange,¹⁷⁷ oxime exchange,¹⁷⁸ alkene metathesis,¹⁷⁹ alkyne metathesis,¹⁸⁰ disulfide exchange,¹⁸¹ Diels-Alder/retro-Diels-Alder reactions,¹⁸² metal-ligand exchange,¹⁸³ and hydrogen-bond exchange.¹⁸⁴ In order for these reactions to undergo DCC, the reversible reaction needs to meet several requirements: (a)

reversibility needs to be accomplished on a reasonable time scale; (b) reversible reaction needs to be compatible with experimental conditions; (c) reaction conditions need to not interfere with noncovalent interactions; (d) all components need to be soluble; (e) reactions should be able to be stopped under kinetic control to isolate and analyze all components; and lastly (f) all reaction components should be close to isoenergetic to reduce the likelihood of forming mixtures that are heavily biased towards certain products. Of the aforementioned requirements, the last one is the hardest to achieve in macrocyclic reactions because of entropic penalty of cyclization, however several reactions have been successful in producing macrocycles utilizing these requirements.

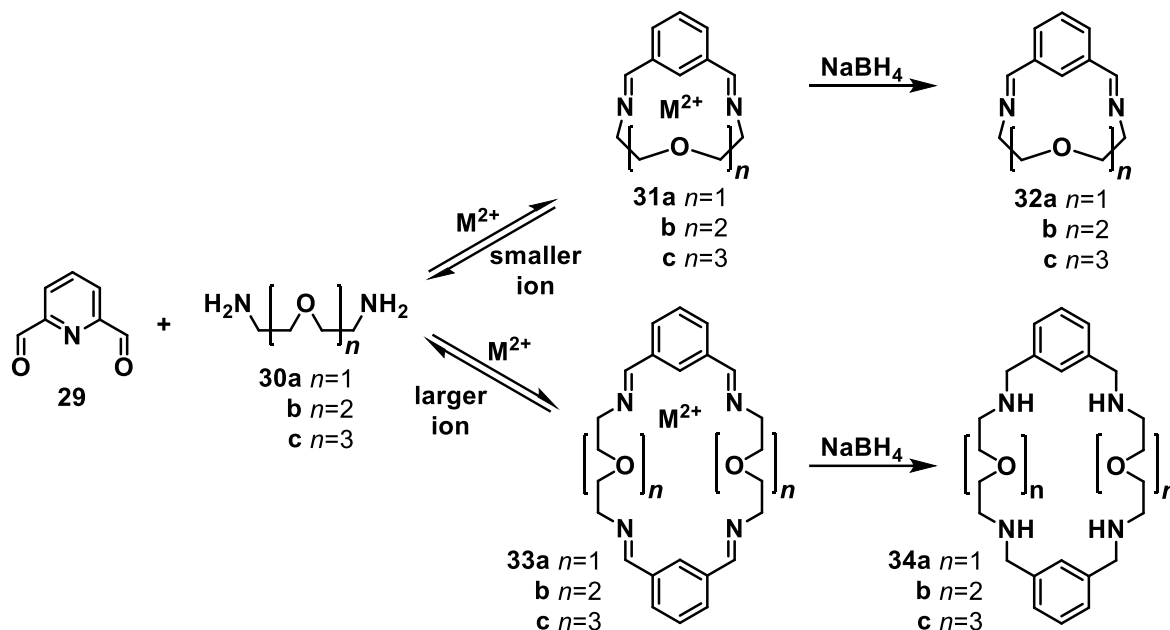
The first macrocycles generated using DCC were prepared via transesterification. Initial reactions used building blocks with methyl ester and hydroxyl functional groups. The focus was placed on using cyclocholates with different substituents on the two central rings.¹⁸⁵ To compare thermodynamic and kinetic conditions, cyclic oligomers **25–28** were synthesized under kinetic control as well.¹⁸⁶ For thermodynamically controlled conditions, the most successful transesterification catalyst was found to be 5 mol% of the complex of potassium methoxide and dicyclohexyl-18-crown-6, which was added to a dissolved solution of cholate in refluxing toluene with 4 Å molecular sieves in a Soxhlet extractor (Scheme 1.8). The product distribution was dependent on the R₁ and R₂ substituent groups. Cyclic dimer **25a** was present only when R₂ was a hydrogen, however all other substituents showed a preference for trimer formation. To show the reaction is under thermodynamic control, pure cyclic oligomers were treated as starting materials and the same ratio of products was obtained. Regardless of whether

starting materials were linear or cyclic, the same ratio of macrocyclic products was observed indicating the true reversibility and thermodynamic control of this reaction.



Scheme 1.8 Synthesis of first class of macrocycles utilizing DCC control.

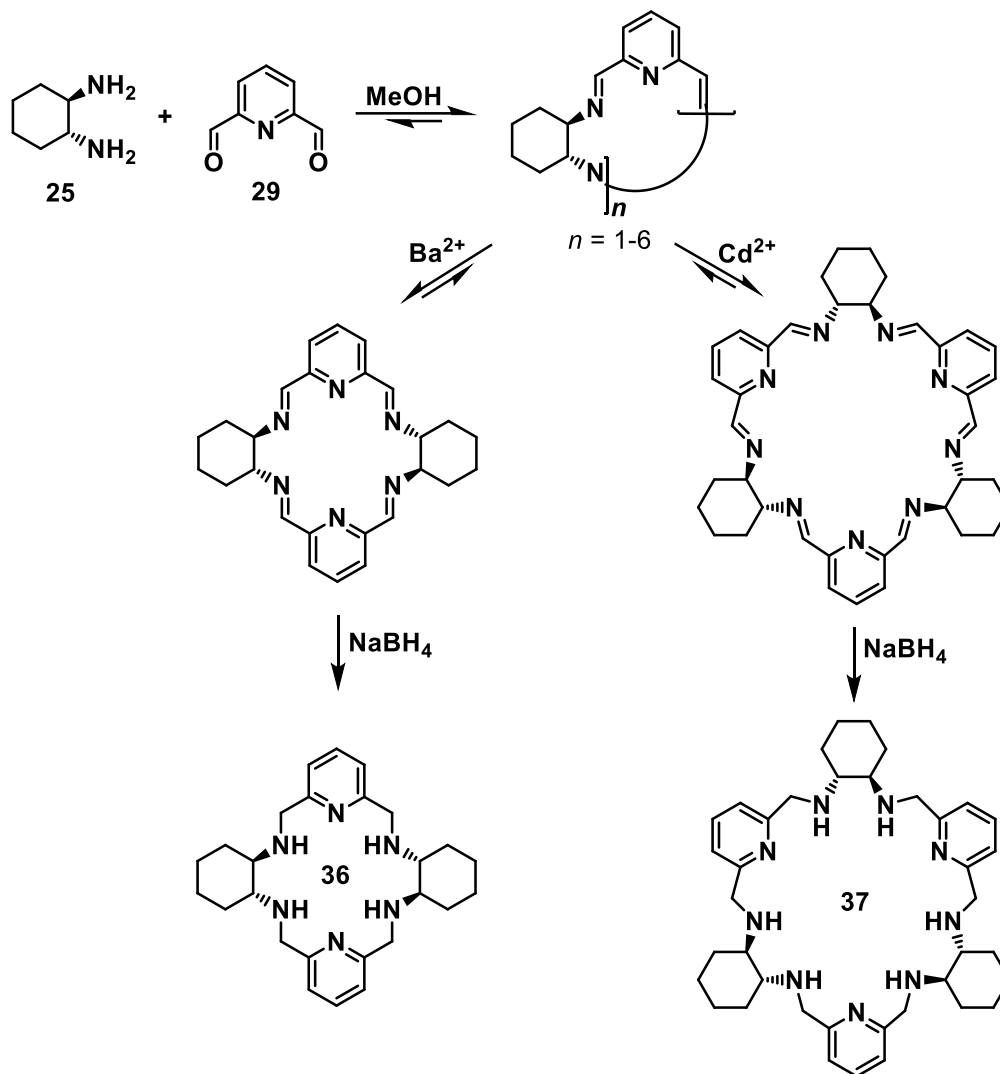
Imine exchange has been used to create a variety of macrocycle receptors for metal-ion templates by Storm and Lüning.^{187,188} By mixing pyridine-1,2-dicarboxaldehyde (**29**) with diamines of varying chain lengths, an assortment of macrocycles was obtained depending on which metal cations were in solution (Scheme 1.9). Reactions were analyzed by reducing the imines to amines first. This step stops the equilibration, locking the ratio of products, also in



Scheme 1.9 Synthesis of templated imine macrocycles.

the amine form the macrocycles no longer coordinate to the metals present. When the reaction was run without templating metals, the only macrocycle found was **31b** in 9% yield. When Mg^{2+} was added into the reaction of **29** and **30a**, upon reduction **32a** was isolated at 86% yield. When larger cations like Ca^{2+} and Sr^{2+} were used, a different macrocycle, **34a**, was detected which was not observed with Mg^{2+} . The length of the diamine and the number of repeating units that a macrocycle will be composed of is determined by the size of the cation present in the reaction.

The reversibility of the imine bond was also highlighted by Gotor and co-workers in their macrocyclic reactions.¹⁸⁹ They used (*R,R*)-cyclohexane-1,2-diamine (**35**) and pyridine-1,2-dicarboxaldehyde (**29**) to create macrocycles of two and six units of each (Scheme 1.10). Again, to analyze the reaction mixture, macrocycles were reduced to remove the metal cation from its coordination environment. When the reaction was run with Ba^{2+} the [2+2] macrocycle



Scheme 1.10 Synthesis of templated imine macrocycles.

(36) was exclusively formed, while the addition of Cd²⁺ resulted in the [3+3] macrocycle (37).

The interconversion was tested by running the reaction initially with Ba²⁺ present, once the reaction had reached equilibrium an excess of Cd²⁺ was added. Upon reduction, only 37 was observed. Expanding the understanding of this templating, Gotor looked at what would happen if a mixture of (*R,R*) and (*S,S*)-*trans*-cyclohexane-1,2-diamine were used.¹⁹⁰ When the reaction was run in the absence of a template, mostly dimer was detected with the trimer as a minor product. Assuming the same pattern is observed as before, Ba²⁺ should yield dimer macrocycles.

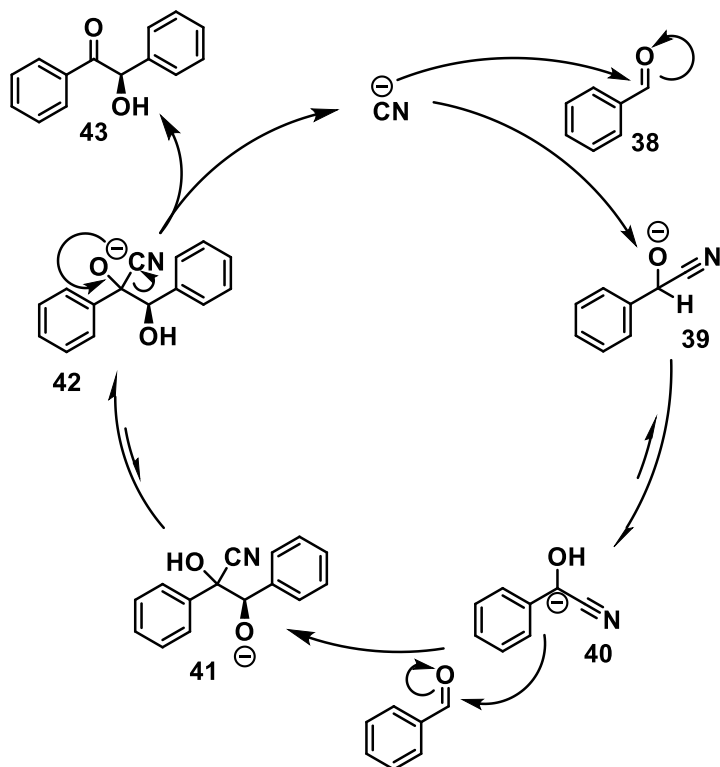
When Ba²⁺ was used as the template, nuclear magnetic resonance (NMR) indicated that two

products were formed, a dimer with two possible diastereomers. Comparing these results when Cd^{2+} was used as a template, NMR and high-pressure liquid chromatography (HPLC) results confirmed that only one diastereoisomer of the trimer was formed. This observation indicates that Cd^{2+} amplification is completely diastereoselective as only one diastereoisomer of the trimer was formed.

1.4 Benzoin Condensation

1.4.1 Reaction Discovery and Development

Chemical reactions that form new C–C bonds are important reactions to build new compounds. The benzoin condensation, discovered by Wöhler and Liebig in 1832 during their work with bitter almond oil, forms a new C–C bond between two aromatic aldehydes.¹⁹¹ The original reaction conditions were developed by Zinin, who utilized a cyanide ion as a catalyst.¹⁹² Several years later, in 1904, Lapworth proposed a mechanism which is shown in Scheme 1.11.¹⁹³ First, nucleophilic attack of the cyanide anion to the benzaldehyde (**38**) results in a cyanohydrin anion (**39**). Proton transfer results in a carbanionic intermediate (**40**), which acts as an electrophile and attacks a second benzaldehyde forming a new C–C bond (**41**). A second proton transfer results in intermediate **42** which enables the ability to expel the cyanide ion and provide the desired benzoin product (**43**). While no small molecule is lost in this mechanism, the name condensation has remained for historical purposes. Through this reaction a single stereocenter is formed, however the achiral cyanide catalyst has no enantiocontrol. Cyanide



Scheme 1.11 Lapworth's proposed benzoin condensation mechanism.

poses some other difficulties in that it is highly toxic, and it requires one of the co-solvents to be water, which greatly limits the solubility of organic starting materials. The desire to expand the usefulness of the benzoin condensation led to the further development of reaction conditions.

In order to make a different catalyst appealing, it would need to improve upon the abilities of cyanide either in yield or selectivity. The first successful catalyst found to perform the benzoin condensation was thiamine.¹⁹⁴ Thiamine is an *N*-heterocyclic carbene (NHC) precursor, which upon deprotonation yields a carbene, which has been shown to be successful at catalyzing a number of organic reactions.¹⁹⁵ Several NHC salts have been used in C–C bond forming reactions (Figure 1.9); cyclic formamidinium salts (**44**), oxazolium salts (**45**), thiazolium salts (**46**), and pyrrolium salts (**47**). In the mechanism proposed by Breslow in

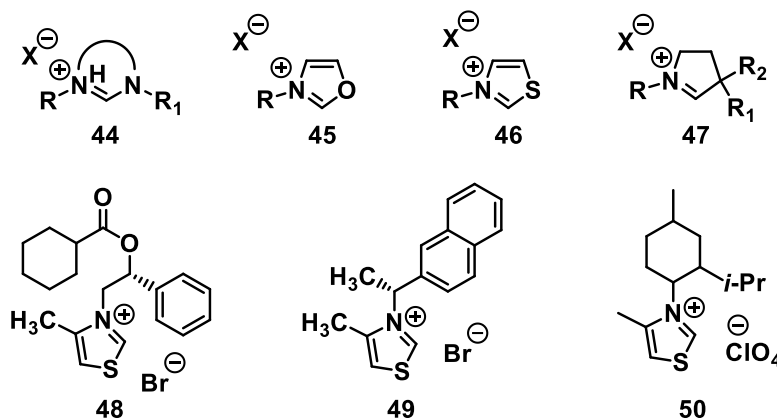


Figure 1.9 General structure of NHC salts successfully used for benzoin condensation reactions.

1958,¹⁹⁶ the catalytically active species is a thiazolin-2-ylidene, formed by the deprotonation of thiamine. Setter and coworkers found that aliphatic¹⁹⁷ and aromatic¹⁹⁸ aldehydes can undergo benzoin condensation utilizing different catalysts. The first sterically controlled benzoin condensation was achieved by placing bulky groups on the nitrogen. While the yields were minimal (6%), two catalysts showed enantiomeric excess (*ee*) of 22% (**48**)¹⁹⁹ and 51% (**49**),²⁰⁰ respectively. A micellar two-phase system with a methyl substituted thiazolium salt (**50**) achieved a similar enantiomeric excess (*ee*) of 35%, however with an improved yield of 20%.²⁰¹ Combining the micellar two-phase conditions and the thiazolium salt with a bulky group substituted on the nitrogen, obtained moderate *ee* of 47–57% and yields of 20–30%.²⁰²

Triazolium salts were next explored for asymmetric benzoin condensation.²⁰³ Investigations were found to indicate that catalytic activity is highly dependent on the substitution pattern (Figure 1.10).^{203,204} The most active species, compound **51**, was found to give 95% *ee* with a yield of 66%, resulting in one of the highest yields and *ee* of the aromatic benzoin condensation. When the same system was applied to aldehydes that were either more or less electron rich than benzaldehyde the same success was not found.²⁰⁵ Introduction of bicyclic thiazolium salts by Enders and Leeper²⁰⁶ achieved an *ee* of 21–90% which could also

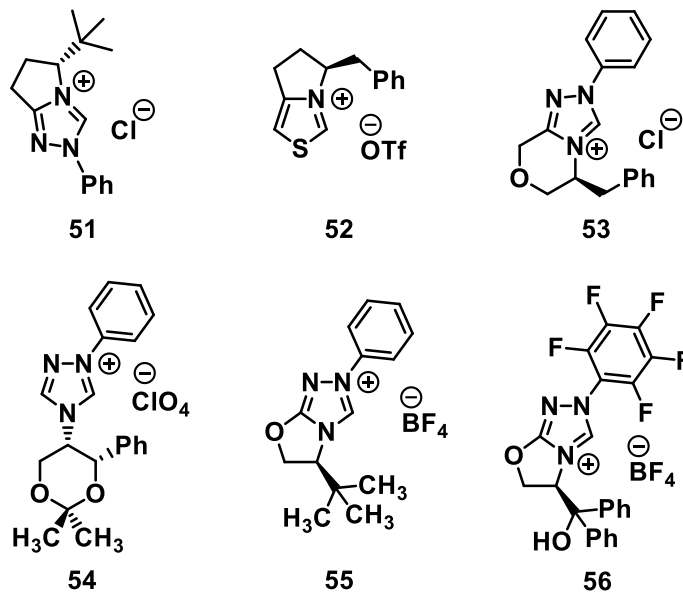


Figure 1.10 NHC salt catalysts development through increasing selectivity.

be obtained with asymmetric benzoin condensation (52–55). Continued work with bicyclic thiazoliums found that salts that can engage in hydrogen bonding control stereochemical outcomes. When the bicyclic system included a pentafluorobenzene substituent (56), a yield of 90% with a greater than 99% *ee* was reported, giving the highest enantiopurity for benzoin condensation.²⁰⁷ The wide variety of successful catalysts has made the benzoin condensation applicable to several different reactions and conditions.

1.4.2 Applications of Benzoin Condensation

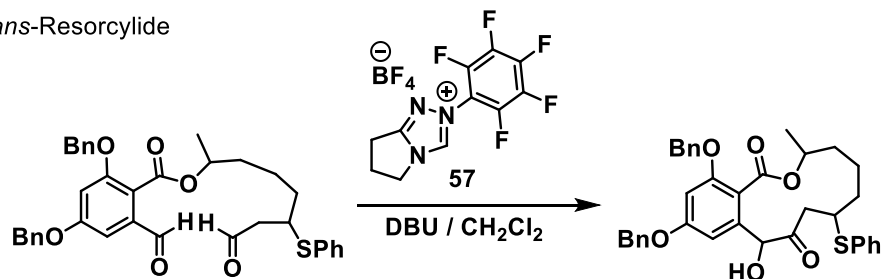
While the initial benzoin condensation was developed using cyanide, several limitations were found in the usefulness of the reaction. The growing need to control the stereoselectivity lead to an increase in the application potential. From the initial discovery of the benzoin condensation in 1832, several years passed before a different catalyst was utilized in 1943. From here, extensive work has been done developing catalysts for specific reaction conditions

and control. Electron-rich (hetero)aromatic rings are present in a vast majority of natural products and pharmaceuticals.^{207,208} Therefore, attention has been given to optimizing synthesis which resulted in new methods for their regio-, chemo-, and stereoselective functionalization. The ability to couple two aldehydes or an aldehyde and ketone is a valuable transformation in natural product synthesis. Utilizing chiral NHCs has resulted in the successful synthesis of several different natural products.

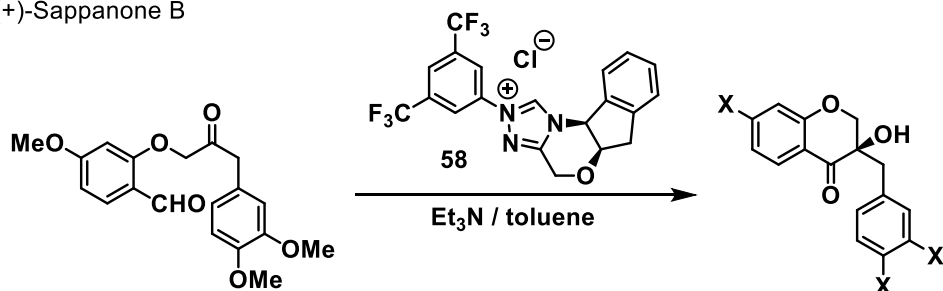
The following synthetic pathways of natural products have all utilized the benzoin condensation by undergoing intermolecular cyclization, summarized in Scheme 1.12. Several natural products, reported in 2007, were selectively synthesized with the utilization of a variety of NHC catalysts. The first reported synthesis was of *trans*-resorcyllide, a twelve-member lactone, by Mennen and Miller.¹⁹⁷ Triazolium salt **57** resulted in a mixture of diastereomers with a 21% yield. Takikawa and Suzuki reported the synthesis of (+)-sappanone B in 92% yield with 95% *ee*.²¹⁰ The 3,5-trifluoromethyl substituents on the NHC (**58**) were tuned for selectivity of the asymmetric coupling. Next, the first stereoselective synthesis of cassialoin was reported by Suzuki and coworkers.²¹¹ The synthesis of Cassialoin utilized a thiazolium salt which yielded **59** in 99% yield with a 20:1 diastereoselectivity (d.r.). Lastly, kinamycins and the monomeric unit of lomaiviticins were successfully synthesized with triazolium salt **57** with 78% yield and 3:1 d.r. From this, three different kinamycins were selectively synthesized in thirteen steps. With the similarities in structure of kinamycins and lomaiviticins, the synthesis was easily transferred to two lomaiviticins. This has direct applications in antitumor and antibiotic activities against a variety of cancer cell lines and bacteria.

With several asymmetric intermolecular reactions proving successful in natural product synthesis, work on intramolecular reactions had been focused on symmetrical aldehydes.

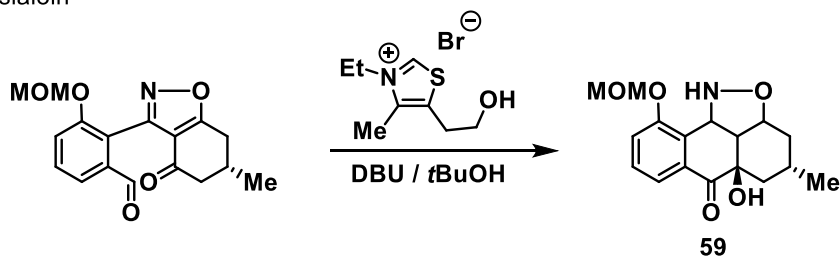
trans-Resorcyllide



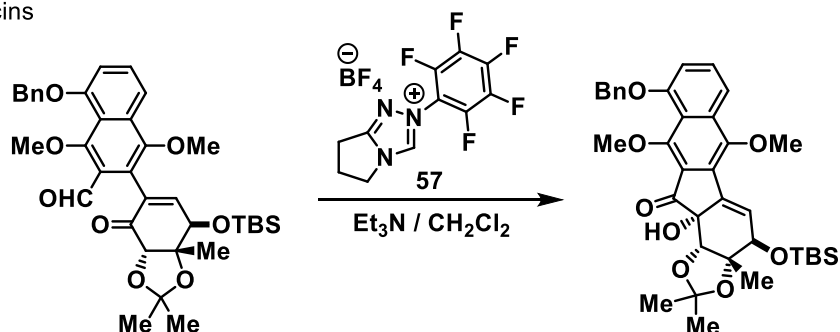
(+)-Sappanone B



Cassialoin



Kinamycins



Scheme 1.12 Summary of highlighted natural product syntheses utilizing benzoin condensation by NHC salt catalysts. All synthetic routes only show the step where the benzoin condensation was used.

Continued development with NHCs have shown that intramolecular synthesis of asymmetric mixed benzoin is also possible. Asymmetric synthesis has desirable applications in organic and pharmaceutical chemistry.²¹² The racemic compounds can be synthesized by a cyanide-

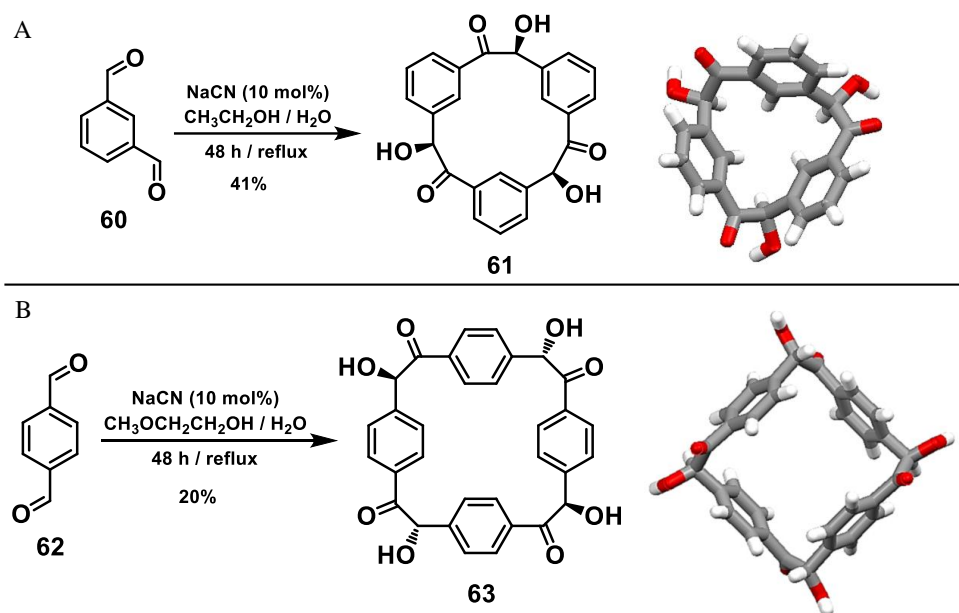
catalyzed cross-benzoin condensation.²¹³ Observing the same insolubility issues with cyanide as described before, other catalysts were explored. Thiamine diphosphate (ThDP)-dependent enzymes benzaldehyde lyase (BAL) were shown to catalyze the production of enantiopure benzoin.²¹⁴ Utilizing the inherent properties of enzymes, a variety of aldehydes were tested, with a focus on aldehydes that did not undergo symmetric benzoin condensation.²¹⁵ Starting with two different aldehydes results in the possibility to form four different products. The BAL enzyme was found to be selective for one product of at least 70%, with an average of 80% conversion. It was also shown to have a wider range in substrate scope than other tested enzyme catalysts. This one-step synthesis showed a large improvement over the previous method of using phenyl-Grignard derivatives.²¹⁶

1.4.3 Macrocycle Synthesis by Benzoin Condensation

Initial work with the benzoin condensation focused on aromatic aldehydes and was expanded to aliphatic aldehydes with NHC catalysts, but most reaction development has focused on single aldehydes. Dialdehydes were first studied by Grimaux, who attempted a benzoin reaction of terephthalaldehyde, but concluded that they only observed polymeric products.²¹⁷ Oppenheimer also studied terephthalaldehyde in 1886 and concluded that the reaction yielded a dimer as its main product.²¹⁸ The same reaction was analyzed for a third time in 1955 by Jones and Tinker and they concluded that it produced a polymeric material in 90% yield.²¹⁹ While the molecular weight was not very high, they disputed Oppenheimer's conclusion that the product was a dimer. Upon acidic workup, the collected solid was analyzed by elemental analysis where the calculated values matched an oligomer composed of seven terephthalaldehyde units with two terminal carboxylic acid groups, formed from the oxidation

of aldehyde by the acidic work up. In 2015, the Miljanić group reexamined this reaction under different conditions.

The initial reaction reported by Jones and Tinker was run in a 10% aldehyde solution in ethanol at room temperature, this was changed to a 6% solution in ethanol:water (1:1) at reflux.²²⁰ The first aldehyde used was isophthalaldehyde (**60**). After heating at reflux for 48 h, a precipitate formed. Upon isolation, recrystallization from 2-methoxyethanol resulted in pure **61** in 41% yield (Scheme 1.13A). The NMR showed no aldehyde or acid peaks, as seen previously,



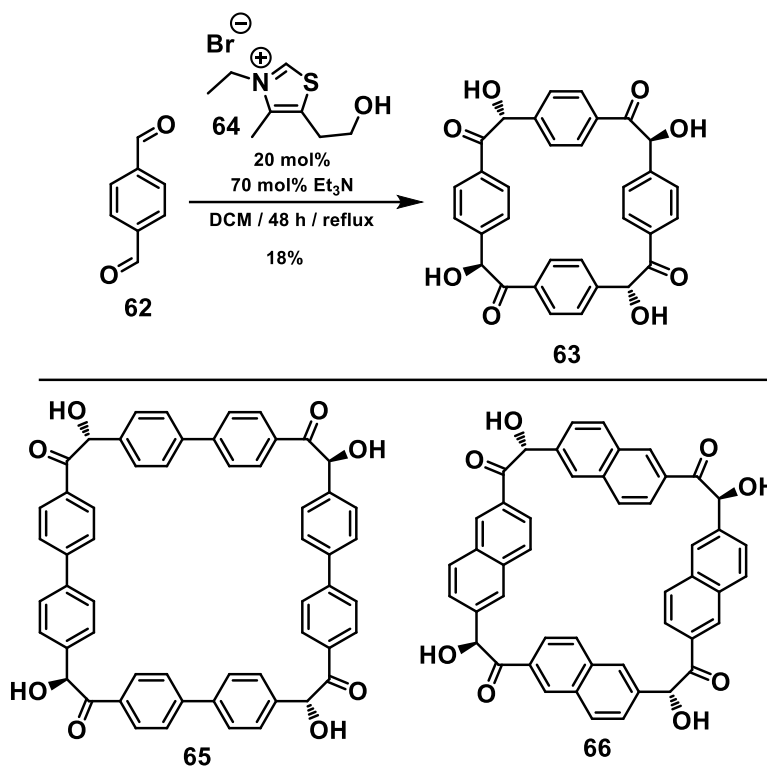
Scheme 1.13 A) Synthesis (left) and crystal structure (right) of cyclotribenzoin. B) Synthesis (left) and crystal structure (right) of cyclotetrabenzoin. Element colors: C—grey, O—red, H—white.

indicating the isolated material was different from that reported earlier. Single crystals were grown by vapor diffusion of CHCl₃ into THF, X-ray crystal analysis confirmed the synthesis of the first macrocycle, cyclotribenzoin, by benzoin condensation. Following this success, terephthalaldehyde (**62**) was engaged into a reaction under similar conditions (Scheme 1.13B).²²¹ The first conditions yielded a precipitate that contained a mixture of products, however by mass spectrometry it was suspected that **63** (or its diastereomers) were present in

the mixture. Under these conditions, **63** could not be obtained as a pure compound, and due to the high polarity purification by column chromatography was not possible. Substituting ethanol for 2-methoxyethanol and lowering the concentration, however, resulted in a precipitate that consisted almost entirely of **63**. Recrystallization from DMSO/MeOH resulted in a white solid in 21% yield. Characterization by NMR also showed no aldehyde or acid peaks, as observed in cyclotribenzoin, indicating that the product could be cyclic. Single crystals were grown by dissolving the precipitate in warm DMSO followed by vapor diffusion of MeOH. X-ray crystal analysis confirmed the synthesis of cyclotetrabenzoin (**63**).

These two macrocycles indicate the usefulness of DCC to influence the products produced in a reaction. While the final reaction conditions no longer create a thermodynamic equilibrium, changing the external conditions yielded two macrocycles from equilibrium systems that initially reported polymer products. When trying to expand to create larger macrocycles, the starting materials were found to be insoluble in the ethanolic and aqueous solvents. This limits the ability to modify the conditions to improve yield, efficiency, or push the equilibrium to yield a different macrocycle. However, moving into different solvent conditions would require the use of a different catalyst as cyanide salts are not soluble in organic solvents. Following previous work with the benzoin condensation, NHC catalysts were explored to move out of aqueous conditions. Cyclotetrabenzoin (**63**) could also be produced using 3-ethyl-5-(2-hydroxyethyl)-4-methyl thiazolium bromide (**64**, Scheme 1.14),²²² indicating an opportunity to expand this class of macrocycles. While in early development, indications have shown that larger macrocycles can be synthesized. So far, 4,4'-biphenyldicarbaldehyde (**65**) and 2,6-diformylnaphthalene (**66**) have successfully yielded tetrameric macrocycles. Continued research to expand the size is being conducted by Andrew

Eisterhold and applications of this novel class of macrocycles is being conducted by myself, Maymounah Alrayyani and Thamon Puangsamlee still ongoing.



Scheme 1.14 Synthesis of cyclotetrabenzoin with NHC salt catalysts and other two successfully synthesized macrocycles with same NHC salt catalysts.

1.5 Conclusions and Outlook

Porous materials have undergone a lot of development in the last decade to include materials composed of inorganic components, organic components, and a combination of both. Development of MOFs and PMCs has yielded materials that do not collapse upon solvent removal and can be tested by gas sorption isotherms showing permanent porosity. With such a large class of materials, applications now vary from petroleum refining to drug delivery. However, MOF synthesis still requires cost reduction for effective commercialization. Another limitation of MOFs and PMCs is the unpredictability of noncovalent interactions which can

decrease the stability of these materials. Continued work with understanding molecular tendencies and computations could enable better prediction of stable frameworks.

Macrocycles present a unique challenge in synthesis as they are not entropically favored. To access a family of macrocycles, DCC was used to create systems where all products could interconvert to form the most stable product. Templating has been the most successful in using DCC to create several macrocycles by changing templating agents. Macrocycles have been successfully used to facilitate host-guest interactions from ion-sequestering to household cleaning products. However, macrocycles have not been explored as building blocks for PMCs. The class of macrocycles has continued to grow through the discovery of cyclobenzoin. While these macrocycles are easily synthesized, they are not soluble in most organic solvents which prevents the ability to create larger macrocycles by ring-opening and inserting another monomer. A second catalyst has been able to create larger macrocycles, but the solubility issue remains. This thesis will address the solubility issues in Chapter 2, explore applications utilizing the central pore of cyclobenzoin in Chapter 3 and determine reaction by-products through purification in Chapter 4.

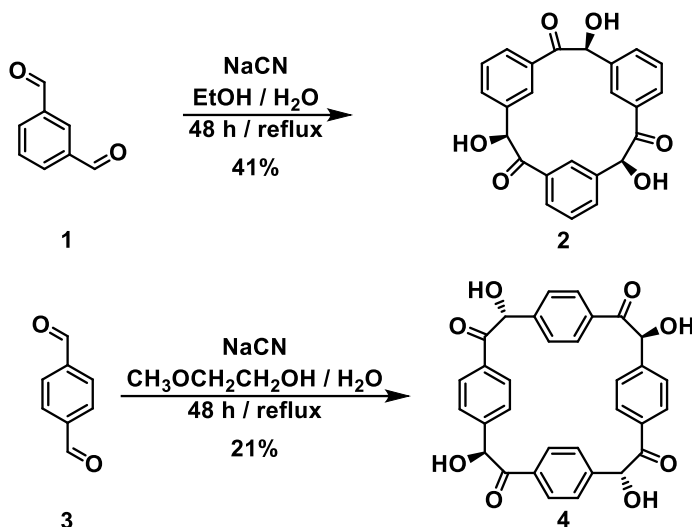
Chapter Two Porosity and Guest Inclusion in Cyclobenzoin Esters

2.1 Introduction

Porous molecular crystals (PMCs)^{21,24,74–80,224} are a unique subset of porous materials as they are composed of discrete molecules and are not polymeric in nature. This research on PMCs has expanded rapidly in the past two decades^{224–230} due to their possible applications in energy,^{231,232} environment,^{233,234} and the fundamental challenges associated with developing materials with noncollapsible voids. Since PMCs are composed of discrete molecules, their porosity can either be extrinsic or intrinsic; that is, voids can be formed between at least two molecules or within the molecule itself, respectively.²⁴ Intrinsically porous PMCs have most commonly been constructed from three-dimensional cage molecules.^{99,235–246} Using two dimensional macrocycles as building blocks for PMCs has historically been underexplored.

Macrocycles have been proven to be suitable building blocks for intrinsically porous materials in solution phase,^{180,247} but not in the solid state. Macrocycles have also been incorporated into porous materials;^{234,248–252} however, strong covalent or metal-ligand bonds were required to coerce them into a porous arrangement. While only a handful of macrocycles have been found to show permanent porosity on their own, their assembly was mediated by directed noncovalent interactions such as hydrogen bonds.^{96,253–258} We have been able to utilize the benzoin condensation to synthesize two organic macrocycles in one-pot syntheses, as shown in Scheme 2.1. While the synthesis of cyclobenzoin²⁵⁹ is simple, purification proved difficult because of the high polarity and low solubility of these macrocycles; this problem made exploring their applications challenging. To circumvent this issue, several post-synthetic modifications were attempted to facilitate further study of cyclobenzoin: reduction of their carbonyl group, oxidation of their hydroxyl groups, alkylation, esterification, or silylation of

their hydroxyl functionalities, as well as ring contractions. The successful modifications will be highlighted in this chapter.



Scheme 2.1 Synthesis of cyclotribenzoin (**2**) and cyclotetrabenzoin (**4**).

2.2 Cyclotribenzoin Synthesis²²⁰ and Reduction²⁶⁰

The reaction of isophthalaldehyde (**1**) with NaCN in a 1:1 ratio of EtOH to water produced cyclotribenzoin (**2**) in good yield. Diffraction-quality single crystals of **2** were grown by dissolving the sample in THF and then slowly diffusing CHCl₃ vapors into that solution. In the crystal form, for every three molecules of **2** there were three molecules of THF disordered over three orientations. The crystal structure shows that all three stereocenters have the same orientation, *S* as shown in Figure 2.1. The macrocycle is also conical in shape, which relieves all of the potential strain—all carbon atoms have bonding angles within $\pm 2^\circ$ of their ideal angles. The crystal packing diagram of **2** shows the molecules are oriented parallel to each other. Each molecule established twelve short [C–H \cdots O] contacts with twelve of its neighbors. The larger (top) side of the conical shape is formed by all six functional groups and three

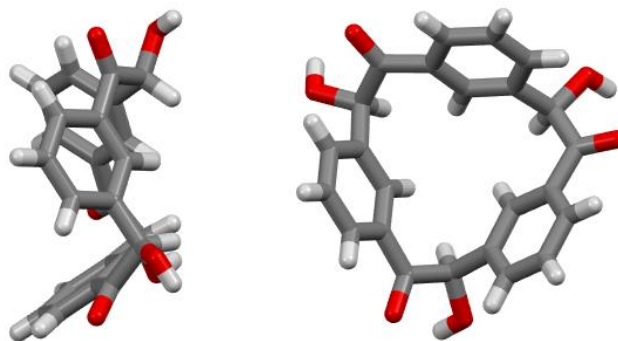
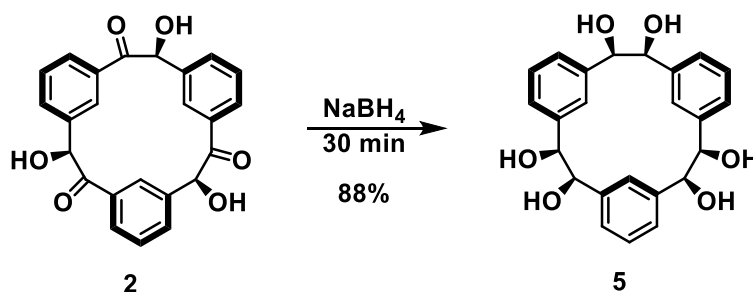


Figure 2.1 X-ray crystal structure of **2**. On the left, the side view showing the conical shape with the convergent oriented C–H groups pointing to the left. On the right, the top-down view of the intrinsic pore. The disordered THF molecules inside the pore have been removed for clarity. Element colors: C—grey, O—red, H—white.

carbons between the two meta-substituted carbons of the aromatic rings. The smaller (bottom) side is composed of one carbon of the aromatic ring and the hydrogen attached to the carbon with the hydroxyl group. In this conformation it appears that six C–H groups—three aromatic and the three C–H groups directly connected to the hydroxyl group—all point to a single spot. This suggests that perhaps **2** and its derivatives could be used as receptors for anions.

Reduction of **2** using NaBH₄ (Scheme 2.2) proceeds in an almost fully diastereoselective fashion producing an all-*cis* hexaol **5**. In the absence of a chelating species, this



Scheme 2.2 Reduction of cyclotribenzoin (**2**) into all-*cis* hexaol **5**.

diastereoselectivity is unusual.²⁶¹ This selectivity is believed to be achieved due to the conical shape of **2**, which forces the hydride to approach from the less sterically hindered side, pushing the newly formed –OH groups into a *syn* relationship with the existing –OH groups and the

benzene rings. X-ray diffraction quality crystals of **5** were grown by dissolving the reduced macrocycle in off-the-shelf THF and slow vapor diffusion of *n*-hexane into the solution. The resulting molecular structure is significantly different from that of the parent molecule **2**. In **5**, all of the –OH groups point in the same direction, as do two of the three benzene rings; the third is flipped and the larger portion points away from the molecule. Unlike **2**, whose molecules stack parallel to each other forming intrinsic channels, compound **5** shows the formation of apparent foci where molecules meet but leave space for H₂O molecules. Each molecule of **5** crystallizes with three molecules of H₂O, which are presumed to originate from the off-the-shelf THF used for crystallization. The H₂O molecules form discrete pentameric clusters within the pores formed by the crystal packing of **5**. Compound **5** is also stabilized by a series of interactions with the –OH groups of the H₂O molecules and the benzene rings. This synthesis showed a simple reduction modification resulted in substantial structure change and enabled the formation of small functional pores.

2.3 Cyclotetrabenzoin Synthesis,²² Oxidation, and Diamine Condensation²⁶²

The reaction of terephthalaldehyde (**3**) with NaCN in a 1:1 ratio of 2-methoxyethanol and H₂O produced cyclotetrabenzoin (**4**) in good yield. Diffraction-quality crystals were grown by slow vapor diffusion of MeOH into a dilute DMSO solution of **4**. The crystal structure has no residual solvent molecules present (Figure 2.2). The four stereocenters alternate between *R* and *S* configurations around the macrocycle. The molecule adopts a square shaped intrinsic pore measuring 6.9×6.9 Å, defined by the centroids of the benzene rings opposite the molecule. The molecule is not strained as all carbon atoms have bonding angles within ± 2° of their idealized geometries. It is also observed that all α-hydroxyketone functional groups point away from the

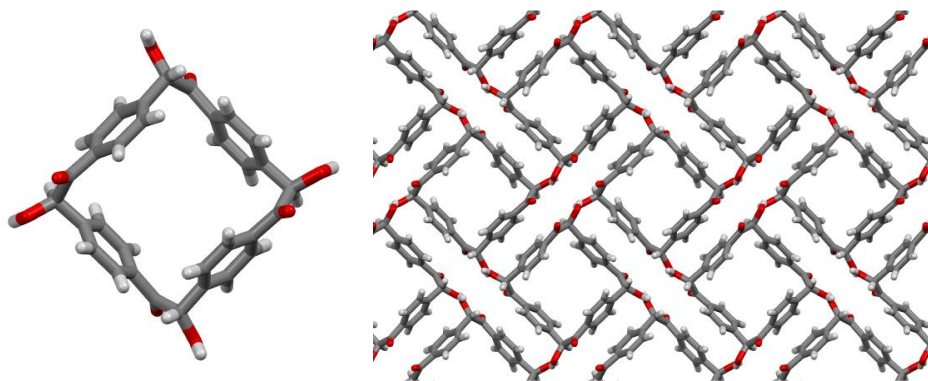
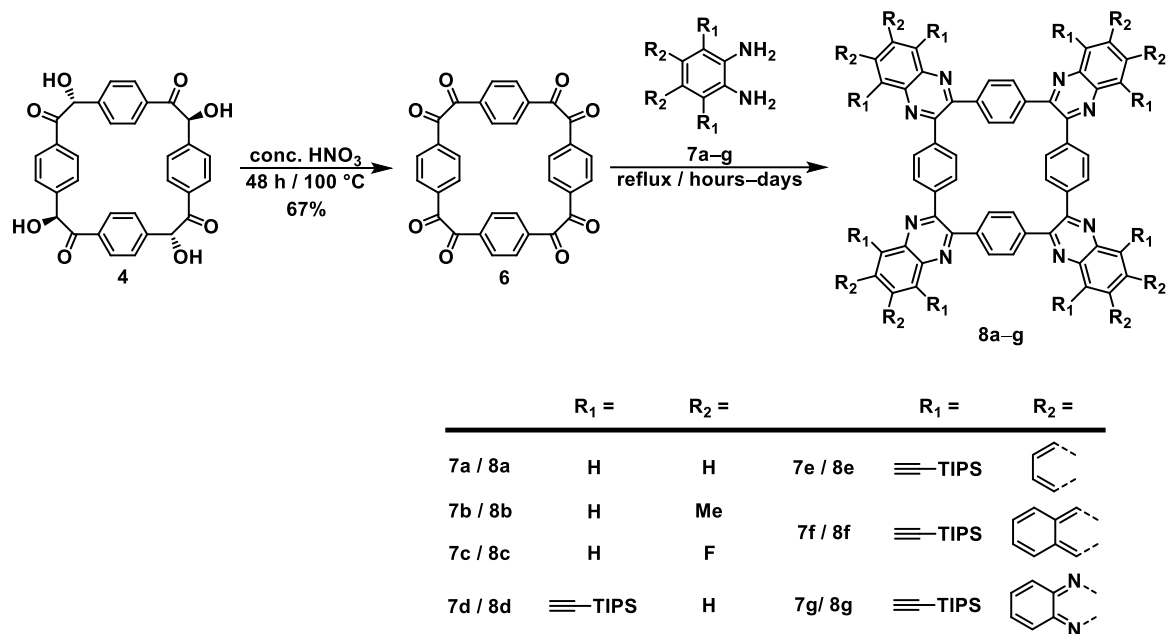


Figure 2.2 X-ray crystal structure of cyclotetrabenzoin (**4**). On the left, shows the square shape of the molecule. On the right, the packing pattern of **4** forming hydrogen bonds on the four corners of each molecule. Both images are viewed along the crystallographic *c* axis. Element colors C—grey, O—red, H—white.

central cavity. This results in their ability to form hydrogen bonds with their counterparts in neighboring molecules, which stabilize the crystal structure. These hydrogen bonds are found between the benzoin O–H hydrogen and oxygen atoms from both the carbonyl (C=O \cdots H distance of 2.11 Å) and hydroxyl groups (H–O \cdots H distance of 2.16 Å) of the neighboring molecule. These interactions are repeated on all four sides of **4**. Individual molecules of **4** stack perfectly on top of each other, resulting in square-shaped channels throughout the structure. With empty channels present, gas sorption was probed using N₂ as the guest and cyclotetrabenzoin was found to have a low Brunauer-Emmett-Teller (BET) surface area of 42 m² g⁻¹. Cyclotetrabenzoin is an easily synthesized, shape-persistent, intrinsically porous all-organic macrocycle that could serve as the progenitor of an entirely new class of macrocycles.

The oxidation of **4** with nitric acid yields octaketone **6** in 76% yield (Scheme 2.3); this octaketone was named cyclotetrabenzil. The resulting 1,2-diketones known as benzils are important building blocks in the synthesis of pharmaceuticals²⁶³ and porphyrins,²⁶⁴ and common photoinitiators for free radical polymerizations.²⁶⁵ The synthesis of cyclotetrabenzil lead to the opportunity to expand into the chemistry of azaacenes. Azaacenes are synthesized



Scheme 2.3 Oxidation of cyclotetrabenzoin (**4**) into cyclotetrabenzil (**6**) followed by condensation with a variety of 1,2-phenylenediamines **7a–g** produces heteroacenes **8a–g**.

by the condensation of 1,2-diketones with 1,2-phenylenediamines, thus making **6** a potentially interesting precursor for azaacene synthesis. Several fully π -conjugated functionalized heteroaromatic macrocycles have been synthesized through diamine condensation (Scheme 2.3). Optical and electronic properties of **8d–g** were studied, and were found to be dominated by the linear acene fragments. X-ray quality crystals, grown by vapor diffusion, showed that the macrocyclic molecules are twisted into a saddle shape caused from the rigidifying of the bonds around the central cavity. Recently, cyclotetrabenzil (**6**) has also been found to crystallize with chlorinated solvents, where the chlorine atoms interact with the central cavity.²⁶⁶ The reduction of **3** resulted in the ability to crystalize water clusters, while the oxidation of **4** resulted in a precursor for azaacene synthesis, with continued applications still ongoing.

2.4 Synthesis of Cyclobenzoin Esters²⁶⁷

The aforementioned post-synthetic modifications either increased the overall polarity or greatly changed the overall shape of the macrocycle, eliminating the ability to understand and explore the original central pore. Several modifications to the benzoin product have been previously accomplished including amidation,²⁶⁸ α -amino ketones,²⁶⁹ deoxygenation,²⁷⁰ substituted imidazothiazolones,²⁷¹ *O*-alkylation,²⁷² reduction,²⁶⁰ oxidation,²⁶² and esterification.²⁷³ We speculated that an *O*-alkylation would increase the solubility while not affecting the macrocycle shape. We tried this by simply dissolving **4** in dimethylformamide (DMF) at 50 °C for 24 hours with different bases and alkylating agents (Table 2.1). In all

Table 2.1 Alkylation reaction conditions

solvent	alkylating agent	equiv. alkylating agent	base	equiv. base	yield (%)
DMF	bromobutane	4.0	<i>t</i> -BuOK	4.0	79
DMF	bromohexadecane	4.0	<i>t</i> -BuOK	4.0	49
DMF	bromobutane	16.5	K ₂ CO ₃	4.0	61
DMF	iodohexane	20.0	K ₂ CO ₃	6.0	50
DMF	bromobutane	4.0	Na	4.0	40

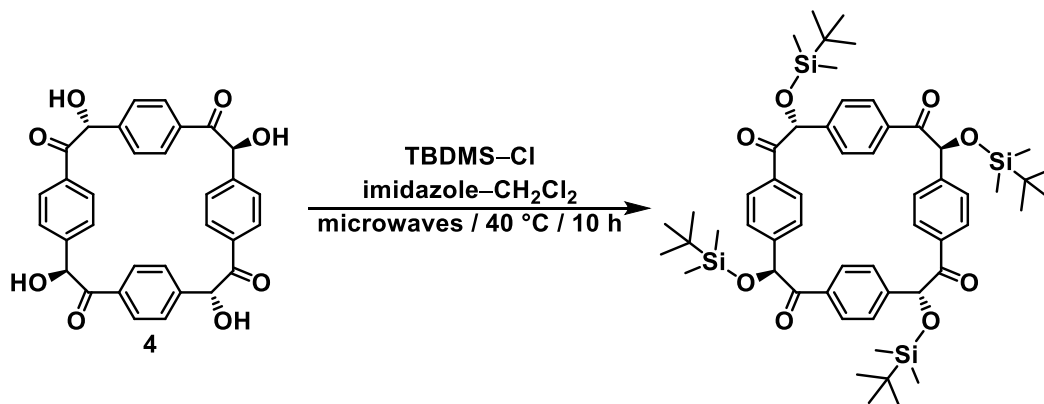
reactions, a precipitate was formed and examined by thin layer chromatography (TLC). Mother liquor analysis by TLC showed remaining alkylating agent, base, and unreacted **4**. Each reaction showed at least one mobile spot by TLC, however upon NMR analysis it was shown to be the alkylating agent. Analysis of other chromatographically isolated fractions by NMR showed the loss of the hydroxyl peaks, but also the loss of the benzoin peaks and a complicated aromatic region. This indicated **4** was undergoing decomposition into a mixture of linear polymer chains or terephthalaldehyde and not the desired alkylation.

Since DMF was determined to be a poor solvent for attempted alkylations of **4**, we tried the alkylation using different solvents. Reactions were again run at 50 °C for 24 hours (Table 2.2), and were analyzed by TLC. The same results as before were observed where the spot that

Table 2.2 Alkylation reaction solvent conditions

solvent	alkylating agent	equiv. alkylating agent	base	equiv. base	yield (%)
DMSO	bromobutane	4.0	K ₂ CO ₃	4.6	71
Acetone	bromobutane	4.0	K ₂ CO ₃	4.6	85
DCM	bromobutane	4.0	K ₂ CO ₃	4.6	30
Acetonitrile	bromobutane	4.0	K ₂ CO ₃	4.6	20
MeOH	bromobutane	4.0	KOH	4.2	70

moved by TLC was found to be the alkylating agent. When the reaction was run in dimethyl sulfoxide (DMSO), we were able to isolate a second spot where NMR analysis again showed decomposition of **4** by the loss of benzoin peaks. All other reaction conditions resulted in the isolation of unreacted **4**, due to its insolubility in the reaction solvent. Since **2** was able to form a silylated derivative⁵⁰ under microwave conditions, we tried the same conditions with **4** (Scheme 2.4). We were able to isolate two products, one was *tert*-butyldimethylsilyl chloride,



Scheme 2.4 Microwave assisted silylation of **4**.

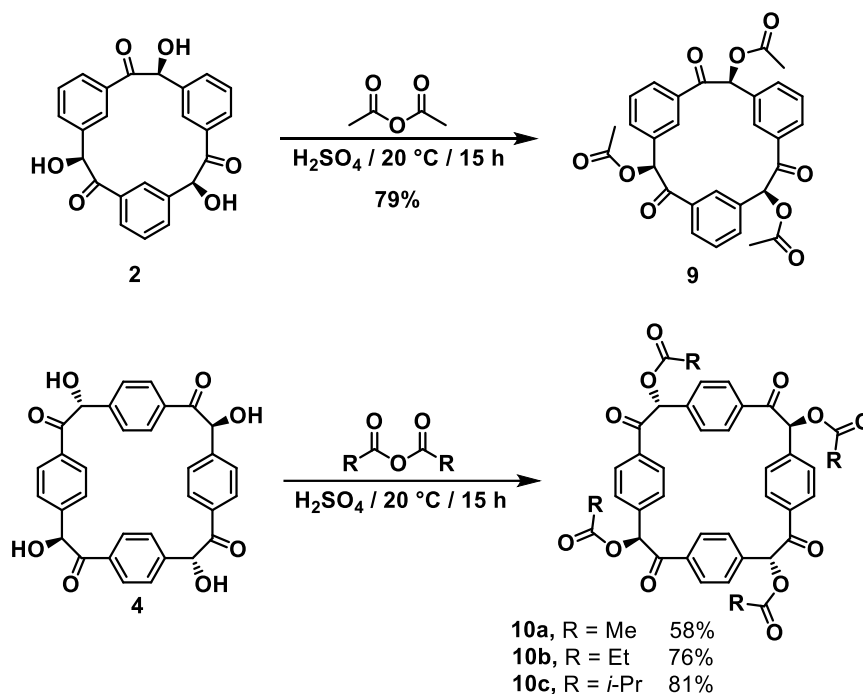
and the second was unreacted **4**. Analysis by NMR shows that **3** and **4** are present in a ratio of 2:1, most likely indicating the starting material was not pure **4**. With unsuccessful attempts to accomplish simple *O*-alkylation, we decided to try esterification.

We started by using acetyl chloride with either triethylamine (TEA) and *N,N*-diisopropylethylamine (DIPEA) as the base in different solvents. We also ran this reaction with acetyl chloride as the solvent and the esterification agent. (Table 2.3). Reactions were all run at 50 °C for 48 hours under nitrogen. After 48 hours, reaction mixtures had turned clear and

Table 2.3 Esterification reaction conditions

solvent	alkylating agent	equiv. alkylating agent	base	equiv. base	yield (%)
MeOH	acetyl chloride	5.0	TEA	5.0	70
DCM	acetyl chloride	5.0	TEA	5.0	72
DCM	acetyl chloride	6.0	DIPEA	6.0	53
THF	acetyl chloride	8.0	DIPEA	8.0	64
	acetyl chloride	184.8	DIPEA	6.0	78

remained clear upon cooling. Extraction removed all organic products from the initial reaction mixture. Analysis by TLC did not successfully separate products, and analysis by NMR showed a large aldehyde peak and a complicated aromatic region. Comparing all previous reaction conditions, it appeared that under basic conditions we observed decomposition of **4** as the major product, so we looked at using acidic conditions. We added **4** to acetic anhydride with stirring to form a homogenous suspension, then two drops of sulfuric acid were added. Upon acid addition, solution slowly went from cloudy to clear. Reaction was neutralized with 1M NaOH, then added to CH₂Cl₂ and extracted with water. This created a cloudy white emulsion which was allowed to separate, then the organic layer was collected and dried yielding a white solid. Column chromatography yielded pure **10a** in 58% yield. Other acyl anhydrides with catalytic amounts of H₂SO₄ were found to esterify cyclobenzoin **2** and **4** in good yields (Scheme 2.5).⁶⁴ As predicted, the removal of the –OH group made cyclobenzoin esters more soluble in common organic solvents.



Scheme 2.5 Esterification of cyclobenzoin macrocycles **2** and **4**.

Diffraction quality crystals of **9** were grown by slow evaporation of its chloroform solution. Solvated cyclotribenzoin acetate $9 \cdot n\text{CHCl}_3$ shows no discernible pores, although its packing is quite different from that of parent **2**. Due to its smaller central pore, 3.79 Å across the top and 2.00 Å across the bottom, **2** has been studied less than **4**. Cyclotribenzoin acetate **9** adopts a cone-shaped conformation and has a cavity size similar to that of **2**, with Ph–C–C–Ph dihedral angles of 66.6–69.7°. The added ester groups stick out along the bottom edge of the macrocycle, enabling efficient packing in the solid state, where the ester group can interlock with another molecule. The ester groups eliminate the possibility to form hydrogen bonds, but instead establishes a series of short contacts. These short contacts are formed between (a) ketone oxygen and AcOC–H (2.91 Å, Figure 2.3A), (b) ketone oxygen and ester methyl hydrogen (2.32 Å, Figure 2.3A), (c) ester carbonyl and ester methyl hydrogen (2.54 and 2.65 Å, Figure

2.3A), (d) ketone oxygen and aromatic hydrogen (2.53 and 2.67 Å, Figure 2.3B), and (e) ester carbonyl and aromatic hydrogens (2.48 Å, Figure 2.3B).

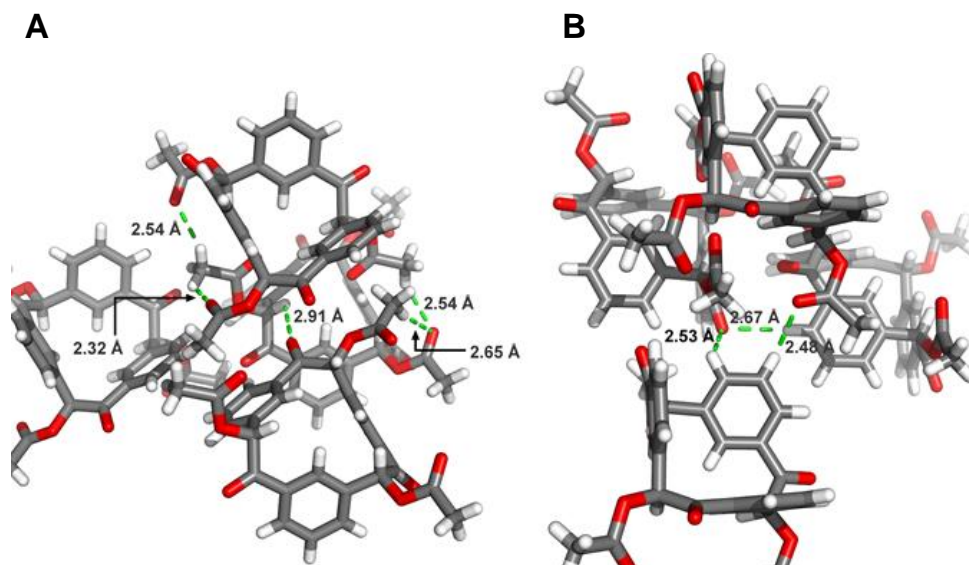


Figure 2.3 Short contacts in the crystal structure of **9** are established between A) ketone oxygen and AcOC–H, as well as ester carbonyl and ester methyl hydrogen, and B) between ketone oxygen and an aromatic hydrogen, as well as ester carbonyl and aromatic hydrogen. Element colors: C—grey, O—red, H—white.

With a larger central pore, **4** has been the focus of possible applications. The first diffraction-quality crystal of **10a** was fortuitously grown in a chromatography column fraction tube. However, when a similar experiment was attempted with other esters, it proved unsuccessful. Slow evaporation crystal growth of various solvents was utilized to grow diffraction-quality single crystals. Successful conditions were as follows: Me₂CO and EtOAc/hexanes for **10a**, Me₂CO for **10b**, and CS₂ for **10c**. In each crystal, the solvent molecules were incorporated into the structures. In the case of **10a**, solvent molecules could be removed by supercritical CO₂ drying, leaving the diffraction-quality crystals uncompromised. Crystals grown from either Me₂CO or EtOAc/hexanes conditions could be dried, resulting in crystal structures of three different solvates of **10a**. The resulting molecular structures of all cyclotetrabenzoin esters are shown in Figure 2.4, with solvent molecules removed for clarity.

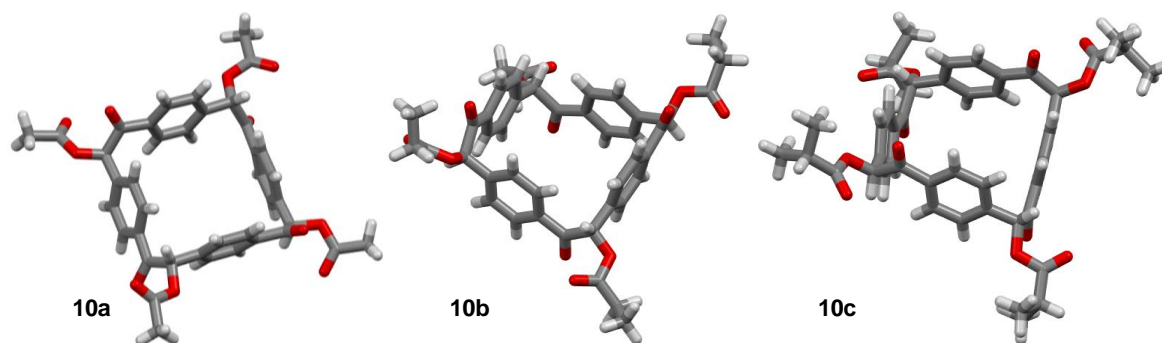


Figure 2.4 Crystal structures of cyclobenzoin esters **10a–c**. Element colors C—grey, O—red, H—white.

As the three crystals for **10a** show a similar molecular structure, only the solvent-free structure will be discussed. Molecules of **10a** are roughly square-shaped, with angles between the planes of aromatic rings on the opposite sides of the macrocycle in the $15.3\text{--}21.2^\circ$ range, depending on the solvent. The acetyl group is pointing away from the aromatic rings with the torsional angles of $159.5\text{--}159.7^\circ$. In contrast, **10b** is significantly more twisted, the Ph–C–C–Ph dihedral angles between 59.8 and 78.3° , compared to $66.9\text{--}68.6^\circ$ for **10a**. The isobutyric ester **10c** is also twisted, but in a symmetric fashion, with Ph–C–C–Ph dihedral angles of 72.9° .

While molecular structures of **10a–c** appeared quite similar, their packing diagrams, shown in Figure 2.4, differ drastically. The three solvates of **10a** are shown in the top row of Figure 2.4, viewed along the crystallographic *c* axis. The packing motif is that of a square grid with two distinct kinds of one-dimensional pores. One, square shaped (7.1×7.1 Å, measured between centroids of benzene rings on opposite sides of the macrocycle), is formed by the vertical alignment of molecules of **10a** into extended nanotubes, similar to the published structure of **4** (Figure 2.5, top left). The other, diamond-shaped (10.9×5.2 Å, measured between the ester and ketone oxygens in macrocycles within the same layer), is a consequence of crystal packing, and its analog was not observed in the structure of **4**. In the three structures, these pores get progressively filled with disordered solvent molecules. The empty structure is free of

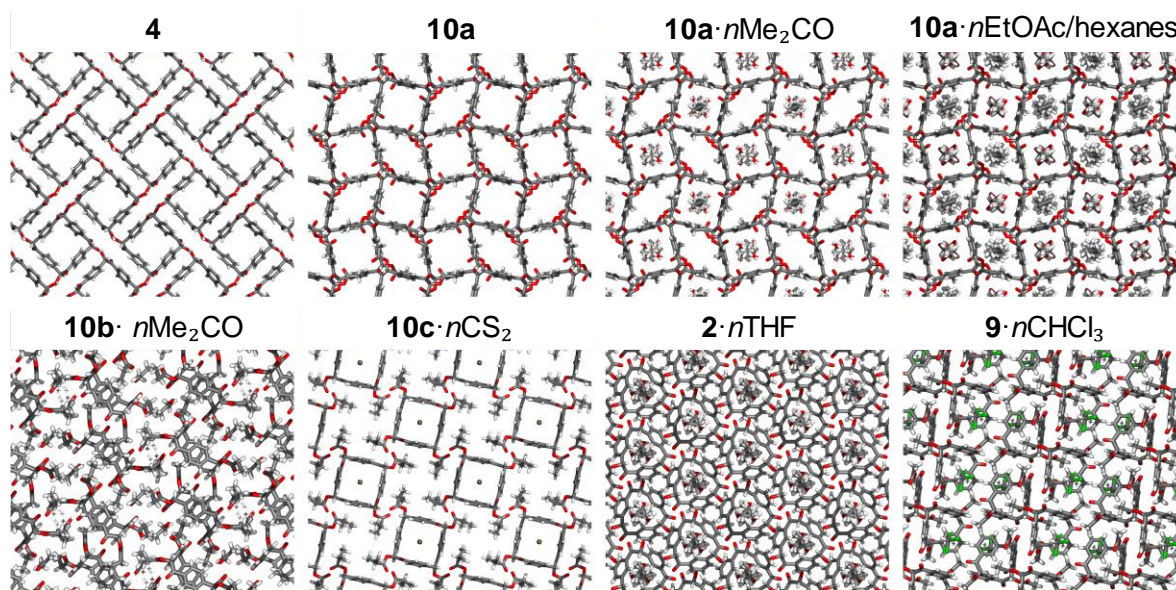


Figure 2.5 Packing diagrams for cyclobenzoin **2** and **4**, and their esters **9** and **10a–c**. All structures are shown along the crystallographic *c* axis, except **10b**·*n*Me₂CO and **4**·*n*CHCl₃ which are shown along their crystallographic *b* axis for better visibility. Element colors: C—gray, O—red, H—white, S—yellow, Cl—green. Disordered solvent molecules are explicitly shown.

solvent. In the case of **2a**·Me₂CO, only the square-shaped pores are filled; in **2a**·EtOAc/hexanes, both kinds of pores are occupied by solvent molecules.

Curiously, the organization of molecules of **10a** into two-dimensional sheets involves no discernible strong noncovalent interactions. Notable are only short (2.53 Å) contacts established between the hydrogens of the methyl group on one molecule and the ester carbonyl oxygens on another molecule (Figure 2.6). These contacts repeat themselves on each of the four corners of **10a**, organizing the molecules into a square grid. Neighboring sheets are rotated by $\pm 25.4^\circ$ (measured as the angle between the planes of benzene rings in molecules of **10a** in neighboring sheets) with respect to each other. Again, vertical alignment involves no strong directional interactions. Neighboring sheets are connected by [C–H···O] contacts between (a) ketone oxygen in one molecule and hydrogens on two aromatic rings in its neighbor (2.63 and 2.69 Å, Figure 2.7A); (b) ester carbonyl oxygen on one molecule and hydrogens on two

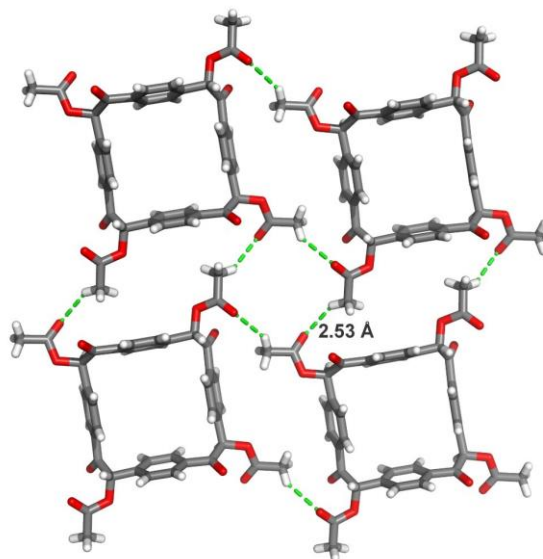


Figure 2.6 Contacts in the plane of the ring of **10a** are established between the methyl hydrogen and ester carbonyl oxygens. Element colors: C—grey, O—red, H—white.

aromatic rings in its neighbor (2.62 and 2.7 Å, Figure 2.7B), and (c) ketone oxygen in one molecule and AcOC—H hydrogen in its neighbor (2.17 Å, Figure 2.7C). In its solvated structures, the molecules of **10a** within the same layer establish no direct short contacts, as disordered solvent molecules separate them; the vertical organization of layers remains largely identical to that observed in the solvent-free crystal structure of **10a**.

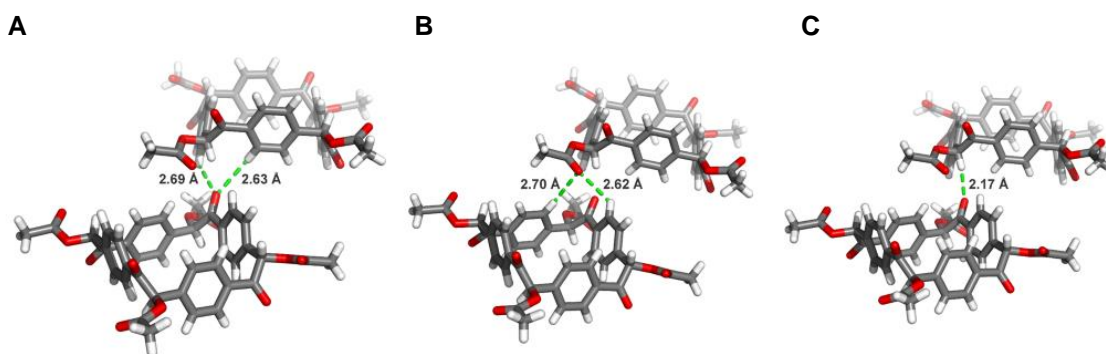


Figure 2.7 Contacts in the plane perpendicular to the ring plane of **10a** are established between A) ketone oxygen and hydrogens on two aromatic rings, B) ester carbonyl oxygen and hydrogens on two aromatic rings, and C) ketone oxygen and AcOC—H hydrogen. Element colors: C—grey, O—red, H—white.

In the packing diagram of **2b**·Me₂CO, no analogous channels are observed. The bending of the macrocyclic structure enables efficient packing, eliminating pores. The ester's terminal CH₃ group appears to be partially included into the cyclobenzoin cavity of the neighboring

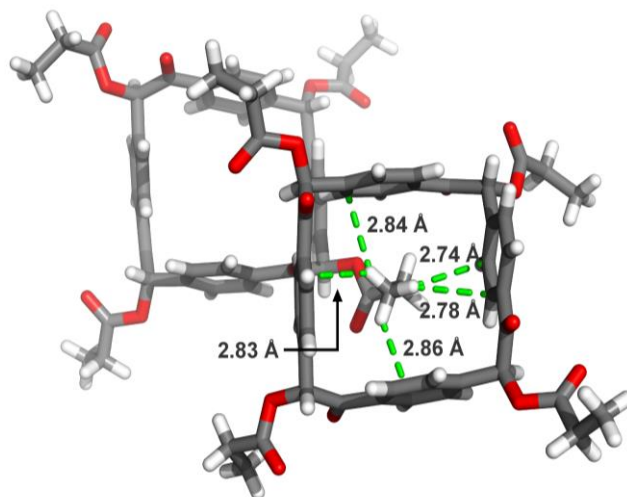


Figure 2.8 Short contacts between the terminal methyl group and the aromatic rings lining the intrinsic pore of **10b**. Element colors: C—grey, O—red, H—white.

molecule, establishing short [C—H···C] contacts that range in length between 2.74 and 2.86 Å (Figure 2.8). Other hydrogens of the ethyl group are in short contacts with the carbonyl oxygen

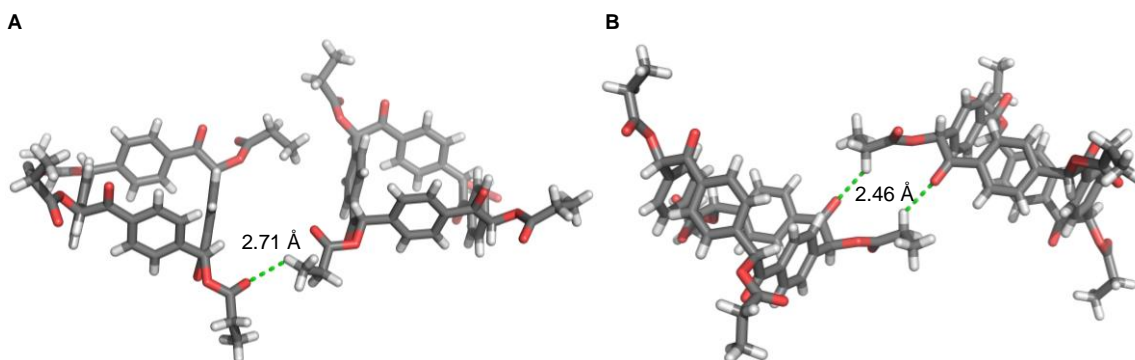


Figure 2.9 Short contacts between A) ethyl group hydrogens and ester carbonyl and B) ethyl group hydrogens and ketone. Element colors: C—grey, O—red, H—white.

atoms in the ester (2.71 Å, Figure 2.9A) and ketone (2.46 Å, Figure 2.9B) moieties of their neighboring molecules.

Ester **10c** crystallizes with CS₂ solvent disordered over four symmetry-equivalent positions that form a continuous column along the ring axis of **10c**. The packing diagram of **10c**·CS₂ is reminiscent of that observed for **10a**, with two distinct channels. The smaller one, formed by the cyclobenzoin rings, is occupied by CS₂ solvent molecules. The larger one, resulting from inefficient packing, is ~11 Å across and largely filled by the pendant *i*-Pr groups of **10c**. Within each layer (Figure 2.10), those *i*-Pr groups establish short contacts with each other (H–H distances of 2.30 Å, Figure 2.10A) and with the oxygen atom of the ester group in the neighboring molecule (2.40 Å, Figure 2.10B). Closest contacts between the adjacent layers along the crystallographic *c* axis are established between the ketone oxygen atoms and aromatic ring hydrogens (2.28 Å, Figure 2.10B), as well as between aromatic hydrogens on adjacent molecules of **10c** (2.30 Å, Figure 2.10B).

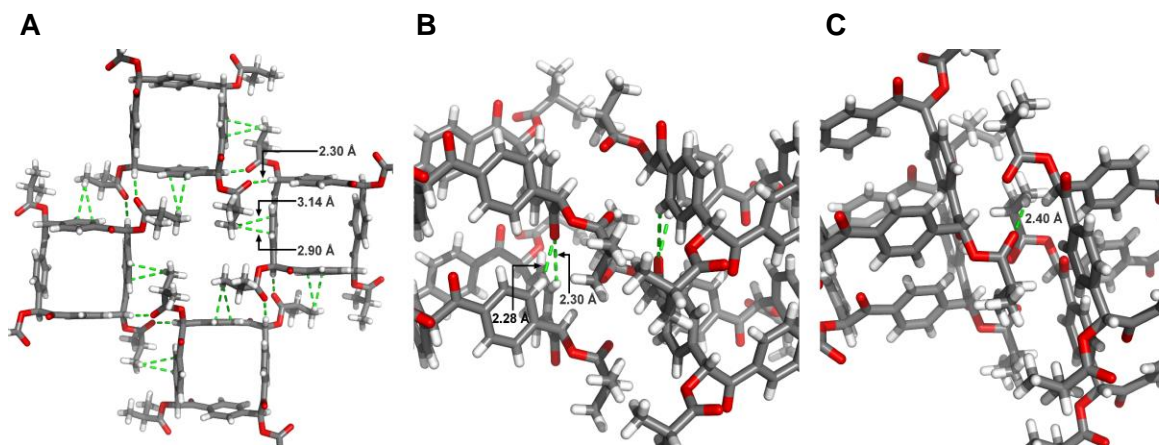


Figure 2.10 On the left, short contacts in the plane of the ring of **10c** are established between A) ester carbonyl and AcOC–H hydrogen, as well as between ester methyl hydrogens and one aromatic carbon. Contacts in the plane perpendicular to the plane of the ring are established between B) ketone oxygen and two aromatic hydrogens in molecule below and C) between ester carbonyl and ester methyl hydrogen. Element colors: C—grey, O—red, H—white.

Viewed along the crystallographic *b* axis, the structure of **10c**·CS₂ is particularly intriguing (Figure 2.11). While disordered, molecules of CS₂ all aligned along the single axis that passes through the center of the cyclobenzoin ring. This arrangement suggests that **10c** and

its analogs can act as supramolecular hosts for guests that are thin enough to fit into their cavities.

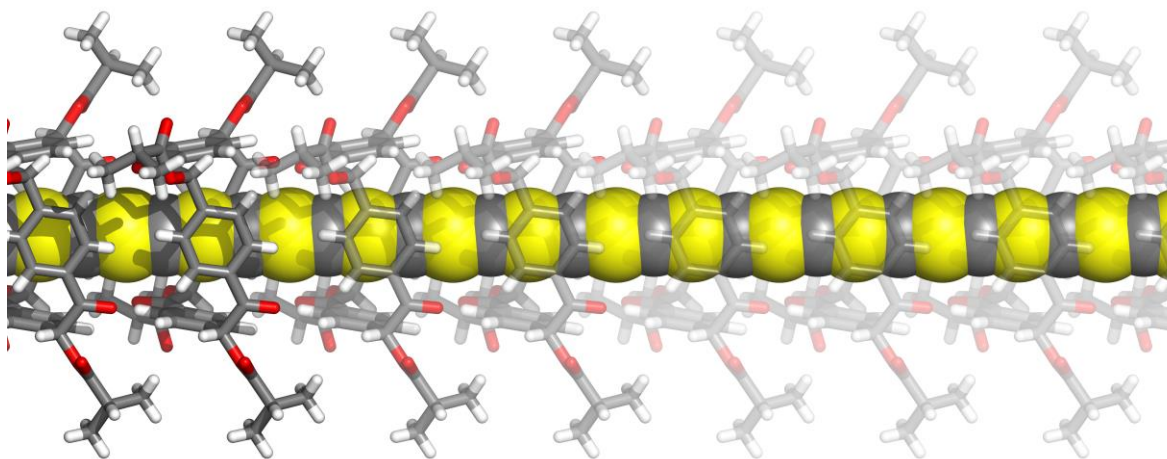


Figure 2.11 Viewed along the crystallographic *b* axis, the crystal structure of **10c**·*n*CS₂ shows well-aligned cavities of molecules of **10c** including linearly disordered molecules of CS₂, in an arrangement which resembles an insulated wire. Element colors: C—gray, O—red, H—white, S—yellow.

As the packing diagrams of **10a** and **10c**·CS₂ revealed one-dimensional channels, we examined whether the crystals of these two materials were permanently porous. Gas sorption was probed using N₂ as the guest, and the samples were activated by drying with super critical CO₂ followed by degassing at 30 °C and 10 mmHg for 15 h. The two resulting isotherms are very different. Compound **10a** has a type I isotherm, characteristic of a microporous system, while activated crystals of **10c** show no measurable uptake of N₂ (Figure 2.12, squares and diamonds, respectively). The uptake of **10a** was unexpected since **4** had minimal uptake of N₂. On the basis of the isotherm the Brunauer-Emmett-Teller (BET) surface area was determined to be 572±16 m² g⁻¹, a dramatic increase from the BET surface area of 42 m² g⁻¹ of parent

compound **4**.⁵³ Pore volume within crystals of **10a** was $0.18 \text{ cm}^3 \text{ g}^{-1}$. Crystals of **10a** absorb a similar volume of CO_2 at 195 K (Figure 2.13) as N_2 .

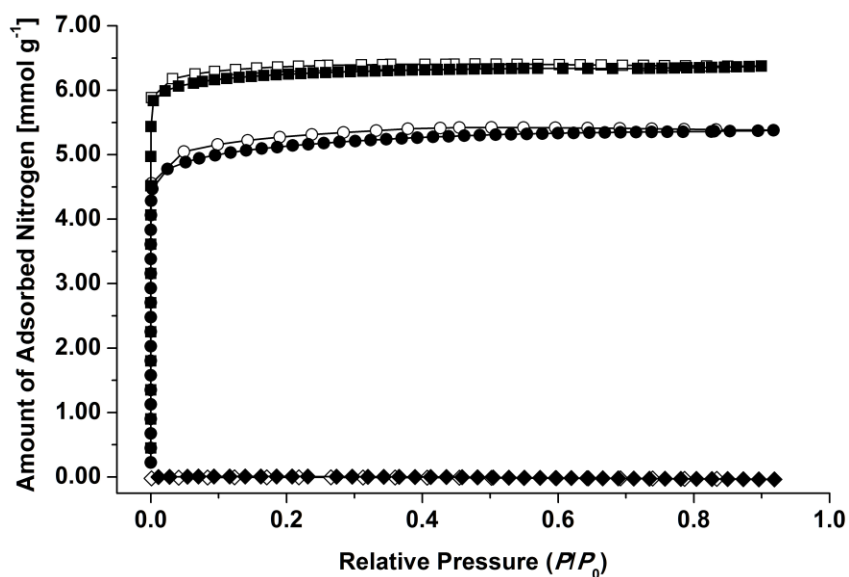


Figure 2.12 Nitrogen adsorption and desorption isotherms for compounds **10a** in the form of single crystals (squares) and a polycrystalline powder (circles), and the activated crystals of **2c** (diamonds). All isotherms were measured at 77 K, following activation. Solid symbols correspond to adsorption, empty ones to desorption.

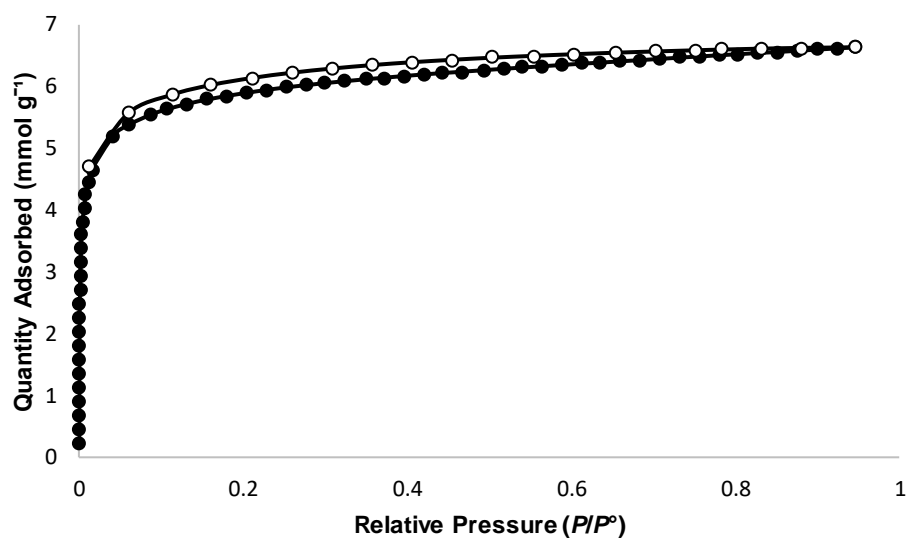


Figure 2.13 Carbon dioxide gas sorption (195 K) plot for crystals of **10a**. Filled symbols indicate adsorption, empty one desorption.

Powder X-ray diffraction (PXRD) of a powder sample of **10a** obtained after column purification and solvent evaporation showed that this material is microcrystalline (Figure 2.14). Since the experimental PXRD pattern matched the simulated pattern based on the single crystal structure data, we performed gas sorption on the microcrystalline powder of **10a**. Using the same conditions as on the single-crystalline samples of **10a** a similar type I isotherm was obtained (Figure 2.12, circles) with a slightly lower BET surface area of $453 \pm 13 \text{ m}^2 \text{ g}^{-1}$.

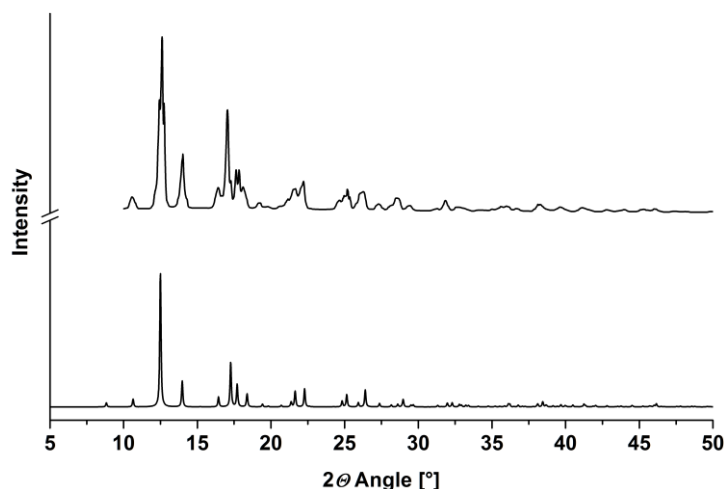


Figure 2.14 Comparison of PXRD patterns of compound **10a**: on the top, the pattern measured on the purified and dried powder sample; on the bottom, the pattern simulated from single crystal X-ray data.

Since **10a** can be produced from terephthalaldehyde in two simple steps, its synthesis is easily scaled up. We produced as much as 14.7 g of **10a** in a single batch; the yield of the esterification increased slightly (66%) relative to the millimolar-scale preparation. Combining the initial cyanide-catalyzed cyclobenzoin preparation with an *in-situ* acid-catalyzed esterification risked the release of gaseous HCN, which is why the two-step procedure was deemed safer.

2.5 Conclusion

In conclusion, we have demonstrated that the esterification of cyclobenzoin not only enhances their solubility and processability, but also creates new molecules with unique and useful properties. The acetic ester of **4** is permanently porous, with relatively moderate BET surface area, but high stability, extremely easy synthesis, and low cost. Cyclotetrabenzoin isobutyrate **10c** organizes into similar one-dimensional channels in the solid state, but these channels now hold an atomically thin guest molecule. The two structures are not held in place by any discernible strongly directional noncovalent interactions, but simply result from the optimal organization of these square-shaped species in the solid state. We are presently preparing cyclobenzoin esters derived from larger aromatic dialdehydes in the hope of obtaining materials with higher surface areas. The encapsulation of CS₂ in the cavity of **10c** confirms the suspicion that cyclobenzoin and their derivatives can act as competent supramolecular hosts. The ability to modify cyclobenzoin in different ways has expanded the usefulness of these macrocycles. Chapter 3 will continue to explore the generality of the supramolecular host behavior, seeking to extend it to the solution phase, and quantify its energetics both experimentally and computationally.

2.6 Experimental Section

2.6.1 General Methods

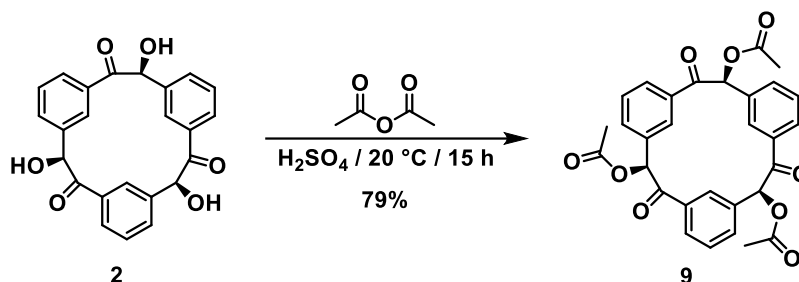
Column chromatography was performed on silica gel 60 (32–63 μm). Analytical TLC was performed on J. T. Baker plastic-backed silica gel IB-F plates. NMR data was collected on a JEOL ECA-500 MHz or ECA-600 MHz spectrometers, with working frequencies (for ¹H nuclei) of 500 and 600 MHz, respectively. Chemical shifts are given in ppm (δ) and are

referenced to the residual CDCl_3 solvent peak at 7.26 ppm (^1H NMR) and 77.16 ppm (^{13}C NMR) or $(\text{CD}_3)_2\text{SO}$ solvent peak at 39.52 ppm (^{13}C NMR). Conventional one-dimensional (1D) ^1H NMR and $^{13}\text{C}\{^1\text{H}\}$ NMR experiments were recorded at room temperature under routine conditions. All ^{13}C NMR spectra were recorded with the simultaneous decoupling of ^1H nuclei. NMR data was analyzed using Delta NMR data processing software. Melting points were measured in a Barnstead International Mel-TEMP apparatus and are uncorrected. Infrared spectra were recorded on a Nicolet iS10 FT-IR spectrometer equipped with a Thermo Scientific iTR for multi-purpose ATR sampling. High Resolution Mass Spectra (HRMS) were performed at the University of Texas at Austin mass spectrometry facility on an Agilent 6530 Q-TOF spectrometer.

All reactions were performed at room temperature in clean oven dried glassware. The following starting materials and solvents were obtained from the respective commercial sources and used without further purification: terephthalaldehyde and 2-methoxyethanol (Oakwood); isophthalaldehyde (AKSci); NaCN , Ac_2O , and propionic anhydride (Sigma); isobutyric anhydride (EMD Millipore); dichloromethane (Fisher); H_2SO_4 (Macron); CDCl_3 , CD_3CN (Cambridge Isotope Labs). Compounds **2** and **4** were prepared as previously reported.^{50,53}

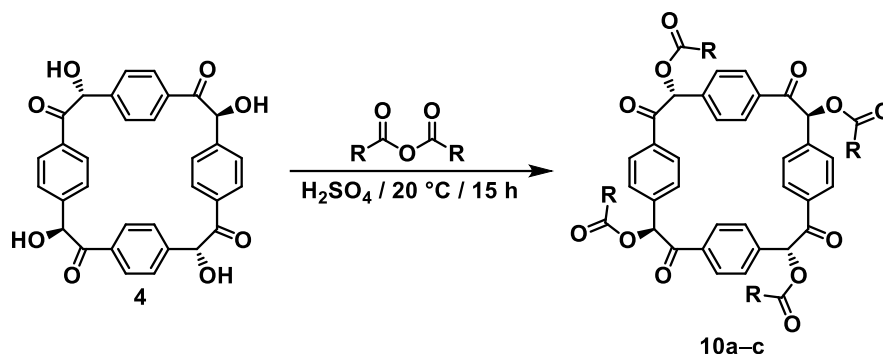
2.6.2 Synthetic Procedures and Characterization

Synthesis of **9**



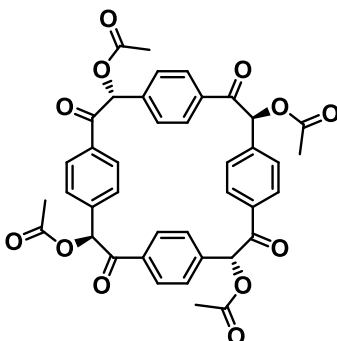
Cyclotribenzoin (**2**, 250 mg, 0.31 mmol) and Ac_2O (1.70 g, 17.0 mmol) were added to a 10 mL round bottom flask equipped with a stir bar. Mixture was stirred until homogenous and then H_2SO_4 (few drops) was added. The mixture was stirred at room temperature for 15 h, and then neutralized with 1M solution of NaOH (1 mL) and added to a separatory funnel containing CH_2Cl_2 (100 mL) and H_2O (100 mL). Shaking of the reaction mixture produced a white suspension, which was left to stand, allowing the layers to separate. White organic layer was collected, and the solvent was evaporated by rotary evaporator to obtain a white solid. Purification by column chromatography on silica gel (EtOAc/hexanes 8:2) yielded compound **9** as a white solid (259 mg, 79%). mp 255–256 $^\circ\text{C}$. ^1H NMR (CDCl_3 , 600 MHz) δ : 8.54 (s, 3H), 7.82 (d, $J=7.8$ Hz, 3H), 7.58 (d, $J=7.8$, 3H), 7.33 (t, $J=7.2$, 3H), 7.1 (s, 3H), 2.35 (s, 9H) ppm. ^{13}C NMR (CDCl_3 , 150 MHz) δ : 191.98, 171.47, 134.08, 133.53, 133.36, 130.05, 129.6, 76.85, 21.08 ppm. FTIR $\tilde{\nu}$: 2936, 1740, 1694, 1371, 1221, 1179, 1058, 990, 795, 691, 536, 514 cm^{-1} . HRMS (ESI, $[\text{M}+\text{Na}]^+$) m/z calculated for $\text{C}_{30}\text{H}_{24}\text{O}_9$: 551.1313, found 551.1317. Anal. calculated for $\text{C}_{30}\text{H}_{24}\text{O}_9$: C, 68.18; H, 4.58. Found: C, 67.83; H, 4.34.

Synthesis of 10a–c



Cyclotetrabenzoin (**4**, 250 mg, 0.466 mmol) and an acyl anhydride (26.5 mmol) were added to a 10 mL round bottom flask equipped with a stir bar. Mixture was stirred until homogenized, and then H_2SO_4 (few drops) was added.³ Reaction mixture was stirred at room temperature for 15 h. Then, the mixture was neutralized with 1M solution of NaOH (1 mL) and added to a separatory funnel containing CH_2Cl_2 (100 mL) and H_2O (100 mL). Shaking the reaction mixture produced a white suspension, which was left to settle, and the layers were allowed to separate. White organic layer was collected and then solvent was evaporated by rotary evaporator to get a white solid. Purification by column chromatography on silica gel (EtOAc/hexanes, 8:2) yielded the desired white solid.

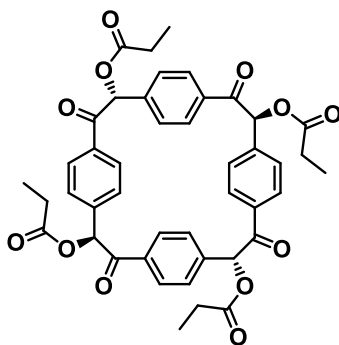
Synthesis of 10a



Refer to the general procedure above. Upon purification, compound **10a** was obtained as a white solid (192 mg, 58%), mp $271\text{--}273\text{ }^\circ\text{C}$. ^1H NMR (CDCl_3 , 600 MHz) δ : 7.88 (d, $J=8\text{ Hz}$, 8H),

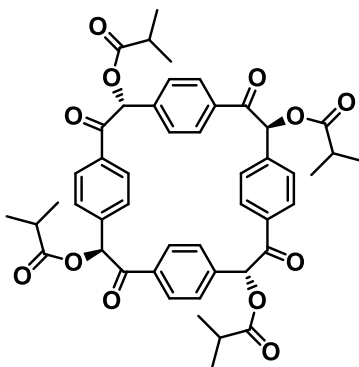
7.43 (d, $J=8$ Hz, 8H), 7.03 (s, 4H), 2.08 (s, 12H) ppm. ^{13}C NMR (DMSO- d_6 , 150 MHz) δ : 192.36, 170.09, 139.25, 134.10, 130.04, 130.00, 77.26, 20.85 ppm. FTIR: $\tilde{\nu}$: 2968, 1742, 1693, 1610, 1368, 1227, 1064, 981, 862, 819, 705, 598 cm^{-1} . HRMS (ESI, $[\text{M}+\text{Na}]^+$) m/z calculated for $\text{C}_{40}\text{H}_{32}\text{O}_{12}$: 727.1796, found 727.1786. Anal. calculated for $\text{C}_{40}\text{H}_{32}\text{O}_{12}$: C, 68.18; H, 4.58. Found: C, 67.18; H, 4.02.

Synthesis of 10b



Refer to general procedure above. Upon purification, compound **10b** was obtained as a white solid (269 mg, 76%), mp 265–267 °C. ^1H NMR (CDCl_3 , 600 MHz) δ : 7.76 (d, $J=8.4$ Hz, 8H), 7.32 (d, $J=8.4$ Hz, 8H), 6.73 (s, 4H), 2.47 (m, 8H), 1.16 (t, $J=7.8$ Hz, 12H) ppm. ^{13}C NMR (CDCl_3 , 150 MHz) δ : 191.48, 173.60, 136.98, 134.00, 129.80, 129.18, 77.22, 27.36, 9.02 ppm. FTIR $\tilde{\nu}$: 2983, 2942, 1730, 1693, 1607, 1342, 1165, 1082, 957, 924, 811, 708, 538 cm^{-1} . HRMS (ESI, $[\text{M}+\text{Na}]^+$) m/z calculated for $\text{C}_{44}\text{H}_{40}\text{O}_{12}$: 783.2412, found 783.2429. Anal. calculated for $\text{C}_{44}\text{H}_{40}\text{O}_{12} \cdot (\text{CH}_3)_2\text{O}$: C, 68.35; H, 5.35. Found: C, 68.50; H, 5.07.

Synthesis of **10c**



Refer to the general procedure above. Upon purification, compound **10c** was obtained as a white solid (0.308 g, 81%, mp 276–278°C). ¹H NMR (CDCl₃, 600 MHz) δ : 7.77 (d, J =8.4 Hz, 8H), 7.33 (d, J =8.4 Hz, 8H), 6.7 (s, 4H), 2.69 (septet, 4H), 1.23 (d, J =6.6 Hz, 12H), 1.17 (d, J =6.6 Hz, 12H) ppm. ¹³C NMR (CDCl₃, 125 MHz) δ : 191.65, 176.24, 138.99, 134.04, 129.76, 128.95, 77.18, 33.84, 19.03, 18.80 ppm. FTIR $\tilde{\nu}$: 2975, 1729, 1699, 1609, 1228, 1186, 1143, 1073, 965, 933, 808, 702 cm⁻¹. HRMS (ESI, [M+Na]⁺) m/z calculated for C₄₈H₄₈O₁₂: 839.3038, found 839.3048. Anal. calculated for C₄₈H₄₈O₁₂: C, 70.58; H, 5.92. Found: C, 70.15; H, 5.63.

2.6.3 Crystal Growth Conditions and X-ray Crystallographic Analysis

All diffraction measurements were performed on a Bruker DUO platform diffractometer equipped with a 4K CCD APEX II detector and an Incoatec 30 W Cu microsource with compact multilayer optics. A hemisphere of data (2713 frames at 4 cm detector distance) was collected using a narrow-frame algorithm with scan widths of 0.50 % in omega and an exposure time of 25 s/frame. The data were integrated using the Bruker-Nonius SAINT program, with the intensities corrected for Lorentz factor, polarization, air absorption, and absorption due to variation in the path length through the detector faceplate. The data were scaled, and an absorption correction was applied using SADABS. Redundant reflections were averaged. Final

cell constants were refined using independent reflections having $I > 10\sigma(I)$. All of the solvent sites contain some disorder, resulting in an average of the solvent orientation at the specific location.

Crystal Growth of **9**

Purified solid of **9** (2 mg) was dissolved in CHCl₃ (1 mL) in a vial. Vial was covered with parafilm with small holes formed with 30-gauge needle and allowed to slowly evaporate. These crystals were colourless and cubic-shaped.

Table 2.4 Crystal Data and Structure Refinement Parameters for Compound **9**·*n*CHCl₃

Empirical formula	C ₃₁ H ₂₅ Cl ₃ O ₉	
Formula weight	647.86	
Temperature	123(2) K	
Wavelength	1.54178 Å	
Crystal system	Triclinic	
Space group	$P\bar{1}$	
Unit cell dimensions	$a = 9.0924(2)$ Å	$\alpha = 76.930(1)^\circ$
	$b = 10.4187(3)$ Å	$\beta = 78.049(1)^\circ$
	$c = 15.9902(4)$ Å	$\gamma = 86.009(1)^\circ$
Volume	1443.13(6) Å ³	
<i>Z</i>	2	
Density (calculated)	1.491 Mg/m ³	
Crystal size	0.23 × 0.05 × 0.03 mm ³	
Reflections collected	16238	
Independent reflections	4955 [$R(\text{int}) = 0.0239$]	

Table 2.4 Continued

Refinement method	Full-matrix least-squares on F^2
Data / restraints / parameters	4955 / 90 / 428
Goodness-of-fit on F^2	1.032
Final R indices [$I > 2\sigma(I)$]	$R_1 = 0.0553$, $wR_2 = 0.1529$
R indices (all data)	$R_1 = 0.0574$, $wR_2 = 0.1550$
Largest diff. peak and hole	0.80 and $-0.55 \text{ e}/\text{\AA}^{-3}$

Crystal Growth of **10a**

Single crystals of **10a**·*n*EtOAc were fortuitously grown in column fractional tubes upon purification. Colourless cubic-shaped crystals grew on the walls of the test tubes and were of sufficient quality for single crystal X-ray diffraction. The second batch of crystals was grown by dissolving purified solids of **10a** (2mg) in 1 mL of Me₂CO in a vial covered in parafilm and punctured with a 30-gauge needle. After three days of slow evaporation colourless cubic-shaped crystals were produced. To produce “empty” crystals of **10a**, single crystals of **10a**·*n*Me₂CO (prepared as just described) were dried with supercritical CO₂ using a Samdri-PVT-3D apparatus. Crystals were loaded into the holding chamber in dry EtOH, and then flushed with CO₂ until EtOH was no longer present in the purge tube.

Table 2.5 Crystal Data and Structure Refinement Parameters for Compound **10a**·*n*EtOAc/Hex

Empirical formula	C ₄₀ H ₃₂ O ₁₂ , C ₄ H ₈ O ₂ , 0.2(C ₆ H ₁₄)
Formula weight	809.99
Temperature	132(2) K
Wavelength	1.54178 Å

Table 2.5 Continued

Crystal system	Tetragonal	
Space group	$P\bar{4}2_1c$	
Unit cell dimensions	$a = 14.2340(3) \text{ \AA}$	$\alpha = 90^\circ$
	$b = 14.2340(3) \text{ \AA}$	$\beta = 90^\circ$
	$c = 10.2135(4) \text{ \AA}$	$\gamma = 90^\circ$
Volume	2069.32(7) \AA^3	
Z	2	
Density (calculated)	1.300 Mg/m ³	
Crystal size	0.30 × 0.30 × 0.15 mm ³	
Reflections collected	14186	
Independent reflections	1928 [$R(\text{int}) = 0.0253$]	
Refinement method	Full-matrix least-squares on F^2	
Data / restraints / parameters	1764 / 5 / 152	
Goodness-of-fit on F^2	1.080	
Final R indices [$I > 2\sigma(I)$]	$R_1 = 0.0331$, $wR_2 = 0.0901$	
R indices (all data)	$R_1 = 0.0340$, $wR_2 = 0.0923$	
Largest diff. peak and hole	0.243 and $-0.217 \text{ e/\AA}^{-3}$	

Table 2.6 Crystal Data and Structure Refinement Parameters for Compound **10a**· $n\text{Me}_2\text{CO}$

Empirical formula	$\text{C}_{40}\text{H}_{32}\text{O}_{12} \cdot \text{C}_{3.41}\text{H}_{6.82}\text{O}_{1.14}$
Formula weight	770.63
Temperature	123(2) K
Wavelength	0.71073 \AA
Crystal system	Tetragonal

Table 2.6 Continued

Space group	$P\bar{4}2_1c$	
Unit cell dimensions	$a = 14.2362(17) \text{ \AA}$	$\alpha = 90^\circ$
	$b = 14.2362(17) \text{ \AA}$	$\beta = 90^\circ$
	$c = 10.2880(12) \text{ \AA}$	$\gamma = 90^\circ$
Volume	$2085.1(6) \text{ \AA}^3$	
<i>Z</i>	2	
Density (calculated)	1.227 Mg/m^3	
Crystal size	$0.81 \times 0.62 \times 0.40 \text{ mm}^3$	
Reflections collected	15450	
Independent reflections	2583 [$R(\text{int}) = 0.0150$]	
Refinement method	Full-matrix least-squares on F^2	
Data / restraints / parameters	2583 / 177 / 198	
Goodness-of-fit on F^2	1.076	
Final <i>R</i> indices [$I > 2\sigma(I)$]	$R_1 = 0.0329$, $wR_2 = 0.0887$	
<i>R</i> indices (all data)	$R_1 = 0.0335$, $wR_2 = 0.0894$	
Largest diff. peak and hole	0.27 and -0.15 e/\AA^{-3}	

Table 2.7 Crystal Data and Structure Refinement Parameters for Compound **10a**

Empirical formula	$\text{C}_{40}\text{H}_{32}\text{O}_{12}$
Formula weight	704.65
Temperature	123(2) K
Wavelength	1.54178 \AA
Crystal system	Tetragonal
Space group	$P\bar{4}2_1c$

Table 2.7 Continued

Unit cell dimensions	$a = 14.1566(6) \text{ \AA}$	$\alpha = 90^\circ$
	$b = 14.1566(6) \text{ \AA}$	$\beta = 90^\circ$
	$c = 10.2623(4) \text{ \AA}$	$\gamma = 90^\circ$
Volume	$2056.66(19) \text{ \AA}^3$	
Z	2	
Density (calculated)	1.138 Mg/m^3	
Crystal size	$0.41 \times 0.22 \times 0.18 \text{ mm}^3$	
Reflections collected	13454	
Independent reflections	1816 [$R(\text{int}) = 0.0271$]	
Refinement method	Full-matrix least-squares on F^2	
Data / restraints / parameters	1816 / 0 / 119	
Goodness-of-fit on F^2	1.088	
Final R indices [$I > 2\sigma(I)$]	$R_1 = 0.0250$, $wR_2 = 0.0685$	
R indices (all data)	$R_1 = 0.0250$, $wR_2 = 0.0685$	
Largest diff. peak and hole	0.20 and -0.12 e/\AA^{-3}	

Crystal Growth of 10b

Purified solids of **10b** (2mg) were dissolved in 1 mL of Me₂CO in a vial which was covered in parafilm and punctured with a 30-gauge needle. After four days colourless needle-like crystals were produced.

Table 2.8 Crystal Data and Structure Refinement Parameters for Compound **10b**·*n*Me₂CO

Empirical formula	C ₅₀ H ₅₂ O ₁₄
Formula weight	876.91

Table 2.8 Continued

Temperature	123(2) K	
Wavelength	1.54178 Å	
Crystal system	Monoclinic	
Space group	$P2_1/n$	
Unit cell dimensions	$a = 16.8259(4)$ Å	$\alpha = 90^\circ$
	$b = 10.7519(3)$ Å	$\beta = 94.1570(10)^\circ$
	$c = 24.8956(6)$ Å	$\gamma = 90^\circ$
Volume	4492.0(2) Å ³	
Z	4	
Density (calculated)	1.297 Mg/m ³	
Crystal size	0.10 × 0.07 × 0.04 mm ³	
Reflections collected	29206	
Independent reflections	7878 [$R(\text{int}) = 0.0385$]	
Refinement method	Full-matrix least-squares on F^2	
Data / restraints / parameters	7878 / 90 / 600	
Goodness-of-fit on F^2	1.026	
Final R indices [$I > 2\sigma(I)$]	$R_1 = 0.0467$, $wR_2 = 0.1223$	
R indices (all data)	$R_1 = 0.0560$, $wR_2 = 0.1288$	
Largest diff. peak and hole	0.31 and -0.33 e/Å ⁻³	

Crystal Growth of 10c

Purified solids of **10c** (2mg) were dissolved in 1 mL of CS₂ in a vial covered in parafilm which was punctured by a 30-gauge needle. Several vials were set up at the same time and placed

inside a secondary container and closed and left in the hood. After several weeks colourless needle-like crystals were produced.

Table 2.9 Crystal Data and Structure Refinement Parameters for Compound **10c**·*n*CS₂

Empirical formula	C _{48.62} H ₄₈ O ₁₂ S _{1.23}	
Formula weight	863.78	
Temperature	123(2) K	
Wavelength	1.54178 Å	
Crystal system	Tetragonal	
Space group	<i>P</i> 4/ <i>n</i>	
Unit cell dimensions	<i>a</i> = 18.8252(7) Å	<i>α</i> = 90°
	<i>b</i> = 18.8252(7) Å	<i>β</i> = 90°
	<i>c</i> = 6.6536(4) Å	<i>γ</i> = 90°
Volume	2358.0(2) Å ³	
<i>Z</i>	2	
Density (calculated)	1.217 Mg/m ³	
Crystal size	0.22 × 0.04 × 0.01 mm ³	
Reflections collected	8717	
Independent reflections	2078 [<i>R</i> (int) = 0.0565]	
Refinement method	Full-matrix least-squares on <i>F</i> ²	
Data / restraints / parameters	2078 / 114 / 166	
Goodness-of-fit on <i>F</i> ²	1.123	
Final <i>R</i> indices [<i>I</i> > 2σ(<i>I</i>)]	<i>R</i> ₁ = 0.0755, w <i>R</i> ₂ = 0.1962	
<i>R</i> indices (all data)	<i>R</i> ₁ = 0.0869, w <i>R</i> ₂ = 0.2032	
Largest diff. peak and hole	0.34 and −0.24 e/Å ^{−3}	

2.6.4 Gas Sorption Experiments

A Micromeritics ASAP2020 plus physisorption instrument was used for all porosity measurements. Data collected were analyzed using MicroActive data processing. Single crystals were grown in respective slow evaporation conditions. Samples were active by drying with supercritical CO₂ using a Samdri-PVT-3D apparatus. Crystals were loaded into the holding chamber in dry EtOH, and then flushed with CO₂ until EtOH was no longer present in the purge tube, the degassing at 30 °C for 15 h in vacuo.

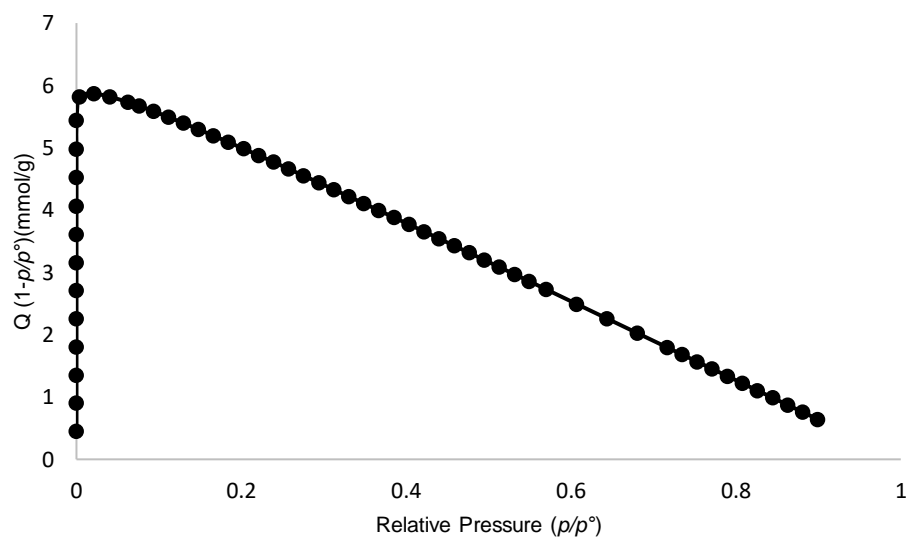


Figure 2.15 Rouquerol plot for N₂ gas sorption within the crystals of **10a**.

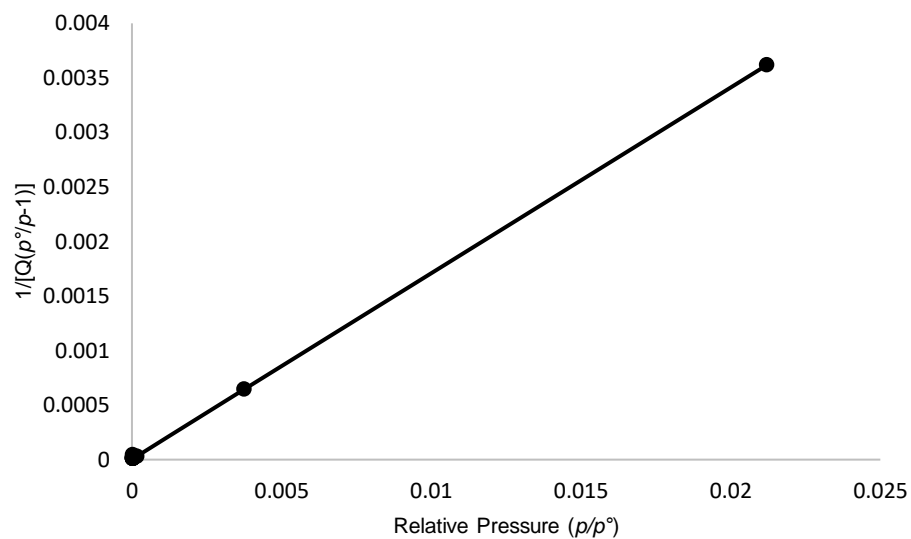


Figure 2.16 BET surface area plot for gas sorption within crystals of **10a**. BET surface area: $572.4 \pm 0.3135 \text{ m}^2 \text{ g}^{-1}$; C Constant = 58769.07; $R^2 = 0.9999996$.

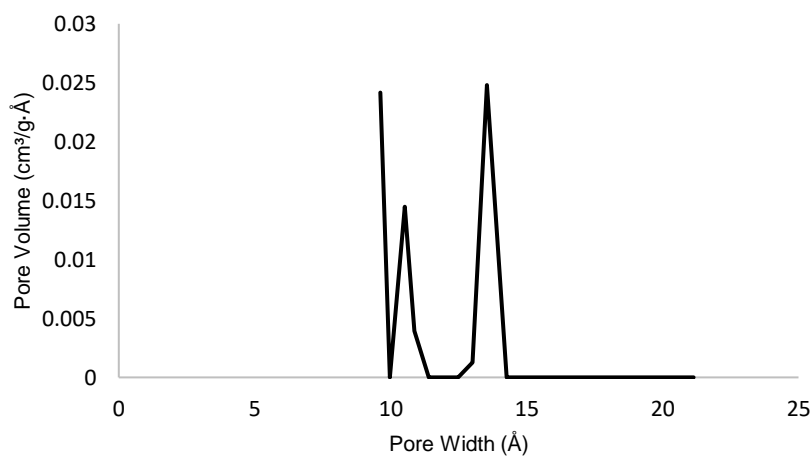


Figure 2.17 NLDFT pore size distribution for crystals of **10a**.

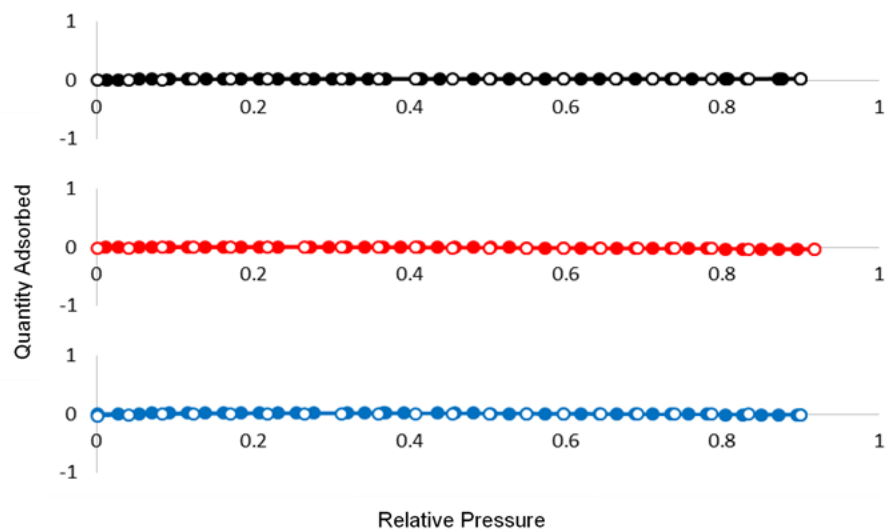


Figure 2.18 Nitrogen gas sorption (77 K) plot for crystals of **10b**, **10c**, and **9** in black red and blue successively. Filled symbols indicate adsorption, empty symbols indicate desorption.

Chapter Three Cyclobenzoin Esters as Hosts for Thin Guests

3.1 Crystal Types and Crystal Growth

A crystalline material is a solid composed of molecules, atoms, or ions organized in a highly ordered lattice. For a solid to be a crystal, the components need to form a periodic arrangement. These repeating units are characterized by a unit cell, which is a small imaginary box that includes the smallest non-repeating components. To form the entire structure these unit cells can be repeated and stacked without leaving any gaps; in other words, they possess translational symmetry. This class of solids can be further subdivided into quasicrystals, polycrystals, and single crystals. These three groups differ in the microscopic arrangement of the lattice components. Quasicrystals are solids whose structure is ordered but not periodic. While the lattice pattern can continuously fill available space, it lacks translational symmetry. The first naturally occurring quasicrystal— $\text{Al}_{63}\text{Cu}_{24}\text{Fe}_{13}$ —was reported in 2009.²⁷⁴ It was discovered in a rock sample from the Koryak Mountains in Russia and was found to have icosahedral symmetry.²⁷⁵ The second natural quasicrystal was isolated in 2015 from the same rock sample, and is the first natural known quasicrystal with decagonal symmetry.²⁷⁶ While quasicrystals have an ordered structure, polycrystalline materials are composed of several crystals fused together while lacking order. A common example of this is ice, as water begins to freeze small crystals form until they fuse with other crystals, forming a polycrystalline structure. Common polycrystalline materials include metals, ceramics, and rocks.

Since crystals have other symmetry operators, there are 219 possible crystallographic space groups. These space groups can be split into seven categories based on symmetry: cubic, hexagonal, monoclinic, orthorhombic, tetragonal, triclinic, and trigonal.²⁷⁷ All of these symmetry groups will form solids that have flat faces and sharp angles often visible on the

macroscopic level. Their specific arrangement lends each crystal unique mechanical,^{278,279} optical,²⁸⁰ and electrical properties.²⁸¹ Of these—quasicrystals, polycrystals, and single crystals—single crystals are of greater interest to us as they enable structure determination by X-ray diffraction.

In 1971, Schmidt was the first to coin the term *crystal engineering* when working on photodimerization of cinnamic acid.²⁸² He defined it specifically in relation to photodimers and the ability to predict configuration and neighbors, dependence of crystal texture on *cis* or *trans* reaction pathway, and packing principles of organic molecules to construct light-stable crystals. He broke crystal engineering down into four phases (a) the experimental correlation of crystal structure with stability, (b) limits of topological correlation of physical structure and chemical behavior, (c) intermolecular forces responsible for the stability of crystalline lattice, and (d) ability to control molecular packing arrangements. A broader definition by Desiraju in 1988 was introduced, defining crystal engineering as the utilization of known supramolecular interactions in crystal packing to design new solids with desired physical and chemical properties.²⁸³ Weak non-covalent interactions are the dominant driving force in growing crystals in porous molecular crystals (PMCs). Commonly studied non-covalent interactions are hydrogen bonding and π – π stacking; both have proven strong enough to support PMCs.^{112,221} These interactions form between known groups, which enables predictions in possible directional interactions. However, as seen before, van der Waals forces, which are the weakest non-covalent interactions can be strong enough to support PMCs also.²⁶⁷ To obtain single crystals, careful control of environment is necessary to facilitate the organization of crystal components as even minor vibrations can disrupt the alignment of molecules. With previous successful crystal growth by vapor diffusion and slow evaporation conditions, we continued to

utilize these conditions. Crystal growth mechanisms of porous materials with directional interactions^{284–286} are not well understood and our understanding in a system lacking directional interactions are deficient as well. Our PMCs form easily reproducible crystals indicating the inherent stability of packing interactions; however, mechanistic studies and calculations need to be done to have a full understanding of the packing formation.

3.2 Host-Guest Complexes with Thin Molecular Guests

Host-guest chemistry is an area of supramolecular chemistry that describes complexes that are composed of two or more molecules which are held together in a unique structural relationship. Of the two interacting components the “host” is defined as the larger molecule and it incorporates the smaller “guest” into its structure.²⁸⁷ These relationships are not held together by covalent bonds, but instead by non-covalent interactions. These interactions can be divided into five categories: ionic bonding, hydrogen or halogen bonds, π – π stacking, Van der Waals forces, and hydrophobic interactions.²⁸⁸ A variety of molecules, including macrocycles, cages, planar π -conjugated compounds, and hydrogen-bonding molecules have been synthesized as host compounds.^{74,289–293} Common guest molecules include aromatics, alcohols, amides, cycloalkanes, and carboxylic acids have been found to create host-guest complexes.^{294–302} Alkynes are a group of particular interest as they are commonly used as reagents for catalysis and subunits of medicinal drugs.³⁰³ Complexes formed with alkynes have been studied for their molecular shapes, conformations, and intermolecular interactions.^{304–306} Several alkyne sensing interactions take place through coordination bonds to facilitate desired reactions to take place,^{309–311} while there are a few examples that show alkyne sensing by Van der Waals interactions.

The design and development of host molecules for linear alkynes has been around since Yuhas and coworkers reported urea crystalizing with a variety of alkynes.³¹² They were able to crystalize complexes containing urea with several alkynes composed of nine or ten carbons out of a methanol solution. Monoalkylacetylene and dialkylacetylene as well as substituted dialkylacetylene successfully formed complexes when the alkyne was located close to the terminus of the chain. Ureas were found to form inclusion compounds with long chain liquid alkynes stabilized by van der Waals interactions from the zigzag conformation of aliphatic alkynes.

Acyclic v-shaped disubstituted adamantane compounds were initially shown to form discrete cyclic dimers upon crystallization, that could accommodate small molecules.³⁰⁷ The adamantane compounds substituted with electron-rich phenol derivatives were found to complex with electron-deficient guest molecules through donor-acceptor interactions.³¹³ Modification of the phenol groups to chloropyrazine or chloropyrimidine were found to form host-guest complexes with various cycloalkanes, cycloalkenes, and aromatics.^{314,315} Further extension of the adamantane substituted arms were able to then include 2-hexyne and 3-hexyne as guest molecules.³⁰³ Upon crystallization, dimers formed which were held together through $\text{CH}\cdots\pi$ interactions between the hydrogen atoms of the methylene and adamantane units. Two dimers of the complex are held together through $\text{CH}\cdots\text{O}$ interactions between the benzene rings and oxygen of the methoxy groups. This arrangement forms channels that are composed of four host molecules and two guest molecules (Figure 3.1). The guests are stabilized by short contacts of the type: (a) $\text{CH}\cdots\pi$ formed between the aromatic hydrogens and alkyne and (b) $\text{CH}\cdots\text{O}$ between guest hydrogens and host methoxy oxygens. When a mixture of 1-hexyne and 2- or 3-

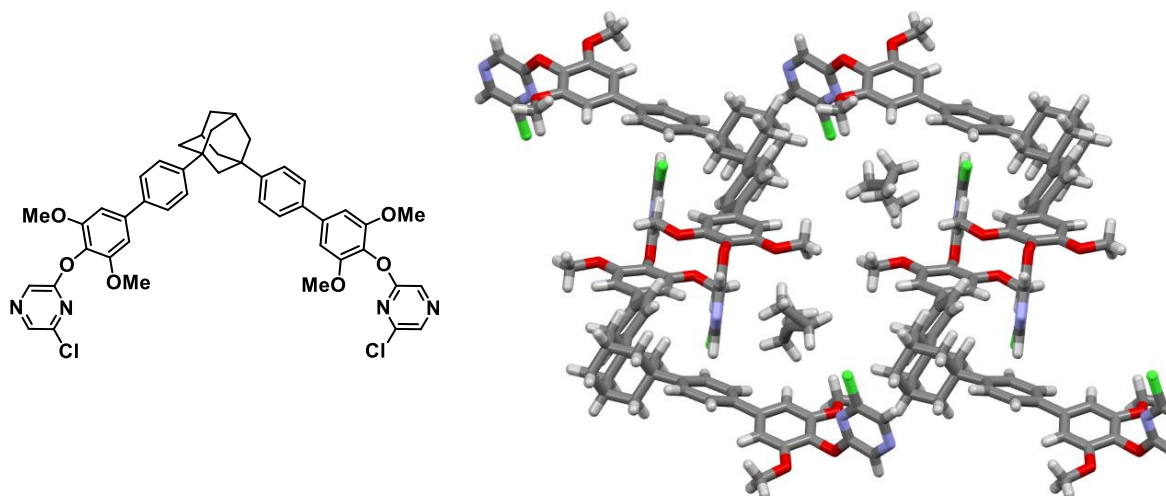


Figure 3.1 Structure of adamantane derivative and resulting crystal structure with two molecules of 3-hexyne located in the created channels, viewed along the crystallography *a* axis. Element colors: C—grey, O—red, N—blue, Cl—green, H—white.

hexyne were used as co-solvents, crystals only containing 2- or 3-hexyne were found. It was concluded that this was due to the lack of CH_2 groups on both sides of the alkyne to stabilize the guest within the host channels. The authors were able to develop a host that could crystalize liquid alkynes, utilizing van der Waals interactions for stabilization.

In the context of gas separation, control over the size, shape, and chemistry of the pores has led to the expansion of new classes of materials. Designing of materials for acetylene (C_2H_2) separation from ethylene (C_2H_4) for industrial processes are necessary for production of pure products for polymerization.^{316–320} It was found that MOFs with a secondary binding unit (SBU) of SiF_6^{2-} had a high affinity for binding C_2H_2 . The metal cluster of SiF_6^{2-} is weakly basic while C_2H_2 is weakly acidic, creating a preferential binding.^{321,322} While MOFs and zeolites^{323–326} have shown selectivity in gas separation, new ultramicroporous materials have shown superior selectivity. This is due to the tight binding sites that are highly selective towards specific gas molecules.³²⁷ Ultramicroporous materials are often octahedral metal centers, with equatorially bound nitrogen-donor linker ligands and inorganic linker anions. The nitrogen-donor ligands

cross-link metal centers to give square grids that are pillared by the inorganic anions. The pore size and electrostatics of the crystal structure can be controlled by either the nitrogen-donor or inorganic anion respectively. While size exclusion was proven successful in gas studies, we explored if the same principles could be utilized with liquid guest molecules. Herein we report the selective encapsulation of thin guest molecules in a PMC with small intrinsic pores.

3.3 Thin Guest Inclusion

Previously we have shown the simple synthesis of cyclotetrabenzoin esters and determined their crystal structures.²⁶⁷ Crystal structures of cyclotetrabenzoin esters showed both intrinsic and extrinsic pores (**10a** and **10c**, Figure 3.2), while **10b** showed no discernible pores. Compound **10a** could be crystalized from two different solvents while resulting in the

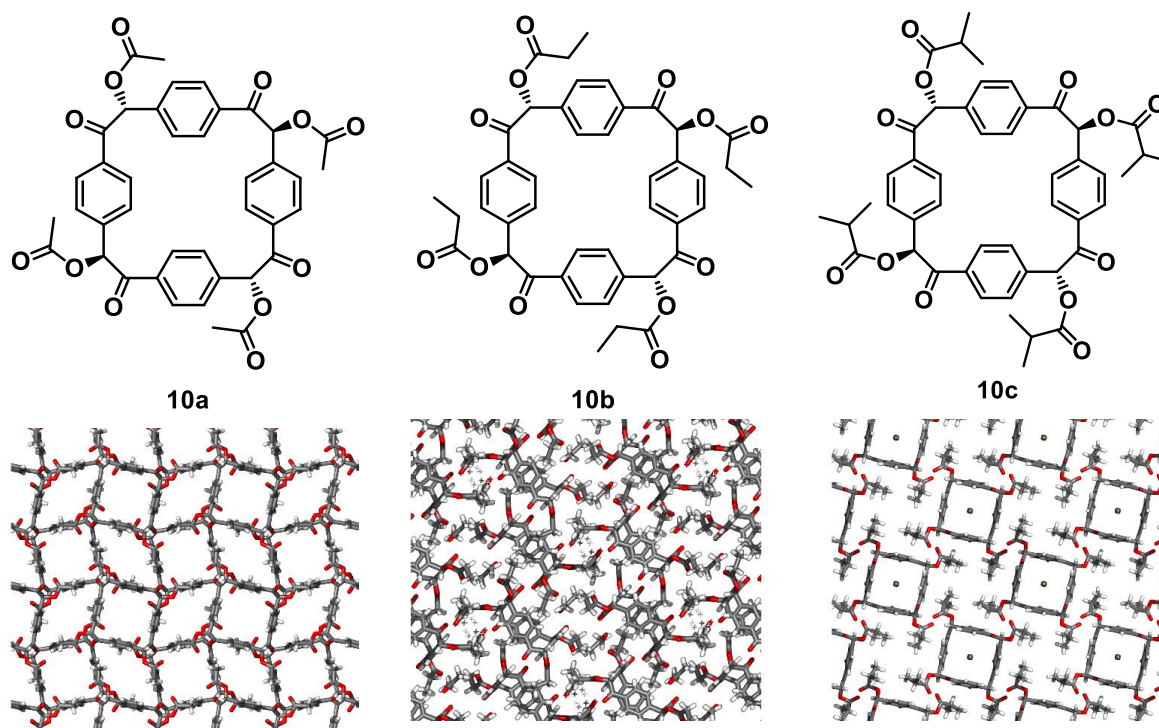


Figure 3.2 Cyclotetrabenzoin ester structures and the resulting crystal packing.

same packing method. It was also found to be permanently porous upon solvent removal which resulted in a BET surface area of $572 \pm 16 \text{ m}^2 \text{ g}^{-1}$, calculated from N_2 isotherm, a respectable value for a structure composed of only a macrocycle compared to other reported BET surface areas of $494\text{--}760 \text{ m}^2 \text{ g}^{-1}$.^{98,99,242,328,329} Also reported was the ability to host a thin guest within the small central cavity, **10c**. Viewed along the crystallographic *b* axis, disordered CS_2 molecules were all aligned along the axis that passes through the center of the cyclotetrabenzoin ring, in an overall arrangement which resembled an insulated wire. This arrangement suggests that **10a–c** can act as supramolecular hosts for guests that are thin enough to fit into their cavities. While in the solid-state arrangements of the macrocycles are all different, the intrinsic square pore remains roughly the same with size measuring between 6.93×6.93 and 7.08×7.08 Å. To explore the possible applications of the intrinsic pore, mimicking the geometry of CS_2 was explored by first using acetonitrile as the solvent. We presumed the terminal nitrile would behave in the same manner as CS_2 . Since acetonitrile has a low boiling point, slow evaporation crystal growth experiments with **10a–c** were set up and produced single cubic crystals of **10a**, while **10b** and **10c** only generated amorphous or polycrystalline precipitates. Upon X-ray diffraction analysis, the packing pattern of **10a** is the same as what was previously reported,²⁶⁷ however the acetonitrile solvent molecules were located with the cyano group inside the intrinsic pore. The acetonitrile molecules are disordered over four orientations, when viewed along the crystallographic *b* axis the nitrogen atom is clearly visible inside the pore of **10a** (Figure 3.3).

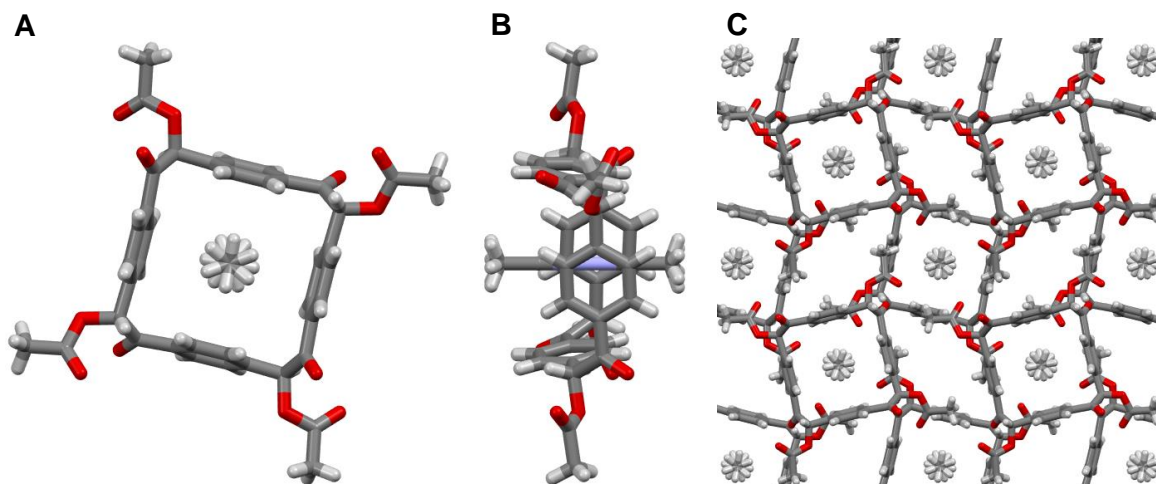


Figure 3.3 A) Viewed along the crystallographic *c* axis shows the acetonitrile disordered inside the intrinsic pore of **10a**. B) Viewed along the crystallographic *b* axis where the nitrogen is clearly visible inside **10a**. C) Packing structure of the crystal viewed along the crystallographic *c* axis. Element colors: C—grey, O—red, N—blue, H—white.

The organization of molecules of **10a** into two-dimensional sheets with acetonitrile involves no discernible strong noncovalent interactions. Notable are only short (2.95 Å) contacts established between the hydrogens of the methyl group on one molecule and the ester carbonyl oxygens on another molecule (Figure 3.4). These contacts repeat themselves on each

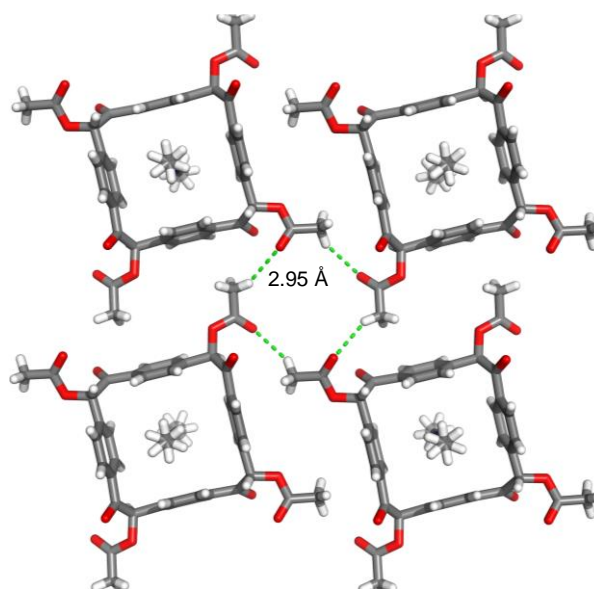


Figure 3.4 Contacts in the plane of the ring of **10a** are established between the methyl hydrogen and ester carbonyl oxygens. Element colors: C—grey, O—red, N—blue, H—white.

of the four corners of **10a**, organizing the molecules into a square grid. Neighboring sheets are rotated by $\pm 27.8^\circ$ (measured as the angle between planes of benzene rings in molecules of **10a** in neighboring sheets) with respect to each other. Again, vertical alignment involves no strong directional interactions. Neighboring sheets are connected by [C–H \cdots O] contacts between (a) ketone oxygen in one molecule and hydrogens on two aromatic rings in its neighbor (2.72 and 2.84 Å, Figure 3.5A), (b) ester carbonyl oxygen in one molecule and hydrogens on two aromatic rings in its neighbor (2.78 and 2.81 Å, Figure 3.5B), and (c) ketone oxygen in one molecule and AcOC–H hydrogen in its neighbor (2.28 Å, Figure 3.5C). The molecules of acetonitrile form four additional short contact with **10a** within the same layer between the nitrogen and the π system of each benzene ring (3.54 Å, Figure 3.6 measures as the distance from the centroid of the benzene ring).

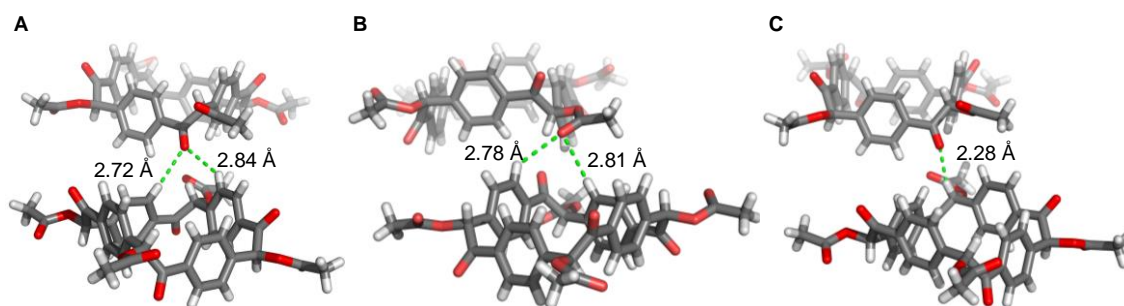


Figure 3.5 Contacts in the plane perpendicular to the ring plane of **10a** are established between A) ketone oxygen and hydrogens on two aromatic rings, B) ester carbonyl oxygen and hydrogens on two aromatic rings, and C) ketone oxygen and AcOC–H hydrogen. Element colors: C—grey, O—red, N—blue, H—white.

Encouraged by this success, we expanded our study to a variety of thin guest molecules, including liquid and solid guests. Slow evaporation was chosen as the method for crystal growth for two reasons; first, this was the method that has successfully produced crystals of the parent macrocycles, and second, no potentially competing guest molecules would be added to the environment. For both liquid-liquid diffusion and vapor diffusion crystal growth methods two liquids are required, which would introduce solvent molecules which could compete with the

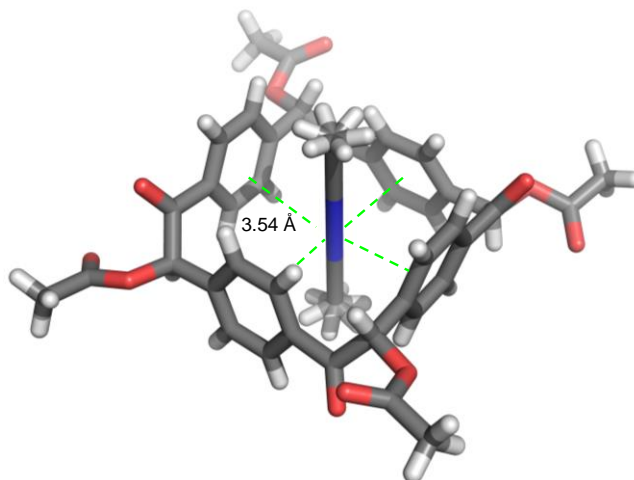


Figure 3.6 Four repeating short contacts formed between the nitrogen of acetonitrile and the centroid of each benzene ring. Element colors: C—grey, O—red, N—blue, H—white.

desired guest molecule. Explored guest molecules included liquid and solid aliphatic and aromatic alkynes and nitriles (Figure 3.7). Solid guests were dissolved in a small amount of a

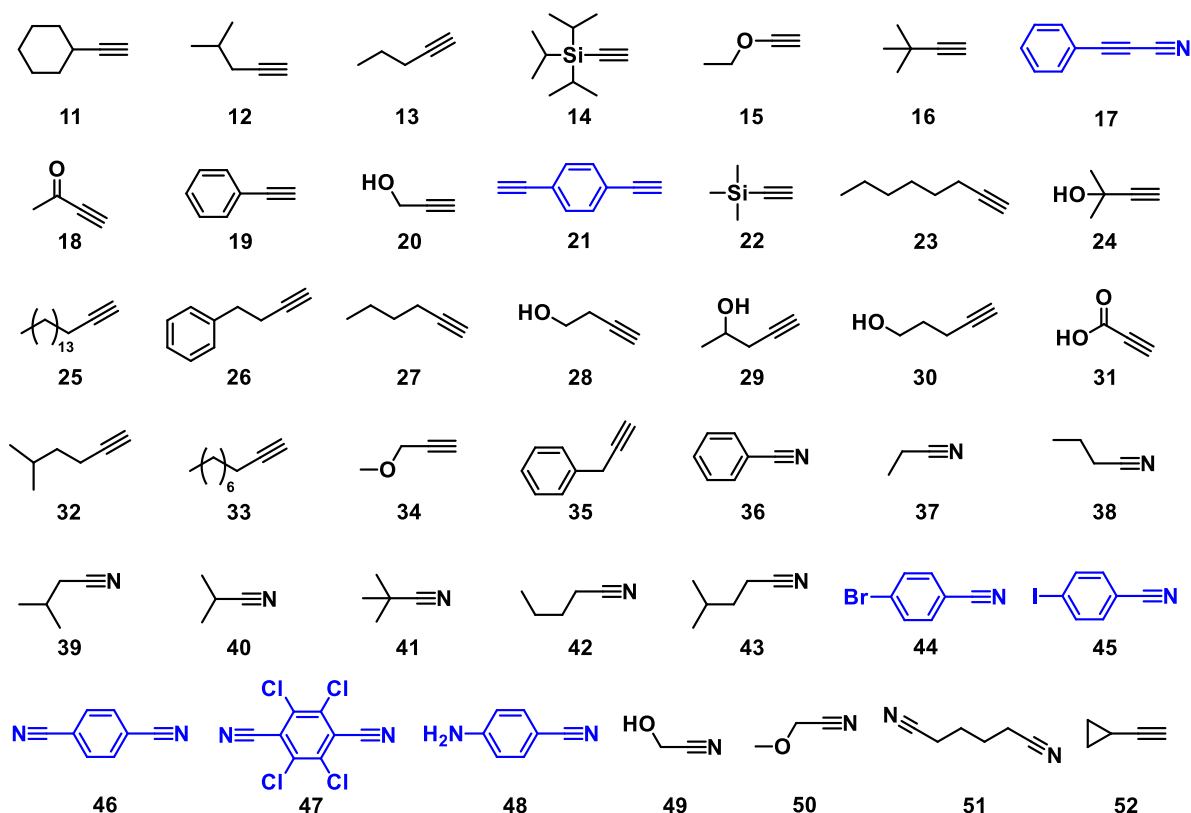


Figure 3.7 Thin guest molecules used for co-crystallization experiments with **10a–c**. Liquid guests are shown in black, and solid guests in blue.

solvent along with the macrocycle, while the liquid guests were used with no added solvent. Several single crystals were obtained from both liquid and solid guest samples. Upon X-ray analysis, crystals from liquid guests were found to contain both the guest and macrocycle. While several crystals with solid guests we obtained, all were found to be of pure guest molecules, and not of a complex with a cyclotetrazabenzoin ester. Successful crystals will be divided into aliphatic and aromatic guest molecules for analysis.

3.3.1 Inclusion of Aliphatic Alkyne and Nitrile Guests

In addition to acetonitrile, three other aliphatic guests were successfully crystallized with a macrocyclic host: 3-butyne-2-one (**18**), propargyl alcohol (**20**), and 4-phenyl-1-butyne (**16**). While **10a–c** were all tested with each guest, **10a** was the only host that produced X-ray diffraction quality crystals of complexes. Analyzing the three structures, all three thin guests

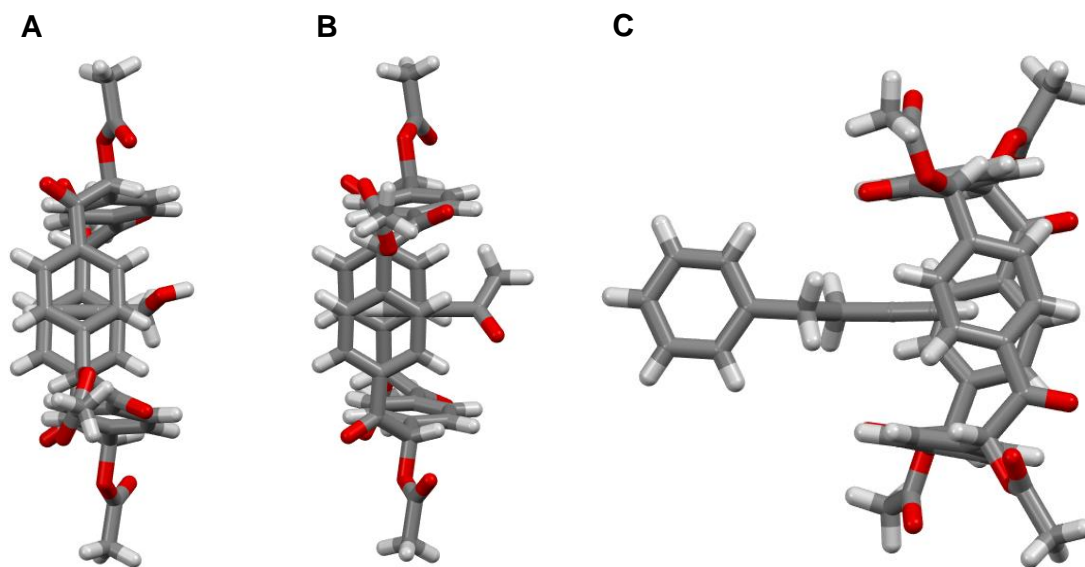


Figure 3.8 Crystal structure of **10a** with thin guests located inside the central pore. A) Guest molecule **18**, viewed along the crystallographic *b* axis. B) Guest molecule **20**, viewed along the crystallographic *b* axis. C) Guest molecule **16**, viewed along the crystallographic *c* axis. Element colors: C—grey, O—red, H—white.

are located with the terminal C≡C–H group in the center of the intrinsic pore (Figure 3.8). Guest molecules **18** and **20** are disordered over four different orientations, while guest **16** is disordered over two orientations. A notable short contact (3.58– 3.60 Å) measured between the terminal carbon of the alkyne and centroid of the aromatic rings is present in each host-guest interaction. Additional stabilizing contacts are found in the packing pattern of the crystal. Since **18** and **20** are similar in size to acetonitrile, it is not surprising that the crystal packing pattern is the same (Figure 3.9A and B respectively). We will look closer at the short contacts present in the crystals of **18** and **20** first.

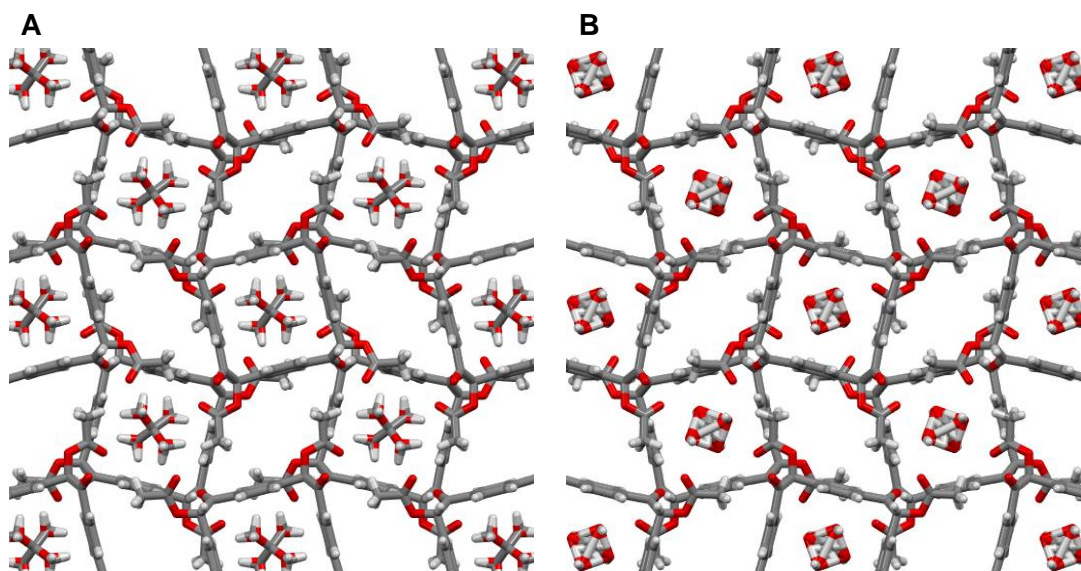


Figure 3.9 Crystal packing of **10a** with thin guest located inside the central pore. A) Guest **18** viewed along the crystallographic *c* axis. B) Guest **20** viewed along the crystallographic *c* axis. Element colors: C—grey, O—red, H—white.

The organization of the molecules of **10a** with guest **18** and **20** have the same short contacts throughout the entirety (± 0.04 Å) of the crystal structure, except for the contacts of **10a** directly with guest molecules. The molecules of **18** form two additional short contacts with **10a** within the same layer (a) between the ester carbonyl and hydrogen of methyl group of **18** (2.89 Å, Figure 3.10) and (b) between a hydrogen on the methyl group of **10a** and the ketone (2.97 Å, Figure 3.10). The molecules of **20** form one additional short contact with **10a** within

the same layer between the oxygen of the alcohol and an aromatic hydrogen (2.33 Å, Figure 3.11).

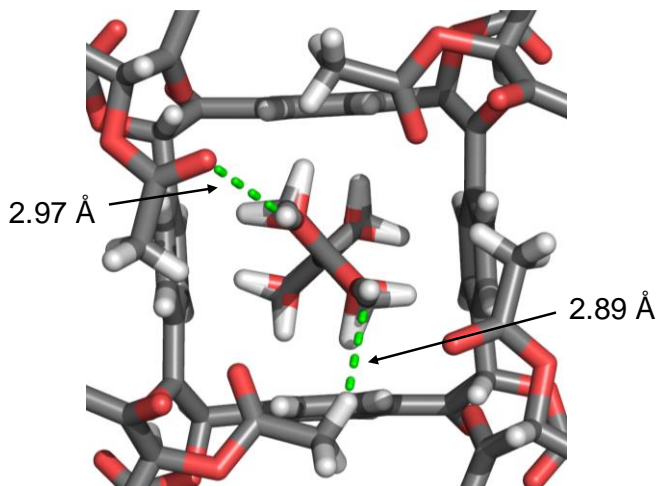


Figure 3.10 Contacts between ester carbonyl oxygen and hydrogens of methyl group on **18** and methyl group hydrogens and oxygen of alcohol. Element colors: C—grey, O—red, H—white.

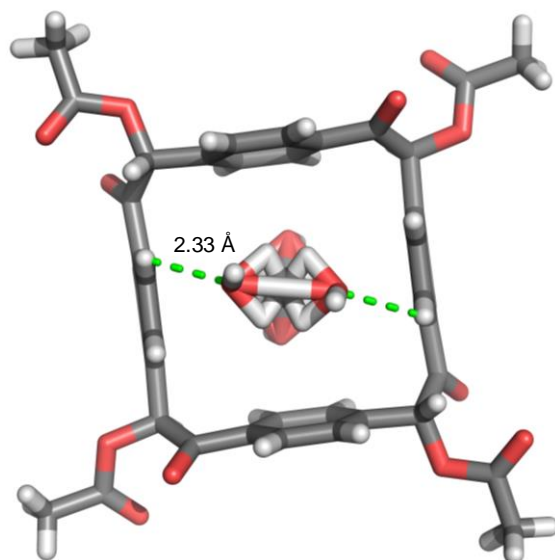


Figure 3.11 Contacts between alcohol oxygen of **20** and aromatic hydrogens of **10a**. Element colors: C—grey, O—red, H—white.

Crystal organization of **10a** with molecules of **16** packing motif is very different than previously seen. In this structure there is one square pore from the intrinsic pore of **10a** with disordered molecules of **16** oriented with the alkyne in the central pore (Figure 3.12A), visible

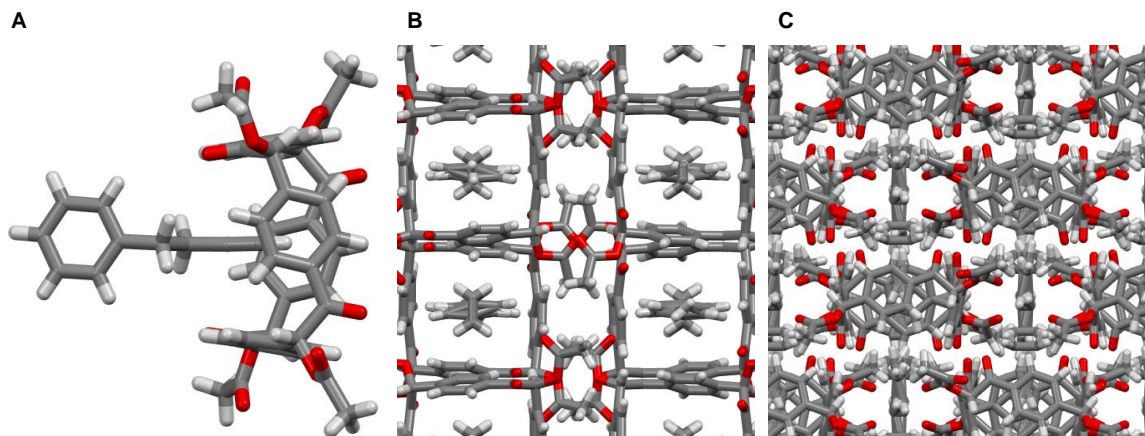


Figure 3.12 Crystal packing of **10a** with **16** partially in the central pore. A) Viewed along the crystallographic *c* axis with the terminal alkyne in the central pore, with disordered solvent molecules removed for clarity. B) Viewed along the crystallographic *a* axis with the guest **16** visible in the intrinsic pores and ester group clusters. B) viewed along the crystallographic *b* axis and vertical stacking of sheets. Element colors: C—grey, O—red, when viewed along the crystallographic *a* axis (Figure 3.12B), with the ester groups clustering in a narrow channel between macrocycles. Vertical sheets stack offset where the macrocycles are not directly on top of one another (Figure 3.12C). These sheets are held together by a series of short contacts. Two-dimensional sheets are connected by [C–H···O] contacts between (a) ester carbonyl oxygen and AcOC–H hydrogen in its neighbor (2.28 Å, Figure 3.13) and (b)

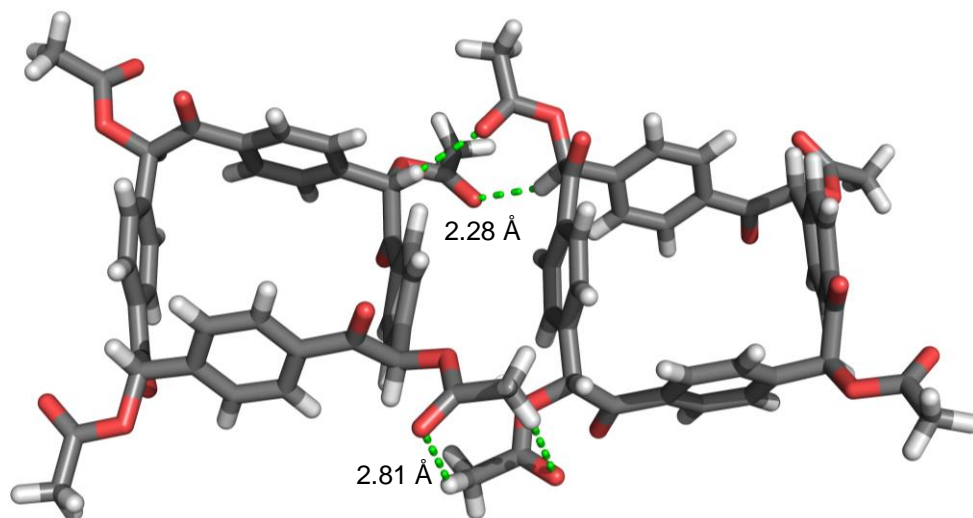


Figure 3.13 Contacts between ester carbonyl and AcOC–H hydrogen (top) and ester carbonyl and hydrogens of the methyl group (bottom). Element colors: C—grey, O—red,

ester carbonyl oxygen of one molecule and the hydrogen of the methyl group on another molecule (2.81 Å Figure 3.13).

Neighboring sheets are connected by [C–H···O] contacts between (a) ketone oxygen in one molecule and an aromatic hydrogen on its neighbor (2.39, 2.83, 2.92 Å, Figure 3.14A), (b) ketone oxygen in one molecule and hydrogens on the methyl group on its neighbor (2.58 Å, Figure 3.14B), and (c) ester carbonyl oxygen of one molecule and hydrogens on the methyl group on its neighbor (2.78 Å, Figure 3.14C). We have shown that aliphatic thin guests including acetonitrile, 3-butyne-2-one (**18**), propargyl alcohol (**20**), and 4-phenyl-1-butyne (**16**) are able to place the nitrile or terminal alkyne group into the intrinsic pore.

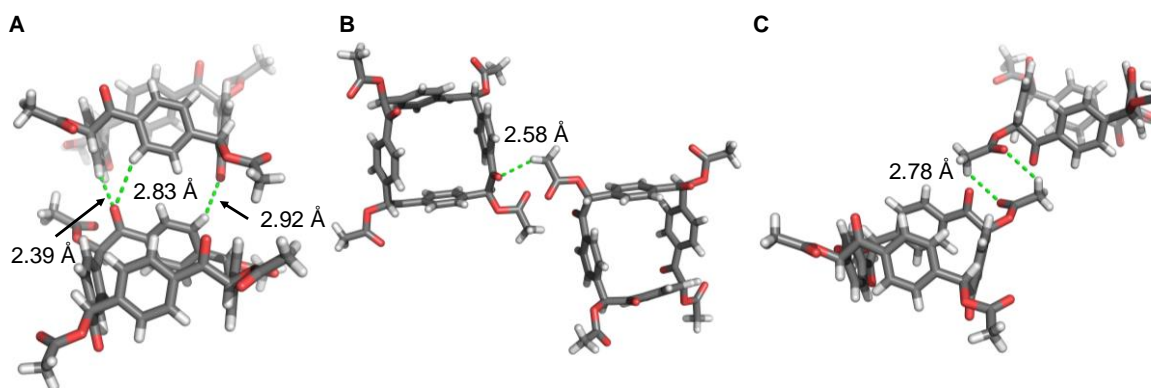


Figure 3.14 A) Contacts between carbonyl oxygen and hydrogens on three aromatic rings. B) ketone carbonyl and methyl hydrogen. C) ester carbonyl oxygen and methyl hydrogen. Element colors: C—grey, O—red, H—white.

3.3.2 Aromatic Alkyne and Nitrile Guest Inclusion

The other category of potential guests we examined were aromatic. We were able to obtain three X-ray diffraction quality crystals with aromatic guests. The first crystal was of **10b** and benzonitrile (**26**) which formed no discernible pores when viewed along any crystallographic axis (Figure 3.15B & C). The guest molecules of **26** are also located outside

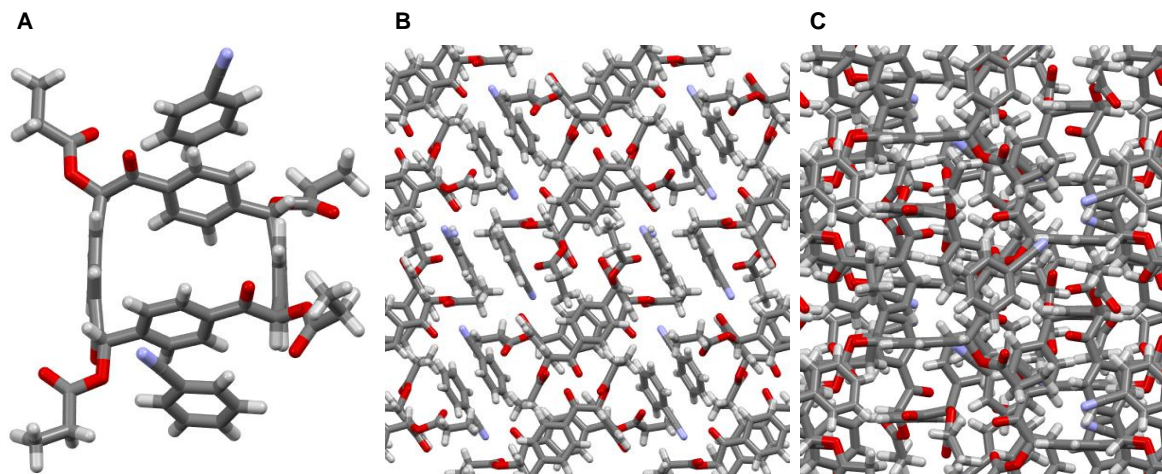


Figure 3.15 Crystal packing of **10b** with **26**. A) Showing **26** is disordered in two orientations outside of the central pore of **10b**. B) Viewed along the crystallographic *b* axis, indicating no pores. C) Viewed along the crystallographic *c* axis, indicating no pores. Element colors: C—grey, O—red, N—blue, H—white.

the central pore (Figure 3.15A). The ethyl group of the ester is found to pack directly below the cyclobenzoin cavity, establishing short [C—H \cdots C] contacts that range in length from 2.88 to 3.36 Å (Figure 3.16A). Other contacts include [C—H \cdots O] contacts between (a) ester's alkoxy

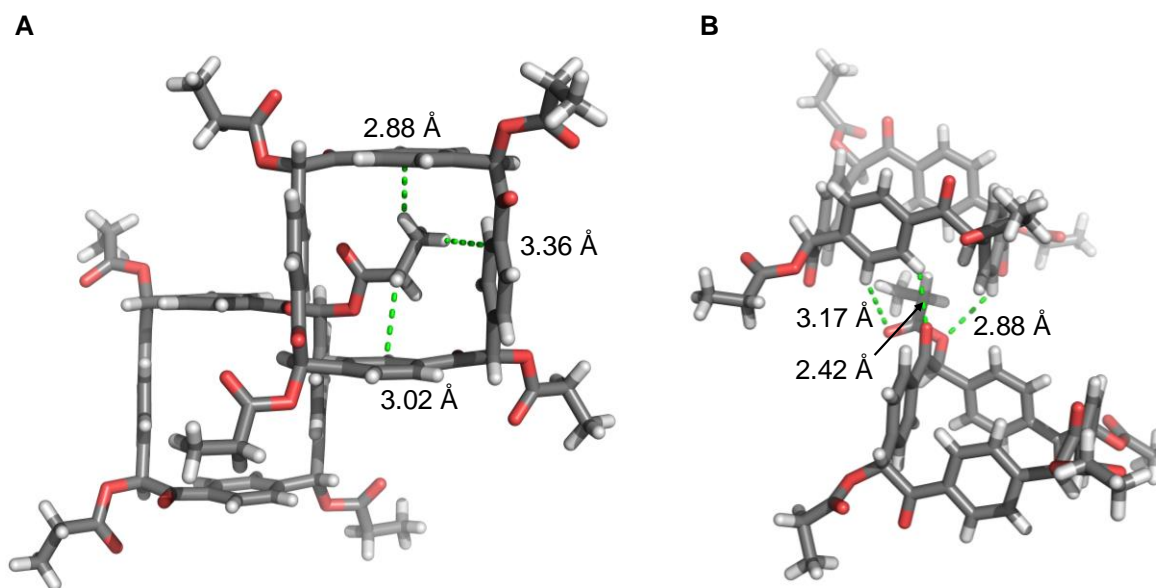


Figure 3.16 A) Contacts between hydrogens on the ethyl group and aromatic rings around the intrinsic pore of **10c**, B) vertical contacts between three aromatic hydrogens on two different rings and ester ether oxygen, ester carbonyl oxygen, and ketone oxygen. Element colors: C—grey, O—red, H—white.

oxygen and an aromatic hydrogen (2.88 Å Figure 3.16B), (b) ketone oxygen and an aromatic hydrogen (2.42 Å Figure 3.16B), and (c) ester carbonyl oxygen and an aromatic hydrogen (3.17 Å Figure 3.16B). A few important contacts are also formed between **10b** and **26**, two [C–H···O] contacts between (a) ester carbonyl oxygen and two aromatic hydrogens of **26** (2.83 and 2.77 Å, Figure 3.17A) and (b) ketone oxygen and an aromatic hydrogen of **26** (2.45 Å, Figure 3.17A). There are also two [C–N···H] contacts between two aromatic hydrogens on two aromatic rings of **10b** (2.71 and 2.90 Å, Figure 3.17B). The only observed short contract

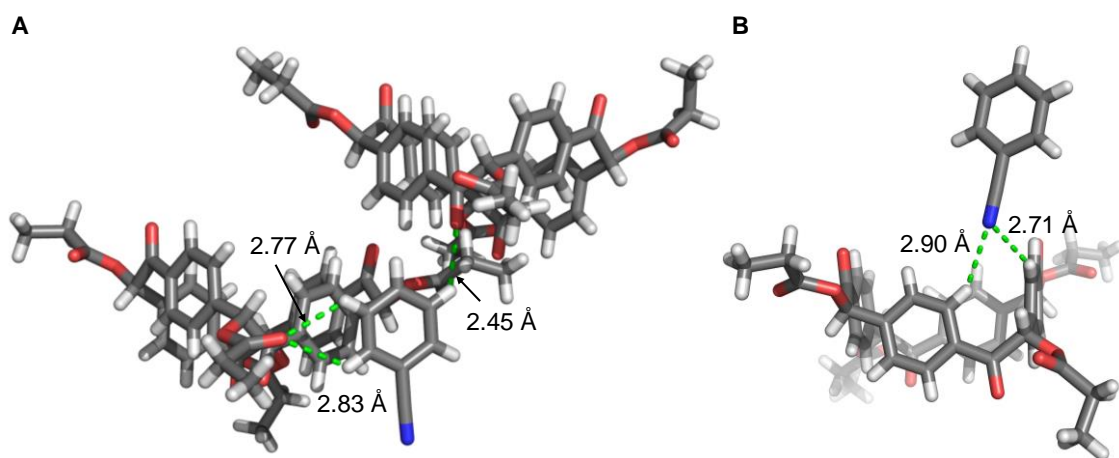


Figure 3.17 Contacts between aromatic hydrogens on **26** with an ester carbonyl oxygen and ketone oxygen (left) and the nitrogen of **26** with two aromatic hydrogens on two aromatic rings (right). Element colors: C—grey, O—red, N—blue, H—white.

between **10b** and **26** is a π - π stacking interaction where the distance is measured between two calculated centroids of neighboring aromatic rings, (3.67 Å, Figure 3.18).

Macrocycle **10c** also crystallizes with guest **26**, where the guest is also located outside of the intrinsic pore (Figure 3.19A). Again, we see no discernable pores established due to efficient packing from the ester group stacking in the cyclobenzoin cavity (Figure 3.19A & B), establishing short [C–H···C] contacts that range in length from 2.84 to 3.12 Å (Figure 3.20A). Other contacts include [C–H···O] contacts between (a) ketone oxygen and (CH₃)₂C–H hydrogen (2.62 Å, Figure 3.20B) and (b) ketone oxygen and two aromatic hydrogens on two

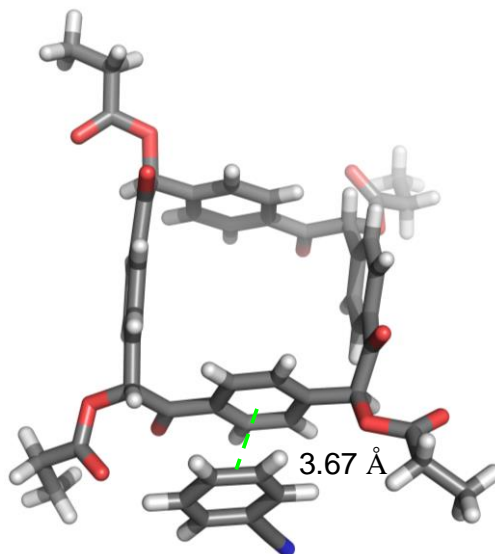


Figure 3.18 Short contact established by π - π stacking formed between **26** and **10b**. Element colors: C—grey, O—red, N—blue, H—white.

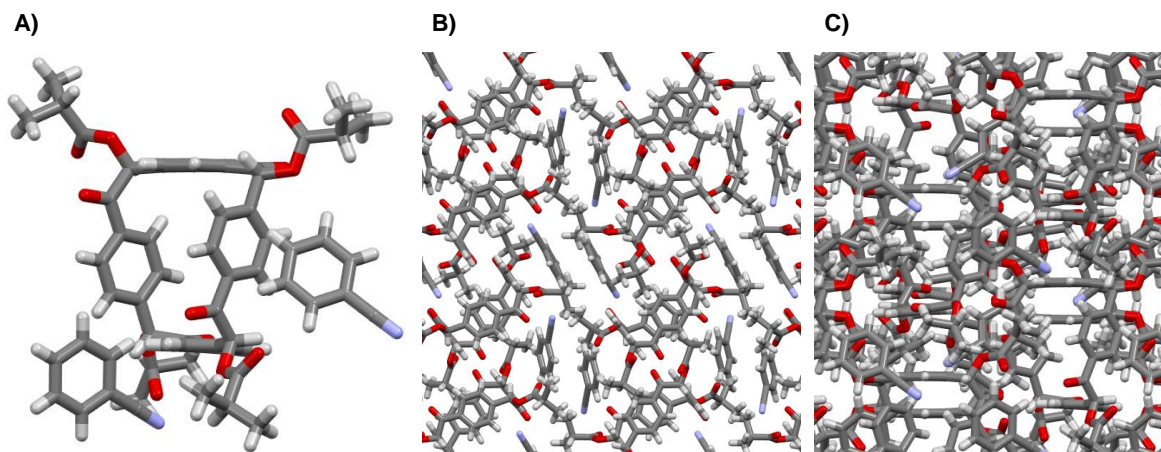


Figure 3.19 Crystal packing of **10c** with **26**. A) Showing **26** is disordered in two orientations outside of the central pore of **10c**. B) Viewed along the crystallographic *b* axis, indicating no pores. C) Viewed along the crystallographic *c* axis, indicating no pores. Element colors: C—grey, O—red, N—blue, H—white.

aromatic rings (2.47 and 2.65 Å, Figure 3.20B). A few important contacts are also formed between **10c** and **26**, four [C—N \cdots H] contacts between the nitrogen of the nitrile and four hydrogens on four aromatic rings (2.55, 2.86, 2.89 and 2.89 Å, Figure 3.21).

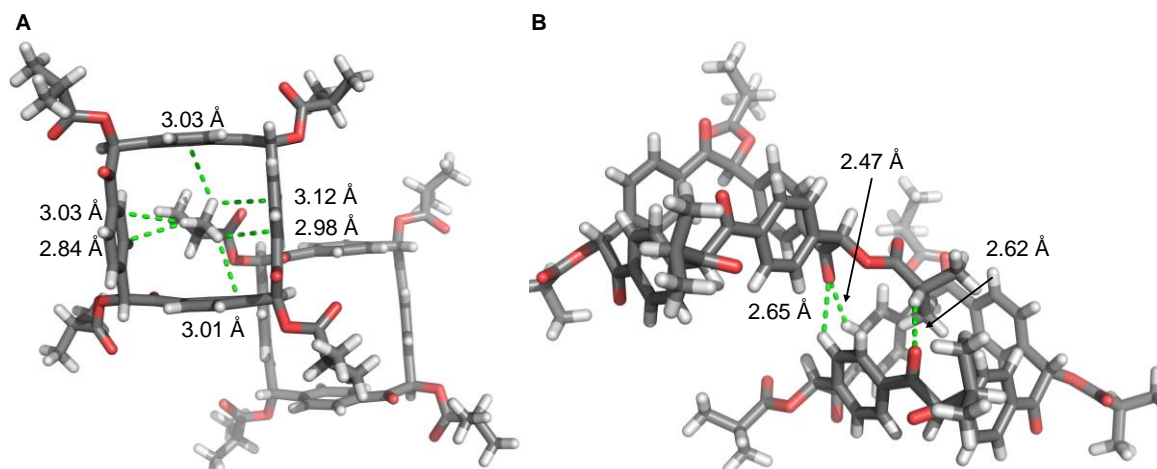


Figure 3.20 Contacts between A) hydrogens on the isopropyl group and the aromatic rings around the intrinsic pore, B) ketone oxygen between two aromatic hydrogens on two aromatic rings and ketone oxygen and $\text{CH}_3\text{C-H}$ hydrogen. Element colors: C—grey, O—red, H—white.

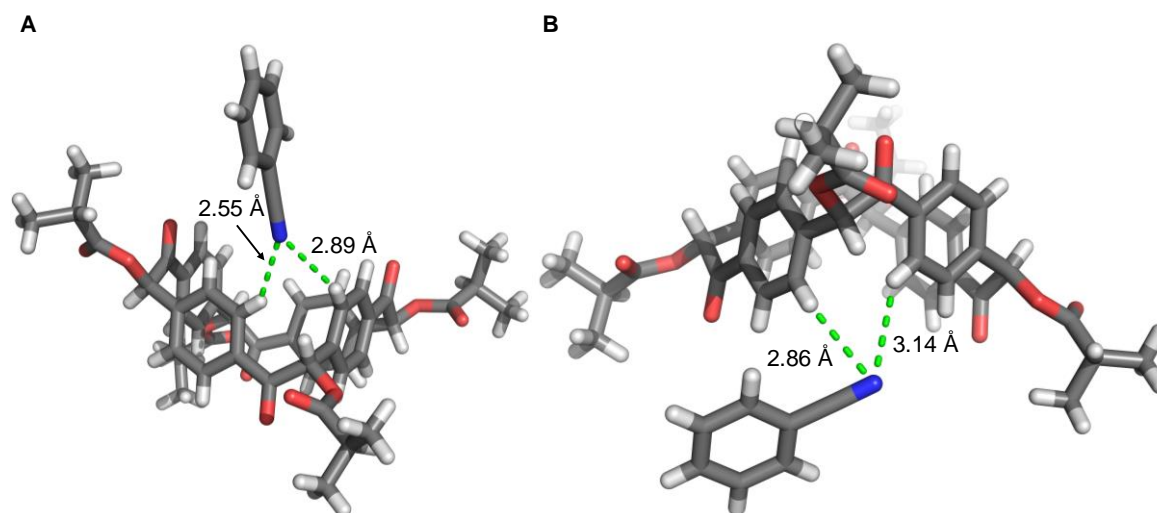


Figure 3.21 Contacts between nitrogen of two different molecules of **26** and three aromatic hydrogens on three different aromatic rings. Element colors: C—grey, O—red, N—blue, H—white.

The last crystal produced was also of **10c** with phenylacetylene (**19**) as the guest, where the guest was also located outside of the central pore (Figure 3.22A). Molecules of **10c** pack in such a way that two different pores are visible when viewed along the crystallographic *c* axis (Figure 3.22B), one square shape from the intrinsic pore and a second oval shape formed between two molecules of **10c**. The guest molecules of **19** are located within these oval pores.

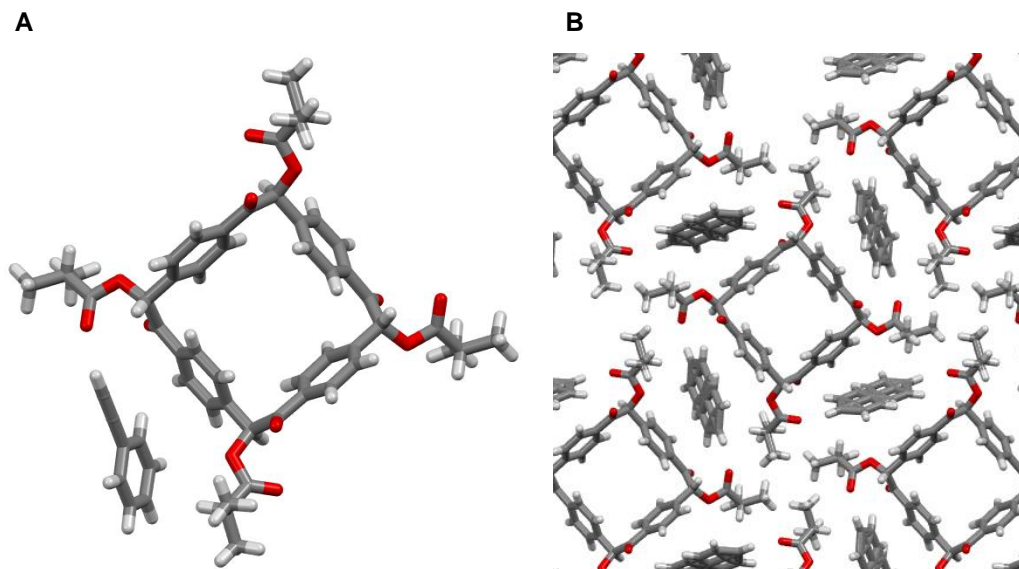


Figure 3.22 Crystal packing of **10c** with **19**. A) Showing **19** is disordered in two orientations outside of the central pore of **10c**. B) Viewed along the crystallographic *c* axis showing two different pores, intrinsic square pore and the extrinsic pore housing guest molecules **19**. Element colors: C—grey, O—red, H—white.

The oval pores are held together by four short [C—H···O] contacts between the ester carbonyl oxygen and the hydrogens of the CH₃ group (2.86 and 3.00 Å, Figure 3.23A). To create a two-dimensional motif, there are a series of short contacts between (a) ketone oxygen and two aromatic hydrogens on two aromatic rings (2.71 and 2.75 Å, Figure 3.23B) and (b) ketone

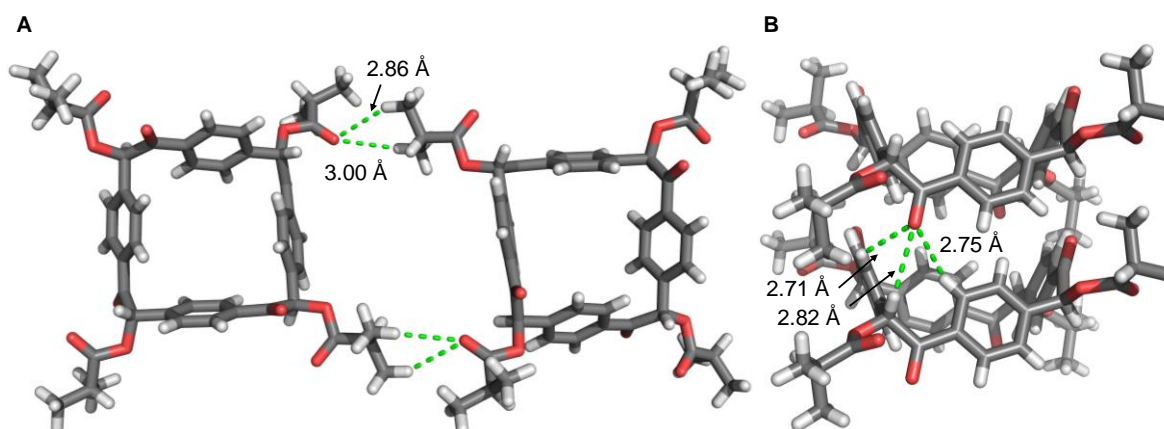


Figure 3.23 Contacts between A) ester carbonyl oxygen and hydrogens on isopropyl group and B) three contacts established between the ketone oxygen and two aromatic hydrogens on two aromatic rings and AcCO—H hydrogen. Element colors: C—grey, O—red, H—white.

oxygen and AcOC–H hydrogen on its neighbor (2.82 Å, Figure 3.23B). There are also three contacts formed between **10c** and **19**, one aromatic hydrogen of **19** between the ketone oxygen and the ester carbonyl oxygen (3.00 and 2.49 Å, Figure 3.24) and another aromatic hydrogen of **19** between the ketone oxygen (3.00 Å, Figure 3.24). Since the crystal has two distinct pores, we tried drying the crystals to see if the crystals could show permanent porosity, however upon removal of solvent molecules crystallinity was lost.

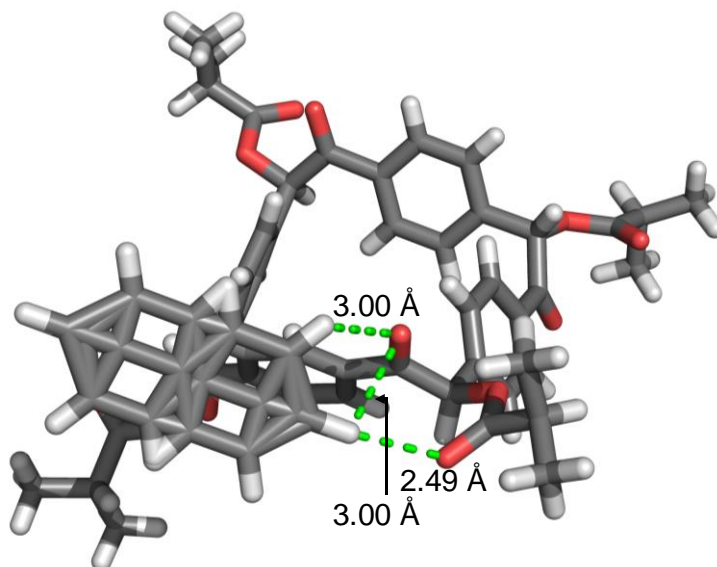


Figure 3.24 Contacts established between **10c** and two aromatic hydrogens of **19** with ketone oxygen and ester carbonyl oxygen. Element colors: C—grey, O—red, H—white.

3.3.3 Aliphatic vs. Aromatic Guest Selectivity

In addition to crystal growth experiments with a single guest, we also looked at a mixed guest solvent to see if one guest would selectively form a complex with **10a** and crystallize. To do this, we wanted to use a guest that we already knew crystallized with the macrocycle, and find molecules that had similar boiling points, so they would evaporate at equal rates. Since successful crystal growth resulted from slow evaporation, if one guest evaporated before the

others it would change the ratio and not determine selectivity. We looked at a guest molecule that successfully formed a crystal complex with **10a**, and then looked up double and single bond analogs to see if boiling points were similar. We found that **18**, **53**, and **54** (Figure 3.25) all

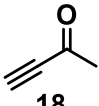
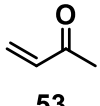
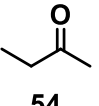
 18		 53		 54
1	:	1	:	1
2	:	1	:	1
1	:	2	:	1
1	:	1	:	2

Figure 3.25 Family of related guest molecules for crystal growth to determine selectively. The table shows the ratios of guests used in crystal growth conditions.

have similar boiling points and functional groups, besides the terminal bonds of interest. Along with single guest crystal conditions, we also went with a mixture of all three guests (Figure 3.25 table). Unfortunately, other than the crystal previously described in Figure 3.9 with **10a** and **18**, no crystals were grown under any attempted conditions. The inability to form crystals from a mixed solvent system indicates **10a** most likely cannot selectively form complexes with alkynes and crystalize.

Looking at the crystal structures and the relationship between host and guest molecules, it appears that aliphatic guests enter the pores of cyclotetrabenzoin esters while aromatic guests do not. To further understand this relationship, we collaborated with Dr. Wu's group to perform calculations and determine if there is a difference in stabilization energies. Calculations were done with several different guest molecules and different parts of the molecules interacting with **10a**. Calculations were performed using a density functional theory (DFT) type calculation, which investigates electronic structures based on spatial electron density, with guest molecule positions not fixed. All calculations analyzed interactions in the gas phase, and it was found

that all interactions showed similar stabilizing energies for most guests (Table 3.1). When

Table 3.1 Calculated stabilization energies for host-guest interactions. Bold atom(s) are interacting with the intrinsic pore of **10a**

guest	kcal/mol	guest	kcal/mol
Ph-C- CH	-13.5	NO ₂ -Ph-C- CH	-18.4
Ph -C-CH	-14.5	NH ₂ -Ph-C- CH	-15.9
CH ₃ - C -C-CCCH ₃	-17.9	CH ₃ O-Ph-C- CH	-18.3
CH₃ -C-C-CCCH ₃	-14.8	CH ₃ -CO-C- CH	-13.3
OH -CH ₂ -C-CH	-14.7	O-C- O	-9.1
OH-CH ₂ -C- CH	-15.9		

comparing stabilization energies for **18** and **19** with the alkyne hydrogen interacting with the pore the stabilization energies were the same, $-13.5 \text{ kcal mol}^{-1}$ and $-13.3 \text{ kcal mol}^{-1}$ respectively, however only **18** crystalized inside the pore. Comparing other calculated energies shows the interacting group has little impact on overall stabilization. To get a better understanding of how these molecules are interacting, we analyzed stabilizing energies as the guest molecule is approaching **10a** and entering the pore. The optimized complexes with guest molecules **19**, **55**, and **56**, had calculated stabilization energies of -18.0 , -18.4 , and $-18.3 \text{ kcal mol}^{-1}$ respectively when the alkyne was in the central pore relative to no molecule interaction. These energies are represented as 0.0 in Figure 3.26, and the plotted data is the energy difference from the optimized interaction. The same pattern is observed for all three host-guest complexes, indicating electronics has little impact on the ability of the complex to form. Since calculations were not indicating what guest molecules would enter the pore, we calculated the stabilizing energies of molecules interacting outside of the pore to see if we could see any patterns. We calculated π - π stacking interactions with the aromatic ring of **19** and of the triple bond of **18** when hydrogen bonded to the ester carbonyl oxygen to facilitate these interactions (Figure

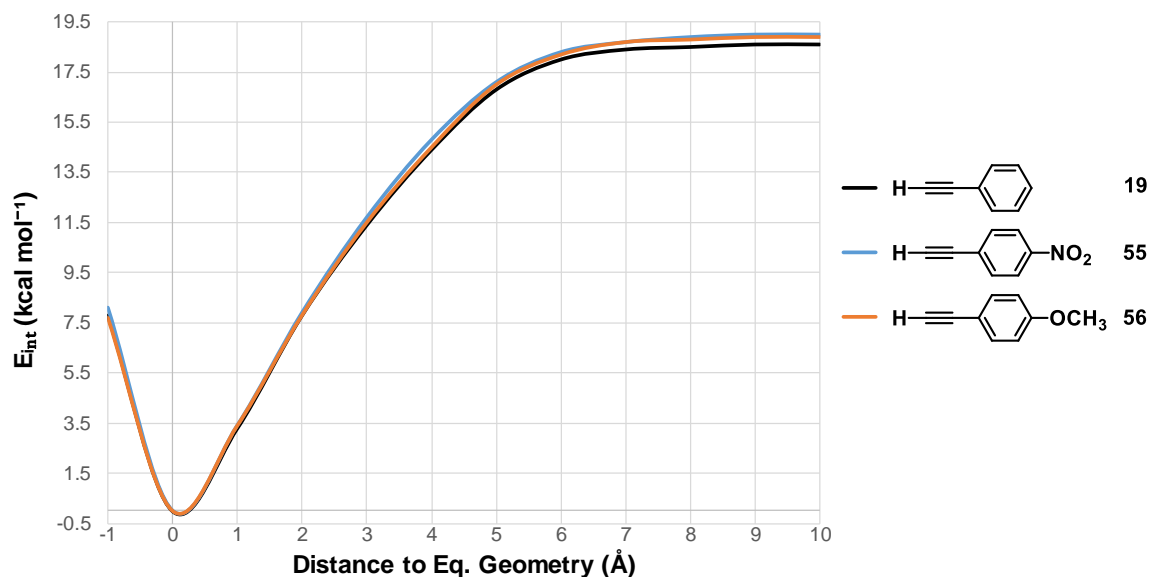


Figure 3.26 Calculated interaction energies as **19**, **55**, and **56** approach and enter the intrinsic pore of **10a**. Reported values are the difference in energy from the optimized complex which is given an energy of 0.0 kcal mol⁻¹.

3.27). Calculations resulted in -10.6 and -9.0 kcal mol⁻¹ of stabilization for **19** and **18** respectively, indicating that **19** shows no difference between stabilizing energies inside or

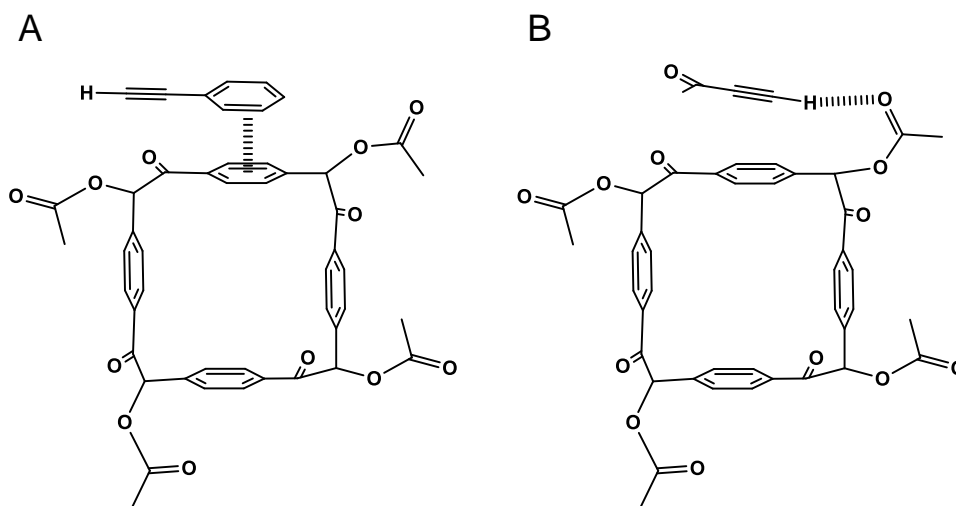


Figure 3.27 Calculated geometries for π - π stacking energies of A) the aromatic ring with **19** and B) the aromatic ring with **18** when hydrogen bonded to ester carbonyl.

outside of the pore. While calculations showed that interactions between the host and guest

molecules were energetically stabilizing, experimentally the calculations did not seem to match the system in its entirety.

3.4 CO₂ Capture

In recent years, CO₂ separation out of mixed gasses containing CH₄,³³⁰ C₂H₂,³²² and fossil fuel processing emissions³³¹ has gained attention due to the increasingly prominent greenhouse effect. As most countries will continue to rely on fossil fuels in the future, the challenge will continue to be to capture CO₂ and decrease humans' carbon footprint. While work has been done to find alternative energy resources, they are not yet a global solution due to cost, scalability, storage, and safety considerations.³³² During the past two decades various kinds of porous materials have been investigated for CO₂ capture, separation, and storage. These materials include MOFs,²³² nanoporous ionic organic networks (NIONs),³³³ covalent organic frameworks (COFs),³³⁴ covalent triazine-based frameworks (CTFs),³³⁵ and porous organic polymers (POPs).³³⁶ Using the known physical properties of CH₄, N₂, and CO₂, materials can be synthesized to selectively interact with gases to create the desired separation by modifying the host pore size, shape, polarity, polarizability, coordination, and conformation.^{337–339} Using physisorbents to do reversible CO₂ sorption has proven to be energy-efficient compared to chemisorbents which require high energy to remove the captured CO₂.³⁴⁰ MOFs have been extensively studied in gas storage^{341–346} and gas separation.^{330,331,347–}
³⁵⁰ A common strategy to increase the capture of CO₂ molecules is to utilize functional groups that facilitate strong interactions. Preparing MOFs with functionalized surfaces have been successful by postsynthetic modifications^{351,352} and utilizing exposed metal cation sites.^{353–357} While single-component adsorption isotherms have shown adsorption capacities of porous

materials, mixed gas isotherms are more impactful for material applications. Several applications of CO₂ capture have been explored including its use in power plants, natural gas processing, transportation emissions, and direct air capture.^{358–363}

With CO₂ being a highly talked about and researched molecule, based on its geometry it could fit into the intrinsic pores of **10a**. Since the crystal structure of **10a** is stable upon solvent removal, we decided to try to utilize the evacuated pores to see if CO₂ could be captured and organized inside of them. To do this, we fixed a dried crystal to the inside of a tapered glass capillary tube that is sealed on the small end and open on the larger end. Using a mortar and pestle, dry ice was crushed into fine pieces to fit into the open end of the tapered capillary tube. The capillary tube was used to collect several dry ice pieces and then quickly sealed by holding over a Bunsen burner to melt the glass and pulled to seal (Figure 3.28). The sealed capillary

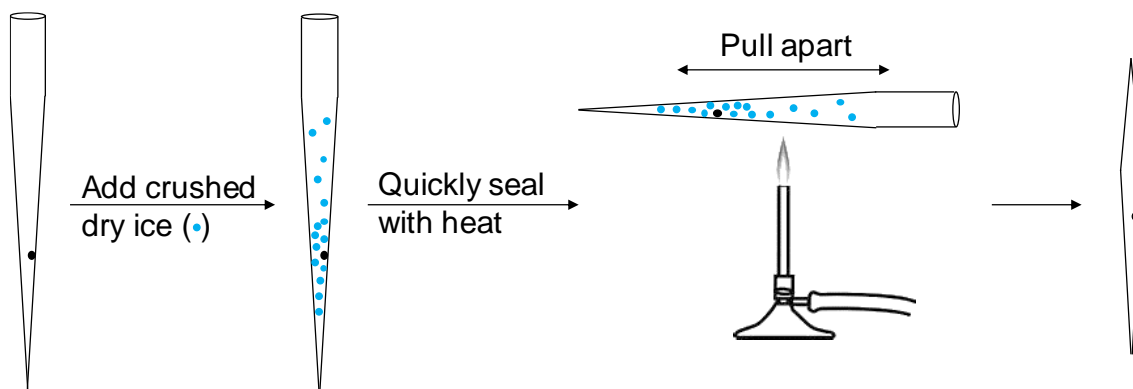


Figure 3.28 Method to make X-ray quality sample with CO₂ captured starting with the crystal sample, black circle, fixed to the capillary tube. Crushed dry ice, blue circles, added to capillary tube and sealed over Bunsen burner. The resulting sealed capillary tube can be placed directly into the X-ray sample holder.

was able to be analyzed by X-ray diffraction and was shown to have CO₂ inside the crystal structure. The location of the CO₂ molecules in relation to **10a** was found to depend on the concentration of CO₂. In the first experiment the concentration of CO₂ was very low, with 0.12 molecules of CO₂ for every one molecule of **10a**. The occupancy of CO₂ molecules inside the

central pore is 7% while there is a 5% occupancy of each location outside of the central pore. In Figure 3.29 the molecules of CO₂ can be seen in three locations, two outside of the central pore and one inside. Viewed along the crystallographic *b* axis we can see the two orientations

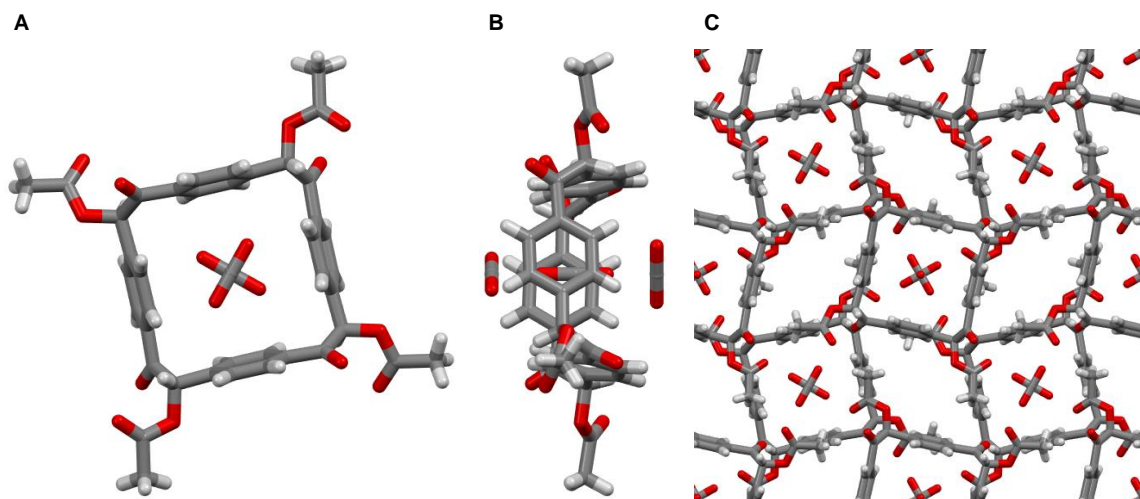


Figure 3.29 CO₂ molecules inside the intrinsic pore of **10a**. A) Viewed along the crystallographic *c* axis with two visible CO₂ molecules. B) Viewed along the crystallographic *b* axis showing three CO₂ molecules inside and outside the intrinsic pore. C) Crystal packing viewed along the crystallographic *c* axis showing the three orientations of disordered CO₂ guest molecules. Element colors: C—grey, O—red, H—white.

of the CO₂ molecules, both inside and outside the central pore. There are several short [C–H···O] contacts established between CO₂ outside the central pore between four aromatic hydrogens on four aromatic rings with each oxygen of CO₂ (2.92 and 3.05 Å, Figure 3.30A). There are also short [C–H···O] contacts established with the CO₂ molecule in the central pore between four aromatic hydrogens on two aromatic rings with each oxygen of the CO₂ molecule (3.40 and 3.45 Å, Figure 3.30B). There are also short contacts established between the partially positive carbon of CO₂ and the aromatic π clouds of the four aromatic rings (3.58 Å, measured from centroid of benzene ring to carbon of CO₂ Figure 3.30B). Upon repeating the same procedure, we were able to get more dry ice into the capillary tube and sealed before the CO₂

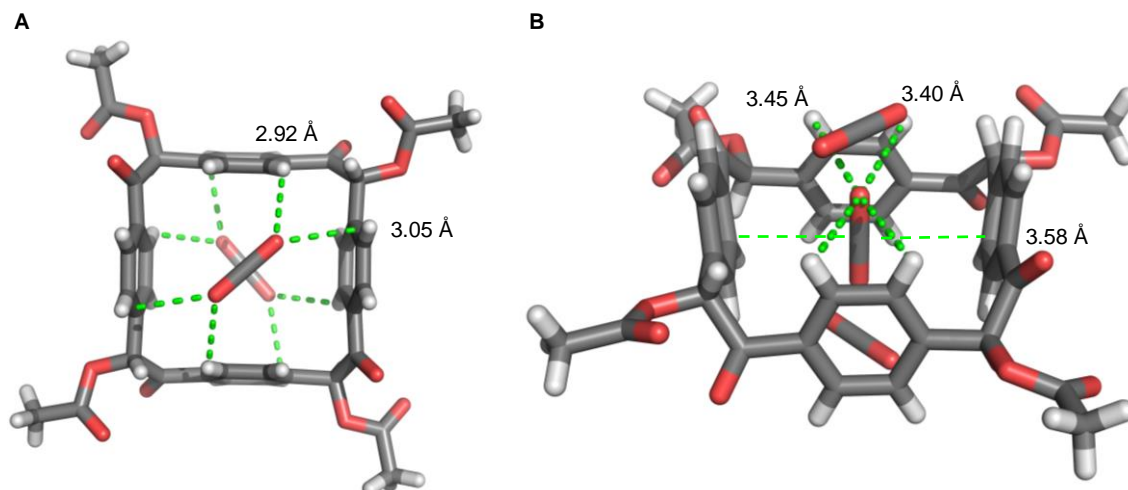


Figure 3.30 Contacts established between A) four aromatic hydrogens of **10a** and both oxygens of CO₂, repeated on both molecules outside of the intrinsic pore, and B) four short contacts established between four aromatic hydrogens with each oxygen of CO₂ in the intrinsic pore and pi interactions of the carbon of CO₂ and π clouds of four aromatic rings. Element colors: C—grey, O—red, H—white.

sublimed. In the second crystal structure, it was observed that the CO₂ molecule in the central cavity was no longer present, only the two molecules outside the central pore (Figure 3.31).

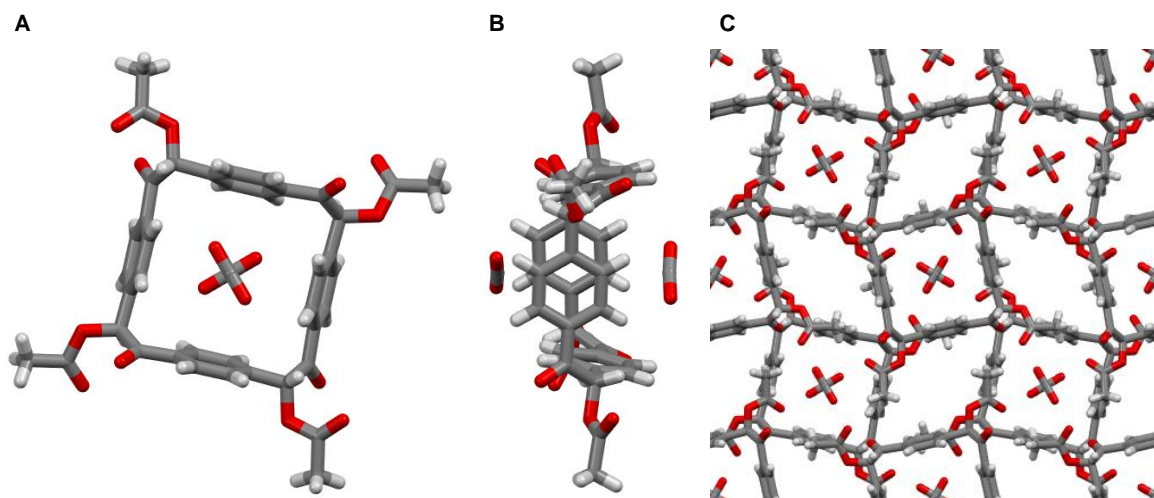


Figure 3.31 CO₂ molecules inside the crystal of **10a**. A) Viewed along the crystallographic *c* axis with the CO₂ molecules just above and below the intrinsic pore. B) Viewed along the crystallographic *b* axis showing CO₂ molecules are located just above and below the intrinsic pore. C) Crystal packing viewed along the crystallographic *c* axis showing the two orientations of disordered CO₂ guest molecules. Element colors: C—grey, O—red, H—white.

Viewed along the crystallographic *b* axis, we can see the CO₂ molecule located right above the central pore of **10a** (Figure 3.31B). In this orientation there are two short [C–H···O] contacts between four aromatic hydrogens on four benzene rings with each oxygen of CO₂ (3.06 and 3.25 Å, Figure 3.32) When viewed along the crystallographic *c* axis, the CO₂ molecules align with the square intrinsic pore and are shown to be disordered in two orientations (Figure 3.31A & C). Composition of the crystal is 1:0.94 (**10a**:CO₂) with each CO₂ orientation having 0.47 occupancy, indicating that while the current crystal shows an almost 1:1 relationship, it could in principle be increased to a 1:2 ratio. Comparing these two crystal structures speculates that the central cavity could be used to facilitate CO₂ molecules at low concentration to enter the crystal structure where they become locked outside of the central pore as concentration increases. These two crystal structures show the possible function of the central pore in the ability of **10a** to uptake CO₂.

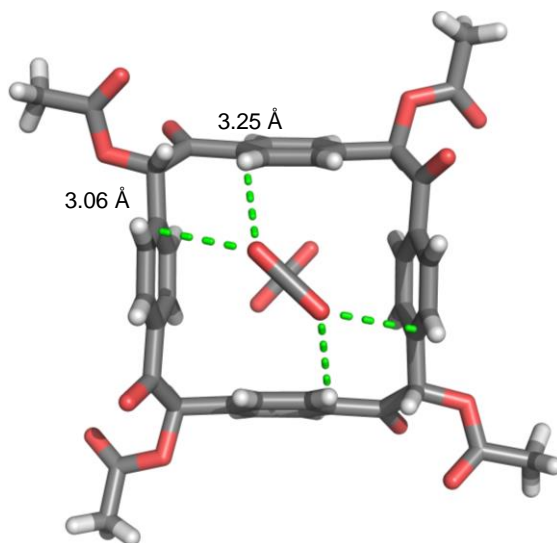


Figure 3.32 Contacts established between four aromatic hydrogens of **10a** and both oxygens of CO₂. Element colors: C—grey, O—red, H—white.

While these crystal structures show CO₂ can enter the crystal, it does not indicate it can capture or separate CO₂. To test the ability to separate gas mixtures, we collaborated with Dr. Chen at the National Cheng Kung University in Taiwan, who tested the ability of **10a** to separate CO₂ from N₂ and CH₄. Preliminary breakthrough curves show that crystalline **10a** can separate CO₂ from N₂ (red and black traces in Figure 3.33, respectively). To show this, a 50/50 gas mixture was passed through the material and the concentration of the outlet gas was determined. Initially only N₂ was detected, but after 40 min CO₂ starts to be detected and after continued flow the ratio detected returns to the 50/50 gas mixture. This preliminary data shows that **10a** can completely separate CO₂ from N₂, and it takes 40 min for the material to become saturated. More work is being done to optimize the separation conditions, and continued testing on other gas mixtures to determine the complete abilities of this material.

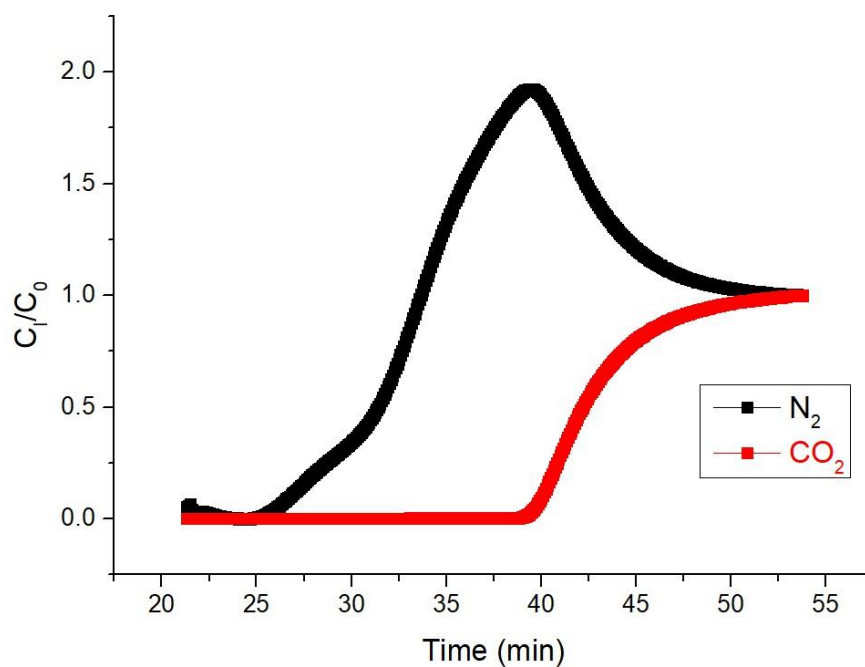


Figure 3.33 Breakthrough curves of gas separation of **10a**.

3.5 Conclusion

We have been able to show that the central pore of cyclobenzoin can be used to form host-guest complexes with thin guests. Crystal growth of host-guest complexes showed that $\text{C}\equiv\text{N}$ and $\text{C}\equiv\text{C}-\text{H}$ groups of aliphatic guests can enter the pores of **10a-c**, while those of aromatic guests cannot. Calculations did not support these findings, indicating instead that all these complexes should be equally stable and both aromatic and aliphatic guests should enter the pore. This could be due to the guest molecules influence on the geometry of the macrocycle which alters the arrangement of multiple macrocycles, which is not captured computationally. While the calculations cannot predict which guest molecules will form host-guest complexes, they do show that these interactions are stabilizing, confirming that thin geometry is essential for guest inclusion into cyclotetrazinoids' pore. We have also shown that **10a** can capture CO_2 inside the crystal motif. When samples with low concentration of CO_2 were analyzed by X-ray crystallography, three orientations of CO_2 were present in the crystal structure with a higher percentage of molecules being found in the intrinsic pore. However, when the same experiment was done with higher concentration of CO_2 only two orientations were seen. What this finding may suggest is that the central pore facilitates the entry of the CO_2 molecules into the crystal structure before locking into one of the other two positions outside of the intrinsic pore. These crystals show the ability of **10a** to interact with CO_2 , but it does not show the ability to capture and separate CO_2 . Expanding on the ability to show CO_2 encapsulation, we have also done gas separation of CO_2 from N_2 and were successfully able to show complete separation of the two gasses in a breakthrough experiment. Continued work is being done to optimize separation conditions and then will continue to try other gas mixtures. With continued success in gas separations, cyclotetrazinoid acetic ester could be applied in simple gas purification systems.

3.6 Experimental Section

3.6.1 General Methods

Crystal growth experiments were set up using solvents and guest samples without further purification. All experiments were set up utilizing slow evaporation in a place with minimal air flow and vibrations. Purified samples of **10a–c** were obtained as previously described. To each vial, 2 mg of a given cyclobenzoin ester were added. If the guest molecule was liquid, enough liquid was added to just dissolve the macrocycle host. If guest was solid, a slight molar excess of it was measured out and added to vial, then enough acetone, acetonitrile, chloroform, ethyl acetate, or dichloromethane was added to just dissolve both the macrocycle and the guest. Vials were monitored daily to see if crystals formed.

3.6.2 Crystal Growth Conditions and Crystallographic Tables

Table 3.2 Crystal Data and Structure Refinement Parameters for Compound **10a**·CH₃CN

Empirical formula	C ₄₂ H ₃₅ NO ₁₂	
Formula weight	745.71	
Temperature	123(2) K	
Wavelength	1.54178 Å	
Crystal system	Tetragonal	
Space group	<i>P</i> $\bar{4}$ 2 ₁ <i>c</i>	
Unit cell dimensions	<i>a</i> = 14.1724(4) Å	α = 90°
	<i>b</i> = 14.1724(4) Å	β = 90°

Table 3.2 Continued

	$c = 10.2805(3) \text{ \AA}$	$\gamma = 90^\circ$
Volume	2064.91(13) \AA^3	
<i>Z</i>	2	
Density (calculated)	1.199 g/cm ³	
Crystal size	0.21 × 0.12 × 0.08 mm ³	
Reflections collected	7723	
Independent reflections	1814 [$R_{\text{int}} = 0.0304$]	
Data / restraints / parameters	1814 / 2 / 125	
Goodness-of-fit on F^2	1.079	
Final R indexes [$I \geq 2\sigma(I)$]	$R_1 = 0.0512$, $wR_2 = 0.1377$	
R indexes (all data)	$R_1 = 0.0514$, $wR_2 = 0.1383$	
Largest diff. peak/hole	0.75/−0.21 e \AA^{-3}	

Table 3.3 Crystal Data and Structure Refinement Parameters for Compound **10a** with **18**

Empirical formula	C ₄₄ H ₃₆ O ₁₃
Formula weight	772.73
Temperature	173(2) K
Wavelength	0.71073 \AA
Crystal system	Tetragonal
Space group	$P\bar{4}2_1c$

Table 3.3 Continued

Unit cell dimensions	$a = 14.2202(8) \text{ \AA}$	$\alpha = 90^\circ$
	$b = 14.2202(8) \text{ \AA}$	$\beta = 90^\circ$
	$c = 10.3528(6) \text{ \AA}$	$\gamma = 90^\circ$
Volume	2093.5(3) \AA^3	
<i>Z</i>	2	
Density (calculated)	1.226 g/cm ³	
Crystal size	0.480 × 0.440 × 0.160 mm ³	
Reflections collected	13827	
Independent reflections	2611 [$R_{\text{int}} = 0.0167$]	
Data / restraints / parameters	2611 / 58 / 157	
Goodness-of-fit on F^2	1.034	
Final R indexes [$I \geq 2\sigma(I)$]	$R_1 = 0.0468$, $wR_2 = 0.1313$	
R indexes (all data)	$R_1 = 0.0476$, $wR_2 = 0.1329$	
Largest diff. peak/hole	0.65/−0.20 e \AA^{-3}	

Table 3.4 Crystal Data and Structure Refinement Parameters for Compound **10a** and **20**

Empirical formula	$\text{C}_{43.41}\text{H}_{38.82}\text{O}_{13.14}$
Formula weight	770.63
Temperature	123(2) K
Wavelength	0.71073 \AA

Table 3.4 Continued

Crystal system	Tetragonal	
Space group	$P\bar{4}2_1c$	
Unit cell dimensions	$a = 14.2362(17) \text{ \AA}$	$\alpha = 90^\circ$
	$b = 14.2362(17) \text{ \AA}$	$\beta = 90^\circ$
	$c = 10.2880(12) \text{ \AA}$	$\gamma = 90^\circ$
Volume	$2085.1(6) \text{ \AA}^3$	
Z	2	
Density (calculated)	1.227 g/cm^3	
Crystal size	$0.81 \times 0.62 \times 0.40 \text{ mm}^3$	
Reflections collected	15450	
Independent reflections	2583 [$R_{\text{int}} = 0.0150$]	
Data / restraints / parameters	2583 / 177 / 198	
Goodness-of-fit on F^2	1.076	
Final R indexes [$I \geq 2\sigma(I)$]	$R_1 = 0.0329$, $wR_2 = 0.0887$	
R indexes (all data)	$R_1 = 0.0335$, $wR_2 = 0.0894$	
Largest diff. peak/hole	$0.27/-0.15 \text{ e \AA}^{-3}$	

Table 3.5 Crystal Data and Structure Refinement Parameters for Compound **10a** and **16**

Empirical formula	$\text{C}_{50}\text{H}_{42}\text{O}_{12}$	
Formula weight	834.83	
Temperature	110 K	
Wavelength	1.54184 Å	
Crystal system	Orthorhombic	
Space group	<i>Pnna</i>	
Unit cell dimensions	$a = 12.42660(4)$ Å	$\alpha = 90^\circ$
	$b = 22.67555(7)$ Å	$\beta = 90^\circ$
	$c = 14.83842(5)$ Å	$\gamma = 90^\circ$
Volume	4181.17(2) Å ³	
<i>Z</i>	4	
Density (calculated)	1.326 g/cm ³	
Crystal size	0.1 × 0.1 × 0.02 mm ³	
Reflections collected	247862	
Independent reflections	4489 [$R_{\text{int}} = 0.0522$]	
Data / restraints / parameters	4489 / 103 / 327	
Goodness-of-fit on F^2	1.045	
Final R indexes [$I \geq 2\sigma(I)$]	$R_1 = 0.0486$, $wR_2 = 0.1394$	
R indexes (all data)	$R_1 = 0.0509$, $wR_2 = 0.1418$	
Largest diff. peak/hole	0.30/−0.25 e Å ^{−3}	

Table 3.6 Crystal Data and Structure Refinement Parameters for Compound **10b** and **26**

Empirical formula	$\text{C}_{58}\text{H}_{50}\text{N}_2\text{O}_{12}$	
Formula weight	967.00	
Temperature	123(2) K	
Wavelength	1.54178 Å	
Crystal system	Monoclinic	
Space group	$P2_1/c$	
Unit cell dimensions	$a = 16.7695(5)$ Å	$\alpha = 90^\circ$
	$b = 10.9246(3)$ Å	$\beta = 96.96(2)^\circ$
	$c = 27.5038(8)$ Å	$\gamma = 90^\circ$
Volume	5001.6(3) Å ³	
Z	4	
Density (calculated)	1.284 g/cm ³	
Crystal size	0.18 × 0.12 × 0.01 mm ³	
Reflections collected	44497	
Independent reflections	9084 [$R_{\text{int}} = 0.0343$]	
Data / restraints / parameters	9084 / 780 / 726	
Goodness-of-fit on F^2	1.005	
Final R indexes [$I \geq 2\sigma(I)$]	$R_1 = 0.0503$, $wR_2 = 0.1419$	
R indexes (all data)	$R_1 = 0.0578$, $wR_2 = 0.1503$	
Largest diff. peak/hole	0.49/−0.26 e Å ^{−3}	

Table 3.7 Crystal Data and Structure Refinement Parameters for Compound **10c** and **26**

Empirical formula	$\text{C}_{62}\text{H}_{58}\text{N}_2\text{O}_{12}$	
Formula weight	1023.10	
Temperature	123(2) K	
Wavelength	1.54178 Å	
Crystal system	Monoclinic	
Space group	$P2_1/c$	
Unit cell dimensions	$a = 16.9106(4)$ Å	$\alpha = 90^\circ$
	$b = 10.9781(2)$ Å	$\beta = 93.017(10)^\circ$
	$c = 28.9134(6)$ Å	$\gamma = 90^\circ$
Volume	5360.22(19) Å ³	
Z	4	
Density (calculated)	1.268 g/cm ³	
Crystal size	0.22 × 0.12 × 0.01 mm ³	
Reflections collected	39634	
Independent reflections	9726 [$R_{\text{int}} = 0.0314$]	
Data / restraints / parameters	9726 / 570 / 693	
Goodness-of-fit on F^2	1.019	
Final R indexes [$I \geq 2\sigma(I)$]	$R_1 = 0.0397$, $wR_2 = 0.1026$	
R indexes (all data)	$R_1 = 0.0461$, $wR_2 = 0.1079$	
Largest diff. peak/hole	0.45/−0.37 e Å ^{−3}	

Table 3.8 Crystal Data and Structure Refinement Parameters for Compound **10c** and **19**

Empirical formula	$\text{C}_{64}\text{H}_{60}\text{O}_{12}$	
Formula weight	1021.12	
Temperature	123(2) K	
Wavelength	1.54178 Å	
Crystal system	Tetragonal	
Space group	$P4_2/n$	
Unit cell dimensions	$a = 22.1162(11)$ Å	$\alpha = 90^\circ$
	$b = 22.1162(11)$ Å	$\beta = 90^\circ$
	$c = 5.7139(3)$ Å	$\gamma = 90^\circ$
Volume	$2794.8(3)$ Å ³	
Z	2	
Density (calculated)	1.213 g/cm ³	
Crystal size	$0.48 \times 0.03 \times 0.02$ mm ³	
Reflections collected	17616	
Independent reflections	9726 [$R_{\text{int}} = 0.0470$]	
Data / restraints / parameters	2540 / 206 / 210	
Goodness-of-fit on F^2	1.142	
Final R indexes [$I \geq 2\sigma(I)$]	$R_1 = 0.0660$, $wR_2 = 0.1637$	
R indexes (all data)	$R_1 = 0.0708$, $wR_2 = 0.1666$	
Largest diff. peak/hole	$0.45/-0.29$ e Å ⁻³	

Table 3.9 Crystal Data and Structure Refinement Parameters for Compound **10a**·CO₂ low concentration CO₂

Empirical formula	C _{40.12} H ₃₂ O _{12.25}	
Formula weight	710.03	
Temperature	123(2) K	
Wavelength	0.71073 Å	
Crystal system	Tetragonal	
Space group	$P\bar{4}2_1c$	
Unit cell dimensions	$a = 14.1598(2)$ Å	$\alpha = 90^\circ$
	$b = 14.1598(2)$ Å	$\beta = 90^\circ$
	$c = 10.2990(2)$ Å	$\gamma = 90^\circ$
Volume	2064.95(7) Å ³	
Z	2	
Density (calculated)	1.142 Mg/cm ³	
Crystal size	0.45 × 0.38 × 0.36 mm ³	
Reflections collected	16370	
Independent reflections	2592 [$R_{\text{int}} = 0.0287$]	
Data / restraints / parameters	2592 / 2 / 125	
Goodness-of-fit on F^2	1.048	
Final R indexes [$I \geq 2\sigma(I)$]	$R_1 = 0.0375$, $wR_2 = 0.1034$	
R indexes (all data)	$R_1 = 0.0392$, $wR_2 = 0.1050$	
Largest diff. peak/hole	0.31/−0.15 e Å ^{−3}	

Table 3.10 Crystal Data and Structure Refinement Parameters for Compound **10a**·CO₂ high concentration CO₂

Empirical formula	C _{40.94} H ₃₂ O _{13.88}	
Formula weight	746.11	
Temperature	123(2) K	
Wavelength	0.71073 Å	
Crystal system	Tetragonal	
Space group	$P\bar{4}2_1c$	
Unit cell dimensions	$a = 14.1449(7)$ Å	$\alpha = 90^\circ$
	$b = 14.1449(7)$ Å	$\beta = 90^\circ$
	$c = 10.2901(5)$ Å	$\gamma = 90^\circ$
Volume	2058.8(2) Å ³	
Z	2	
Density (calculated)	1.204 Mg/cm ³	
Crystal size	0.55 × 0.48 × 0.42 mm ³	
Reflections collected	11027	
Independent reflections	2389 [$R_{\text{int}} = 0.0285$]	
Data / restraints / parameters	2389 / 0 / 134	
Goodness-of-fit on F^2	1.061	
Final R indexes [$I \geq 2\sigma(I)$]	$R_1 = 0.0374$, $wR_2 = 0.1012$	
R indexes (all data)	$R_1 = 0.0412$, $wR_2 = 0.1043$	
Largest diff. peak/hole	0.251/−0.162 e Å ^{−3}	

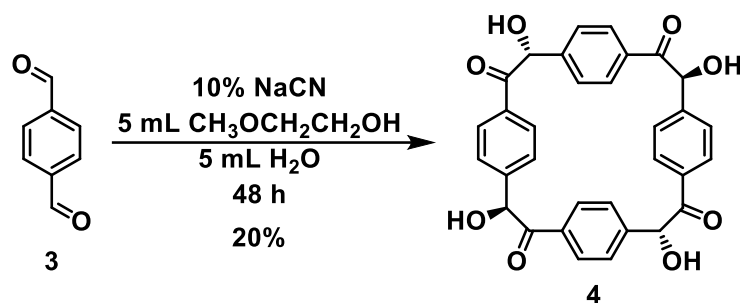
Chapter Four Cyclotetrabenzoin Purification and By-Product Analysis

4.1 Benzoin Condensation

The benzoin condensation is a carbon-carbon bond forming reaction, discovered in 1832¹⁹¹ by Wöhler and Liebig, which produces an α -hydroxyketone from two aldehydes. In the original reaction conditions, cyanide adds to one benzaldehyde, increasing the acidity of the aldehydic proton.³⁶⁴ After a proton transfer, the formed intermediate was proposed to account for the umpolung transformation in the following step.³⁶⁵ In the addition of the second aldehyde, the first aldehyde acts as a nucleophile to attack the second aldehyde.³⁶⁶ The α -hydroxyketone is a useful synthetic building block for the formation of natural products and biomolecules,³⁶⁷ such as fungicides,³⁶⁸ antidepressants,³⁶⁹ bio-active oxygenated heterocycles,³⁷⁰ and urease inhibitors.³⁷¹ The expansion of the utilization of the benzoin condensation came when Ukai³⁷² and Breslow¹⁹⁶ reported the use of thiazolium salts as pre-catalysts. Since then, *N*-heterocyclic carbenes (NHC)^{365,373} and biocatalysts^{367,374} were successfully shown to enantioselectively catalyze the production of benzoin. Challenges remain in the chemoselectivity of cross-benzoin condensations.³⁷⁵ The electronic nature, substitution pattern, and steric bulk of the substrates have a large impact on the catalyst selectivity. In most cases, ortho-substituted aromatic aldehydes lead to low catalyst activity.^{206,376,377}

The discovery of cyclobenzoin in 2015 utilized the benzoin condensation to synthesize two macrocycles in a one-step reaction.^{220,221} Both macrocycles precipitated out of solution and were isolated by simple filtration. While both reactions yielded novel macrocycles, we were more interested in cyclotetrabenzoin (**4**) which had a larger pore for potential applications in ion sequestering,¹²⁷ small molecule capture,¹²⁰ and as a synthetic building block.³⁷⁸ The four α -hydroxyketone groups could be utilized as a building block that is already arranged in a fixed

conformation. Our one-step synthesis of macrocycle **4** is a simple reaction, which results in a relatively low yield of 20% (Scheme 4.1).²²¹ With such a low yield, we were curious what other products were formed by this reaction.



Scheme 4.1 Synthesis of cyclotetrabenzoin (**4**).

4.2 Reaction Condition Modifications

Published reaction conditions for the preparation of **4** use a 1:1 solvent mixture of water and 2-methoxyethanol, heated at reflux for 48 hours. Under these conditions, **4** precipitates out of the solution in a 40% crude yield. Purification is accomplished by dissolving the solid in dimethyl sulfoxide (DMSO) under nitrogen at 50 °C with stirring for 12 hours. This solution is then filtered, mother liquor is placed in a round bottom flask and boiling methanol is slowly layered on top. Upon filtration there is a white solid that is removed, however its NMR spectrum shows no peaks. The round bottom flask is filled with nitrogen and sealed with a septum. After seven days a white precipitate is collected by filtration yielding **4** at 21%. Accidental lowering of the reaction temperature resulted in higher crude yields collected, however upon purification

Table 4.1 Increased crude yields compared to isolated purified yields

reaction temperature (°C)	crude yield (%)	purified yield (%)
reflux	30	15
reflux	47	19
70	79	22
70	94	23

the yields did not indicate the same increase (Table 4.1). To determine if the purification method was isolating all of **4** out of the reaction precipitate, we calculated yields by NMR spectroscopy using 1,4-dinitrobenzene as the internal calibration standard. We found that with an average of 84% crude yield resulted in 53% calculated pure yield by NMR (Table 4.2), indicating we were not isolating all of **4** through the published purification method. Along with trying to improve the purification method, we also sought to increase the yield of **4** by modification of reaction conditions.

Table 4.2 Increased crude yields compared to calculated NMR pure yields

reaction temperature (°C)	crude yield (%)	NMR yield (%)
70	87	53
70	82	52
70	81	55
70	89	52

Several reaction conditions were modified to determine if the yield of cyclotetrabenzoin could be increased: solvent, reaction temperature, atmosphere, and catalyst loading. Since the starting materials have limited solubility in the original solvent mixture, we tried to see if changing the solvent ratio would increase the yield of **4**. Since the starting materials are not soluble in water and **4** is not soluble in 2-methoxyethanol, we lowered the concentration of water to see if that would keep intermediates soluble to produce more **4**. Upon decreasing the concentration of water, we found that a precipitate was not formed and analysis by NMR spectroscopy did not indicate the presence of **4** after workup of the reaction. We saw similar results when ethanol was used instead of 2-methoxyethanol as well. In the mechanism of the benzoin condensation two proton transfers occur: in step II, which enables the first aldehyde to act as a nucleophile and in step IV, to produce the α -hydroxyketone and regenerate the catalyst (Figure 4.1) to facilitate the mechanism. Since the reaction solvents contain an alcohol and water both can be utilized as a proton source, the absence of **4** upon workup is unexpected.

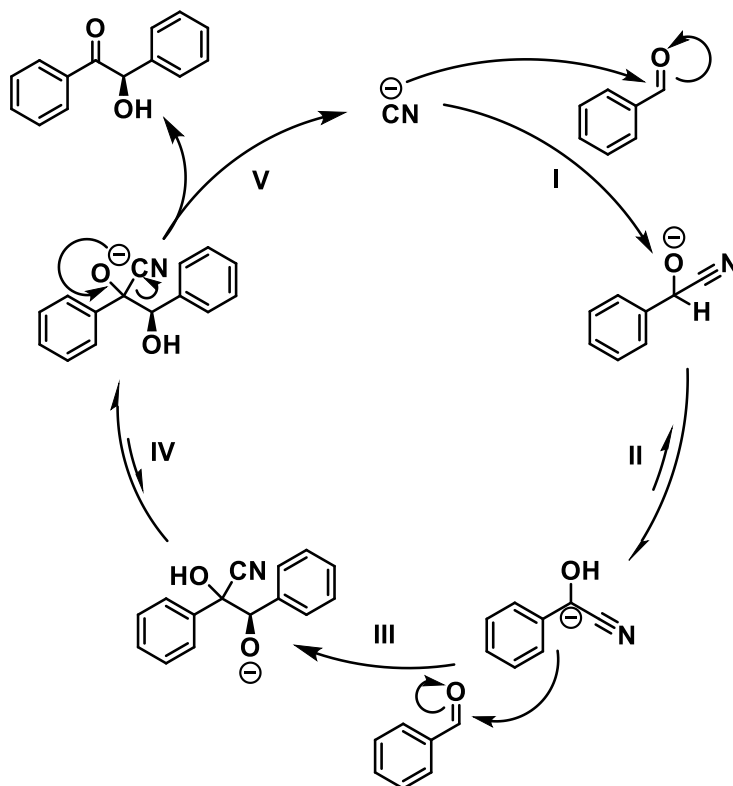


Figure 4.1 Mechanism of benzoin condensation.

We next examined whether lowering the temperature would increase the yield of **4**. Since we saw an initial increase in crude and NMR yields by lowering the temperature to 70 °C, we looked at temperatures lower than this. We again compared the crude and calculated NMR yields (Table 4.3) and found that 60 °C resulted in the highest crude yield and the highest

Table 4.3 Comparison of crude yield and calculated NMR yield at lower temperatures

reaction temperature (°C)	crude yield (%)	NMR yield (%)
50	37	19
50	25	15
60	80	48
60	80	53
70	43	21
70	33	17

calculated NMR yield. These studies have indicated that the published conditions do not result in the highest possible yield of **4**. However, the purification method is the most limiting in always producing around 20% yield regardless of crude yield. Comparing isolated purified

yields with calculated NMR yields of reactions run at different temperatures confirms what had been seen previously (Table 4.4). The lower yield at 80 °C is unexpected given conditions at reflux result in a higher yield. While the isolated pure yields are lower than the calculated NMR yields, they indicate that only around 50% of the calculated pure material is isolated.

Table 4.4 Comparison of crude, calculated NMR, and isolated purified yields of reactions at different temperatures

reaction temperature (°C)	crude yield (%)	NMR yield (%)	purified yield (%)
60	53	32	13
60	73	42	23
70	43	21	12
80	23	10	7

We also tested if the atmosphere under which the reaction was performed had any impact on the yields. Under published conditions, the atmosphere and condenser were filled with nitrogen, but not exchanged. Since we previously concluded that running the reaction at 60 °C results in the highest yield, we conducted the following experiments at that temperature. We tested if bubbling nitrogen through the solvent mixture, as opposed to just filling the headspace with nitrogen, had any impact. Since we were no longer running at reflux, we compared a sealed container to those with a condenser under a constant flow of nitrogen. Results are summarized in Table 4.5, which show that nitrogen purging has no impact on crude or calculated NMR yields compared to previous experimental results. We also compared

Table 4.5 Comparison of nitrogen atmosphere on reaction yields at 60 °C

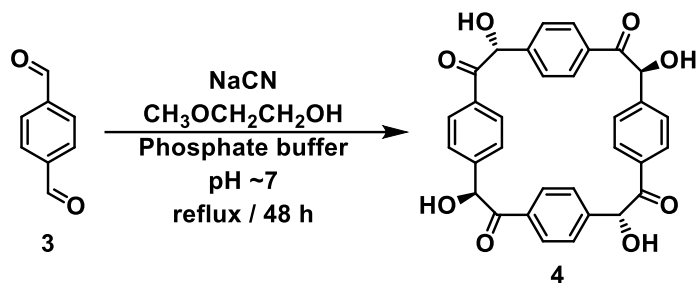
heat source	nitrogen purging method	crude yield (%)	NMR yield (%)
oven	bubbled, sealed	81	44
oven	headspace, sealed	83	58
oil	bubbled, condenser	64	48
oil	headspace, condenser	80	41
oil	bubbled, sealed	47	23
oil	headspace, sealed	83	53

running the reaction in an oil bath to an oven and found no difference in crude or calculated NMR yields.

Of the mentioned reaction conditions studied, we have shown that decreasing the temperature to 60 °C resulted in the highest crude yield, which also resulted in the highest calculated pure NMR yield of **4**. These higher crude yields and calculated NMR yields were shown to be consistent across several reactions, indicating that isolated yield of **4** could be increased with an improved purification method. However, in my hands, no purification method resulted in higher isolated yield than that published in the literature.

4.3 Cyanide Impact on Reaction Yield

The final reaction condition we examined was catalyst loading. We started by testing if the cyanide catalyst remained present throughout the course of the reaction. Since cyanide should not be consumed through the course of the reaction, it was expected to remain in solution at the end of the reaction. Cyanide detection can be easily done by completing a Prussian blue test. This test takes iron(II) sulfate in a cyanide solution acidified by HCl to give $\text{Fe}^{\text{III}}_4[\text{Fe}^{\text{II}}(\text{CN})_6]_3$ which is blue in color, giving the test its name. This test is very sensitive, so even small amounts of cyanide will turn the solution blue. We used this method to test for cyanide at several points during the reaction. Control samples of the cyanide solution and the reaction solution after the initial addition of cyanide both resulted in a blue solution. Initial testing of the mother liquor after 48 hours showed no blue color, indicating cyanide is no longer present in the solution. This implies that cyanide is not being regenerated as the catalyst. To test for HCN gas, reactions were run in a phosphate buffer solution calibrated to a pH of 7 to



Scheme 4.2 Synthetic reaction of **4** using a buffered reaction solvent.

prevent the protonation of cyanide (Scheme 4.2). While NMR analysis indicated that reaction produced **4**, the isolated yields remained around the same as in previous reactions, around 40% crude with a lower calculated NMR yield of 15%. Prussian blue testing indicated that cyanide was not present at the completion of the reaction. We also ran the reaction in a pressure vessel to keep all the reactants and intermediates contained; if HCN was being formed, it would remain trapped in the vessel. Again, Prussian blue testing showed that no cyanide was present at the completion of the reaction. In both the buffered solution and the closed system, we saw no difference in the outcome compared to the published results and cyanide was no longer present in solution.

Published reaction conditions add 10 mol% NaCN to the reaction solution once all the starting materials are dissolved. After 48 hours the reaction was determined to be complete by Prussian blue testing, which indicated cyanide was no longer present. We wondered if adding 20 mol% NaCN would increase the amount of **4** precipitated from solution, and if cyanide would then remain in solution. Initial reactions resulted in a slightly higher crude yield of 55%, but an isolated yield of 20%, and after 48 hours cyanide was not present. Repeating the reaction, Prussian blue testing was done after 24 hours and no cyanide was present. Regardless of whether 10 or 20 mol% of NaCN was initially added, both conditions show cyanide is no longer

present after 24 hours. This observation would imply that the reaction is complete after 24 hours as NaCN is no longer present to catalyze the reaction.

Instead of doubling the initial concentration of NaCN, a second addition was attempted in two ways. First, we added a second portion of 10 mol% after 24 hours to the main reaction mixture and second, we filtered the precipitate as published, then added an additional 10 mol% to just the mother liquor. When the second addition was performed after 24 hours, the solution turned darker in color, similar to the deep red coloration that develops after initial loading, and the color slowly dissipated over the next 24 hours. Prussian blue testing was done after the second addition as a control to show that cyanide was present, followed by a second test after 24 hours which also showed cyanide was still present in the reaction solution. Precipitates were filtered and the same 20% isolated yields were observed, indicating the addition of cyanide did not result in an increase in isolated yield and the presence of cyanide upon the completion of the reaction indicated there was no more benzoin condensation taking place.

The second way we added NaCN was by running the reaction for 48 hours, filtering out the precipitate and adding cyanide to the mother liquor and heating that solution at reflux for another 48 hours. Prussian blue testing confirmed at the end of the first 48 hours no cyanide was present. Upon addition of NaCN to the mother liquor a control showed that cyanide was initially present, and after the second 48 hours cyanide was still present as seen with the previous second addition of NaCN. Again, we saw no change in yield after the first 48 hours and no precipitate was formed upon the second addition. While changing the amount of cyanide did not impact the results of the reaction, we did learn that after 24 hours the reaction is complete. We also learned that whatever has not precipitated out of solution does not precipitate

with additional NaCN and Prussian blue testing indicated that cyanide was still present, confirming the benzoin condensation did not continue after the first 24 hours.

Of the tested conditions—temperature, atmosphere, and catalyst amount—temperature was the only condition that resulted in a change in reaction outcome. We were able to show that decreasing the temperature from reflux (100 °C) to 60 °C increased the crude and calculated NMR yields. Utilization of published purification methods however did not translate into higher isolated yields. We found that regardless of crude yield, around 20% was always the isolated pure yield. The rest of this chapter will discuss our attempts to find a better purification method.

4.4 Purification Methods

Purification, defined as the removal of contaminants, is an important process in several everyday applications. These purification methods can range from simple processes one does at home daily to highly specialized industrial processes. Purification methods include; chromatography,^{379,380} crystallization,^{381,382} filtration,^{383–388} extraction,³⁸⁹ and distillation.³⁹⁰ Each method utilizes unique characteristics found in each system where components need to be separated and not every method will work for each system. Finding a successful method depends on the types of molecules that need to be separated, how they interact with one another, and what method provides an environment that disrupts molecule interactions to facilitate separation. Chromatography will be the most utilized purification strategy in this thesis.

Chromatography utilizes the same principles of extraction, with the addition of solid phase and one mobile phase that passes through the solid phase.^{391–394} In all methods separations require the sample to be dissolved in the mobile phase. Components that are more retained by

the stationary phase move slowly through the stationary phase, while components that are weakly retained move rapidly. Liquid chromatography is the most widely used of all analytical separation techniques.³⁸⁰ The popularity is due to its sensitivity, adaptability, automation, nonvolatile separation, thermally fragile separation, and applicability to industrially important substances. Molecular exclusion chromatography—also called size exclusion, gel filtration, or gel permeation chromatography (GPC)—is similar to liquid chromatography, however, GPC separates molecules by size.³⁹⁵ Common gels for the stationary phase include sephadex and Bio-Gel P, which are crosslinked polymer compounds with varying pore sizes.³⁹⁶ Small molecules are able to penetrate the pores in the stationary phase, while larger molecules pass through therefore eluting first. Depending on the interactions or types of molecules desired to be separated, more than one method of purification could be necessary to effectively separate all components. We looked to utilize several different methods to determine what other products are being made in the reaction of **4**.

4.4.1 Cyclotetrabenzoin Purification

In the previous studies we have learned that the calculated NMR yields indicate **4** has a higher pure yield than 20%, but we have not been able to show this through isolated yields. To improve the ability to purify **4** we started by doing a solvent sweep to determine what solvents we could use to improve isolated pure yields. Upon testing several solvents (Table 4.6) we found that only dimethyl sulfoxide (DMSO) and hot dimethylformamide (DMF) were able to dissolve all precipitated material. As discussed in Chapter 2, it was found that DMF decomposes **4** when used as a solvent in reactions—for the same reason pyridine was also not used—so

Table 4.6 Solubility testing of **4** in common organic solvents at room temperature and heating until solvent was boiling

Solvent	20 °C	Boiling	Solvent	20 °C	Boiling
Acetic acid	No	No	Ethylene glycol	No	No
Acetone	No	No	Hexane	No	No
1-Butanol	No	No	Methanol	No	No
<i>t</i> -Butanol	No	No	2-Methoxyethanol	No	No
Carbon tetrachloride	No	No	Nitric acid	No	No
Chlorobenzene	No	No	Nitromethane	No	No
Chloroform	No	No	1-Pentanol	No	No
Cyclohexane	No	No	1-Propanol	No	No
1,2-Dichloroethane	No	No	Pyridine	Cloudy	Cloudy
Diethylene glycol	Cloudy	Cloudy	Toluene	No	No
1,2-Dimethoxy ethane	No	No	Triethylamine	No	No
Dimethylformamide	Cloudy	Yes	<i>p</i> -Xylene	No	No
Dimethyl sulfoxide	Yes	Yes	Xylenes	No	No
Ethanol	No	No	Tripropylamine	No	No
Ethyl acetate	No	No	Water	No	No

DMSO is the only solvent able to dissolve **4**. With a high boiling point and high polarity, DMSO is not an ideal solvent to work with in most purification processes. Instead of trying to dissolve **4**, we decided to try to selectively dissolve all other precipitated products. Reaction precipitates of two reactions were used, starting with the least polar solvents and slowly increasing polarity. Precipitates were added to an excess of solvent then sonicated with slight heat, filtered, and mother liquor was removed to isolate any dissolved products. In both cases, tetrahydrofuran (THF) was the only solvent to dissolve a measurable amount of product. NMR analysis showed a complicated spectrum, with a variety of aldehydic, aromatic, and benzoin peaks. In these NMR spectra, the benzoin and alcohol proton areas were too crowded to allow us to separate these signals, this possibly indicating that polymers were formed. Comparison of the initial precipitate (Figure 4.2 green) to the spectra of the compounds isolated by THF (Figure 4.2 brown) showed four clear aldehyde singlets, indicating possibly four different linear compounds (Figure 4.2 brown). Comparison of NMR spectra taken before and after the removal of products by THF (Figure 4.2 blue) shows some purification with the removal of all aldehyde

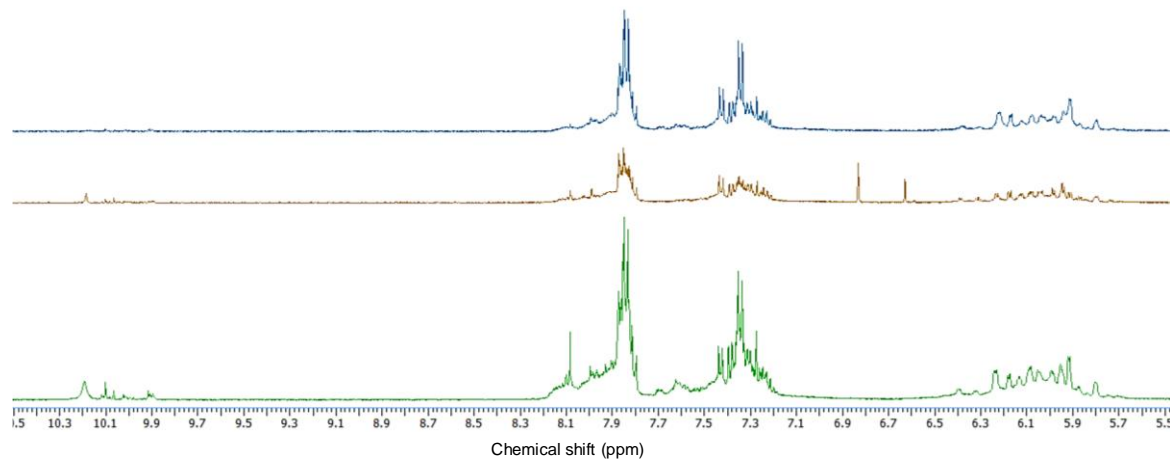


Figure 4.2 Reaction precipitates of **4** were dissolved in THF, which by NMR analysis showed removal of all aldehydic peaks from the starting precipitate, however, multiple products were removed with the crowded aromatic and benzoin peak areas. Green—starting precipitate, brown—THF dissolved acyclic products, blue—remaining reaction solids.

peaks, but the final product is still not pure **4**. With no remaining aldehyde peaks, other remaining products could be macrocycles. However, product analysis by thin layer chromatography (TLC) of both the linear products in THF and potential macrocycles showed no movement or separation under any conditions. Assuming the remaining products have similar polarities to **4**, similar insolubility would also be observed making products difficult to elute.

Without being able to dissolve products selectively, we tried to selectively precipitate products from the mother liquor. Running the synthesis of **4** under published conditions, the initial precipitate was filtered out and the orange mother liquor was heated to boiling with a heat gun. A second precipitate formed upon cooling, which was filtered out. The remaining mother liquor was placed into the freezer overnight, which produced the third precipitate. Upon filtering the precipitate, the mother liquor remained a light-yellow color, so we removed the remaining solvent and got a fourth solid. Analysis of the three precipitates isolated from the mother liquor by NMR showed peaks in the desired aromatic and benzoin areas, however, peaks

were crowded and not well-defined. Some separation of products was achieved as aldehyde peaks were diminished in the fourth precipitate (Figure 4.3 blue). The three resulting precipitates were sent for mass spectrum analysis, which revealed several potential peaks of

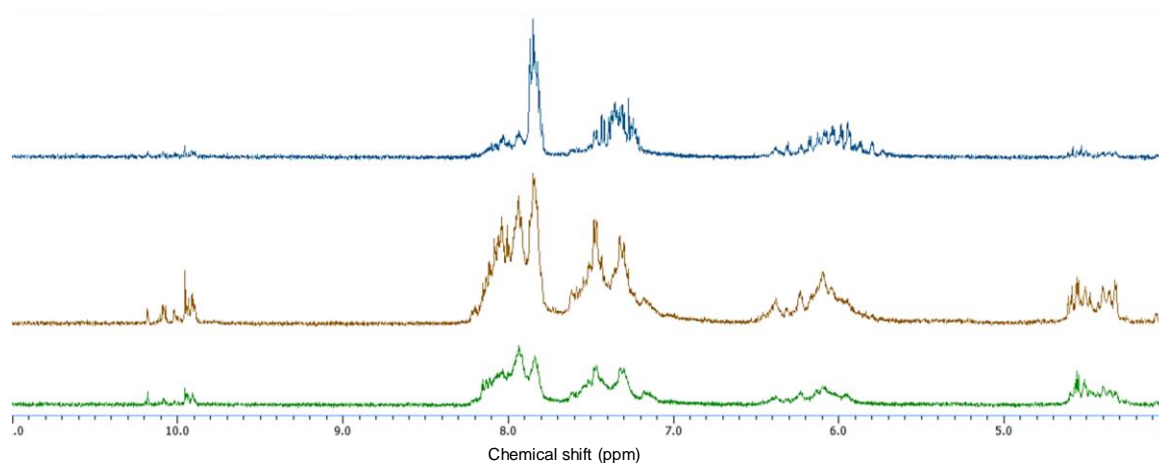


Figure 4.3 Stacked NMR spectra of three precipitated products from the mother liquor. Green—precipitate isolated by heating mother liquor to boiling, brown—precipitate isolated by placing remaining mother liquor in freezer, blue—precipitate isolated by removing remaining mother liquor solvent.

interest. Mass spectrum showed five peaks that matched products ranging in size from dimer to hexamer, highlighted in Figure 4.4, with both linear and cyclic products having the same mass. In the benzoin condensation mass is conserved as the aldehydic proton from one aldehyde is transferred to form the hydroxyl group with the other aldehyde. Comparing the mass spectrum with NMR spectra we see the disappearance of aldehyde peaks which correspond to the disappearance of pentamer and hexamer masses, indicating these two species are linear. With the removal of aldehyde peaks by NMR, the third precipitate could be composed of cyclic products. Corresponding mass spectrum indicates the smaller chains are cyclic, which is less desired as the central pores would be smaller than the pore in **4**. Comparing with mass spectrum, it does show a minor amount of presumed dimer and trimer with the majority of precipitate composed of unknown products. Induced precipitation resulted in the first indication that

desired products other than **4** are found in the reaction solution, however, upon replication we were unable to isolate precipitates corresponding to the observed side products.

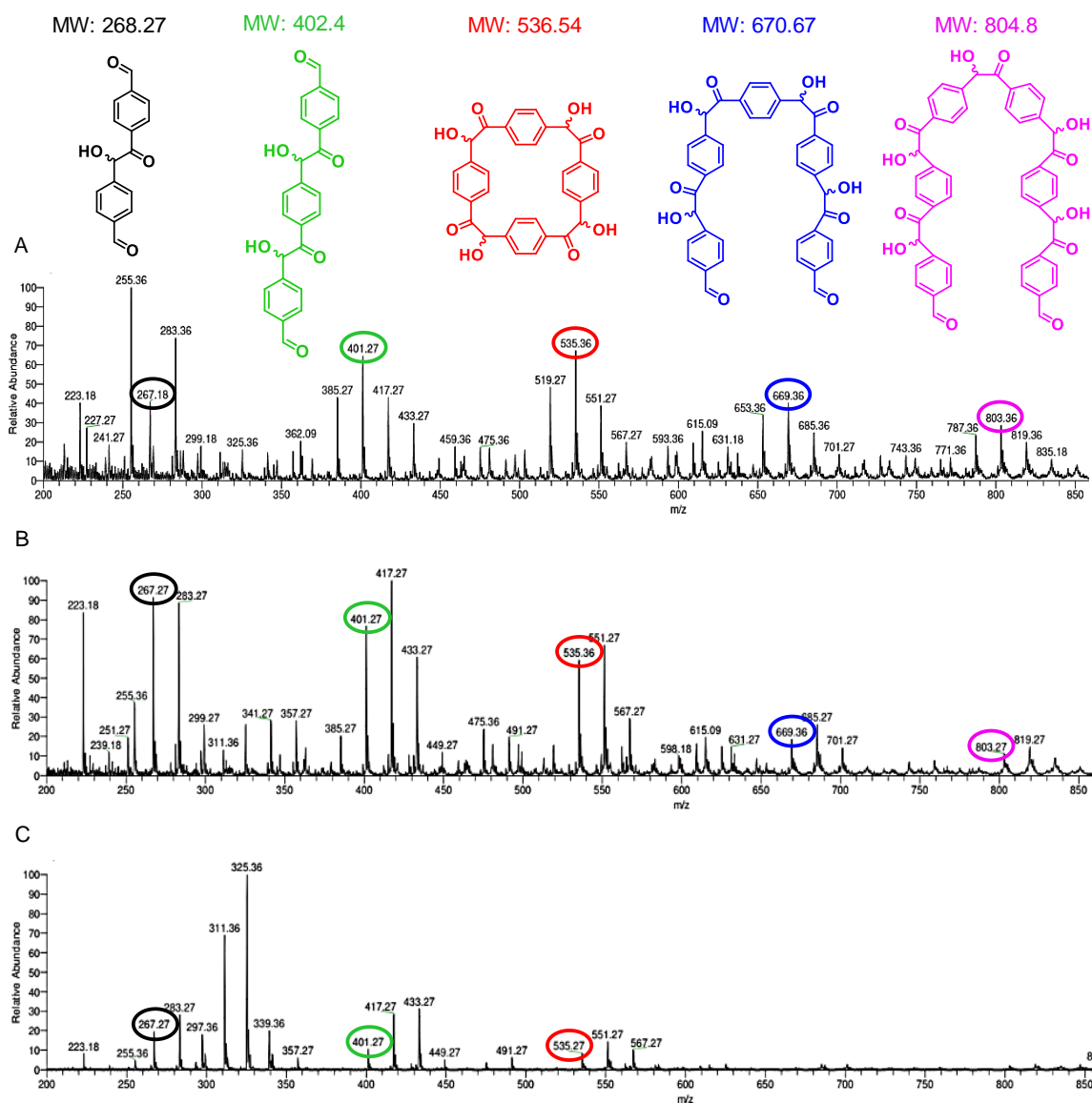


Figure 4.4 Mass spectrum analysis of three precipitated solids from the mother liquor. Potential products that match peaks of interest in the spectrum are colored to match their respective peaks. Linear and cyclic products are shown as there is no mass difference in these products.

We continued trying to selectively dissolve products from the mother liquor by doing extraction with a variety of organic solvents. The only solvent found to dissolve any compounds was ethyl acetate. The collected NMR spectra of the solids dissolved in ethyl acetate showed

aldehyde and aromatic peaks with minimal benzoin peaks, indicating that most of the isolated product was unreacted. Since all products showed limited solubility in common organic solvents, we tried Soxhlet extraction to try to increase the amount of products dissolved while using minimal amounts of solvent. To do this, we evaporated the mother liquor to dryness, yielding a red/orange sticky solid that was placed in the thimble for extraction. Solvents were used in the order of increasing polarity: chloroform, ethyl acetate, and acetone were able to dissolve reaction components. All three collected solids were analyzed by mass spectrometry, unfortunately all three spectra had the most abundant peak between 169.18 and 191.18 m/z units, which is too large to be terephthalaldehyde (**3**), but too small to be a dimer. If cyanide were to attack both aldehydes of **3**, the resulting intermediate with two negatively charged oxygens could be protonated instead of completing the proton transfer (step II in Figure 4.1). This would produce a product with two hydroxyl groups and two nitrile groups resulting in a mass of 188.06 m/z units, which falls in the range of the observed mass spectrum peaks. With the reversibility of the reaction, it is unlikely that these products are trapped intermediates; however, the masses found do not match any desired products.

With no success in selectively dissolving products, we tried to simply precipitate more of the desired compound under the published conditions. As discussed before, we showed that calculated NMR yields were around 50% higher than any of the isolated pure yields, indicating that the method of purification we are using is not isolating all of **4** from the DMSO solution. We looked to change the purification method by increasing the length of time allowed for a precipitate to form, increasing the amount of methanol used in the precipitation, and changing methanol to a different solvent. We first looked to increase the amount of methanol used to precipitate out **4** by repeating the addition of boiling methanol after the first seven days of

precipitation. Following published procedures after the first precipitate was filtered, the mother liquor was returned to the round bottom flask and a second portion of boiling methanol was layered on top and allowed to precipitate for another seven days. After seven days a precipitate formed and was filtered. Mother liquor was again returned to the round bottom flask and a third amount of boiling methanol was layered on top and let to precipitate for seven days. This time however, no precipitate formed, so boiling water was added to the round bottom flask and allowed to stand for seven days. A precipitate did form and was filtered from solution. This process was repeated twice, the findings are shown in Table 4.7, showing an increase of isolated

Table 4.7 Extended purification results with following precipitates and isolated yields

Trial	1 st Precipitate (g)	2 nd Precipitate (g)	3 rd Precipitate (g)	Total (g)	Yield (%)
1	0.2573	0.0273	0.1089	0.3935	29.3
2	0.2338	0.0624	0.3096	0.6058	45.2

yields by almost 50% compared to the published 20%. The substantial increase between trial 1 and 2 is unexpected as the same procedure was followed. To check the purity of the collected precipitates, NMR spectra were analyzed, however this showed a drastic decrease in the purity after the first precipitate. The first collected precipitate showed pure **4**, however the other two collected precipitates showed similar spectra with an additional set of peaks in the aromatic region. Since neither spectrum had aldehyde peaks, they are not oligomers or polymers, but most likely the additional peaks are due to the isomers of **4**. The final modification to the purification method we tried was replacing methanol with another solvent. We tried acetonitrile, as it is less polar in comparison to methanol and is not an alcohol, although it proved to precipitate out the same amount of pure **4** as methanol. Unfortunately, no tested modifications showed any improvements in the isolated pure yields.

Lastly, we tried to purify this reaction mixture by a variety of different column conditions. Normal phase silica was tried, knowing that **4** would most likely not come off the column, we could potentially identify other products from this reaction. This column was run with the most polar solvent mixtures possible without dissolving silica. After several attempts, no products could be isolated from the column, indicating that all products from this reaction are too polar to be eluted with normal phase silica. Switching to reverse phase silica should enable the polar products to move down the column and be isolated. While **4** could be isolated off the column, yield and purity were no higher than under the published conditions. We then switched to size exclusion chromatography by using activated charcoal as the stationary phase in the column. Separation of compounds would be achieved by the smaller components interacting with the pores in the charcoal, while larger components would move through the column. After several attempts with a variety of solvents, no products could be isolated using this method. We then switched the stationary phase to Sephadex, which is another size exclusion chromatography media. Sephadex is a cross-linked dextran gel that is used to separate molecules by size. Before use, Sephadex needs to be activated by soaking in solvent. Since DMSO is the only solvent able to dissolve all reaction components, it was the chosen as the eluent to run this column. Several fractions could be isolated from the column using pure DMSO as the mobile phase. Analysis by NMR shows that the last three fractions (Figure 4.5 pink, teal, purple) contain pure **4**, while the first three fractions (Figure 4.5 green, brown, blue) show no benzoin peaks. We were able to utilize Sephadex to isolate **4** from the other products, however, the yield did not increase and it also did not lend any insight into what other products are produced in this reaction. Limitations to this method are the slow flow rate through the gel media and the need to use heating tape to prevent the DMSO—with a melting point of 19 °C—

from freezing in the column. Replication of these results also did not prove successful as reaction components could not be separated and isolated from the column.

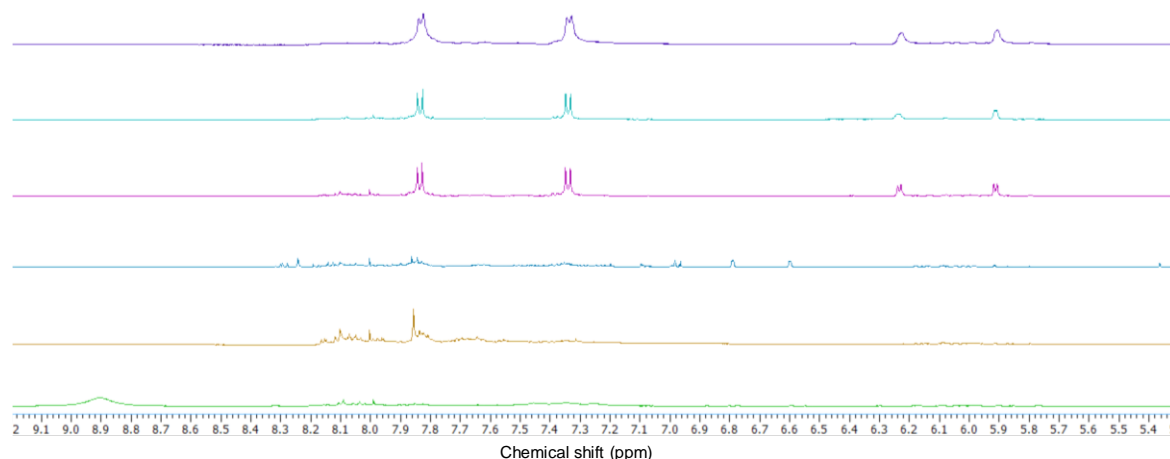


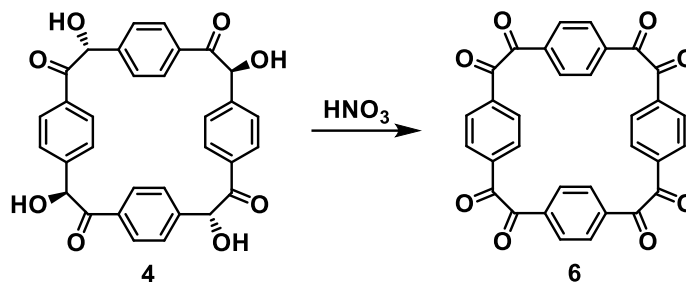
Figure 4.5 Comparison of NMR spectra of fractions from the reaction precipitate of **4** collected from Sephadex column. First three fractions, green, brown, and blue, show no desired peaks that match **4**. They also show no benzoin peaks to show the condensation reaction has taken place. Last three fractions, pink, teal, and purple, show the desired matching peaks of **4**.

To see if other products could be produced in this reaction, we replaced the 2-methoxyethanol with DMSO and ran the reaction as otherwise published. Since DMSO is the only solvent able to dissolve **4**, these conditions could keep all products dissolved and an equilibrium could be established to possibly create a different product than **4**. After several days a precipitate started to form in the reaction, which was filtered and analyzed by TLC. Several fractions were collected, and NMR analysis revealed that none of the fractions contained peaks that matched **4**. There were also no benzoin or alcohol peaks found in any fraction. While there seems to be a reaction taking place, as starting material is not isolated, NMR does not show benzoin peaks which indicates that a benzoin reaction is not taking place under these conditions. While multiple different purification methods were implemented, no improvements were found when compared to published conditions. Some limiting factors to purifying **4** were its high

polarity which limits the choice of solvents that can be utilized in purification methods. We also were unsuccessful in identifying any other products formed during the reaction.

4.4.2 Purification After Oxidation to Cyclotetrabenzil

As shown before, we have been able to oxidize cyclotetrabenzoin (**4**) to cyclotetrabenzil (**6**) (Scheme 4.3).²⁶² Cyclotetrabenzil (**6**) could be purified by Soxhlet extraction with chloroform, indicating its increased solubility. With the increased solubility, we were hopeful that we could then separate all components of this reaction. First, we oxidized the entire crude



Scheme 4.3 Synthesis of cyclotetrabenzil (**6**) from cyclotetrabenzoin (**4**).

reaction precipitate without any purification. Column chromatography resulted in the isolation of two fractions. Analysis of the first collected fraction by NMR showed several aromatic peaks with two minor acidic peaks indicating that most products collected were cyclic. Upon oxidation, stereocenters are removed resulting in all aromatic protons becoming equivalent and a single aromatic peak in **6**, which is also the expected pattern for larger macrocycles. Further purification by TLC of cyclic products showed no separation of any products: while samples showed movement by TLC, all products eluted together. The second isolated fraction showed only aliphatic peaks and residual solvent by NMR analysis. Several column chromatographic separations were attempted but resulted in the same results of a crowded aromatic region with the inability to separate these products further for characterization.

Since column chromatography did not seem to produce efficient separation, we tried to use sublimation. Again, the crude product of **4** was oxidized, then sublimed by slowly increasing the temperature under vacuum until 300 °C, which resulted in six fractions collected and some product that did not sublime. All fractions were analyzed by NMR spectroscopy, with the first fraction matching the spectrum of terephthalic acid, oxidized product of starting material **3**, showing an acid peak and a singlet aromatic peak. Other collected sublimation fractions showed multiple aromatic peaks and minimal acid peaks, indicating they could be cyclic. Comparison of the collected NMR of sublimed fractions with the NMR collected from the first fraction off the column show a similar aromatic pattern, indicating both methods result in potential cyclic products or oxidized linear products with a terminal cyanide, however neither method was able to effectively separate products.

We also analyzed all stages of this reaction by gel permeation chromatography (GPC) which is a size exclusion chromatography method. To get a full understanding of the reaction of **4** several stages were analyzed including published purification methods. A large-scale reaction of **4** was run, with the crude product being split into three groups to analyze all components. The first sample (A) was purified by published conditions in DMSO/methanol solution, then oxidized, and purified by Soxhlet extraction. This fraction should be the purest section going through both published purification methods. The second sample (B) was purified by published conditions in DMSO/methanol solution, then oxidized, and analyzed as is. The third sample (C) was not purified and oxidized as a crude product. Analysis of these three samples going from purest (A) to least pure (C) should be able to show how many compounds are removed by each purification method. The mother liquor of the initial reaction was evaporated to dryness, and isolated solids were oxidized and analyzed as well. While analysis

by GPC should give us a good indication of how many products are present in the reactions, it will not tell us exactly what the products are. Retention time from GPC could indicate whether products are larger or smaller in weight than **6**, as larger molecules will elute faster than smaller molecules. Analysis of collected spectra shows that sample A has one major product (Figure 4.6 red), with a retention time around 18 minutes, and two larger products, with retention times around 15 min. Comparison to sample B (Figure 4.6 green) shows products with similar retention times with an increase in intensity of the larger molecules. While the peak heights of the impurities appear to stay the same, the ratio of impurity to **6** increases from sample A to sample B. Sample C (Figure 4.6 blue), which should be the most impure, shows the same two

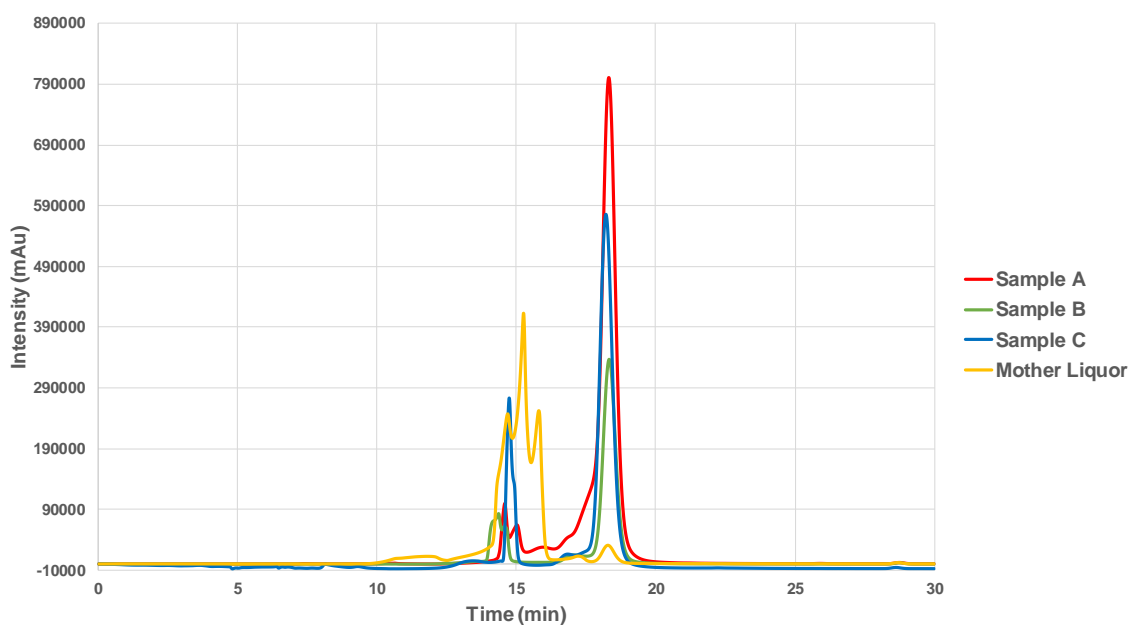


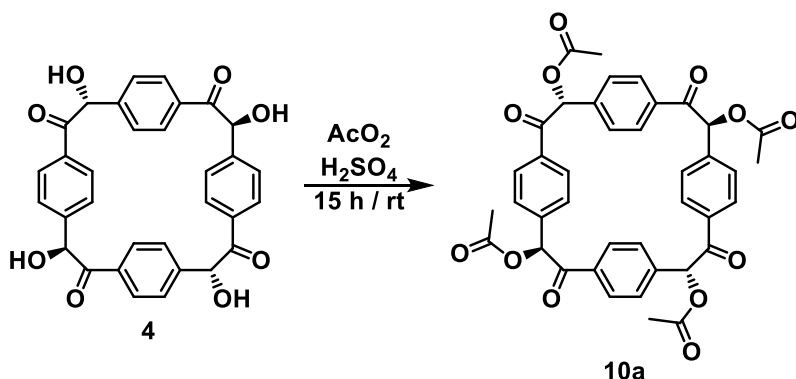
Figure 4.6 GPC traces at various points throughout the published purification process of the synthesis of **4** and **6**. Sample A should be the purest sample having gone through purification processes of both **4** and **6**, sample B was only purified after synthesis of **4**, and sample C should be the most impure having not been purified by either method. Mother liquor sample was evaporated to dryness after synthesis of **4** and solids were oxidized. Analysis of sample A shows the major product **6** along with a minor impurity, larger in size than **6**, which also remains in samples B and C. The mother liquor sample shows potentially the same product is present, along with two other products also larger in size than **6**. The mother liquor also shows the majority of **4** is isolated from the reaction with the initial filtration.

products as the other two samples. These three samples show the same impurities are, to some extent, present throughout the entire purification process of macrocycles **4** and **6**. The oxidized products of the mother liquor (Figure 4.6 yellow) show very little **6** remained and three larger products are the main components of the precipitated solids. Of those three products, two do not seem to appear in any other sample, indicating they are completely soluble in the reaction solvent mixture. Further characterization of these products was unsuccessful as the DMF that was used as the solvent decomposed the products over time. Attempted modification to decrease flow rate to separate peaks was unsuccessful as no additional peak separation was achieved—only peak broadening. We learnt that there is minimal amount of **4** that is not precipitated out of solution, along with at least three other larger products present in the mother liquor. Upon oxidation, any regioisomers that were formed in the first reaction are now all the same, minimizing the number of products present in solution. Full characterization of products has still not been achieved with decomposition of samples and the inability to further separate overlapping product peaks through GPC analysis.

Analysis of oxidized products allowed us to use purification methods that we were not able to before. We were able to isolate two fractions by column chromatography; one showed several aromatic peaks while the second sample contained aliphatic and solvent peaks. These results are also supported by GPC analysis, where sample C shows two compounds are present and confirms the second compound is larger in size than **6**. While neither method has been able to fully characterize any additional components, we have learned there is another product larger than **6** present in the reaction precipitate and the mother liquor contains an additional two products also larger in size. Whether these products are cyclic or linear has not conclusively been determined.

4.4.3 Purification After Esterification of Reaction Components

The second synthetic modification we have achieved to cyclobenzoin is the esterification of alcohol groups. This simple esterification increased the solubility of cyclobenzoin in common organic solvents enough to be purified for the first time utilizing normal phase silica. With the added solubility, we wanted to conduct the same experiments to determine all reaction components as we did before. Of the previously published esterification macrocycles,²⁶⁷ acetic anhydride was chosen to do the esterifications (Scheme 4.4). The first



Scheme 4.4 Esterification synthesis yielding major product of **10a**.

components we tried to purify were the esterified products of the crude precipitate of **4**. Column chromatography resulted in 76% yield of pure **10a**, confirming that it could be possible to isolate more than 20% of **4**, as reported previously. While we have been able to increase the isolated yield of **4**, however we were not able to identify what the impurities were. This reaction was repeated, with purification by preparative thin layer chromatography plates instead of column chromatography isolate all products. Separation of two compounds were observed, one that moved and one that remained on the base line. Analysis by NMR showed the compound that moved was pure **10a** while the compound that remained on the baseline had no peaks of interest. This indicates the by-product of this reaction that does not move by TLC could be the

same solid that was the second fraction isolated by column after oxidation as the NMR of this fraction also contained no aromatic peaks. As the esterified solids and oxidized solids were not purified through the DMSO/methanol process, the solids isolated that show no aromatic peaks could be the same product that is removed during the purification of **4**.

After the completion of the synthesis of **4**, the precipitate was isolated, the mother liquor was evaporated to dryness and the remaining solids were subjected to the same esterification conditions and purified by column chromatography. Two fractions were isolated off the column, with NMR analysis showing both spots are most likely a mix of linear products with several aldehyde peaks. This matches the conclusion previously observed when analyzing the mass spectrum of induced precipitated products from the mother liquor. This purification was also repeated using preparative TLC where the first plate isolated two compounds where the compound that moved remained impure by NMR analysis, so the compound was collected and subjected to a second separation by preparative TLC. Separation on the second plate resulted in three compounds, all of which showed minor benzoin peaks by NMR analysis. Unfortunately, neither method was successful in characterizing any component of the mother liquor. However, fractions isolated by column chromatography did support the previous findings of analysis of original mother liquor products that the remaining products are linear.

We also tried to purify the reaction without removing the initial precipitate to use as a control to monitor how other components move through purification. To accomplish this, upon completion of the reaction all solvents were evaporated to dryness to leave all reaction solids together, which were then esterified. Purification by column chromatography was able to isolate two individual fractions. Analysis by NMR of the first isolated fraction showed some aldehyde peaks with a crowded aromatic region. The area where the expected benzoin peak were

expected to be had several peaks, however they were relatively minor, indicating a benzoin reaction may not have taken place. What is more confusing about this fraction is the lack of **10a** peaks. Since **10a** was not removed from the initial solution, we would expect to see a large amount of **10a** present. The second isolated fraction did not show any aromatic peaks by NMR, corresponding to previous studies where the compounds remaining on the baseline are not benzoin products. We also tried to purify this mixture by preparative TLC. In the first round of TLC, three compounds were isolated. Two of the three compounds moved off the baseline and showed complicated patterns of peaks by NMR while the compound that remained on the baseline showed no peaks of interest, as seen with other purifications. The two compounds that moved were analyzed by a second preparative TLC plate. The compound that moved the furthest the first time was further separated into two compounds. The first compound had a crowded aromatic area with a few aldehyde peaks, while the second compound again showed no aromatic peaks. In the second compound that was re-separated by preparative TLC was further separated into four compounds and analyzed by NMR. Of the four isolated compounds, only the compound that moved the furthest had any aromatic peaks by NMR. These peaks correspond to peaks of **10a** with some of the impurities being linear products with a small amount of aldehyde peaks present. Through these studies we have not been able to identify any other products of the reaction of **4**. Column chromatography and preparative TLC of esterified products continued to confirm what we have seen in previous purification with other isolated products not containing aromatic peaks by NMR analysis.

Unable to isolate additional macrocycles from the crude mixture, we looked to change the established equilibrium of the reaction by replacing 2-methoxyethanol with DMSO. Since DMSO is the only solvent able to dissolve all of **4**, all reaction products should remain in solution continuing to establish an equilibrium. All other reaction conditions were repeated and to our surprise, after 24 hours there was a precipitate that formed in the reaction. The precipitate was filtered and subjected to column chromatography where three fractions were able to be isolated. Analysis of the first fraction by NMR shows pure **10a**, which was confirmed by mass spectrum. The second fraction showed NMR peaks in similar locations, but the peaks were not as well defined, and there were additional peaks in the aromatic region and peaks reappear in the area similar to where the hydroxyl protons of **4** appear (Figure 4.7). Mass spectrum analysis of this product showed a molecular ion peak at 643.2 m/z units, which corresponds to **4** with

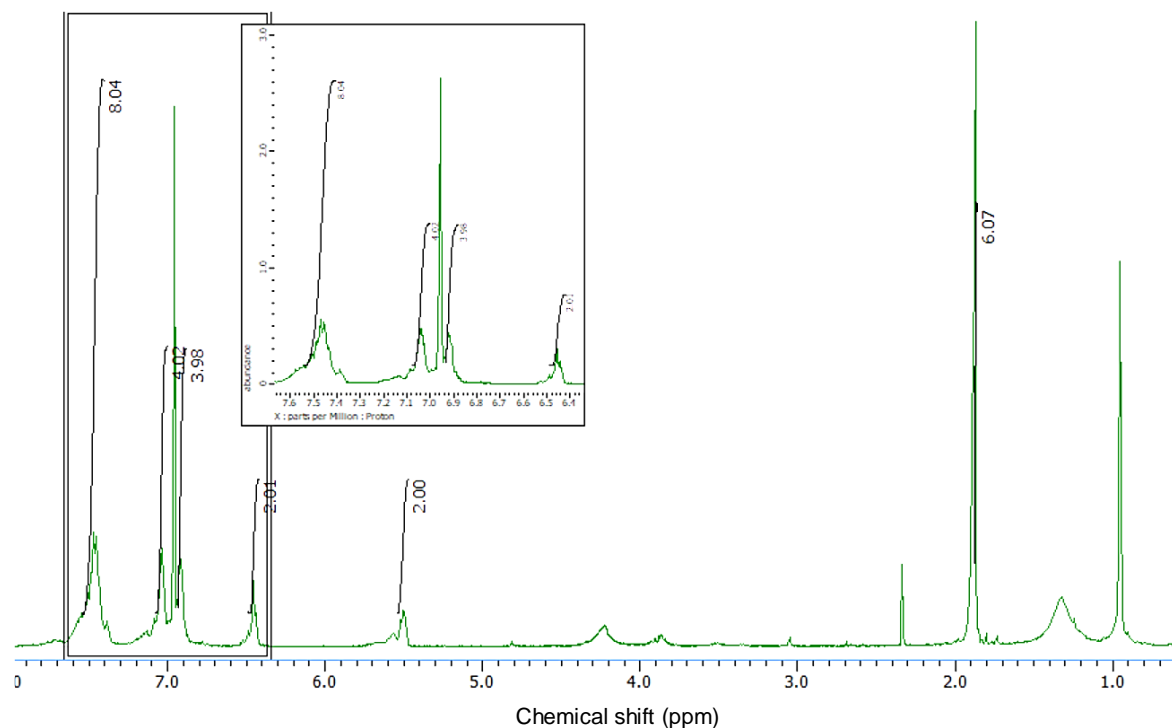


Figure 4.7 NMR spectrum of the first isolated fraction of esterified products from column chromatography of the precipitate collected from reaction with DMSO/water as reaction solvent. Integration shows a ratio of 8:4:4:2:2:6 which could correspond to **4** with two ester and two hydroxyl groups (**57**, **58**).

two ester groups and two hydroxy groups (**57**, **58**) (Figure 4.8). The two isomers shown are the most likely products, however other isomers are also possible since the NMR peaks are not

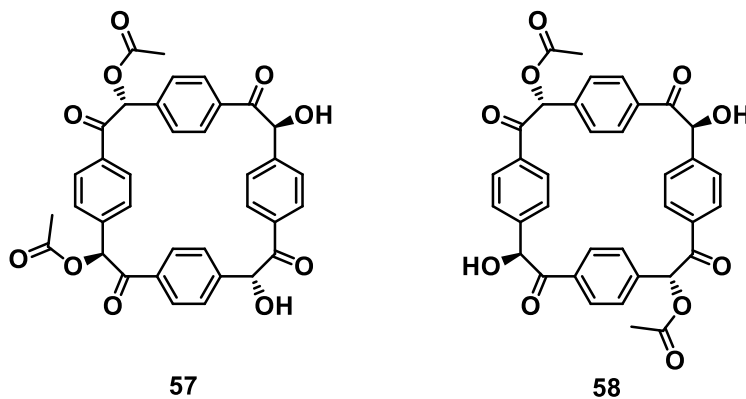


Figure 4.8 Most likely isomer products isolated in second fraction purified through column chromatography.

well-defined to determine other isomers. The last isolated fraction again showed peaks in similar locations to the second fraction, however there was even less definition and the hydroxyl peak was larger than the benzoin peak. Mass spectrum showed a molecular ion peak of 601.1 m/z units, which corresponds to cyclotetrabenzoin with one acetyl group and three hydroxyl groups (**59**) (Figure 4.9). The remaining mother liquor was evaporated to dryness and the remaining solids were esterified. Column chromatography isolated three fractions. The first fraction was analyzed by NMR and matched the peaks of **10a**. The second fraction's NMR spectrum matched the peaks of the previously isolated **59**. The last collected fraction again

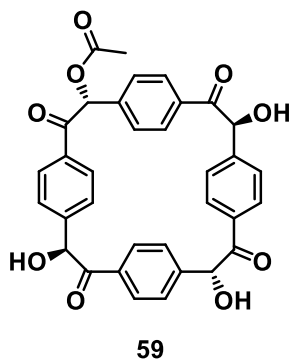


Figure 4.9 Isomer product isolated in the third fraction purified by column chromatography.

contained no aromatic peaks by NMR analysis. We have shown that changing the reaction solvent to an equal mixture of water and DMSO results in the same substitution as the previously published **4**. Column chromatography was able to isolate two additional products that were characterized to be different degrees of incomplete esterification of **4**. Changing the reaction conditions to increase solubility and keep an established equilibrium did not result in isolation of any solid that indicates there is another macrocycle present.

We wanted to see if keeping all products in solution would change the equilibrium, so the amount of water was reduced in relation in DMSO. After 48 hours at reflux no precipitate had formed in the reaction. To induce precipitation, water was added while the reaction was still warm, which caused a precipitate to form that could be filtered and esterified. Column chromatography resulted in the collection of four fractions. The first fraction that was isolated off the column was analyzed by NMR and showed that the majority of the peaks matched product **10a**. The second fraction isolated had most of the same peaks with an additional peak around 6 ppm, which matches the NMR spectrum of **57**, **58**. Both fractions had aldehyde peaks as well, indicating neither fraction was completely pure. The last two collected fractions did not have any benzoin peaks, indicating that a benzoin reaction did not take place. Aromatic peaks were also minimal, which has also been seen in all other purification methods in the last isolated fraction or compounds. Changing of the reaction solvent did not change the major product observed in this reaction: we could still only isolate **10a**.

Through esterification, we were able to confirm previously seen results in identifying other reaction components. Aside from the isolation of esterified **4**, completely or partially esterified, NMR analysis showed that most other isolated compounds did not have aromatic peaks. This has also been observed in the purification of oxidized components. Reaction

conditions were modified to include DMSO as a reaction solvent to hopefully change the major product, however, it was found that again **4** was the major product after esterification and no indication of other macrocycles were present.

4.5 Conclusion

The synthesis of cyclotetrabenzoin (**4**) is a simple one pot synthesis that results in a single isomer macrocycle, while a significant portion of starting materials are unaccounted for. With the benzoin condensation reaction being an equilibrium reaction, we looked to modify reaction conditions to shift the equilibrium and produce other products. These proved to be unsuccessful as **4** was the only isolated product regardless of conditions. Analysis of calculated NMR yields indicated pure yield was higher than the previously reported 20%, however no purification methods were found to increase the isolated yields. We then tried to isolate other components of this reaction. Starting with the parent reaction of **4** the purification was unsuccessful, due largely to the insolubility of **4** in common organic solvents necessary for separation techniques. Increased solubility was observed by oxidation in the discovery of **6**, so we applied the same purification techniques to oxidized products with the ability to use common organic solvents. Through GPC analysis we were able to show there are three other products that are larger than **6** present in the mother liquor, however characterization was not achieved as products decomposed in DMF and product separation was not achieved. The most success in increasing solubility came with esterification in producing **10a** which could be purified by column chromatography. We again used this synthetic modification to analyze reaction components but were unsuccessful in identifying reaction components other than the cyclic tetramer. The only products we were able to identify were **57**, **58**, and **59** which were confirmed

by mass spectrum and NMR. When taking a crude sample of **4** and esterifying all products, we were able to get a 70% yield, indicating the true yield of **4** is much larger than 20%. Through all purification analysis at different times throughout the course of the reaction we were not able to characterize a larger macrocycle or a different isomer of **4**. Several purification processes resulted in isolated solids that contained either no benzoin, aromatic or both types of peaks in the NMR.

4.6 Experimental Section

4.6.1 General Methods

Column chromatography was performed on silica gel 60 (32–63 μm). Analytical TLC was performed on J. T. Baker plastic-backed silica gel IB-F plates, EDM Millipore glass-backed silica gel F₂₅₄ plates. Preparative TLC was performed on Analtech Uniplate glass-backed silica gel UV₂₅₄ plates. NMR data was collected on a JEOL ECA-500 MHz or ECA-600 MHz spectrometers, with working frequencies (for ¹H nuclei) of 500 and 600 MHz, respectively. Chemical shifts are given in ppm (δ) and are referenced to the residual CDCl₃ solvent peak at 7.26 ppm (¹H NMR) and 77.16 ppm (¹³C NMR) or (CD₃)₂SO solvent peak at 39.52 ppm (¹³C NMR). Conventional one-dimensional (1D) ¹H NMR and ¹³C{¹H} NMR experiments were recorded at room temperature under routine conditions. All ¹³C NMR spectra were recorded with the simultaneous decoupling of ¹H nuclei. NMR data was analyzed using Delta NMR data processing software. High Resolution Mass Spectra (HRMS) were collected at the University of Texas at Austin mass spectrometry facility on an Agilent 6530 Q-TOF spectrometer. GPC analysis was done using Shimadzu HPLC instrument with Shodex column packed with DMF.

All commercially available reagents were used as received unless otherwise stated. Synthetic procedures were followed as previously published for **4**, **6**, and **10a**.^{221,262,267}

4.6.2 NMR Spectra of Isolated Compounds from Various Purification Methods

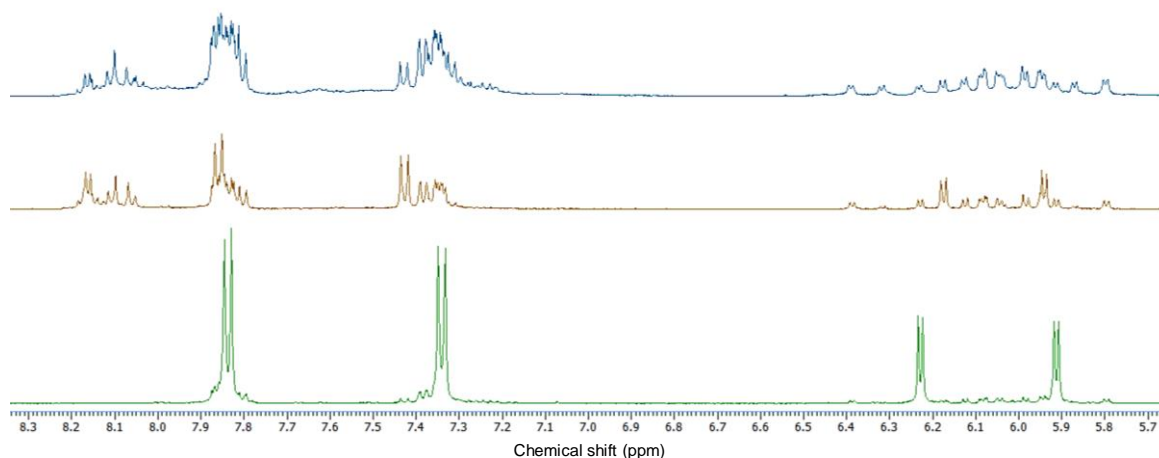


Figure 4.10 Stacked NMR spectra of precipitates isolated from modifications to published purification method of **4**. Comparison of collected precipitates shows a decrease in purity from green to blue. The additional aromatic peaks around 8.1 ppm could correspond to different isomers of **4**. Peaks that correspond to **4** can be found in all three spectra, however, most of **4** is removed in the first precipitate. Green—first precipitate collected after published conditions with no modification, brown—second precipitate collected after a second addition of boiling methanol and precipitation for seven days, blue—third precipitate isolated after addition of water to precipitate all remaining compounds.

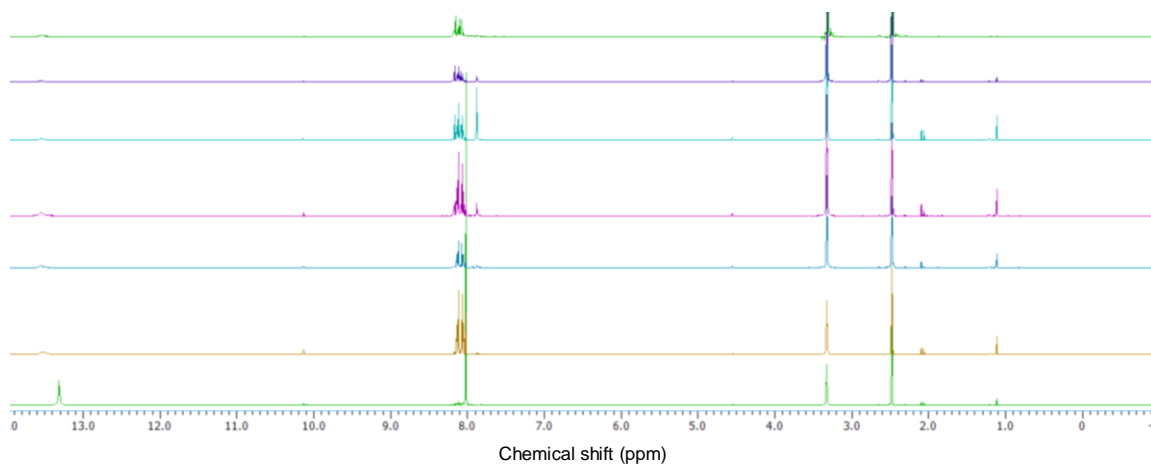


Figure 4.11 Stacked NMR spectra of sublimation fractions of oxidized crude reaction precipitate. NMR spectra are stacked in order of isolation, with the bottom green spectra being the first isolated fraction and the top green spectra being the fraction that did not sublime. The first isolated fraction, bottom green spectrum, matches terephthalic acid which is the oxidation product of starting material **3**. All other collected fractions show similar NMR spectra with several aromatic peaks and minimal acid peaks, indicating a mixture of cyclic products. In fractions collected through sublimation, we were not able to isolate a single product other than the oxidized starting materials.

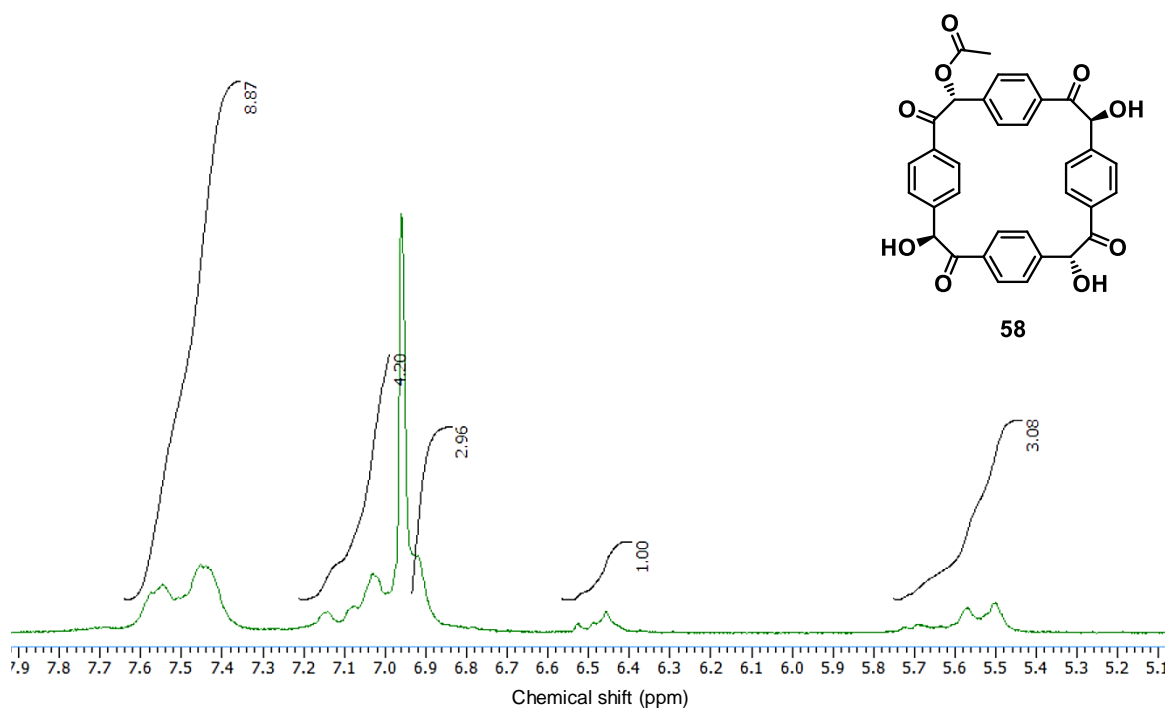


Figure 4.12 NMR analysis of the third isolated fraction from column chromatography of esterified precipitate from reaction containing DMSO/water as solvent system. Three aromatic regions of peaks are present, along with a small benzoin peak around 6.4 ppm and a larger hydroxyl peak around 5.5 ppm. These peaks correspond to **58** which was confirmed by mass spectrum.

Bibliography

1. Schüth, F.; Sing, K. S. W.; Weitkamp, J. *Handbook of Porous Solids*, John Wiley & Sons: Hoboken, NJ, **2002**.
2. Rouquerol, J.; Avnir, D.; Fairbridge, C. W.; Everett, D. H.; Haynes, J. H.; Pernicone, N.; Ramsay, J. D. F.; Sing, K. S. W.; Unger, K. K. *Pure Appl. Chem.* **1994**, *66*, 1739–1758.
3. Akhtar, F.; Andersson, L.; Ogunwumi, S.; Hedin, N.; Bergetröm, L. *J. Eur. Ceramic Soc.* **2014**, *34*, 1643–1666.
4. Król, M.; Mozgawa, W.; Jastrzębski, W. *J. Porous Mater.* **2016**, *23*, 1–9.
5. Degnan Jr., T. F. *Top. Catal.* **2000**, *13*, 349–356.
6. Cheung, O.; Hedin, N. *RSC Adv.* **2014**, *4*, 14480–14494.
7. Mofarahi, M.; Gholipour, F. *Microporous Mesoporous Mater.* **2014**, *200*, 1–10.
8. Breck, D. W. *Zeolite Molecular Sieves: Structure, Chemistry and Use*, John Wiley & Sons, Inc.: New York, NY, **1974**.
9. Breck, D. W. *J. Chem. Educ.* **1964**, *41*, 678–689.
10. Čejka, J.; Corma, A.; Zones, S. I. *Zeolites and Catalysis: Synthesis Reactions and Applications*, Wiley, Weinheim, Germany, **2010**.
11. Moliner, M. *Dalton Trans.* **2014**, *43*, 4197–4208.
12. Cui, Y.; Li, B.; He, H.; Zhou, W.; Chen, B.; Qian, G. *Acc. Chem. Res.* **2016**, *49*, 483–493.
13. Bosch, M.; Yuan, S.; Rutledge, W.; H. C. *Acc. Chem. Res.* **2017**, *50*, 857–865.
14. Liu, D.; Zou, D.; Zhu, H.; Zhang, J. *Small* **2018**, *14*, 1801454.
15. Yaghi, O. M.; Li, H. *J. Am. Chem. Soc.* **1995**, *117*, 10401–10402.

16. Chui, S. S. Y.; Lo, S. M. F.; Charmant, J. P. H.; Orpen, A. G.; Williams, A. D. *Science* **1997**, *36*, 1725–1727.
17. Kondo, M.; Fujimoto, K.; Ohkubi, T.; Asami, A.; Noro, S.; Kitagawa, S.; Ishii, T.; Matsuzaki, H. *Chem. Lett.* **1999**, *28*, 291–292.
18. Li, H. Eddaoudi, M.; O’Keeffe, M.; Yaghi, O. M. *Nature* **1999**, *402*, 276–279.
19. Abrahams, B. F.; Hoskins, B. F.; Robson, R. *J. Am. Chem. Soc.* **1991**, *113*, 3606–3607.
20. Zaworotko, M. J. *Nature* **1997**, *386*, 220–221.
21. Hashim, M. I.; Hsu, C.-W.; Le, H. T. M.; Miljanić, O. Š. *Synlett* **2016**, *27*, 1907–1918.
22. Han, Y.-F.; Yuan, Y.-X.; Wang, H.-B. *Molecules* **2017**, *22*, 266.
23. Hassell, T.; Copper, A. I. *Nat. Rev. Mater.* **2016**, *1*, 1–14.
24. Holst, J. R.; Trewin, A.; Cooper, A. I. *Nat. Chem.* **2010**, *2*, 915–920.
25. Barrer, R. M.; Ibbitson, D. A. *Trans. Farad. Soc.* **1944**, *40*, 195–206.
26. Maesen, T. *Introduction to Zeolite Science and Practice 3rd ed.*, Elsevier, Amsterdam, **2007**, 1–12.
27. Alkhlel, A.; De Lasa, H. *Ind. Eng. Chem. Res.* **2018**, *57*, 13627–13638.
28. Millar, G. J.; Couperthwaite, S. J.; Alyuz, K.; *Int. J. Chem. Environ. Eng.* **2016**, *4*, 1918–1928.
29. Millar, G. J.; Winnett, A.; Thompson, T.; Couperthwaite, S. J. *J. Water Process Eng.* **2016**, *9*, 47–57.
30. Wen, J.; Dong, H.; Zeng, G. *J. Clean. Prod.* **2018**, *197*, 1435–1446.

31. Poursaeidesfahani, A.; Andres-Garcia, E.; de Lange, M.; Torres-Knoop, A.; Rigutto, M.; Nair, N.; Kapteijm, F.; Gascon, J.; Dubbeldam, D.; Vlugt, T. J. H. *Microporous Mesoporous Mater.* **2019**, *227*, 237–244.
32. Nakhli, S. A. A.; Delkash, M.; Bakhshayesh, B. E.; Kazemian, H. *Water Air Soil Pollut.* **2017**, *288*, 464.
33. Valpotić, H.; Gračner, D.; Turk, R.; Đuričić, D.; Vince, S.; Folnožić, I.; Lojkić, M.; Žaja, I. Ž.; Bedrica, L.; Maćešić, N.; Getz, I.; Dobranić, T.; Samardžija, M. *Period. Biol.* **2017**, *119*, 159–172.
34. Li, Y.; Li, L.; Yu, J. *Chem* **2017**, *3*, 928–949.
35. Lima, C. G. S.; Moreira, N. M.; Paixão, M. W.; Corrêa, A. G. *Curr. Opin. Green Sustain. Chem.* **2019**, *15*, 7–12.
36. Prech, J. *Catal. Rev. Sci. Eng.* **2018**, *1*, 71–131.
37. Meshram, S. U.; Khandekar, U. R.; Mand, S. M.; Mohan, A. *J. Surfactants Deterg.* **2015**, *18*, 259–266.
38. Kubů, M.; Žilková, N. *Catal. Today* **2019**, *324*, 3–14.
39. Collins, F.; Rozhkovskaya, A.; Outram, J. G.; Millar, G. J. *Microporous Mesoporous Mater.* **2020**, *291*, 109667.
40. Bu, X.; Feng, P.; Gier, T. E.; Zhao, D.; Stucky, G. D. *J. Am. Chem. Soc.* **1998**, *120*, 314–317.
41. Meier, W. M.; Olson, D. H.; Baerlocher, Ch. *Atlas of Zeolite Structure Types*; Elsevier: Boston, MA, **1996**.
42. Čejka, J.; van Bekkum, H.; Corma, A.; Schüth, F. *Stud. Surf. Sci. Catal.* Elsevier, Amsterdam, **2007**.

43. Wilson, S. T.; Lok, B. M.; Messina, C. A.; Cannan, T. R.; Flanigen, E. M. *J. Am. Chem. Soc.* **1982**, *104*, 1146–1147.
44. Khan, M. I.; Meyer, L. M.; Haushalter, R. C.; Schweitzer, A. L.; Zubieta, J.; Dye, J. L. *Chem. Mater.* **1996**, *8*, 43–53.
45. Suib, S. T. *Curr. Opin. Solid State Mater. Sci.* **1998**, *3*, 63–70.
46. Bu, X.; Feng, P.; Gier, T. E.; Zhao, D.; Stucky, G. D. *J. Am. Chem. Soc.* **1998**, *120*, 13389–13397.
47. Gier, T. E.; Bu, X.; Feng, P.; Stucky, G. D. *Nature* **1998**, *13*, 88–91.
48. Werner, A. Z. *Anorg. Chem.* **1893**, *3*, 267–330.
49. Schoedel, A.; Rajeh, S. *Top. Curr. Chem.* **2020**, *378*, 19.
50. Tasiopoulos, A. J.; Vinslava, A.; Wernsdorfer, W.; Abboud, K. A.; Christou, G. *Angew. Chem., Int. Ed.* **2004**, *43*, 2117–2121.
51. Abourahma, H.; Bodwell, G. J.; Lu, J.; Moulton, B.; Pottie, I. R.; Walsh, R. B.; Zaworotko, M. J. *Cryst. Growth Des.* **2003**, *3*, 513–519.
52. Chen, B.; Eddaoudi, M.; Reineke, T. M.; Kampf, J. W.; O’Keeffe, M.; Yaghi, O. M. *J. Am. Chem. Soc.* **2000**, *122*, 11559–11560.
53. Koyama, H.; Saito, Y. *Bull. Chem. Soc. Jpn.* **1954**, *27*, 112–114.
54. Shen, J.-O.; Liao, P.-Q.; Zhou, D.-D.; He, C.-T.; Wu, J.-X.; Zhang, W.-X.; Zhang, W.-X.; Zhang, J.-P.; Chen, X.-M. *J. Am. Chem. Soc.* **2017**, *139*, 1778–1781.
55. Mellot-Draznieks, C.; Dutour, J. Férey, G. *Anorg. Allg. Chem.* **2004**, *630*, 2599–2604.
56. Tranchemontagne, D. J.; Mendoza-Cortés, J. L.; O’Keeffe, M.; Yaghi, O. M. *Chem. Soc. Rev.* **2009**, *38*, 1257–1283.

57. Deng, H.; Doonan, C. J.; Furukawa, H.; Ferreira, R. B.; Towne, J.; Knobler, C. B.; Wang, B.; Yaghi, O. M. *Science* **2010**, *327*, 846–850.
58. Hoskins, B. F.; Robson, R. *J. Am. Chem. Soc.* **1990**, *112*, 1546–1554.
59. Yaghi, O. M.; Li, G. *Angew. Chem. Int. Ed. Engl.* **1995**, *34*, 207–209.
60. Li, H.; Eddaoudi, M.; Groy, T. L.; Yaghi, O. M. *J. Am. Chem. Soc.* **1998**, *120*, 8571–8572.
61. Joaristi, A. M.; Juan-Alcañiz, J.; Serra-Crespo, P.; Kapteijn, F.; Gascon, J. *Cryst. Growth. Des.* **2012**, *12*, 3489–3498.
62. Müller, U.; Puetter, H.; Hesse, M.; Wessel, H. *Patent* WO 2005/049892, **2005**.
63. Geydye, R.; Smith, F.; Westaway, K.; Ali, H.; Baldisera, L.; Laberge, L.; Rousell, J. *Tetrahedron Lett.* **1986**, *27*, 279–282.
64. Taddei, M.; Dau, P. V.; Cohen, S. M.; Ranocchiari, M.; van Bokhoven, J. A.; Costantino, F.; Sabatini, S.; Vivani, R. *Dalton Trans.* **2015**, *44*, 14019–14026.
65. Son, W.-J.; Kim, J.; Ahn, W.-S. *Chem. Commun.* **2008**, *59*, 659–683.
66. Carson, C. G.; Brown, A. J.; Sholl, D. S.; Nair, S. *Cryst. Growth Des.* **2011**, *11*, 4505–4689.
67. Carlier, L.; Baron, M.; Chamayou, A.; Couarraze, G. *Tetrahedron Lett.* **2011**, *52*, 4686–4689.
68. Frišćić, T. *Chem. Soc. Rev.* **2012**, *41*, 3493–3510.
69. Ahmad, M. Z.; Navarro, M.; Lhotka, M.; Zornoza, B.; Tellez, C.; de Vos, W. M.; Benes, N. E.; Konnertz, N. M.; Visser, T.; Semino, R.; Maurin, G.; Fila, V.; Coronas, J. *J. Memb. Sci.* **2018**, *558*, 64–77.
70. Assen, A. H.; Yassine, O.; Shekhah, O.; Eddaoudi, M. *ACS Sens.* **2017**, *2*, 1294–1301.

71. Wu, C.-D.; Zhao, M. *Adv. Mater.* **2017**, *29*, 1605446.
72. Jiang, K.; Zhang, L.; Hu, Q.; Yang, Y.; Lin, W.; Cui, Y.; Yang, Y.; Qian, G. *Matter. Lett.* **2018**, *225*, 142–144.
73. Tian, T.; Zeng, Z.; Vulpe, D.; Casco, M. E.; Divitini, G.; Midgley, P. A.; Silvestre-Albero, J.; Tan, J.-C.; Moghadam, P. Z.; Fairen-Jimenez, D. *Nat. Mater.* **2018**, *17*, 177–180.
74. Cooper, A. I. *ACS Cent. Sci.* **2017**, *3*, 544–553.
75. Evans, J. D.; Sumbly, C. J.; Doonan, C. *Chem. Lett.* **2015**, *44*, 582–588.
76. Zhang, G.; Mastalerz, M. *Chem. Soc. Rev.* **2014**, *43*, 1934–1947.
77. Mastalerz, M. *Synlett* **2013**, *24*, 781–786.
78. Tian, J.; Thallapally, P. K.; McGrail, B. P. *CrystEngComm* **2012**, *14*, 1909–1919.
79. McKeown, N. B. *J. Mater. Chem.* **2010**, *20*, 10588–10597.
80. Barbour, L. J. *Chem. Commun.* **2006**, 1163–1168.
81. Iwamoto, T.; Makano, T.; Morita, M.; Miyoshi, T.; Miyamoto, T.; Sasaki, Y. *Inorg. Chim. Acta.* **1968**, *2*, 313–316.
82. Mathey, Y.; Mazières, C.; Setton, R. *Inorg. Nucl. Chem. Lett.* **1977**, *13*, 1–3.
83. Tomic, E. A. *J. Appl. Polym. Sci.* **1965**, *9*, 3745–3752.
84. Chui, S. Y.; Lo, S. M.-F.; Charmant, J. P. H.; Orpen, A. G.; Williams, I. D. *Science* **1999**, *283*, 1148–1150.
85. Farha, O. K.; Eryazici, I.; Jeong, N. C.; Hauser, B. G.; Wilmer, C. E.; Sargeant, A. A.; Snurr, R. Q.; Nguyen, S. T.; Yazaydin, A. O.; Hupp, J. T. *J. Am. Chem. Soc.* **2012**, *134*, 15016–15021.
86. Ma, W.; Yang, H.; Yu, L.; Chen, Y.; Li, Y. *Materials* **2014**, *7*, 4431 – 4441.

87. García-Martínez, J.; Johnson, M.; Valla, J.; Kunhao, L.; Ying, J. Y. *Catal. Sci. Technol.* **2012**, 2, 987–994.
88. Dey, C.; Kundu, T.; Biswal, B. P.; Mallick, A.; Banerjee, R. *Acta. Cryst.* **2014**, B70, 3–10.
89. Barbour, L. J. *Chem. Commun.*, **2006**, 1163–1168.
90. Pfeiffer, P. *Organic Molecular Compounds*, Stuttgart, **1927**, 213.
91. Feigl, F. *Anais Assoc. Quim. Brasil*, **1944**, 3, 72.
92. Walker, F. G.; Hawthorne, D. G. *Trans. Faraday Soc.* **1967**, 63, 166–174.
93. Iwamoto, T.; Miyoshi, T.; Miyamoto, T.; Sasaki, Y.; Fujiwara, S. *Bull. Chem. Soc. Jpn.* **1967**, 40, 1174–1178.
94. Dianin, J. J. *Russ. Phys. Chem. Soc.* **1914**, 46, 1310–1319.
95. Barrer, R. M.; Shanson, V. H. *J. Chem. Soc., Chem. Commun.* **1976**, 9, 333–334.
96. Atwood, J. L.; Barbour, L. J.; Jerga, A.; Schottel, B. L. *Science* **2002**, 298, 1000–1002.
97. Dalgarno, S. J.; Thallapally, P. K.; Barbour, L. J.; Atwood, J. L. *Chem. Soc. Rev.* **2007**, 36, 236–245.
98. Mastalerz, M. *Chem. Eur. J.* **2012** 18, 10082–10091.
99. Tozawa, T.; Jones, J. T. A.; Swamy, S. I.; Jiang, S.; Adams, D. J.; Shakespeare, S.; Clowes, R.; Bradshwa, D.; Hasell, T.; Chong, S. Y.; Tang, C.; Thompson, S.; Parker, J.; Trewin, A.; Bacsá, J.; Slawin, A. M. Z.; Steiner, A.; Cooper, A. I. *Nat. Mater.* **2009**, 8, 973–978.
100. Ikbal, S. A.; Colombari, C.; Zhang, A.; Delecluse, M.; Brotin, T.; Dufaud, V.; Dustasta, J.-P.; Sorokin, A. B.; Martines, A. *Inorg. Chem.* **2019**, 58, 7220–7728.

101. Kondratenko, A. V.; Peppel, T.; Seeburg, D.; Kondratenko, V. A.; Kalevaru, N.; Martin, A.; Wohlrab, S. *Catal. Sci. Technol.* **2017**, *7*, 366–381.
102. Hoffmann, K. A.; Küspert, F. Z. *Anorg. Chem.* **1897**, *15*, 204–207.
103. Rayner, J. H.; Powell, H. M. *J. Chem. Soc.* **1952**, 319–328.
104. Sozzani, P.; Bracco, S.; Comotti, A.; Ferretti, L.; Simonutti, R. *Angew. Chem. Int. Ed.* **2005**, *44*, 1816–1820.
105. Barbour, L. J. *Chem. Commun.* **2006**, 1163–1168.
106. Mastalerz, M.; Oppel, I. M. *Angew. Chem. Int. Ed.* **2012**, *51*, 5252–5255.
107. Schwiebert, K. E.; Chin, D. N.; MacDonalds, J. C.; Whitesides, G. M. *J. Am. Chem. Soc.* **1996**, *118*, 4018–4029.
108. Pulido, A.; Chen, L.; Kaczorowski, T.; Holden, D.; Little, M. A.; Chong, S. Y.; Slater, B. J.; McHahon, D. P.; Bonillo, B.; Stackhous, C. J.; Stephenson, A.; Kane, C. M.; Clowes, R.; Hassell, T.; Cooper, A. I.; Day, G. M. *Nature* **2017**, *543*, 657–666.
109. Bezzu, C. G.; Helliwell, M.; Warren, J. E.; Allan, D. R.; McKeown, N. B. *Science* **2010**, *327*, 1627–1630.
110. Zhang, Z.; Miljanić, O. Š. *Org. Mater.* **2019**, *1*, 19–29.
111. Hashim, M. I.; Le, H. T. M.; Chen, T.-H.; Chen, Y.-S.; Daugulis, O.; Hsu, C.-W.; Jacobson, A. J.; Kaveevivitchai, W.; Liang, X.; Makarenko, T.; Miljanić, O. Š.; Popovs, I.; Tran, H. V.; Wang, X.; Wu, C.-H.; Wu, J. I. *J. Am. Chem. Soc.* **2018**, *140*, 6014–6026.
112. Chen, T.-H.; Popov, I.; Kaveevivitchai, W.; Chuang, Y.-C.; Chen, Y.-S.; Daugulis, O.; Jacobson, A. J.; Miljanić, O. Š. *Nat. Commun.* **2014**, *5*, 5131.

113. Chen, T.-H. Kaveevivitchai, W.; Jacobson, A. J.; Miljanić, O. Š. *Chem. Commun.* **2015**, *51*, 14096–14098.
114. Zhang, Z.; Hashim, M. I.; Miljanić, O. Š. *Chem. Commun.* **2017**, *53*, 10022–10025.
115. Saenger, W. *Angew. Chem. Ind. Ed. Engl.* **1980**, *19*, 344–362.
116. Franck, B.; Nonn, A. *Angew. Chem. Int. Ed. Engl.* **1995**, *34*, 1795–1811.
117. Pedersen, C. J. *J. Am. Chem. Soc.* **1967**, *89*, 2495–2496.
118. Ogoshi, T.; Kanai, S.; Fujinami, S.; Yamagishi, T.; Nakamoto, Y. *J. Am. Chem. Soc.* **2008**, *130*, 5002–5003.
119. Cram, D. J.; Cram, J. M. *Chem Soc. Rev.* **2015**, *44*, 6494–6518.
120. Wheate, N. J.; Limantoro, C. *Supramol. Chem.* **2016**, *28*, 849–856.
121. Villiers, A. *Compt. Rend. Acad. Sci.* **1891**, *112*, 536 – 538.
122. Freudenberg, K; Meyer-Delius, M. *Eur. J. Inorg. Chem.* **1938**, *71*, 1596–1600.
123. Szejtli, J. *Chem. Rev.* **1998**, *98*, 1743–1754.
124. Corrigan, O. I.; Stanley, C. T. *J. Pharm. Pharmacol.* **1982**, *34*, 621–626.
125. Trinh, T.; Cappel, J. P.; Geis, P. A.; McCarty, M. L; Pilosof, D.; Zwerdling, S. S. *Patent* 5,714,137, Feb 3, **1998**.
126. McCoy, M. *Chem. Eng. News.* **1999**, *77*, 25–27.
127. Pedersen, C. J. *Angew. Chem. Int. Ed. Engl.* **1988**, *27*, 1021–1027.
128. Cram, D. J.; Cram, J. M. *Science* **1974**, *183*, 803–809.
129. Lehn, J.-M. *Supramolecular Chemistry: Concepts and Perspectives*, VCH, Weinheim, **1995**.
130. Lehn, J.-M. *Acc. Chem. Res.* **1978**, *11*, 49–57.
131. Lehn, J.-M. *Science* **1985**, *227*, 849–856.

132. Lehn, J.-M. *Angew. Chem. Int. Ed. Engl.* **1988**, 27, 89–112.
133. Lehn, J.-M. *Pure Appl. Chem.* **1994**, 66, 1961–1966.
134. Lehn, J.-M. *Alkali Metal Complexes with Organic Ligands*, Springer Berlin Heidelberg, **1973**, 1–69.
135. Behrend, R.; Meyer, E.; Rusche, F. *Ann. Chem.* **1905**, 339, 1–37.
136. Freeman, W. A.; Mock, W. L.; Shih, N. Y. *J. Am. Chem. Soc.* **1981**, 103, 7367–7368.
137. Kim, J.; Jung, I.-S.; Kim, S.-Y.; Lee, E.; Kang, J.-K.; Sakamoto, S.; Yamaguchi, K.; Kim, K. *J. Am. Chem. Soc.* **2000**, 122, 540–541.
138. Day, A.; Arnold, A. P.; Blanch, R. J.; Snushall, B. *J. Org. Chem.* **2001**, 66, 8094–8100.
139. Day, A. I.; Blanch, R. J.; Arnold, A. P.; Lorenzo, S.; Lewis, G. R.; Dance, I. *Angew. Chem. Int. Ed.* **2002**, 41, 275–277.
140. Cheng X. J.; Liang, L. L.; Chen, K.; Ji, N. N.; Xiao, X.; Zhang, J. X.; Zhang, Y. Q.; Xue, S. F.; Zhu, Q. J.; Ni, X. L.; Tao, Z. *Angew. Chem. Int. Ed.* **2013**, 52, 7252–7255.
141. Shetty, D.; Khedkar, J. K.; Park, K. M.; Kim, K. *Chem. Soc. Rev.* **2015**, 44, 8747–8761.
142. Isaacs, L. *Acc. Chem. Res.* **2014**, 47, 2052–2062.
143. Ma, X.; Zhao, Y. *Chem. Rev.* **2015**, 115, 7794–7839.
144. Ogoshi, T.; Kanai, S.; Fujinami, S.; Yamagishi, T.-A.; Nakamoto, Y. *J. Am. Chem. Soc.* **2008**, 130, 5022–5023.
145. Zhang, Z.; Luo, Y.; Chen, J.; Dong, S.; Yu, Y.; Ma, Z.; Huang, F. *Angew. Chem. Int. Ed.* **2011**, 50, 1397–1401.

146. Strutt, N. L.; Forgan, R. S.; Spruell, J. M.; Botros, Y. Y.; Stoddart, J. F. *J. Am. Chem. Soc.* **2011**, *133*, 5668–5671.
147. Zhang, H.; Strutt, N. L.; Stoll, R. S.; Li, H.; Zhu, Z.; Stoddart, J. F. *Chem. Commun.* **2011**, *47*, 11420–11422.
148. Tan, L. L.; Li, H.; Tao, Y.; Zhang, S. X.; Wang, B.; Yang, Y. W. *Adv. Mater.* **2014**, *26*, 7027–7031.
149. Wang, W.; Chen, L.-J.; Wang, X.-Q.; Sun, B.; Li, X.; Zhang, Y.; Shi, J.; Yu, Y.; Zhang, L.; Liu, M.; Yang, H.-B. *Proc. Natl. Acad. Sci. U.S.A.* **2015**, *112*, 5597–5601.
150. Sathiyajith, C.; Shaikh, R. R.; Han, Q.; Zhang, Y.; Meguellati, K.; Yang, Y.-W. *Chem. Commun.* **2017**, *53*, 677–696.
151. Si, W.; Xin, P.; Li, Z.-T.; Hou, J.-L. *Acc. Chem. Res.* **2015**, *48*, 1612–1619.
152. Chen, L.; Si, W.; Zhang, L.; Tang, G.; Li, Z.-T.; Hou, J.-L. *J. Am. Chem. Soc.* **2013**, *135*, 2152–2155.
153. Ogoshi, T.; Demachi, K.; Kitajima, K.; Yamagishi, T.-A. *Chem. Commun.* **2011**, *47*, 7164–7166.
154. Ogoshi, T.; Kitajima, K.; Aoki, T.; Fujinami, S.; Yamagishi, T.-A.; Nakamoto, Y. *J. Org. Chem.* **2010**, *75*, 3268–3273.
155. Han, C.; Zhang, Z.; Yu, G.; Huang, F. *Chem. Commun.* **2012**, *48*, 9876–9878.
156. Ogoshi, T.; Kitajima, K.; Fujinami, S.; Yamagishi, T.-A. *Chem. Commun.* **2011**, *47*, 10106–10108.
157. Han, J.; Hou, X.; Ke, C.; Zhang, H.; Strutt, N. L.; Stern, C. L.; Stoddart, J. F. *Org. Lett.* **2015**, *17*, 3260–3263.

158. Schneebeli, S. T.; Cheng, C.; Hartlieb, K. L.; Strutt, N. L.; Sarjeant, A. A.; Stern, C. L.; Stoddart, J. F. *Chem. Eur. J.* **2013**, *19*, 3860–3868.
159. Corbett, P. T.; Leclaire, J.; Vial, L.; West, K. R.; Wietor, J.-L.; Sanders, J. K. M.; Otto, O. *Chem. Rev.* **2006**, *106*, 3652–3711.
160. Hartman, A. M.; Gierse, R. M.; Hirsch, A. K. H. *Eur. J. Org. Chem.* **2019**, 3591–3590.
161. Frei, P.; Hevey, R.; Ernst, B. *Chem. Eur. J.* **2019**, *25*, 60–73.
162. Mondal, M.; Hirsch, A. K. H. *Chem. Soc. Rev.* **2015**, *44*, 2455–2488.
163. Van der Vlag, R.; Hirsch, A. K. H. in: *Compr. Supramol. Chem.* 2, Elsevier, **2017**, 487–509.
164. Liu, B.; Pappas, C. G.; Zangrando, E.; Demitri, N.; Chmielewski, P. J.; Otto, S. *J. Am. Chem. Soc.* **2019**, *141*, 1685–1689.
165. Frydrych, R.; Ślepokura, K.; Bil, A.; Gregoliński, J. *J. Org. Chem.* **2019**, *84*, 5695–5711.
166. Thompson, M. C.; Busch, D. H. *J. Am. Chem. Soc.* **1962**, *84*, 1762–1763.
167. Brady, P. A.; Sanders, J. K. M. *J. Chem. Soc., Perkin Trans. I* **1997**, 3237–3254.
168. Kaiser, G.; Sanders, J. K. M. *Chem. Commun.* **2000**, 1763–1764.
169. Nelson, S. M. Knox, C. V.; Mccann, M.; Drew, M. G. B. *J. Chem. Soc., Dalton Trans.* **1981**, 1669–1677.
170. Lins, R. J.; Flitsch, S. L.; Turner, N. J.; Irving, E.; Brown, S. A. *Angew. Chem. Int. Ed.* **2002**, *41*, 3405–3407.
171. Woll, M. G.; Gellman, S. H. *J. Am. Chem. Soc.* **2004**, *126*, 11172–11174.
172. Shi, B. L.; Greaney, M. F. *Chem. Commun.* **2005**, 866–867.

173. Star, A.; Goldberg, I.; Fuchs, B. *Angew. Chem. Int. Ed.* **2000**, 39, 2685–2689.
174. Sutton, L. R.; Donaubauer, W. A.; Hampel, F.; Hirsch, A. *Chem. Commun.* **2004**, 1758–1759.
175. Wipf, P.; Mahler, S. G.; Okumura, K. *Org. Lett.* **2005**, 7, 4483–4486.
176. Giuseppone, N.; Lehn, J.-M. *J. Am. Chem. Soc.* **2004**, 126, 11448–11449.
177. Rideout, D. *Science* **1986**, 233, 561–563.
178. Nazarpak-Kandlousy, N.; Zweigenbaum, J.; Henion, J.; Eliseev, A. V. *J. Comb. Chem.* **1999**, 1, 199–206.
179. Giger, T.; Wigger, M.; Audetat, S.; Benner, S. A. *Synlett* **1998**, 6, 688–691.
180. Zhang, W.; Moore, J. S. *J. Am. Chem. Soc.* **2005**, 127, 11863–11870.
181. Davidson, S. M. K.; Regen, S. L. *Chem. Rev.* **1997**, 97, 1269–1280.
182. Boul, P. L.; Reutenauer, P.; Lehn, J. M. *Org. Lett.* **2005**, 7, 15–18.
183. Goodman, M. S.; Jubian, V.; Linton, B.; Hamilton, A. D. *J. Am. Chem. Soc.* **1995**, 117, 11610–11611.
184. Cai, M. M.; Shi, X. D.; Sidorov, V.; Fabris, D.; Lam, Y. F.; Davis, J. T. *Tetrahedron* **2002**, 58, 661–671.
185. Brady, P. A.; Bonar-Law, R. P.; Rowan, S. J.; Suckling, C. J.; Sanders, J. K. M. *Chem. Commun.* **1996**, 319–320.
186. Bonar-Law, R. P.; Sanders, J. K. M. *Tetrahedron Lett.* **1992**, 33, 2071–2074.
187. Storm, O.; Lüning, U. *Chem. Eur. J.* **2002**, 8, 793–798.
188. Lüning, U. *J. Incl. Phenom. Macrocycl. Chem.* **2004**, 49, 81–84.
189. González-Álvarez, A.; Alfonso, I.; López-Ortiz, F.; Aguirre, Á.; García-Granda, S.; Gotor, V. *Eur. J. Org. Chem.* **2004**, 2004, 1117–1127.

190. González-Álvarez, A.; Alfonso, I.; Gotor, V. *Chem. Commun.* **2006**, 2224–2226.
191. Wöhler, F.; Liebig, J. *Ann. Pharm.* **1832**, 3, 249–282.
192. Zinin, N. *Ann. Pharm.* **1839**, 31, 329–332.
193. Lapworth, A. *J. Chem. Soc., Trans.* **1904**, 85, 1206–1214.
194. Ugai, T.; Dokawa, T.; Tsubokawa, S. *J. Pharm. Soc. Jpn.* **1943**, 63, 269.
195. Enders, D.; Niemeier, O.; Henseler, A. *Chem Rev.* **2007**, 107, 5606–5655.
196. Breslow, R. *J. Am. Chem. Soc.* **1958**, 80, 3719–3726.
197. Knight, R. L.; Leeper, F. J. *Tetrahedron Lett.* **1997**, 38, 3611–3614.
198. Gerhards, A. U.; Leeper, F. J. *Tetrahedron Lett.* **1997**, 38, 3615–3618.
199. Sheehan, J. C.; Hunneman, D. H. *J. Am. Chem. Soc.* **1966**, 88, 3666–3667.
200. Sheehan, J. C.; Hara, T. *J. Org. Chem.* **1974**, 39, 1196–1199.
201. Enders, D.; Kallfass, U. *Angew. Chem. Int. Ed.* **2002**, 41, 1743–1745.
202. Zhao, C.; Chen, S.; Wu, P.; Wen, Z. *Acta Chem. Sinica* **1988**, 46, 784.
203. Enders, D.; Breuer, K.; Teles, J. H. *Helv. Chim. Acta* **1996**, 79, 1217–1221.
204. Knight, R. L.; Leeper, F. J. *J. Chem. Soc., Perkin Trans. 1* **1998**, 1891–1894.
205. Enders, D.; Han, J. *Tetrahedron: Asymmetry* **2008**, 19, 1367–1371.
206. Baragwanath, L.; Rose, C. A.; Zeitler, K.; Connon, S. J. *J. Org. Chem.* **2009**, 74, 9214–9217.
207. Stark, H.; Kathmann, M.; Schlicker, E.; Schunack, W.; Schlegel, B.; Sippl, W. *Mini-Rev. Med. Chem.* **2004**, 4, 965–977.
208. Meyers, A. I. *Heterocycles in Organic Synthesis*, Wiley, New York, NY, **1974**.
209. Mennen, S. M.; Miller, S. J. *J. Org. Chem.* **2007**, 72, 5260–5269.
210. Takikawa, H.; Suzuki, K. *Org. Lett.* **2007**, 9, 2713–2716.

211. Koyama, Y.; Yamaguchi, R.; Suzuki, K. *Angew. Chem.* **2008**, *120*, 1100–1103.
212. Pirrung, M. C.; Fallon, L.; Lever, D. C.; Shuey, S. W. *J. Org. Chem.* **1996**, *61*, 2129–2136.
213. Buck, J. S.; Ide, W. S.; Adams, R.; Bachmann, W. E.; Blatt, H. A.; Fieser, L. F.; Johnson, J. R.; Snyder, H. R. *Organic Reactions* Wiley, New York, NY, **1949**, 269–304.
214. Demir, A. S.; Pohl, M.; Janzen, E.; Müller, M. *J. Chem. Soc., Perkin Trans.* **2001**, *1*, 633–635.
215. Iding, H.; Dünwald, T.; Greiner, L.; Liese, A.; Müller, M.; Siegert, P.; Grötzinger, J.; Demir, A. S.; Pohl, M. *Chem. Eur. J.* **2000**, *6*, 1483–1495.
216. Hayashi, M.; Matsuda, T.; Oguni, N. *J. Chem. Soc., Chem. Commun.* **1990**, 1364–1365.
217. Oppenheimer, H. *Ber. Dtsch. Chem. Ges.* **1886**, *19*, 1814.
218. Grimaux, E. *Compt. Rend.* **1876**, *83*, 826.
219. Jones, J. I.; Tinker, P. B. *Chem. Soc.* **1955**, 1286–1287.
220. Ji, Q.; Do, L. H.; Miljanić, O. Š. *Synlett* **2015**, *26*, 1625–1627.
221. Ji, Q.; Le, H. T. M.; Wang, X.; Chen, Y.-S.; Makarenko, T.; Jacobson, A. J.; Miljanić, O. Š. *Chem. Eur. J.* **2015**, *21*, 17205–17209.
222. Eisterhold, A. M. *Benign Catalysis and Expansion of Cyclobenzoin*, University of Houston, MS Thesis, **2019**.
223. Hasell, T.; Cooper, A. I. *Nat. Rev. Mater.* **2016**, *1*, doi:10.1038/natrevmats.2016.53.
224. Slater, A. G.; Cooper, A. I. *Science* **2015**, *348*, aaa8075.
225. Ding, S.-Y.; Wang, W. *Chem. Soc. Rev.* **2013**, *42*, 548–568.

226. Côté, A. P.; Benin, A. I.; Ockwig, N. W.; O’Keeffe, M.; Matzger, A. J.; Yaghi, O. M. *Science* **2005**, *310*, 1166–1170.
227. Furukawa, H.; Cordova, K. E.; O’Keeffe, M.; Yaghi, O. M. *Science* **2013**, *341*, 1230444.
228. *Metal-Organic Frameworks: Applications from Catalysis to Gas Storage*, Farrusseng, D. (Ed.); Wiley-VCH: Weinheim, **2011**.
229. *Metal-Organic Frameworks: Design and Application*, MacGillivray, L. R. (Ed.); Wiley: Hoboken, **2010**.
230. Introduction to Metal-Organic Frameworks. Special issue of *Chem. Rev.* **2012**, *112*, 673–1268.
231. Xie, L. S.; Sun, L.; Wan, R.; Park, S. S.; DeGayner, J.; Hendon, C. H.; Dincă, M. *J. Am. Chem. Soc.* **2018**, *140*, 7411–7414.
232. Sumida, K.; Rogow, D. L.; Mason, J. A.; McDonald, T. M.; Bloch, E. D.; Herm, Z. R.; Bae, T. H.; Long, J. R. *Chem. Rev.* **2012**, *112*, 724–781.
233. Kim, H.; Rao, S. R.; Kapustin, E. A.; Zhao, L.; Yang, S.; Yaghi, O. M.; Wang, E. N. *Nat. Commun.* **2018**, *9*, doi: 10.1038/s41467-018-03162-7.
234. Alsbaiee, A.; Smith, B. J.; Xiao, L.; Ling, Y.; Helbling, D. E.; Dichtel, W. R. *Nature* **2016**, *529*, 190–194.
235. Burgun, A.; Valente, P.; Evans, J. D.; Huang, D. M.; Sumby, C. J.; Doonan, C. J. *Chem. Commun.* **2016**, *52*, 8850–8853.

236. Evans, J. D.; Huang, D. M.; Hill, M. R. Sumby, C. J.; Sholl, D. S.; Thornton, A. W.; Doonan, C. J. *J. Phys. Chem. C* **2015**, *119*, 7746–7754.
237. Ono, K.; Johmoto, K.; Yasuda, N.; Uekusa, H.; Fujii, S.; Kiguchi, M.; Iwasawa, N. *J. Am. Chem. Soc.* **2015**, *137*, 7015–7018.
238. Zhang, G.; Presly, O.; White, F.; Oppel, I. M.; Mastalerz, M. *Angew. Chem. Int. Ed.* **2014**, *53*, 5126–5130.
239. Zhang, G.; Presly, O.; White, F.; Oppel, I. M.; Mastalerz, M. *Angew. Chem. Int. Ed.* **2014**, *53*, 1516–1520.
240. Elbert, S. M.; Rominger, F.; Mastalerz, M. *Chem. Eur. J.* **2014**, *20*, 16707–16720.
241. Avellaneda, A.; Valente, P.; Burgun, A.; Evans, J. D.; Markwell-Heys, A. W.; Rankine, D.; Nielsen, D. J.; Hill, M. R.; Sumby, C. J.; Doonan, C. J. *Angew. Chem. Int. Ed.* **2013**, *52*, 3746–3749.
242. Schneider, M. W.; Oppel, I. M.; Ott, H.; Lechner, L. G.; Hauswald, H.-J. S.; Stoll, R.; Mastalerz, M. *Chem. Eur. J.* **2012**, *18*, 836–847.
243. Jones, J. T. A.; Hasell, T.; Wu, X.; Bacsá, J.; Jelfs, K. E.; Schmidtman, M.; Chong, S. Y.; Adams, D. J.; Trewin, A.; Schiffman, F.; Cora, F. Slater, B.; Steiner, A.; Day, G. M.; Cooper, A. I. *Nature* **2011**, *474*, 367–371.
244. Bojdys, M. J.; Briggs, M. E.; Jones, J. T. A.; Adams, D. J.; Chong, S. Y.; Schmidtman, M.; Cooper, A. I. *J. Am. Chem. Soc.* **2011**, *133*, 16566–16571.
245. Mastalerz, M.; Schneider, M. W.; Oppel, I. M.; Presly, O. *Angew. Chem. Int. Ed.* **2011**, *50*, 1046–1051.

246. Mastalerz, M. *Chem. Commun.* **2008**, 4756–4758.
247. Davis, F.; Higson, S. *Macrocycles: Construction, Chemistry and Nanotechnology Applications*, Wiley, Chichester, **2011**.
248. Turunen, L.; Warzok, U.; Puttreddy, R.; Beyeh, N. K.; Schalley, C. A.; Rissanen, K. *Angew. Chem. Int. Ed.* **2016**, 55, 14033–14036.
249. Chen, T.-H.; Popov, I.; Miljanić, O. Š. *Chem. Eur. J.* **2017**, 23, 286–290.
250. Chen, T.-H.; Popov, I.; Chuang, Y.-C.; Chen, Y.-S.; Miljanić, O. Š. *Chem. Commun.* **2015**, 51, 6340–6342.
251. Pei, W. Y.; Xu, G.; Yang, J.; Wu, H.; Chen, B.; Zhou, W.; Ma, J. F. *J. Am. Chem. Soc.* **2017**, 139, 7648–7656.
252. Smaldone, R. A.; Forgan, R. S.; Furukawa, H.; Gassensmith, J. J.; Slawin, A. M. Z.; Yaghi, O. M.; Stoddart, J. F. *Angew. Chem. Int. Ed.* **2010**, 49, 8630–8634.
253. Wang, P.; Wu, Y.; Zhao, Y.; Yu, Y.; Zhang, M.; Cao, L. *Chem. Commun.* **2017**, 53, 5503–5506.
254. Jie, K.; Liu, M.; Zhou, Y.; Little, M. A.; Bonakala, S.; Chong, S. Y.; Stephenson, A.; Chen, L.; Huang, F.; Cooper, A. I. *J. Am. Chem. Soc.* **2017**, 139, 2908–2911.
255. Yao, Y.; Zhang, Y.; Zhang, Y.; Tao, Z.; Ni, X.; Wei, G. *Appl. Mater. Interfaces* **2017**, 9, 40760–40765.
256. Sanna, E.; Escudero-Adán, E. C.; López, C.; Ballester, P.; Rotger, C.; Costa, A. J. *Org. Chem.* **2016**, 81, 5173–5180.

257. Shimizu, L. S.; Salpage, S. R.; Korous, A. A. *Acc. Chem. Res.* **2014**, *47*, 2116–2127.
258. Venkataraman, D.; Lee, S.; Zhang, J.; Moore, J. S. *Nature* **1994**, *371*, 591–593.
259. Alrayyani, M.; Miljanić, O. Š. *Chem. Commun.* **2018**, *54*, 11989–11997.
260. Alrayyani, M.; Wang, X.; Miljanić, O. Š. *Chem. Eur. J.* **2017**, *23*, 16476–16478.
261. Nakata, T.; Tanaka, T.; Oishi, T. *Tetrahedron Lett.* **1983**, *24*, 2653–2656.
262. Hahn, S.; Alrayyani, M.; Sontheim, A.; Wang, X.; Rominger, F.; Miljanić, O. Š.; Bunz, U. H. F. *Chem. Eur. J.* **2017**, *23*, 10543–10550.
263. Wadkins, R. M.; Hyatt, J. L.; Wei, X.; Yoon, K. J. P.; Wierdl, M.; Edwards, C. C.; Morton, C. L.; Obenauer, J. C.; Damodaran, K.; Beroza, P.; Danks, M. K.; Potter, P. *M. J. Med. Chem.* **2005**, *48*, 2906–2915.
264. Friedman, M. *J. Org. Chem.* **1965**, *30*, 859–836.
265. Catalina, F.; Peinado, C.; Blanco, M.; Alonso, A.; Allen, N. S. *J. Photochem. Photobiol., A* **2000**, *131*, 141–146.
266. Alrayyani, M. *Synthesis and Characterization of Novel Macrocycles Based on Cyclobenzoin*, University of Houston, PhD Thesis, **2020**.
267. McHale, C. M.; Stegemoller, C. R.; Hashim, M. I.; Wang, X.; Miljanić, O. Š. *Cryst. Growth Des.* **2019**, *19*, 562–567.
268. Pandolfi, F.; Chiarotto, I.; Rocco, D.; Feroci, M. *Electrochim. Acta.* **2017**, *254*, 358–367.
269. Tamaddon, F.; Tafti, A. D. *Synlett* **2016**, *27*, 2217–2220.
270. Gong, S. W.; He, H. F.; Zhao, C. Q.; Liu, L. J.; Cui, Q. X. *Synth. Commun.* **2012**, *42*, 574–581.

271. Kravchenko, A. N.; Antonova, M. M.; Baranov, V. V.; Nelyubina, Y. V. *Synlett* **2015**, 26, 2521–2526.
272. Temperini, A.; Minuti, L. *Tetrahedron. Lett.* **2012**, 53, 2709–2711.
273. Dalko, M.; Dumats, J. Process for the Synthesis of Trisubstituted Oxazoles. L'Oreal S.A. Paris, FR, **2001**. US Patent 6,333,414.
274. Bindi, L.; Steinhardt, P. J.; Yao, N.; Lu, P. J. *Science* **2009**, 324, 1306–1309.
275. Bindi, L.; Steinhardt, P. J.; Yao, N.; Lu, P. J. *Am. Mineral* **2011**, 96, 928–931.
276. Bindi, L.; Yao, N.; Lin, C.; Hollister, L. S.; Andronicos, C. L.; Distler, V. V.; Eddy, M. P.; Kostin, A.; Kryachko, V.; MacPherson, G. J.; Steinhardt, W. M.; Yudovskaya, M.; Steinhardt, P. J. *Sci. Rep.* **2015**, 5, <https://doi.org/10.1038/srep09111>.
277. Atkins, P.; Overton, T.; Rourke, J.; Weller, M.; Armstrong, F. *Inorganic Chemistry*, Oxford University Press: Oxford, GB, **2006**.
278. Pei, H.; Wen, Z.; Li, Z.; Zhang, Y.; Yue, Z. *Appl. Surf. Sci.* **2018**, 440, 790–803.
279. Li, Z.; Wen, Z.; Gao, H.; Wu, Y. *Materialwiss. Werkstofftech.* **2018**, 49, 1193–1205.
280. Su, W.; Xu, Q.; Wang, R.; Xu, Z.; Liu, S.; Liu, B. *Mater. Des.* **2018**, 141, 296–322.
281. Wu, Y.; Xiang, J.; Yang, C.; Lu, W.; Lieber, C. M. *Nature* **2004**, 430, 61–65.
282. Schmidt, G. M. J. *Pure Appl. Chem.* **1971**, 27, 647–678.
283. Desiraju, G. R. *Angew. Chem. Int. Ed.* **2007**, 46, 8342–8356.
284. Wang, F.; Richards, V. N.; Shields, S. P.; Buhro, W. E. *Chem. Mater.* **2014**, 26, 3212–3225.
285. Davey, R. J.; Schroeder, S. L. M.; ter Horst, J. H. *Angew. Chem. Int. Ed.* **2013**, 52, 2166–2179.
286. Desiraju, G. R. *Nat. Mater.* **2002**, 1, 77–79.

287. Anslyn, E. V.; Dougherty, D. A. *Modern Physical Organic Chemistry* University Science Books, Sausalito CA, **2006**.
288. Lodish, H.; Berk, A.; Kaiser, C. A.; Krieger, M.; Scott, M. P.; Bretscher, A.; Ploegh, H.; Matsudaira, P. *Molecular Cell Biology* W. H. Freeman and Company, New York, NY, **2008**.
289. Vishweshwar, P.; McMahon, J. A.; Bis, J. A.; Zaworotko, M. J. *J. Pharm. Sci.* **2006**, *95*, 499–516.
290. Omachi, H.; Segawa, Y.; Itami, K. *Acc. Chem. Res.* **2012**, *45*, 1378–1389.
291. Cai, J.; Sessler, J. L. *Chem. Soc. Rev.* **2014**, *43*, 6198–6213.
292. Hu, W.-B.; Hu, W.-J.; Liu, Y. A.; Li, J.-S.; Jiang, B.; Wen, K. *Chem. Commun.* **2016**, *52*, 12130–12142.
293. Kobaisi, M. A.; Bhosale, S. V.; Latham, K.; Raynor, A. M.; Bhosale, S. V. *Chem. Rev.* **2016**, *116*, 11685–11796.
294. Báthori, N. B.; Nassimbeni, L. R. *CrystEngComm* **2011**, *13*, 3156–3161.
295. Jacobs, A.; Nassimbeni, L. R.; Silwana, N.; Báthori, N. B.; Weber, E. *CrystEngComm* **2011**, *13*, 7014–7018.
296. Ogoshi, T.; Sueto, R.; Yoshikoshi, K.; Sakata, Y.; Akine, S.; Yamagishi, T. *Angew. Chem. Int. Ed.* **2015**, *54*, 9849–9852.
297. Nassimbeni, L. R.; Báthori, N. B.; Patel, L. D.; Su, H.; Wber, E. *CrystEngComm* **2015**, *51*, 3627–3629.
298. Morohashi, N.; Nanbu, K.; Tonosaki, A.; Noji, S.; Hattori, T. *CrystEngComm* **2015**, *51*, 4799–4808.

299. Ogoshi, T.; Sueto, R.; Hamada, Y.; Doitomi, K.; Hirao, H.; Sakata, Y.; Akine, S.; Kakuta, T.; Yamagishia, T. *Chem. Commun.* **2017**, *53*, 8577–8580.
300. Sykes, N. M.; Su, H.; Weber, E.; Bourne, S. A.; Nassimbeni, L. R. *CrystEngComm* **2017**, *19*, 3682–3688.
301. Morohashi, N.; Ebata, K.; Nakayama, H.; Noji, S.; Hattori, T. *Cryst. Growth Des.* **2017**, *17*, 891–900.
302. Jie, K.; Zhou, Y.; Li, E.; Zhao, R.; Liu, M.; Huang, F. *J. Am. Chem. Soc.* **2018**, *140*, 3190–3193.
303. Kawahata, M.; Tominaga, M.; Fujimaru, K.; Hyodo, T.; Yamaguchi, K. *Tetrahedron* **2019**, *75*, 130576.
304. Tominaga, M.; Masu, H.; Azumaya, I. *Cryst. Growth Des.* **2011**, *11*, 542–546.
305. Tominaga, M.; Masu, H.; Azumaya, I. *CrystEngComm* **2011**, *13*, 5299–5302.
306. Tominaga, M.; Katagiri, K.; Azumaya, I. *Cryst. Growth Des.* **2009**, *9*, 3692–3696.
307. Liu, L.; Fang, Z.; Zheng, X.; Xi, D. *ACS Sens.* **2019**, *4*, 1323–1328.
308. Qing, M.; Xie, S.; Cai, W.; Tang, D.; Tang, Y.; Zhang, J.; Yuan, R. *Anal. Chem.* **2018**, *90*, 11439–11445.
309. Ge, C.; Luo, Q.; Wang, D.; Zhao, S.; Liang, X.; Yu, L.; Xing, X.; Zeng, L. *Anal. Chem.* **2014**, *86*, 6387–6392.
310. Zheng, W.; Li, H.; Chen, W.; Zhang, J.; Wang, N.; Guo, X.; Jiang, X. *Small* **2018**, *14*, 1703857.
311. Shen, Q.; Tang, S.; Li, W.; Nie, Z.; Liu, Z.; Huang, Y.; Yao, S. *Chem. Commun.* **2012**, *48*, 281–283.

312. Radell, J.; Connolly, J. W.; Yuhas, L. D. *Phys. Lab. Mater. Cent.* **1960**, 26, 2022–2025.
313. Kawahata, M.; Tominaga, M.; Maekawa, Y.; Yamaguchi, K. *CrystEngComm* **2017**, 19, 7229–7235.
314. Kawahata, M.; Hyodo, T.; Tominaga, M.; Yamaguchi, K. *CrystEngComm* **2018**, 20, 5667–5671.
315. Hyodo, T.; Kawahata, M.; Hikami, Y.; Komatsu, A.; Tominaga, M.; Yamaguchi, K. *CrystEngComm* **2019**, 21, 1548–1554.
316. Matsuda, R.; Kitaura, R.; Kitagawa, S.; Kubota, Y.; Belosludov, R. V.; Kobayashi, T. C.; Sakamoto, H.; Chiba, T.; Takata, M.; Kawazoe, Y.; Mita, Y. *Nature* **2005**, 436, 238–241.
317. Yang, S.; Ramirez-Cuesta, A. J.; Newby, R.; Garcia-Sakai, V.; Manuel, P.; Callear, S. K.; Campbell, S. I.; Tang, C. C.; Schröder, M. *Nat. Chem.* **2015**, 7, 121–129.
318. Wu, H.; Gong, Q.; Olson, D. H.; Li, J. *Chem. Rev.* **2012**, 112, 836–868.
319. Zhang, J.-P.; Chen, X.-M. *J. Am. Chem. Soc.* **2009**, 131, 5516–5521.
320. Hu, T. L.; Wang, H.; Li, B.; Krishna, R.; Wu, H.; Zhou, W.; Zhao, Y.; Han, Y.; Wang, X.; Zhu, W.; Yao, Z.; Xiang, S.; Chen, B. *Nat. Commun.* **2015**, 6, 7328–7335.
321. Noro, S.; Kitaura, R.; Kondo, M.; Kitagawa, S.; Ishii, T.; Matsuzaka, H.; Yamashita, M. *J. Am. Chem. Soc.* **2002**, 124, 2568–2583.
322. Cui, X.; Chen, K.; Xing, H.; Yang, Q.; Krishna, R.; Bao, Z.; Wu, H.; Zhou, W.; Dong, X.; Han, Y.; Li, B.; Ren, Q.; Zaworotko, M. L.; Chen, B. *Science* **2016**, 6295, 141–144.

323. Nugent, P.; Belmabkhout, Y.; Burd, S. D.; Cairns, A. J.; Luebke, R.; Forrest, K.; Pham, T.; Ma, S.; Space, B.; Wojtas, L.; Eddaoudi, M.; Zaworotko, M. J. *Nature*, **2013**, *495*, 80–84.
324. Chen, K. J.; Scott, H. S.; Madden, D. G.; Pham, T.; Kumar, A.; Bajpai, A.; Lusi, M.; Forrest, K. A.; Space, B.; Perry, J. J.; Zaworotko, M. J. *Chem.* **2016**, *1*, 753–765.
325. Li, B.; Cui, X.; O’Nolan, D.; Wen, H.-M.; Jiang, M.; Krishna, R.; Wu, H.; Lin, R.-B.; Chen, Y.-S.; Yuan, D.; Xing, H.; Zhou, W.; Ren, Q.; Qian, G.; Zaworotko, M. J. *Adv. Mater.* **2017**, *29*, 1704210.
326. Zhang, Z.; Cui, X.; Yang, L.; Cui, J.; Bao, Z.; Yang, Q.; Xing, H. *Ind. Eng. Chem. Res.* **2018**, *57*, 7266–7274.
327. O’Nolan, D.; Kumar, A.; Chen, A.-J.; Mukherjee, S.; Madden, D. G.; Zaworotko, M. J. *ACS. Appl. Nano Mater.* **2018**, *1*, 6000–6004.
328. Zhang, Y.; Duan, J.; Ma, D.; Li, P.; Li, S.; Li, H.; Zhou, J.; Ma, X.; Feng, X. Wang, B. *Angew. Chem., Int. Ed.* **2017**, *56*, 16313.
329. Zhou, Y.; Jie, K.; Zhao, R.; Huang, F. *Adv. Mater.* **2019**, 1904824.
330. Vaidhyanathan, R.; Iremonger, S. S.; Shimizu, G. K. H.; Boyd, P. G.; Alavi, S.; Woo, T. K. *Science* **2010**, *330*, 650.
331. Bloch, E. D.; Queen, W. L.; Krishna, R.; Zadrozny, J. M.; Brown, C. M.; Long, J. R. *Science* **2012**, *335*, 1606–1610.
332. Trickett, C. A.; Helal, A.; Al-Maythaly, B. A.; Yamani, Z. H.; Cordova, K. E.; Yaghi, O. M. *Nat. Rev. Mat.* **2017**, *2*, <https://doi.org/10.1038/natrevmats.2017.45>.
333. Sun, J.-K.; Antonietti, M.; Yuan, J. *Chem. Soc. Rev.* **2016**, *45*, 6627–6656.

334. Huang, N.; Wang, P.; Addicoat, M. A.; Heine, T.; Jiang, D. *Angew. Chem. Int. Ed.* **2017**, *56*, 4982–4986.
335. Kuhn, P.; Antonietti, M.; Thomas, A. *Angew. Chem. Int. Ed.* **2008**, *47*, 3450–3453.
336. Das, A.; Heasman, P.; Ben, T.; Qiu, S. *Chem. Rev.* **2017**, *117*, 1515–1563.
337. Bao, Z.; Chang, G.; Xing, H.; Krishna, R.; Ren Q.; Chen, B. *Energy Environ. Sci.* **2016**, *9*, 3612–3641.
338. Liao, P.-Q.; Huang, N.-Y.; Zhang, W.-X.; Zhang, J.-P.; Chen, X.-M. *Science* **2017**, *356*, 1193–1196.
339. Wang, Y.; Zhao, D. *Cryst. Growth. Des.* **2017**, *17*, 2291–2308.
340. Lin, R.-B.; Xiang, S.; Xing, H.; Zhou, W.; Chen, B. *Coord. Chem. Rev.* **2019**, *378*, 87–103.
341. He, Y.; Zhou, W.; Qian, G.; Chen, B. *Chem. Soc. Rev.* **2014**, *43*, 5657–5678.
342. Li, B.; Wen, H.-M.; Wang, H.; Wu, H.; Tyagi, M.; Yildirim, T.; Zhou, W.; Chen, B. *J. Am. Chem. Soc.* **2014**, *136*, 6207–6210.
343. Li, B.; Wen, H.-M.; Zhou, W.; Xu, J. Q.; Chen, B. *Chem* **2016**, *1*, 557–580.
344. Taylor, M. K.; Runčevski, T.; Oktawie, J.; Gonzalez, M. I.; Siegelman, R. L.; Mason, J. A.; Ye, J.; Brown, C. M.; Long, J. R. *J. Am. Chem. Soc.* **2016**, *138*, 15019–15026.
345. Rowsell, J. I. C.; Yaghi, O. M. *J. Am. Chem. Soc.* **2006**, *128*, 1304–1315.
346. Moreau, F.; da Silca, I.; al Smail, N. H.; Easun, T. L.; Savage, M.; Godfrey, H. G. W.; Parker, S. F.; Manuel, P.; Yang, S.; Schröder, M. *Nat. Commun.* **2017**, *8*, 14085.
347. Nugent, P.; Belmabkhout, Y.; Burd, S. D.; Cairns, A. J.; Luebke, R.; Forrest, K.; Pham, T.; Ma, S.; Space, B.; Wojtas, L.; Eddaoudi, M.; Zaworotko, M. J. *Nature* **2013**, *495*, 80–84.

348. Peng, Y.; Li, Y.; Ban, Y.; Jin, H.; Jiao, W.; Liu, X.; Yang, W. *Science* **2014**, *346*, 1356.
349. Yang, S.; Ramirez-Cuesta, A. J.; Newby, R.; Garcia-Sakai, V.; Manuel, P.; Callear, S. K.; Campbell, S. I.; Tang, C. C.; Schröder, M. *Nat. Chem.* **2015**, *7*, 121–129.
350. Cadiau, A.; Adil, K.; Bhatt, P. M.; Belmabkhout, Y.; Eddaoudi, M. *Science* **2016**, *353*, 137.
351. Wang, Z.; Cohen, S. M. *Chem. Soc. Rev.* **2009**, *38*, 1315–1329.
352. Tanabe, K. K.; Cohen, S. M. *Chem. Soc. Rev.* **2011**, *40*, 498–519.
353. Vimont, A.; Goupil, J.-M.; Lavalley, J.-C.; Daturi, M.; Surblé, S.; Serre, C.; Millange, F.; Férey, G.; Audebrand, N. *J. Am. Chem. Soc.* **2006**, *128*, 3218–3227.
354. Dincă, M.; Long, J. R. *Angew. Chem., Int. Ed.* **2008**, *47*, 6766–6779.
355. Zhou, W.; Wu, H.; Yildirim, T. *J. Am. Chem. Soc.* **2008**, *130*, 15268–15269.
356. Dietzel, P. D. C.; Besikiotis, V.; Blom, R. *J. Mater. Chem.* **2009**, *19*, 7362–7362.
357. Chen, B.; Xiang, S.; Qian, G. *Acc. Chem. Res.* **2010**, *43*, 1115–1124.
358. Li, J.-R.; Kuppler, R. J.; Zhou, H.-C. *Chem. Soc. Rev.* **2009**, *38*, 1477–1504.
359. Keskin, S.; van Heest, T. M.; Sholl, D. S. *ChemSusChem* **2010**, *3*, 879–891.
360. Li, J.-R.; Ma, Y.; McCarthy, M. C.; Sculley, J.; Yu, J.; Jeong, H.-K.; Balbuena, P. B.; Zhou, H.-C. *Coord. Chem. Rev.* **2011**, *255*, 1791–1823.
361. Morris, R. E.; Wheatley, P. S. *Angew. Chem. Int. Ed.* **2008**, *47*, 4966–4981.
362. Phan, A.; Doonan, C. J.; Uribe-Romo, F. J.; Knobler, C. B.; O’Keefe, M.; Yaghi, O. M. *Acc. Chem. Res.* **2010**, *43*, 58–67.
363. Simmones, J. M.; Wu, H.; Zhou, W.; Yildirim, T. *Energy Environ. Sci.* **2011**, *4*, 2177–2185.

364. Luca, L. D.; Mezzetti, A. *Synthesis* **2020**, 52, 353–364.
365. Bugaut, X.; Glorius, F. *Chem. Soc. Rev.* **2012**, 41, 3511–3522.
366. Smith, M. B.; March, J. *In March's Advanced Organic Chemistry*, 5th ed. Wiley, New York, **2001**, 1243.
367. Hoyos, P.; Sinisterra, J. V.; Molinari, F.; Alcántara, A. R.; Domínguez de María, P. *Acc. Chem. Res.* **2010**, 43, 288–299.
368. Gala, D.; DiBenedetto, D. J.; Clark, J. E.; Murphy, B. L.; Schumacher, D. P.; Steinman, M. *Tetrahedron Lett.* **1996**, 37, 611–614.
369. Fang, Q. K.; Han, Z. X.; Grover, P.; Kessler, D.; Senanayake, C. H.; Wald, S. A. *Tetrahedron: Asymmetry* **2000**, 11, 3659–3663.
370. Wildemann, H.; Dünkelfmann, P.; Müller, M.; Schmidt, B. *J. Org. Chem.* **2003**, 68, 799–791.
371. Tanaka, T.; Kawase, M.; Tani, S. *Bioorg. Med. Chem.* **2004**, 12, 501–505.
372. Ukai, T.; Tanaka, R.; Dokawa, T. *J. Pharm. Soc. Jpn.* **1943**, 63, 296.
373. Haghshenas, P.; Langdon, S. M.; Gravel, M. *Synlett* **2017**, 28, 542–559.
374. Schmidt, S.; Pedroso de Almeida, T.; Rother, D.; Hollmann, F. *Green Chem.* **2017**, 19, 1226–1229.
375. Rose, C.; Gundala, S.; Connon, S. J.; Zeitler, K. *Synthesis*, **2011**, 2011, 190–198.
376. Soeta, T.; Tabatake, Y.; Inomata, K.; Ukaji, Y. *Tetrahedron* **2012**, 68, 894–899.
377. O'Toole, S. E.; Rose, C. A.; Gundala, S.; Zeitler, K.; Connon, S. J. *J. Org. Chem.* **2011**, 76, 347–357.
378. Mortensen, K. T.; Osberger, T. J.; King, T. A.; Sore, H. F.; Spring, D. R. *Chem. Rev.* **2019**, 119, 10288–10317.

379. Martin, A. J. P.; Synge, R. L. M. *Nature*, **1952**, *170*, 826–826.
380. Skoog, D. A.; Holler, E. J.; Crouch, S. R. *Principles of Instrumental Analysis*, Thomson Brooks/Cole, Thomas Corporation. Belmont, CA, 2007.
381. Erdemir, D.; Lee, A. Y.; Myerson, A. S. *Acc. Chem. Res.* **2009**, *42*, 621–629.
382. Susuki, M. *J. Chem. Educ.* **1993**, *70*, 821.
383. Harris, D. C. *Quantitative Chemical Analysis*, W. H. Freeman and Company, New York, NY, **2010**.
384. Lee, C. J.; Martin, R. V.; Henze, D. K.; Brauer, M.; Cohen, A.; Donkelaar, A. v. *Environ. Sci. Technol.* **2015**, *49*, 4335–4344.
385. Nowak, D. J.; Hirabayashi, S.; Bodine, A.; Hoehn, R. *Environ. Pollut.* **2013**, *178*, 395–402.
386. Tham, K. W. *Energy Build.* **2016**, *130*, 637–650.
387. Liu, G.; Xiao, M.; Zhang, X.; Gal, C.; Chen, X.; Liu, L.; Pan, S.; Wu, J.; Tang, L.; Clements-Croome, D. *Sustain. Cities Soc.* **2017**, *32*, 375–396.
388. Sabsey, M. D.; Stauber, C. E.; Casanova, L. M.; Brown, J. M.; Elliott, M. A. *Environ. Sci. Technol.* **2008**, *42*, 4261–4267.
389. Michalowaski, T. *J. Chem. Educ.* **2002**, *79*, 1267.
390. Taylor, F. S. *Ann. Sci.* **1945**, *5*, 185–202.
391. Poole, C. F. *The Essence of Chromatography*, Elsevier, Amsterdam, **2003**.
392. Heumann, L. V. *J. Chem. Educ.* **2008**, *85*, 524.
393. Samide, M. J. *J. Chem. Educ.* **2008**, *85*, 1512.
394. Smith, C. A.; Villaescusa, F. W. *J. Chem. Educ.* **2003**, *80*, 1023.

395. Mori, S.; Barth, H. G. *Size Exclusion Chromatography* Springer, New York, NY, **1999**.
396. Wu, C.-S. *Handbook of Size Exclusion Chromatography*, 2nd ed. Marcel Dekker, New York, NY, **2004**.